Modeling Soil Moisture Dynamics in Wetlands

by

Junhao He

A dissertation submitted to the Graduate Faculty of
Auburn University
in partial fulfillment of the
requirements for the Degree of
Doctor of Philosophy

Auburn, Alabama
August 7, 2021

Keywords: Richards Equation, Soil Moisture, Numerical solution,
Wetland Hydrology, Bayesian Monte Carlo

Approved by

Latif Kalin, Chair, Professor of School of Forestry and Wildlife Sciences
Mohamed M. Hantush, Senior Research Scientist, U.S. EPA
Christopher J. Anderson, Professor of School of Forestry and Wildlife Sciences
Sanjiv Kumar, Assistant Professor of School of Forestry and Wildlife Sciences
Xing Fang, Professor of Department of Civil and Environmental Engineering

Abstract

Soil moisture distribution and fluxes are among the fundamental components of the hydrological cycle. One-dimensional Richard's Equation (hereafter RE) (Richards, 1931) is often used to represent the physics of water moisture distribution and flow in soils by the forces of capillarity and gravity at the local-field and watershed scales. However, obtaining an accurate and efficient numerical solution of RE has remained challenging due to its high non-linearity. In this study, a depth-averaged solution to RE was presented to advance the current knowledge of soil moisture modeling in the root zone and vadose zone.

Chapter 1 presented a literature review on modeling soil moisture in saturated/unsaturated soils. The importance of soil moisture and soil moisture modeling was provided. Three forms of RE were explained followed by several issues related to the numerical solution of RE, including nonlinearity, spatial and temporal discretization, and computational costs as well as the problems of applying RE in wetland environment were summarized. In addition, the objectives of this study were presented.

In Chapter 2, a two-layer approximation of RE was developed, which describes vertically-averaged soil moisture content and flow dynamics in the root zone and the unsaturated soil below. The two-layer solution of RE converted the partial differential equation (PDE) of RE into two-coupled ordinary differential equations (ODEs) describing dynamic vertically-averaged soil moisture variations in the two soil zones subject to a deep or shallow water table in addition to

variable soil moisture flux and pressure conditions at the surface. The numerical model was evaluated for three common soil textures with free-drainage and zero-pressure head at the bottom boundary under various atmospheric conditions. Simulated values showed that the new model is numerically stable and generally accurate in simulating vertically-averaged soil moisture in the two layers under various flux and prescribed pressure boundary conditions (BCs). A hypothetical simulation scenario involving desaturation of initially saturated soil profile caused by exponentially declining water table demonstrated robustness of the numerical model in tracking vertically-averaged moisture contents in the roots layer and the lower vadose soil as the water table continued to fall.

In Chapter 3, a comprehensive assessment of the two-layer RE model was presented. First, the two-layer model was evaluated for 231 soil textures under varying soil layer thicknesses, with a prescribed upper boundary and two bottom BCs. The vertical soil profile was assumed to be uniform. Second, the two-layer model was tested for conditions where the top and bottom soil layers have contrasting hydraulic characteristics. Last, a case study of model application at a Soil Climate Analysis Network (SCAN) site was presented. The application was combined with the Bayesian Monte Carlo (BMC) method for model calibration and uncertainty analysis. Results showed that when dealing with a homogeneous soil profile, the two-layer model had excellent performance. 99.8% and 87.5% of the simulations among 92,400 simulations were found to have root mean square error (*RMSE*) of moisture contents smaller than 0.015 m^3/m^{-3} for free-drainage and zero-pressure head bottom BC, respectively. With heterogeneous soil profiles, the soil moisture contents and fluxes from the two-layer model agreed well with those from HYDRUS (Šimůnek et al., 2008). The two-layer model combined with the BMC method showed good agreement with the observed average soil moisture of the root zone and vadose zone below. Soil

moisture observation data, hydroclimate data, and model structural uncertainties contributed to the overall model uncertainty the most. The model input parameters had very small contribution to the overall model uncertainty. The posterior parameter space and their likelihood values obtained by BMC in calibration process were used for model validation. The overall *RMSE* was smaller than 0.023 m^3/m^{-3} and the Nash–Sutcliffe efficiency (*NSE*) was greater than 0.72 for both soil layers during model validation.

In Chapter 4, a multiple layer-averaged solution of RE is developed. The layer-averaged RE (LARE) solution solves the coupled ODEs using Heun's method with time adaptive algorithm and it accounts for prescribed flux and pressure head boundary conditions at the soil surface, including precipitation, ponding, soil evaporation, and plant transpiration, subject to deep and shallow dynamic water table. LARE was evaluated through five testing scenarios by comparison against analytical solutions, HYDRUS 1-D solver, and field soil moisture observations. The model provided accurate estimations of moisture contents for multiple soil layers, and it was computationally efficient in terms of CPU time and storage usage compared to the finite volume RE scheme in accounting for complex, dynamic prescribed boundary conditions without any convergence issues.

The focus of Chapter 5 was modification of soil moisture module and plant growth module in a process-based biogeochemical model *WetQual* for wetland nutrient cycling in the ponded and variably saturated compartments. The Updated model adopted the two-layer model to simulate soil moisture dynamics subjected to various atmospheric conditions at the soil top and changing shallow groundwater level in the variably saturated compartment of the wetland. Plant water uptake was specified for plants in the wetland environment. The primary productivity module was modified to consider environmental factors including temperature stress, water stress, and plant

dormancy. The updated model was evaluated by applying it to a restored wetland located on Kent Island, Maryland, USA, by two numerical experiments using different bottom boundary conditions for moisture movement in the variably saturated compartment. The results showed that the model had good performance in estimating nutrient loads. The moisture contents in the variably saturated compartment had significant differences between the two bottom conditions using deep and shallow water tables. Besides, the use of the zero-pressure head and free-drainage bottom boundary conditions applied in the variably saturated compartment had significant influences on NH_4, TSS, and TOC exports but did not show influences on other nutrient constituents in the ponded compartment. Sensitivity analysis revealed that the parameters' sensitivities in the ponded and variably saturated compartments more or less confirmed the sensitivity results of the Original (Hantush et al., 2013) and the Expanded (Sharifi et al., 2017) models, but the order of sensitivities differed. Nevertheless, N, C, and P cycles did not show sensitivity to soil hydraulic parameters. The mass balance analysis showed that using different bottom boundary conditions for moisture flow in the variably saturated compartment had influences on N, C, and P budgets. The model estimated biomass in the study wetland reflected the effects of temperature and water stress in addition to the period of dormancy. The estimated plant biomass and nutrient uptake had good matches with field measurements.

Acknowledgments

Five-year living and studying in Auburn have been an adventure and delight for me. Without the help of many kindly people, I would not have been able to accomplish my doctoral dissertation. First and foremost, I am eternally grateful to my supervisor Dr. Latif Kalin for his support in developing my research ideas and achieving my scientific goals. He is not only an admirable advisor but also a wonderful friend. It has always been a pleasure to work with him in an atmosphere of warmth and great personal trust. My second appreciation will go to Dr. Mohamed Hantush, one of my committee members who helped me in developing my research vision and made an invaluable contribution to my research. The knowledge and skills I learned from Dr. Kalin and Dr. Hantush are invaluable for my future career. I am also so thankful to other members of my dissertation advisory committee, Dr. Christopher Anderson, Dr. Sanjiv Kumar, and Dr. Xing Fang for their support and suggestions for this research. I would like to appreciate Dr. Sabahattin Isik, who has always been patient and helpful, for his assistance in my research. I also thank Dr. Jasmeet Lamba for reviewing this dissertation.

I want to thank my friends for being in my life and being my friend in Auburn. My special thanks go to Dr. Mehdi Rezaeianzadeh, Mr. Recep Kanber, Mr. Henrique Haas, Dr. Yuanzhi Yao, Mr. Zhuonan Wang, and Mr. Hemendra Kumar.

I would like to express my gratitude to my parents, Juying Li and Hanjun He for their love and unfailing emotional support. It is a life-changing experience to study abroad and be far away from family. It is my great fortune to meet the Warner family in Auburn. I want to express my

sincere appreciation to Mr. William Warner and Ms. Leslie Warner for letting me be part of their family. I deeply appreciate my wife, Dr. Qing Ge, for sharing her life with me. I would thank her for her unending support and love. I also thank my son, William He, who has always been the source of my joy. Last but not least, I would like to thank the U.S. EPA and the School of Forestry and Wildlife Sciences for the funding support they provided.

The U.S. Environmental Protection Agency (U.S. EPA) through its Office of Research and Development partially funded and collaborated in the research reported in this paper under Contract EP-C-11-010 with Auburn University, School of Forestry and Wildlife Sciences. The views expressed in this article are those of the authors and do not necessarily represent the views or the policies of the U.S. Environmental Protection Agency.

Table of Contents

List of Tables

List of Figures

List of Abbreviations

ANN	Artificial Neural Network
BMCML	Bayesian Monte Carlo and Maximum Likelihood Estimation
CLM	Community Land Model
GLUE	Generalized Likelihood Uncertainty Estimation
GSSHA	Gridded Surface/Subsurface Hydrologic Analysis
HTESSEL	Hydrology Tiled ECMWF Scheme for Surface Exchanges over Land
JULES	Joint UK Land Environment Simulator
LARE	Layer-Averaged Richards Equation
LM3	Land Dynamics Model
LSM	Land Surface Model
MCMC	Markov Chain Monte Carlo
ODE	Ordinary Differential Equations
ORCHIDEE	Organizing Carbon and Hydrology in Dynamic Ecosystems
PTF	Pedotransfer Function
RE	Richards Equation

RMSE	Root Mean Square Error
SCAN	Soil Climate Analysis Network
SWAT	Soil and Water Assessment Tool
USDA	United States Department of Agriculture
VIC	Variable Infiltration Capacity
1-D	One dimension
3-D	Three dimension

Chapter 1: Introduction

1. Soil moisture

Soil moisture is commonly defined as the total amount of water that reside in the pores of the soil in the vadose zone, also termed as unsaturated soil zone, the region between the soil surface and the groundwater table. Volumetric water content and soil matric potential are two commonly used parameters for quantifying soil water availability. Volumetric water content is defined as the ratio of the volume of water to the unit volume of the soil and has the unit of $[L^3_{H2O}/L^3_{soil}]$. It can be also expressed as percentage or depth of water per depth of soil $[L_{H2O}/L_{soil}]$. Volumetric water content is applicable to various spatial scales, from field scale to continental scales (e.g. Crave and Gascuel-Odoux, 1997; Raffelli et al., 2017; Roberti et al., 2018). Soil matric potential is a measure of the forces (capillary and adsorptive forces) of the soil particles binding water molecules and it is commonly expressed in pressure unit, such as kPa. It is an important indicator to determine the relative availability of water held in the soil for plants. The force or energy in plants must exceed the soil matric potential in order for plants to extract water from the soil. The moisture contents at saturation (θ_s), field capacity (θ_{fc}), and the permanent wilting point (θ_{wp}) are three major soil characteristics, which are typically defined as corresponding to soil matric potentials of approximately $-0.1\ kPa$, -10 to $-33\ kPa$, and $-1500\ kPa$, respectively (Hillel, 1998). The matric potentials for θ_s, θ_{fc}, and θ_{wp} are similar across different soil types, while the corresponding volumetric moisture contents mainly depend on soil texture (Hillel, 1998).

Soil moisture is one of the key variables regulating many ecosystem processes and feedback loops in the land-atmosphere system and further controling the terrestrial energy and

biochemical cycles (McGuire et al., 2000; Seneviratne et al., 2010). Soil moisture functions as a source of water for the atmosphere through the process of evapotranspiration (Maxwell and Condon, 2016). Land evapotranspiration is the second-largest component of the terrestrial hydrological cycle. It returns more than 60% of land precipitation to the atmosphere (Korzoun, 1978; Oki and Kanae, 2006). Meanwhile, the energy used for land evapotranspiration takes up more than half of the total solar energy absorbed by land surfaces (Trenberth et al., 2009). Through this process, soil moisture controls the fractions of latent and sensible heat fluxes, which have effects on air temperature and precipitation (Koster et al., 2004, 2009; Hirschi et al., 2014).

2. Modeling of variably saturated flow

Soil moisture connects surface water and groundwater through unsaturated flow. Precipitation reaching the ground surface may either infiltrate into the soil or runs off the soil surface (runoff). Within the soil, water moves according to the gradients of the soil water potential. Water may be removed from the soil by evaporation at the soil surface and plant water uptake in the root zone, or be lost to deeper layers by drainage and transported out of the soil by lateral flow. Soil may also get water from groundwater by groundwater discharge. The processes that water moves within the unsaturated soil zone are referred to as variably saturated flow processes.

Variably saturated flow modeling is fundamental for multiple disciplines such as environmental science, agriculture, and hydrology because variably saturated flow is one of the essential processes in these field (Zeng and Decker, 2009). Many numerical models have been developed to describe and solve for variably saturated flow in porous soil media. Among them, the simplest model is the soil water balance bucket model (Manabe, 1969). It represents the major hydrological processes involved in the soil water budget using conceptualized soil layers as

buckets for receiving and retaining all incident water. This method is numerically efficient and stable regarding the calculating time and computational burden, and thus, is used in many hydrological models, such as Laio et al. (2001), Romano et al. (2011), Arnold et al. (2012), Orth et al. (2013), Davis et al. (2017), and Sanchez-Mejia and Papuga (2017). However, the water budget model may be prone to errors and cannot correctly quantify the water transport in the unsaturated zone due to the oversimplification of the physical process. As an alternative, physically-based models provide relatively accurate information about the flow characteristics in the vadose zone. They are generally developed more or less based on the solution of conservation equations of fluid mechanics with appropriate boundary conditions (e.g. Green and Ampt, 1911; Richards, 1931; Philip, 1957). Among different physically-based models, one of the fundamental and well-known equations is often adopted to describe variably saturated flow in porous media is the Richard's Equation (RE) (Richards, 1931). The RE is often used to represent the physics of moisture distribution and flow in soils by the forces of capillarity and gravity at the local-field and watershed scales. The RE combines the mass balance equation and Darcy's equation and often considers a sink/source term. The RE can be written in the volumetric soil moisture form, mixed form, and matric pressure head form, which each having advantages and disadvantages. The commonly used mixed form RE is written as,

$$\frac{\partial \theta}{\partial t} = -\frac{\partial}{\partial z}\left[K(\theta)\left(\frac{\partial \psi(\theta)}{\partial z} + 1\right)\right] - S(z) \quad (1)$$

where θ is the volumetric water content [L^3L^{-3}]; t is time [T]; z is the vertical coordinate [L] (positively oriented downward); $K(\theta)$ is unsaturated hydraulic conductivity [LT^{-1}]; $\psi(\theta)$ is capillary pressure head (negative of porewater pressure head) [L]; and S is a sink term for plant water uptake [T^{-1}]. In the mixed form RE, θ and ψ are the two unknown variables (dependent

variables) and are often solved numerically. Hence, a closure relationship, the soil-water retention function is employed to relate θ and $\psi(\theta)$.

The soil moisture form of RE is written as advection-diffusion form and it is solely a function of the moisture content,

$$\frac{\partial \theta}{\partial t} = -\frac{\partial}{\partial z}\left[D(\theta)\frac{\partial \theta}{\partial z} + K(\theta)\right] - S(z) \tag{2}$$

where $D(\theta)$ is the soil-water diffusivity [L^2T^{-1}], in which $D(\theta) = K(\theta)(d\psi(\theta)/d\theta)$. The term $D(\theta)(\partial\theta/\partial z)$ represents diffusion by capillarity and $K(\theta)$ represents advection due to gravity. The moisture form of RE is mass conservative and has less nonlinearity compared to other forms of RE. However, these advantages only apply to homogeneous relatively dry soil. If soil is saturated, moisture content keeps constant and the derivative $d\psi/d\theta$ becomes zero at smaller than or equal to air-entry capillary pressure, resulting in the soil-water diffusivity being infinity, which could lead to unstable numerical solution. When taking pressure head as the primary variable and using the chain rule, the head form of RE can be written as,

$$C(\psi)\frac{\partial \psi}{\partial t} = -\frac{\partial}{\partial z}\left[K(\psi)\left(\frac{\partial \psi}{\partial z} + 1\right)\right] - S(z) \tag{3}$$

where $C(\psi)$ is the specific moisture capacity [L^{-1}], in which $C(\psi) = d\theta/d\psi$. The head form of RE can be applied in both unsaturated and saturated flow conditions, because the pressure head is continuous over the soil profile, making it capable to solve heterogeneous soil problems. However, the head form RE may experience mass balance error introduced by the nonlinear term $C(\psi)$ (Zha et al., 2017). The special design of the numerical iteration technique needs to be applied to avoid mass balance errors (e.g. Celia et al., 1990; Rathfelder and Abriola, 1994; Tocci et al., 1997; Miller et al., 2006).

3. Problems of solving RE

The common issue among all forms of RE is nonlinearity. RE is known as a highly nonlinear, degenerate elliptic-parabolic partial differential equation (Farthing and Ogden, 2017a). Besides, two empirical, highly nonlinear soil hydraulic functions, unsaturated hydraulic conductivity function $K(\theta)$ and soil-water characteristic curve $\psi(\theta)$, make the solution of RE unstable especially when soil is extremely dry or close to saturation (List and Radu, 2016). Also, when applying RE to the conditions with dynamic upper and lower boundary conditions, the moisture or pressure head could change rapidly in space and time. The numerical solution may experience stability and mass conservation issues in such conditions. To address the nonlinearity of RE and make the RE solution stable and mass conservative, various numerical solutions of RE have been proposed using a special design of spatial and temporal discretization schemes in methods of finite differences (Celia et al., 1990; Ross, 1990; Rathfelder and Abriola, 1994; Herrada et al., 2014), finite volume (Kumar et al., 2009; Caviedes-Voullième et al., 2013; Lai and Ogden, 2015; and Svyatskiy and Lipnikov, 2017), finite element (Forsyth et al., 1995; Lee and Abriola, 1999; Simunek et al., 2008), and combination of these schemes (Helmig, 1997).

When setting the spatial discretization, the size of the mesh is the most important consideration since it determines the accuracy of the numerical solutions (Or et al., 2015). There are three major spatial discretization methods: uniform mesh, non-uniform mesh, and adaptive mesh. The uniform mesh is the simplest, but fine vertical resolution is often needed for the numerical solution to yield relatively accurate results. The non-uniform discretization scheme usually has fine vertical resolution at the soil surface and is coarsened along with depth. The finer mesh at the soil top tracks the rapid variations of fluxes and hydraulic gradient under various

atmospheric boundary conditions, while coarse mesh in deeper soil reduces the computational cost (Downer and Ogden, 2004a; Dickinson et al., 2014). For a thick and dry soil profile, the wetting front creates a sharp hydraulic gradient when moving downward. Adaptive discretization can be employed in this situation. The mesh becomes finer around the wetting front to track the time evolution of the moving wetting front.

The other problem related to RE is the computational expense. The computational cost in terms of the CPU utilization and the time used for convergence of the numerical solution associated with the numerical schemes listed above could vary differently according to the conditions RE being applied. In laboratory or field scale, computation time is not a major concern because the simulation time is relatively short. However, when applying RE in a large watershed model with high vertical resolution or in a distributed regional model having thousands or millions of nodes, the computation time would accumulate during a long simulation period and eventually lead to the total simulation time being undesirably long. One way to avoid high computational costs is to coarsen the spatial discretization at a reasonable resolution to yield relatively accurate results. Another method is to use an adaptive time-stepping scheme to optimize the computational cost by adjusting the time step size (Pop, 2002; Miller et al., 2006). Time step becomes smaller when boundary condition changes rapidly to ensure the accuracy of the solution and it becomes larger to increase the efficiency when numerical solutions converge fast.

The water flow between plant roots and the surrounding soil is one of the essential processes linking the vadose zone hydrology with the atmosphere. Many models simulate plant water uptake by the sink term $S(z)$ applied in RE, which assumes the entire root system as a single unit to simulate the compound effects of individual roots (e.g. Feddes et al., 1976; Molz and Remson, 1971; Molz, 1981; Van Genuchten, 1987). Among them, Feddes et al. (1978) model is

one of the fundamental models that considers partitioning potential transpiration over depth according to root density and applying a water-stress response function. New generation of models borrowed this concept (Dogan and Motz, 2005; Ojha and Rai, 1996; Perrochet, 1987; Prasad, 1988; Van Genuchten, 1987). They extended this concept by adding more physical processes in the sink term such as soil-water pressure head, root growth, root permeability, and root water extraction. The selection of the proper mathematical model for certain plant type and environmental conditions can impact the accuracy of the prediction of plant water uptake.

4. Modeling soil moisture dynamics in wetland environments

Wetlands are defined as those environments with soils intermittently covered with shallow water or with water present either at or near the soil surface, and vegetation adapted to saturated soil conditions (Mitsch and Gosselink, 2000). Wetland hydrology is one of the important characteristics that determine wetland ecosystems and functions. Wetland soils are often made of fine-texture clay-rich soils and often flooded and saturated or near-saturated, but during different states of hydroperiod, wetland soils can experience saturation and unsaturated conditions. Moisture content in wetland soil is sensitive to the wetland water budget. Small changes in water inputs can have significant effects on the moisture status of the soil. The switch between saturated and unsaturated conditions of the wetland soils regulates oxygen level in the soils, which further influence the soil microbial community structure and microbial respiration, thereby control the biogeochemical processes of the wetland (Reddy and DeLaune, 2008; Manzoni et al., 2012; Moyano et al., 2013; Chen et al., 2015; Limpert et al., 2020). When soil is getting wet but not fully saturated, soil moisture is positively correlated with microbial activity (Brockett et al., 2012; Manzoni et al., 2012). Wickland and Neff (2008) reported that the soil organic decomposition rate

increased with the increase of soil moisture. It reached the highest value when the relative saturation rate was about 0.5 to 0.75, then it decreased when soil is close to saturation. The frequent dry/wet events increased the activity of autotrophic nitrifier populations (Fierer and Schimel, 2002). The maximum nitrogen mineralization occurred at intermediate soil moisture (Sleutel et al., 2008). Decreasing of soil moisture content increases air-filled porosity, which leads to reduction of nitrification rate (Manu et al., 2021). Soil moisture has a strong impact on greenhouse gas emissions. Schaufler et al. (2010) found that nitrous oxide emissions were positively correlated with soil moisture, while NO emission was negatively correlated with soil moisture. The highest CO_2 emissions occurred at intermediate soil moisture. Oxygen level decreases with increased moisture content resulting in decreased redox potential in wetland soils (Picek et al., 2000). Consequently, as conditions become more anoxic and reducing, microorganisms tend to use alternative electron acceptors, which would change the dominant metabolic activity in the soil (Mitsch and Gosselink, 2000).

Although the soil in the wetland area is often saturated or close to saturation, understanding the variations of moisture content of wetland soil is still necessary for precisely evaluating the biochemical process in the wetland. Sharifi A. et al., (2017) applied and slightly modified the finite difference numerical solution to RE developed by van Dam and Feddes (2000) to simulate soil moisture dynamics in variably saturated soil around ponding area of the wetland. This RE solution was integrated into a wetland hydrology and nutrient model, *WetQual*. The solution considers various flux or head-controlled top boundary conditions including precipitation, soil evaporation, plant water uptake, and surface ponding. The bottom boundary condition can be head controlled or flux controlled depending on the position of the groundwater level. However, Sharifi A. et al., (2017) reported that the finite difference solution to RE crashed frequently during simulations

especially when the soil was close to saturation due to the hyperbolic nature of RE and the high non-linearity of soil hydraulic functions. The overall model stability was interrupted because of the multiple crashes of the numerical model. In addition, the plant growth module in *WetQual* were modeled using simple mass balance equations (Hantush et al., 2013). However, it did not consider detailed seasonal plant phenology (such as plant dormancy and maturity) and the effect of environmental stress on plant growth, such as temperature and water stress.

5. Study Objectives

The first objective of this study was to develop and verify a two-layer approximation of RE (called the two-layer model). The two-layer model is later integrated into the *WetQual* model (objective 4). The solution of the two-layer model converts the partial differential equation of RE into two coupled ordinary differential equations. It describes vertically averaged soil moisture content and flux dynamics in the root zone and the unsaturated vadose zone below as well as it accounts for various upper atmospheric conditions including precipitation, evapotranspiration, and ponding and handles dynamic groundwater level within or below the soil column. The two-layer model is numerically stable and computationally efficient and it yields relatively accurate estimations of layer-averaged soil moisture contents and boundary fluxes. Numerical experiments were conducted to evaluate the performance of the two-layer model including three soil textures with different permeability and various atmospheric conditions subject to a dynamic groundwater level at the bottom boundary. The derivations of the two-layer model, numerical solutions, and testing scenarios are presented in Chapter 2.

The strength and weakness of the two-layer model in simulating soil moisture content under complex and changing environments were not fully explored in Chapter 2. Accordingly, **the**

second objective was to perform an in-depth assessment of the two-layer model. The two-layer model was first evaluated for uniform soil profiles made up of 231 soil textures with varying soil layer thicknesses, under a prescribed upper boundary and two bottom boundary conditions. Then, the two-layer model was tested with stratified layers. Last, the developed model was applied at field scale to a Soil Climate Analysis Network (SCAN) site. The Bayesian Monte Carlo and Maximum Likelihood estimation (BMCML) methodology was performed for model calibration and predictive uncertainty estimation. The model evaluation results were compared against HYDRUS and field observations. The methodology, numerical experiments, and application scenarios are explained in Chapter 3.

Although the two-layer model was comprehensively tested in Chapter 3 for its performance under various environmental conditions, it has some structural shortcomings. If modeling soil moisture content and fluxes is desired at higher vertical resolution, a multi-layer scheme can be implemented. Consequently, **the third objective** of this study was to extend the two-layer solution of depth-averaged RE to a multiple **L**ayer-**A**veraged **RE** solution, called LARE. The solution of LARE simulates average moisture contents of multiple predefined soil layers governed by several coupled ordinary differential equations. The coupled governing equations are solved explicitly by Heun's method integrated with a time adaptive algorithm. Additionally, the numerical scheme LARE was evaluated against analytical solutions, HYDRUS 1-D solver, and field soil moisture observations. The numerical derivations and solutions of LARE as well as numerical experiments and application scenarios are presented in Chapter 4.

The moisture content estimation module in *WetQual* developed by Sharifi et al. (2017) reported numerically unstability issues in the wetland environment. There is a need to improve the soil moisture estimation module in *WetQual*. Besides, the plant growth/death module in *WetQual*

is too simple that cannot appropriately capture the seasonal growth/death pattern of the wetland plants. Consequently, **the fourth objective** was to improve the soil moisture module and plant growth/death module in *WetQual*. The two-layer model was integrated into *WetQual* and it was used for simulating moisture content for the variably saturated compartment of the wetland and estimating actual plant water uptake to regulate plant growth. The plant growth/death module was improved for taking into account temperature stress, water stress on plant growth, and plant dormancy. The improved *WetQual* model was evaluated by two numerical experiments using the generalized likelihood uncertainty estimation technique (GLUE) and global sensitivity analysis (GSA) methods. The plant growth/death module was assessed by comparing the results of estimated biomass with field measurements. The improvements of model components and evaluation scenarios are presented in Chapter 5.

6. Dissertation Organization

The structure of the dissertation is organized as follows:

Chapter 1 describes the background and the motivation of this research, presenting the research objectives.

Chapter 2 provides detailed description of the two-layer model including the derivation of the governing equations and the numerical method for solving the equations. The numerical scheme was verified with two numerical tests by comparing the model outputs with the benchmark model HYDRUS 1-D in response to the first objective.

Chapter 3 presents the methodology, numerical experiments, and case study application for a thorough assessment and validation of the two-layer model in response to the second

objective of this study. Meanwhile, the model parameter sensitivity and prediction uncertainty were also evaluated using a Bayesian framework.

Chapter 4 describes the methods of the development of the multiple Layer Averaged Richards Equation (LARE) and the description of the associated numerical method in response to the third objective. This chapter also provides five testing scenarios for LARE against analytical solutions, HYDRUS 1-D solver, and field soil moisture observations in response to the third objective.

Chapter 5 provides the improvements of unsaturated flow and plant growth modules in *WetQual* and presents three numerical scenarios for model evaluation in response to the fifth objective. Each chapter from Chapter 2 to Chapter 5 was written as standalone journal paper.

Chapter 6 summarizes the entire research and presents the significant findings through this study. Potential improvements and suggestions for future work are also provided.

Chapter 2: Two-Layer Vertically-Averaged Soil Moisture Dynamics: Numerical Model

Abstract

Simulating water moisture flow in variably saturated soils with a relatively shallow water table is challenging due to the high nonlinear behavior of Richards' equation (RE). A two-layer approximation of RE was derived in this paper, which describes vertically-averaged soil moisture content and flow dynamics in the root zone and the unsaturated soil below. To this end, the partial differential equation (PDE) describing RE was converted into two-coupled ordinary differential equations (ODEs) describing dynamic vertically-averaged soil moisture variations in the two soil zones subject to a deep or shallow water table in addition to variable soil moisture flux and pressure conditions at the surface. The coupled ODEs were solved numerically using the iterative Huen's method for a variety of flux and pressure-controlled top and bottom boundary conditions (BCs). The numerical model was evaluated for three typical soil textures with free-drainage and mixed flux-pressure head at the bottom boundary under various atmospheric conditions. The results of soil water contents and fluxes were validated using HYDRUS-1D as a benchmark. Simulated values showed that the new model is numerically stable and generally accurate in simulating vertically-averaged soil moisture in the two layers under various flux and prescribed pressure BCs. A hypothetical simulation scenario involving desaturation of initially saturated soil profile caused by exponentially declining water table demonstrated the robustness of the numerical model in tracking vertically-averaged moisture contents in the roots layer and the lower vadose soil as the water table continued to fall. The two-layer model can be used by researchers to simulate variably saturated soils in wetlands and by water resources planners for efficient coupling of land-surface systems to groundwater and management of conjunctive use of surface and groundwater.

1. Introduction

Soil moisture distribution and fluxes are fundamental components in the hydrological cycle. They connect surface water and groundwater and function as a source for evaporation demand, including plant transpiration (Maxwell and Condon, 2016). Besides, soil moisture is also known to control terrestrial biogeochemical processes by regulating the soil microbial respiration (Orchard and Cook, 1983; Liu et al., 2009). Soil moisture and fluxes should be well represented by hydrological and biogeochemical models as they play important roles for water resources planning and management and tracking water and solute mass budgets of a watershed.

One of the fundamental and well-known equations to describe unsaturated flow in porous media is Richard's Equation (hereafter RE) (Richards, 1931). It is often used to represent the physics of water distribution and flow in soils (root and vadose zones) by the forces of capillarity and gravity at the local-field and watershed scales. The RE is obtained by substituting Darcy's equation into the continuity equation and considering applicable sink/source terms. The one-dimensional form of RE can be written as

$$\frac{\partial \theta}{\partial t} = -\frac{\partial}{\partial z}\left[K(\theta)\left(\frac{\partial \psi}{\partial z} + 1\right)\right] - S(z) \quad (1)$$

where θ is the volumetric water content [L^3L^{-3}]; K is unsaturated hydraulic conductivity [LT^{-1}]; ψ is capillary pressure head (negative of soil water pressure head) [L]; t is time [T]; S is a sink term for plant roots' uptake [T^{-1}]; and z is the vertical coordinate [L] (positively oriented downward).

RE is known as a highly nonlinear, elliptic-parabolic partial differential equation (PDE). Although numerous studies have been done to address the non-linearity of RE, obtaining an accurate and efficient numerical solution of RE has remained challenging (Farthing and Ogden, 2017). Besides, RE is coupled with two empirical, highly nonlinear soil hydraulic functions:

unsaturated hydraulic conductivity function $K(\theta)$ and soil-water characteristic curve $\psi(\theta)$. A condition known as degeneration can be introduced to the solution of RE when either or both of the values of unsaturated hydraulic conductivity and capillary-pressure head are close to zero (List and Radu, 2016). Algorithms have been developed for solving RE numerically in saturated and unsaturated flow problems. Various numerical solutions of RE have been proposed using spatial and temporal discretization schemes in methods of finite differences (Celia et al., 1990; Ross, 1990; Rathfelder and Abriola, 1994; Herrada et al., 2014), finite volume (Kumar et al., 2009; Caviedes-Voullième et al., 2013; Lai and Ogden, 2015; and Svyatskiy and Lipnikov, 2017), and finite element (Forsyth et al., 1995; Lee and Abriola, 1999; Šimůnek et al., 2008). Ross (1990) presented an efficient finite difference scheme for solving RE using hyperbolic Sine transformation of matric potential considering soil infiltration. Caviedes-Voullième et al. (2013) applied an implicit finite volume scheme based on the mixed form of RE and implemented Celia et al. (1990) method to infiltration and column drainage flow scenarios. They concluded that this scheme is mass conservative and can solve the equation under saturated conditions and when soil transitions from unsaturated to saturated conditions. Further, for numerical stability and efficiency, it is better to use relatively large time steps with coarse meshes. Varado et al. (2006) expressed flux in terms of matrix (Kirchoff) potential and presented and validated a finite difference scheme expressed in terms of soil saturation. Besides demonstrating efficiency of the numerical solution, they concluded that it is necessary to use finer spatial discretization near the soil surface for accurately modeling the cumulative infiltration in fine-textured soils. Despite these efforts and many others, the spatial and temporal discretization of RE continue to pose a challenge, especially for soils with initially low moisture contents and high heterogeneity due to mass balance errors and numerical oscillation and dispersion (e.g., Belfort et al., 2013; and Caviedes-Voullième et al., 2013).

Although application of RE at the laboratory and field scales has been relatively successful (Lai and Ogden, 2015; Liu et al., 2018; Zha et al., 2013), application of RE to larger scale systems such as wetlands and watersheds can be even more challenging. Using the numerical scheme proposed by van Dam and Feddes (2000), Sharifi et al. (2017) reported the frequent crashing of the RE solver, especially when soil is near saturation. In that study, high resolution of soil moisture values with depth was irrelevant and only layer-average values were important in simulating nitrogen and carbon cycling. Contemporary medium or large-scale soil moisture models often consider simplified representation of RE for moisture dynamics to decrease the computational burden. Some examples to this include RE coupled mass conservation equation (Zhu et al., 2016), analytical solution of RE (Huang and Wu, 2012; Su et al., 2018), coarse finite difference resolution (Downer and Ogden, 2004), and simpler functions for water retention parameters (Hayek, 2016).

Watershed and land surface models often rely on average soil moisture content than point values to simulate energy balance and biochemical processes such as CLM (Oleson et al., 2010), GSSHA (Downer and Ogden , 2004) and SVAT (Sellers et al., 1986). In these approaches, average moisture content for each soil layer is calculated either by integrating computed soil moisture over the layer or by selecting a nodal value to represent the average soil moisture content. Although RE estimates soil moisture from a physical perspective, the numerical schemes can be unstable and computational cost can increase exponentially at such scales. This is especially true when a solution is required over large areas and repetitive model simulations are needed to quantify model predictive uncertainty using, e.g., Monte Carlo simulations. Moreover, estimation of soil moisture values at high vertical resolution might be redundant and unnecessary (Cao and Yue, 2014) and can be unreliable in some applications (Farthing et al., 2003). Although several simplified approaches have been proposed to calculate moisture content for certain depth of soil in watershed

scale applications, such as the soil water balance bucket model (Sanchez-Mejia and Papuga, 2017), these approaches cannot account for the complexities of soil water movement as RE does. Therefore, a stable and efficient numerical solution of RE is needed for large-scale soil moisture estimations and when modeling the coupling land surface and surface water to groundwater. The solution should be able to deal with the interactions between unsaturated soil and fluctuating groundwater levels by the actions of recharge, accretion or evaporative losses. Furthermore, a numerical scheme should be designed to approximate vertically-averaged volumetric soil moisture content with some mathematical rigor, with quantifiable errors to eliminate the need for high-resolution details and thus reduce computational resource usage in terms of computation time and memory storage.

Despite presenting integrated form of Eq. (1) (e.g., Lee and Abriola, 1999; Herrada et al., 2014; and Lai and Ogden, 2015), analyses often proceeded with essentially finite-differences approximation of point values. All these schemes were proposed to obtain solutions at high vertical resolution, by discretizing the flow domain into multiple numerical cells. They are not designed to obtain moisture content averaged over vertically delineated soil layers (e.g., root zone and intermediate vadose zone), unless solutions are further processed. Worth noting is the work by Kumar (2004) where RE was averaged over a sloping soil to describe depth-averaged mean moisture content considering the effect of soil heterogeneity. The analysis emphasized relative contributions of various components of the lateral flow, but a solution was not presented and verified. While much of the literature has focused on numerical algorithms for solving RE at the point scale, much less effort has been devoted to the solution of layer-averaged forms with emphases on numerical efficiency and presence of water table at relatively shallow depth.

The interaction between saturated and unsaturated zone plays a critical role in the hydrological cycle (Zeng and Decker, 2009; Bizhanimanzar et al., 2019; Dai et al., 2019). Water table fluctuations can affect soil moisture in the root zone and regulate soil evaporation and plant water uptake (Sulis et al., 2011). During dry periods, soil profile can receive upward water flux from the water table, which could potentially be a crucial source of water to plants. The interactions between unsaturated (typically root zone) and saturated zone can be one-directional when water table is relatively deep (e.g., Celia et al., 1990; Varado et al., 2006; Herrada et al., 2014; Lai and Ogden, 2015; Hayek, 2016; Zhang et al., 2016; Rahman et al., 2019), and two-directional when the water table is relatively shallow and has significant effects on the water storage in the vadose soil. The numerical solution of RE becomes degenerate when the water table is within the root zone and close to the surface (Ogden et al., 2017). This further underscores the need for a stable, efficient and operational numerical model that can couple soil surface to groundwater and simulate saturation and desaturation close to the surface under highly variable climate conditions and fluctuating water table.

This paper presents a new numerical model for two-layer vertically-averaged RE describing one-dimensional vertical water movement in the root zone and the vadose layer below. The solution is derived from first-order approximation (truncated error of order $(\Delta z)^2$) of vertically-averaged soil moisture content and the mixed form of RE. It converts the PDE to two-coupled ODEs describing vertically-averaged moisture content and flow in two layers. The numerical model considers various atmospheric conditions along with plant water uptake and water movement between soil and fluctuating water table. The objectives of this paper are to: 1) derive a vertically-averaged and mass-conservative approximation of RE; 2) verify the model performance by comparison with the reference model HYDRUS considering various types of BCs;

and 3) demonstrate the capability of the model in simulating the presence of a dynamic water table. The overarching goal is to develop a numerically stable and efficient module for field and watershed-scale soil moisture and flux simulations.

In the following sections, the mathematical derivation of the two-layer model is first described. This is followed by sections describing soil hydraulic properties, methods of plant water uptake and soil evaporation, and numerical scheme. The model is then evaluated by comparing the results of soil moisture and fluxes with those from HYDRUS-1D model for different soil texture and various BCs. The application concludes with a hypothetical scenario demonstrating model ability to simulate average soil moisture between ground surface and a dynamic water table. The manuscript ends with summary and conclusions.

2. Methodology

2.1. Water table below the root zone layer (two-layer model)

The equation governing one-dimensional vertical water movement in soils is the flow continuity equation:

$$\frac{\partial \theta}{\partial t} = -\frac{\partial q}{\partial z} - S \tag{2}$$

where, θ is volumetric water content [L^3L^{-3}]; t is time [T]; z is soil depth below the surface [L], positive downward; S is a soil moisture sink term (e.g. plant transpiration) [$L^3L^{-3}T^{-1}$]; and q is flux per unit area [$L^3T^{-1}L^{-2}$], given by Darcy's law:

$$q = K\frac{\partial \psi}{\partial z} + K \tag{3}$$

where, K is unsaturated hydraulic conductivity [LT^{-1}]; and ψ is negative of soil pressure head (capillary pressure head or matric potential) [L].

Figure 2.1 is a schematic illustration of a soil profile with a root zone of thickness h and water table at depth $H(t)$ and time t. Two layers are delineated; the first layer with thickness h denotes the root zone. The second layer with thickness (H-h) corresponds to vadose soil extending from the bottom of the first layer to the water table. We derive coupled ODEs of average moisture contents $\bar{\theta}_1$ and $\bar{\theta}_2$ for the root zone layer and the second layer, respectively. First, let us assume groundwater level is initially below the first layer ($H(t) > h$), $\bar{\theta}_1$ and $\bar{\theta}_2$ are defined as

$$\bar{\theta}_1(t) = \frac{1}{h}\int_0^h \theta(z,t)\, dz \tag{4}$$

$$\bar{\theta}_2(t) = \frac{1}{H(t)-h}\int_h^{H(t)} \theta(z,t)\, dz \tag{5}$$

We start by integrating Eq. (2) from z = 0 to z = h:

$$\int_0^h \frac{\partial \theta}{\partial t} dz = -\int_0^h \frac{\partial q}{\partial z} dz - \int_0^h S\, dz \tag{6}$$

which yields

$$h\frac{d\bar{\theta}_1}{dt} = q|_{z=0} - q|_{z=h} - h\bar{S} \tag{7}$$

where, $q|_{z=0}$ is flux at soil surface [LT^{-1}]; $q|_{z=h}$ is interface flux between the first layer and the second layer [LT^{-1}]; and $\bar{S}$ is average transpiration rate over the root zone [$L^3L^{-3}T^{-1}$]: $\bar{S} = \int_0^h S\, dz\, /h$. Integrating (2) over the second layer, from $z = h$ to $z = H(t)$, and taking out the S term

$$\int_h^{H(t)} \frac{\partial \theta}{\partial t} dz = -\int_h^{H(t)} \frac{\partial q}{\partial z} dz \tag{8}$$

and applying Leibnitz rule yields

$$(H-h)\frac{d\bar{\theta}_2}{dt}-\theta_{2s}\frac{dH}{dt}=q|_{z=h}-q|_{z=H} \tag{9}$$

where, θ_{2s} is the saturated moisture content of the second layer [L^3L^{-3}]; $q|_{z=H}$ is the flux at bottom of the second layer [LT^{-1}].

At the interface of two layers ($z = h$), $q|_{z=h}$ is given by:

$$q|_{z=h}=K|_{z=h}\left.\frac{\partial\psi}{\partial z}\right|_{z=h}+K|_{z=h} \tag{10}$$

Taylor series expansion of ψ around z = h is

$$\psi(z,t)=\psi(h,t)+\left.\frac{\partial\psi}{\partial z}\right|_{z=h}(z-h)+\frac{1}{2}\left.\frac{\partial^2\psi}{\partial z^2}\right|_{z=h}(z-h)^2+\cdots \tag{11}$$

Integrating (11) from z = 0 to z = h and retaining zero and first-order terms yield

$$\bar{\psi}_1\cong\psi(h,t)-\frac{1}{2}\left.\frac{\partial\psi}{\partial z}\right|_{z=h}h \tag{12}$$

thus,

$$\left.\frac{\partial\psi}{\partial z}\right|_{z=h}\cong 2\frac{\psi(h,t)-\bar{\psi}_1}{h} \tag{13}$$

where, $\bar{\psi}_1$ is the average of $\psi_1$in the first layer [L], $\bar{\psi}_1=\int_0^h\psi(z,t)\,dz\ /h$.

Integrating (11) from z = h to z = H and dropping higher-order terms yields

$$\bar{\psi}_2\cong\psi(h,t)+\frac{1}{2}\left.\frac{\partial\psi}{\partial z}\right|_{z=h}(H-h) \tag{14}$$

Hence,

$$\left.\frac{\partial\psi}{\partial z}\right|_{z=h}\cong 2\frac{\bar{\psi}_2-\psi(h,t)}{H-h} \tag{15}$$

where, $\bar{\psi}_2=\int_h^H\psi(z,t)\,dz\,/(H-h)$. Equations (13) and (15) lead to this approximation:

$$2\frac{\psi(h,t)-\bar{\psi}_1}{h}=2\frac{\bar{\psi}_2-\psi(h,t)}{H-h} \tag{16}$$

which can be solved for $\psi(h,t)$,

$$\psi(h,\mathrm{t}) = \beta\bar{\psi}_1 + (1-\beta)\bar{\psi}_2 \tag{17}$$

where, $\beta = \frac{H-h}{H}$, $1-\beta = \frac{h}{H}$.

Substituting (17) into either (12) or (14) yields

$$\left.\frac{\partial\psi}{\partial \mathrm{z}}\right|_{\mathrm{z}=h} = \frac{2}{H}(\bar{\psi}_2 - \bar{\psi}_1) \tag{18}$$

Using the Taylor-series expansion of K around z = h:

$$K(\mathrm{z},\mathrm{t}) = K(h,\mathrm{t}) + \left.\frac{\partial K}{\partial \mathrm{z}}\right|_{\mathrm{z}=h}(\mathrm{z}-h) + \frac{1}{2}\left.\frac{\partial^2 K}{\partial \mathrm{z}^2}\right|_{\mathrm{z}=h}(\mathrm{z}-h)^2 + \cdots \tag{19}$$

Similarly, by integrating (19) from z = 0 to z = h and dropping higher-order terms, one can show

$$\left.\frac{\partial K}{\partial \mathrm{z}}\right|_{\mathrm{z}=h} = 2\frac{K(h,\mathrm{t}) - \overline{K}_1}{h} \tag{20}$$

where, $\overline{K}_1 = \int_0^h K(\mathrm{z},\mathrm{t})\,dz\,/h$. Hereafter, we make the approximation $\overline{K}_1 \cong K_1(\bar{\theta}_1)$.

Integrating (19) from z = h to z = H and dividing by $(H-h)$ yields

$$\left.\frac{\partial K}{\partial \mathrm{z}}\right|_{\mathrm{z}=h} = 2\frac{\overline{K}_2 - K(h,\mathrm{t})}{H-h} \tag{21}$$

where, $\overline{K}_2 = \int_h^H K(\mathrm{z},\mathrm{t})\,dz\,/(H-h) \cong K_2(\bar{\theta}_2)$.

Comparison of (20) with (21) leads to

$$2\frac{K(h,\mathrm{t}) - \overline{K}_1}{h} = 2\frac{\overline{K}_2 - K(h,\mathrm{t})}{H-h} \tag{22}$$

Hence,

$$K(h,\mathrm{t}) = \beta\overline{K}_1 + (1-\beta)\overline{K}_2 \tag{23}$$

Underlying Eq. (23) is the assumption that $K(z,t)$ is a continuous function and differentiable with respect to z.

Substituting (18) and (23) into (10) yields this expression for $q|_{z=h}$:

$$q|_{z=h} = \frac{2}{H}(\beta\bar{K}_1 + (1-\beta)\bar{K}_2)(\bar{\psi}_2 - \bar{\psi}_1) + \beta\bar{K}_1 + (1-\beta)\bar{K}_2 \tag{24}$$

The top flux $q|_{z=0}$ is controlled by precipitation and evaporation,

a) If $i > 0$ and $i < K_{s1}$,

$$q|_{z=0} = i \tag{25}$$

where, K_{s1} is saturation conductivity of the first layer [LT^{-1}]; and i is precipitation rate [LT^{-1}].

b) If $i > 0$ and $i > K_{s1}$, Eq. (25) holds until the first layer is saturated. Ponding occurs immediately after the first layer is saturated. If the ponding depth is *d* [L], we have

$$q|_{z=0} = 2K_{s1}\frac{\bar{\psi}_1 + d}{h} + K_{s1} \tag{26}$$

c) If $i = 0$,

$$q|_{z=0} = -ev_a \tag{27}$$

where, ev_a is soil actual evaporation rate [LT^{-1}].

At z = *H*, flux to the water table is

$$q|_{z=H} = K|_{z=H}\left.\frac{\partial\psi}{\partial z}\right|_{z=H} + K|_{z=H} \tag{28}$$

and

$$K|_{z=H} = K_{s2} \tag{29}$$

Once again, we expand ψ around z = *H* and integrate from z = h to z = *H* to obtain

$$\left.\frac{\partial\psi}{\partial z}\right|_{z=H} = 2\frac{\psi(H,t) - \bar{\psi}_2}{H-h} \tag{30}$$

Let $\psi(H,t) = \psi_b$, where ψ_b is the critical bubbling suction (i.e., negative of air-entry capillary pressure) of the soil. Thus,

$$q|_{z=H} = 2K_{s2}\frac{\psi_b - \bar{\psi}_2}{H-h} + K_{s2} \tag{31}$$

If water table drops deep below *H*, free drainage condition holds at the bottom and $\left.\frac{\partial\psi}{\partial z}\right|_{z=\mathrm{H}} = 0$. It can be shown using Taylor-series expansion of K around z = *H* and noting that $\left.\frac{\partial K}{\partial z}\right|_{z=\mathrm{H}} = 0$ for free drainage BC, that to the first-order, flux $q|_{z=\mathrm{H}}$ becomes

$$q|_{z=\mathrm{H}} = \overline{K}_2 \cong K_2(\bar{\theta}_2) \tag{32}$$

Equations (7) and (9) with flux expressions (24-27) and (31), and interface expressions (17) and (23) collectively form two-coupled ordinary differential equations describing the dynamics of average volumetric water content in the root zone and the lower vadose soil bounded by the water table at the bottom. Here after, we refer to Eqs (7) and (9) with (24) and (31) as the two-layer model.

2.2. Water table within the first layer (one-layer model)

Here, we address the case where groundwater level is within the root zone (first soil layer), $0 < H \leq h$. The average water content in the root zone is calculated by a weighted average of moisture content in both the saturated and unsaturated parts:

$$\bar{\theta}_1(t) = \frac{H\bar{\theta}_{1u}(t) + (h-H)\theta_{1s}(t)}{h} \tag{33}$$

where, $\bar{\theta}_{1u}$ is moisture content of unsaturated part of the first layer [L^3L^{-3}], θ_{1s} is saturation water content of the first layer [L^3L^{-3}].

$\bar{\theta}_{1u}(t)$ is defined as

$$\bar{\theta}_{1u}(t) = \frac{1}{H(t)}\int_0^{H(t)} \theta(z,t)\,dz \tag{34}$$

Following similar steps, Integration of Eq. (2) from z = 0 to z = $H(t)$ yields

$$H\frac{d\bar{\theta}_{1u}}{dt} - \theta_{1s}\frac{dH}{dt} = q|_{z=0} - q|_{z=H} - H\bar{S}_u \tag{35}$$

where, $q|_{z=H}$ is flux at the water table [LT^{-1}]; and $\bar{S}_u = \int_0^H S\, dz\, /H$.

Similar to (31), $q|_{z=H}$ to the first-order is given by

$$q|_{z=H} = 2K_{s1}\frac{\psi_b - \bar{\psi}_{1u}}{H} + K_{s1} \tag{36}$$

where, $\bar{\psi}_{1u}$ is capillary pressure head of the unsaturated part of the first layer [L].

The time-dependent *H* and *dH*/*dt* terms account for the expansion and contraction of the layers over which $\bar{\theta}_1$ and $\bar{\theta}_2$ are computed. In the context of this scenario, the two layers are virtual and not physical; they cease to exist when the water table rises to the surface and the entire soil profile is saturated. The first layer evolves from zero thickness to *H(t)* until the water table drops to the level lower than the root zone where thickness becomes constant at *h*. The second layer then start evolving from zero thickness and expands to *H(t)-h* as the water table continues to fall.

2.3. Unsaturated soil hydraulic properties

The two-layer model uses the Van Genuchten (1980) model for the soil hydraulic characteristic relationships ψ and K:

$$K(S_e) = \begin{cases} K_s S_e{}^{\lambda}\left[1 - \left(1 - S_e{}^{\frac{1}{m}}\right)^m\right]^2 & \psi < 0 \\ K_s & \psi \geq 0 \end{cases} \tag{37}$$

$$\psi(S_e) = \frac{1}{\alpha}\left(S_e{}^{-\frac{1}{m}} - 1\right)^{1-m} \tag{38}$$

$$S_e = \frac{\theta - \theta_r}{\theta_s - \theta_r} \tag{39}$$

$$m = 1 - \frac{1}{n} \tag{40}$$

where, θ_r and θ_s are residual and saturated water content, respectively [L^3L^{-3}], K_s is saturated hydraulic conductivity [LT^{-1}], S_e is effective saturation rate [-], n is an empirical shape-defining parameter [-], λ is the pore size distribution index [-] and α is a fitting parameter [L^{-1}].

2.4. Transpiration estimation

The sink term *S*, which is defined as the volume of water removed from a unit volume of soil per unit time due to plant water uptake, is calculated using the water stress function proposed by Feddes (1982),

$$S(\psi) = \gamma(\psi) S_p \tag{41}$$

where $\gamma(\psi)$ is soil water stress response function of the soil capillary pressure ($0 \leq \gamma \leq 1$) and S_p is potential plant transpiration rate [T^{-1}]. The plant water uptake is calculated by water stress response function as shown in Figure 2.2. When soil is approaching saturation with capillary pressure smaller than ψ_1 or losing water to the point capillary pressure is above ψ_4, plant water uptake ceases ($\gamma = 0$). Water uptake is equal to the potential rate when soil capillary pressure is between certain predefined capillary pressure heads (ψ_2 and ψ_3). As for capillary pressure between ψ_1 and ψ_2 (or ψ_3 and ψ_4), water uptake is calculated as linearly increasing (or decreasing) with ψ.

2.5. Evaporation estimation

Evaporation is calculated from potential evaporation for water content of the first layer greater than wilting point using the relationship,

$$ev_a = ev_p \left(\frac{\bar{\theta}_1 - \theta_{wp}}{\theta_{fc} - \theta_{wp}} \right)^p \quad (42)$$

where, ev_p is potential evaporation rate [LT^{-1}], θ_{wp} is moisture content at wilting point (-33 kPa) [L^3L^{-3}], θ_{fc} is volumetric water content at field capacity (-1500 kPa) [L^3L^{-3}] and p is an exponent coefficient [-]. The value of p was set to 1. Potential transpiration rate (S_p) and potential evaporation rate (ev_p) can be calculated by partitioning of potential evapotranspiration calculated either by process-based or empirical equations, such as Penman-Monteith method (Allen et al., 2005), Hargreaves equation (Jensen et al., 1997) and Priestley-Taylor equation (Priestley and Taylor, 1972).

2.6. Numerical Scheme

The governing equations (7) and (9) with (24) and (31) for the two-layer model are solved explicitly by using the predictor-corrector algorithm Heun's method (Chapra and Canale, 2015). First, the fluxes q_n (q_0 refers to the top flux $q|_{z=0}$, q_1 refers to the interface flux of two layers $q|_{z=h}$ and q_2 refers to bottom flux $q|_{z=H}$) at the boundaries are obtained from $\bar{\psi}$ and $\overline{K}$ of each layer, which are calculated at the beginning of each computational time step using the Van Genuchten soil characteristic relationships (Eqs. 37-40) soil hydraulic model. The time derivative or slope of the function $\bar{\theta}_i(t)$ at the beginning of the computational time interval (Euler's slope) is expressed as

$$\frac{d\bar{\theta}_i}{dt} = f\left(t_j, {q_n}^j\right) \quad (43)$$

where, subscript *i* denotes layer number; subscript *j* indicates time t_j; and $f\left(t_j, {q_n}^j\right)$ can be deduced from Eqs. (7) and (9) after arranging terms; it is evaluated at the beginning of the

computational time step (t_j). Equation (43) is used to extrapolate $\bar{\theta}_i$ linearly to the end of the computational time step

$$\bar{\theta}_i^0 = \bar{\theta}_i{}^j + f\left(t_j, q_n{}^j\right)\Delta t \tag{44}$$

in which the superscript 0 refers to the intermediate prediction of $\bar{\theta}_i$ at time t_{j+1}, which refers to the standard Euler method and Δt is the computational time step [T], $\Delta t = t_{j+1} - t_j$. The fluxes per unit area q_n^0 are obtained from $\bar{\psi}_i^0$ and $\bar{K}_i^0$ which are calculated from $\bar{\theta}_i^0$ and Van Genuchten soil characteristic model. The slope of the function $\bar{\theta}_i(t)$ at the end of the time interval is given by:

$$\frac{d\bar{\theta}_i}{dt} = f\left(t_{j+1}, q_n{}^0\right) \tag{45}$$

where, the superscript $j+1$ refers to time t_{j+1}. The correction for the prediction (44) is calculated using the average slope for the interval:

$$\bar{\theta}_i{}^{j+1} = \bar{\theta}_i{}^j + \frac{f\left(t_j, q_n{}^j\right) + f\left(t_{j+1}, q_n{}^0\right)}{2}\Delta t \tag{46}$$

The slope in (45) is updated based on this correction ($\bar{\theta}_i{}^{j+1}$) and a revised correction is obtained using (46) once again. These steps are repeated until convergence. A termination criterion, ε, for the convergence of the corrector is provided by:

$$\left|\bar{\theta}_i{}^{j+1,p} - \bar{\theta}_i{}^{j+1,p-1}\right| \leq \varepsilon \tag{47}$$

where, $\bar{\theta}_i{}^{j+1,p-1}$ and $\bar{\theta}_i{}^{j+1,p}$ are the results from the prior iteration and the present correction.

2.7. Model Evaluation

We evaluated the two-layer model by comparing scenario simulations of volumetric moisture content and fluxes with corresponding HYDRUS layer-averaged results for three soil

textures with various prescribed upper and bottom BCs as well as a moving water table. The selected soil textures were with high, moderate, and low permeability according to their saturated hydraulic conductivity: sandy loam, loam, and clay loam, respectively. The van Genuchten soil hydraulic characteristics model was used for calculating unsaturated hydraulic conductivity and pressure head. The soil characteristics properties of the three soil textures are shown in Table 1. The thickness of the first layer and depth to the water table were set to $h = 10$ cm and $H = 40$ cm. The upper BCs (q_0) involved two combinations of precipitation and potential transpiration (T_p) scenarios (Table 2). Soil evaporation was not considered in model comparison owing to the different ways this model and HYDRUS estimate actual evaporation. We assumed that the vegetation cover was pasture, for which the root water uptake parameters ψ_1, ψ_2, ψ_3, and ψ_4 in the water stress response function were set to the values obtained from Wesseling et al. (1991), which were: 10 cm, 25 cm, 800 cm, and 8000 cm, respectively. We considered three distinct water table (WT) scenarios: 1) free-drainage at depth *H* (deep WT); 2) WT at depth H below the root zone; and 3) dynamic WT: sudden rise of WT to the surface and exponential decline afterward. The third scenario exemplifies the capability of the model to simulate desaturation of the two soil layers. For the shallow WT scenario, we imposed zero-pressure head BC (Eq. 31) assuming ψ_b = 0. The initial moisture contents for three soil textures were set to 80% of effective saturation rate (S_e). Simulations were performed for a 20-day period with 0.001 days of computational time step (about 1.44 minutes).

In scenario 3, we hypothesize that the soil domain is instantly saturated by a sudden rise of the WT from initial depth H_0 = 40 cm to H = 0 at the soil surface at time t = 0 days followed by a gradual desaturation. During desaturation, we assume an exponential decline of the WT to its initial depth H_0:

$$H(t) = H_0(1 - e^{-0.03t}) \tag{48}$$

This scenario was simulated for 100 days with computational time step of 0.001 day. Without loss of generality, the upper BC was set to zero rain and zero evapotranspiration.

HYDRUS was used as a benchmark to evaluate the two-layer model performance. HYDRUS software package is a computer-based program that solves RE numerically for transient flow in saturated and unsaturated soils using a finite element method with a mass conservative implicit iterative scheme (Šimůnek et al., 2008). The finite element mesh here was constructed by discretizing the soil profile into 101 elements. Because HYDRUS solves RE at multiple discretized nodes, the averaged water contents for two soil layers were calculated by summing the values of water contents over all nodes and dividing by the number of nodes within each layer (nodes are evenly spaced in each layer). The time step used in HYDRUS was the same as that used in the two-layer model for each simulation scenario. For consistency, the adaptive time-stepping scheme was not implemented in HYDRUS. The tolerance in convergence criterion between the iterations (Eq. 47) was set to the water content difference of 0.0001 in both the two-layer model and HYDRUS. We used root mean square error (*RMSE*) to measure the model performance. In practice, the precision of the in-situ soil moisture measurement probes is assumed to be good for *RMSE*≤0.02 (Robinson et al., 2008).

$$RMSE = \sqrt{\frac{1}{N}\sum_{i=1}^{N}(\theta^*{}_i - \theta_{HYDRUS,i})^2} \tag{49}$$

where, $\theta^*{}_i$ is the i^{th} simulated soil moisture by the two-layer model; $\theta_{HYDRUS,i}$ is the i^{th} simulated value by HYDRUS; and *N* is number of simulated days.

3. Results

Figures 2.3-2.6 compare simulated moisture and cumulative fluxes at the surface and bottom of the soil profiled ($z = H$) between the two models under the two weather scenarios in Table 2.2 and free-drainage and WT BCs. The performance statistics *RMSE* is shown in Table 2.3. Figure 2.7 shows the results for simulation Scenario 3, moisture comparison between two models with water table exponentially receding from soil surface to its initial depth H_0 = 40 cm (30 cm below the bottom of the first layer). Overall, the two-layer mode simulated layer-averaged moisture content compared very well with those obtained by integrating the nodal values calculated by HYDRUS.

3.1. Free-drainage BC

Soil moisture contents and fluxes simulated by the two-layer model compared well to the corresponding layer-averaged HYDRUS results with free-drainage BC (Figures 2.3 and 2.4). The *RMSE* values for layer-averaged θ were between 0 to 0.010 and 0 to 0.011 for the first and the second layers, respectively (Table 2.3). Coarse textured soil (sandy loam) showed the fastest rate to reached steady than fine-textured soils, as the moisture content plots in Figures 2.3 and 2.4 show. The estimated moisture content of the second layer by the two-layer model compared better with corresponding HYDRUS values under rainfall scenario (i = 0.5 cm/day, T_p = 0 cm/day) (Figure 2.3) than the scenario of plant water uptake by transpiration (i = 0 cm/day, T_p = 0.2 cm/day) (Figure 2.4).

The top and bottom cumulative flux values of the three soils agreed well with those simulated by HYDRUS. The fluxes were identical to those from HYDRUS (e.g. Figure 2.4b). The temporal behavior of water flux at both boundaries was well captured by the two-layer model. Computed cumulative fluxes in the rainfall scenario had a much better match with those from

HYDRUS than for the transpiration-only scenario. The two-layer model and HYDRUS initially estimated cumulative transpiration at the potential rate, when the soil water potential was between ψ_2 and ψ_3, as depicted by the linear trend in Figure 2.3. When soil moisture of the root zone decreased by the influences of plant extraction and gravity, transpiration rate started to decrease at the time when water potential reached the range between ψ_3 and ψ_4. The two-layer model estimated cumulative transpiration was larger than those estimated by HYDRUS in the transition period toward steady-state values (from about 10 days to 20 days for sandy loam and after about 15 days for loam and clay loam soil in Figure 2.3b). The two-layer model estimated cumulative transpiration compared better in loam and clay loam than in sandy loam. For sandy loam, the lower values of the average soil moisture in the second layer after 10 days was contributed by higher estimated transpiration rates in the two-layer model (Figure 2.3a). The near flat bottom cumulative flux in the second layer implies free drainage has seized after 10 days and the continued decrease of computed average moisture thereafter can only be explained by the second layer contributing to simulated plant uptake in the first layer (root zone).

3.2. Zero-pressure BC (Water Table)

With zero-pressure head BC (Eq. 31), the water table can exchange moisture with the second layer and becomes a source of water moisture to the overlying soil during dry periods. The *RMSE* values for layer-averaged θ ranged between 0.001 to 0.006 and 0.001 to 0.008 for the first and the second layers, respectively (Table 2.3). Similar to the free-drainage scenario, the two-layer mode results for soil water content and cumulative fluxes were in a very good agreement with those obtained from HYDRUS with groundwater at the bottom of the soil domain. In this scenario, the second layer receives water from the saturated zone and contributes flux to the first layer to

meet plant water demand. Except for sandy loam in layer 1 where free drainage dominated, comparison of Figure 2.4(a) with Figure 2.6(a) and Figure 2.3(a) with Figure 2.5(a) shows the effect of shallow water table on moisture build-up in both layers. All simulations reached steady-state relatively fast (in two days). For clay loam, the two-layer model reached steady state faster than HYDRUS with the transpiration scenario, but was slower with the rainfall scenario. Computed cumulative fluxes by the two-layer model were in perfect match with those from HYDRUS. Both models simulated transpiration rates at the potential rate in all simulations as the root zone matric potentials were between ψ_2 and ψ_3. This is supported by the computed linear cumulative transpiration in Figure 2.5(b).

3.3. Dynamic WT

This hypothetical scenario depicts a sudden rise of WT to the surface at t = 0 and subsequent desaturation, assuming an exponential falling rate of the WT (Eq. 48). Numerical results of soil water contents for sandy loam, loam and clay loam are shown in Figure 2.7. Estimated soil moisture for the first and the second layer all showed the same trend with HYDRUS results. The two-layer model showed excellent performance in calculating soil moisture for both layers (Table 2.3). The differences between the moisture content values estimated by the two models decreased as the soil texture became finer. The evolution of $\bar{\theta}_1$ and $\bar{\theta}_2$ was well captured by the current model. The transition from saturated to unsaturated conditions caused by groundwater decline was well captured with no numerical stability problems. Note the initially steady values of $\bar{\theta}_2$ at saturation until around t = 9.6 days when it starts declining. This corresponds to the time when the WT reaches the bottom of layer 1 (H= 10 cm) and the ensuing desaturation

of layer 2 as the water table continues falling to the original position at depth 40 cm. Before t = 9.6 days, the water table is situated within layer 1, and layer 2 consequently is saturated.

4. Discussion

Soil moisture dynamics is normally governed by solving Richard's elliptic-parabolic partial differential equation or a variant of it. Current numerical models are either too simple to achieve the desired accuracy (e.g., Ducoudré et al., 1993; Neitsch et al., 2011) or too complex, time-consuming, and computationally expensive to implement on large spatial scales and finer temporal resolution (Farthing and Ogden, 2017b; Harter et al., 2004; Qi et al., 2018). The vertically-averaged solution to RE describes one-dimensional water movement and soil moisture dynamics averaged over the thicknesses of the root zone and the vadose zone below. The proposed numerical scheme solves for layer-averaged moisture content in each soil zone as opposed to point values (nodal or grid-centered values). This is because the two-layer model is derived based on integrated form of the finite differences approximations and expressed in terms of layer thickness-averaged values. The numerical scheme of the two-layer model involves an adequate parameterization of soil physics and it is relatively simple, stable, and robust. It is accurate and requires less CPU time. The numerical solutions in tested simulations all converged very fast. The predicted top and bottom fluxes as well as plant transpiration compared very well with HYDRUS results for both cases of free-drainage and WT as the bottom BCs. The newly developed two-layer model was able to reproduce salient features of drainage under capillary and gravity forces. The simulation for sandy loam soil showed that coarse soil textures which have relatively high conductivity tend to lose water faster than fine textured soils due to gravity drainage and have moisture content close to wilting point at steady state (Figures 2.3(a) and 2.4(a)). The ability of the two-layer model to

simulate supply of moisture from the WT to both layers was evident in fine-textured soils (Figures 2.5(a) and 2.6(a)). Despite the presence of WT, the model simulated quick drainage of the water by gravity in the two layers for sandy loam and loam very well (Figures 2.5(a) and 2.6(a)). When considering water table at the bottom of the soil profile, groundwater can move upward due to suction forces, and the upward flux from the second layer to the first layer is highly determined by the soil characteristics and layer thicknesses. The finer the soil texture, the higher the soil water contents of the first and the second layer at steady state will be. As shown in Figures 2.5 and 2.6, the second layer of clay loam reaches saturated conditions and the moisture content of the first layer stays close to saturation.

The differences between the two-layer model and HYDRUS can be attributed to truncation errors of order $(\Delta z)^2$. The greater the layer thickness the larger the error and the differences with integrated finer-discretization solution computed by HYDRUS (based on 100 cells here). Higher-order corrections might be needed to improve model performance. Moreover, transpiration rate is computed slightly differently in both models. In the two-layer model, plant roots are assumed to be uniformly distributed within the root zone and transpiration is calculated using the layer-averaged capillary pressure head (matric potential), which, in turn, is calculated from layer-averaged soil moisture content using the soil characteristic relationship. In HYDRUS, however, the sink term is described by the plant root water uptake distribution function, which is non-uniformly distributed in the root zone. This could underestimate the computed transpiration rate in some nodes relative to others during the soil drying process. The averaging approach in the two-layer model is producing higher transpiration than that in HYDRUS, although the average soil moisture contents are similar in both models. (see Figure 3b).

Because only two soil layers are considered in this new model, the two coupled ordinary differential equations involving top, interfacial and bottom fluxes govern water movement in the soil profile. Results showed that Heun's method in the two-layer model is a simple numerical method; it gives stable, robust and relatively accurate results. These simplifications make the computer program taking up less memory and CPU usage than those taken by HYDRUS. In addition, we have tested the 4^{th} order Runge-Kutta method in solving the coupled equations and compared to Heun's method. The results regarding moisture contents for the two soil layers and fluxes (data not shown) matched precisely those obtained using Heun's method. However, the CPU time in Runge-Kutta method was a little longer than the Heun's method. The Runge-Kutta method requires two additional sets of variables compared to Heun's method to allocate the parameters that are used for calculating 3^{rd} and 4^{th} slope. Besides, during the simulation, if the soil moisture change between time steps is small, the numerical solution can converge faster. Four slopes still need to be calculated in one iteration in Runge-Kutta method, while Heun's method only calculates two slopes. Thus, the use of Heun's method with the corrector-predictor algorithm using certain predefined termination criteria in the numerical scheme can ensure the accuracy of the calculation during the iterations and minimize the number of iterations during each time step.

The newly developed two-layer model can be an efficient soil moisture and water fluxes estimation algorithm for coupling surface water and groundwater systems at field and watershed scales or even at larger scales. We showed that the model produces relatively accurate estimations of averaged soil moisture and water fluxes, and is robust enough to account for the effect of fluctuating, shallow water table. In a follow-up paper, we comprehensively evaluate the two-layer model including application to real site soil moisture data and model predictive uncertainty estimation. Distributed watershed models and land surface models need to perform simulations at

hydrologic response unit level or grid level, often for long periods (Fatichi et al., 2016a). Therefore, computational cost is something that needs to be accounted for. Input parameters for this new model are relatively less, which makes it easy to set up and function, and thus ideal for large-scale hydrologic modeling. This model is also suitable in applications where groundwater is relatively shallow and where average soil moisture suffices for estimating biogeochemistry in complex ecosystems (e.g., wetlands), and when determining fluxes between surface water and groundwater systems is of interest. Wetland nutrient and carbon cycling models requiring averaged soil moisture content to simulate biochemical processes in variably saturated/unsaturated soils can greatly benefit from this model (Sharifi A. et al., 2017). In recent years, remote sensing techniques have provided large-scale soil moisture data and continuous surface soil moisture monitoring (Wagner et al., 2013; Babaeian et al., 2018). However, remote sensing observation provides near-surface soil moisture data only (about 0 - 5 cm). The determination of deeper soil moisture content can be equally important and control water fluxes between the surface water and the groundwater systems (Sadeghi et al., 2019).

5. Summary and Conclusion

We have developed a new, stable and robust vertically-averaged form of one-dimensional RE to model vertical unsaturated water movement in a two-layered soil. The two-layer model simulates averaged soil moisture content by connecting hydroclimate conditions to the vadose zone with shallow and deep WTs. The PDE of RE is replaced with two-coupled ODEs and solutions are obtained numerically using the simple Huen's method. A novel feature is the term in the second ODE accounting for a dynamic WT. The numerical method is mass-conservative. The objective of the model is to couple land surface and aquatic ecosystems to the vadose soil and

groundwater to simulate surface water and groundwater interactions at larger than local scales, such as in wetlands and watersheds. At such scales where the areal extent is much greater than the vertical, average fluxes can be well represented by soil moisture averaged over the roots layer and the vadose zone, especially for shallow surficial aquifers. Besides numerical errors caused by truncation of higher-order terms, the model does not simulate horizontal flow nor account for the effect of sloping soil surfaces.

The performance of the two-layer model was investigated in terms of computational accuracy and efficiency by comparison with HYDRUS as a reference model for three simulation scenarios, free drainage at the bottom of the soil profile, WT at the bottom of the soil domain, and falling water table. Three soil textures and different combinations of plant transpiration and rainfall rates were considered. The results showed that the two-layer model was robust and accurate in simulating variably saturated flows. The new model can capture the dynamics of depth-averaged soil moisture under different surface flux BCs in the presence of deep and shallow water table. Overall, simulated cumulative fluxes agreed very well with those from HYDRUS for all scenarios. Although some relatively small discrepancies of moisture estimates between the two models were observed, the *RMSE* values, overall, indicate excellent model performance. Moreover, the two-layer model captured actual evaporation dynamics well in the root zone, mimicking the behavior of the root zone or the biologically active sediment layer in wetlands. Further, numerical simulations conducted for desaturation of an initially saturated soil profile by a falling WT showed that the two-layer model could successfully capture the dynamics of average soil moisture above the water table within the root zone and the lower vadose soil as the WT retreats.

Although the two-layer model proved very promising and accurate under various conditions, there is certainly room for improvement. For instance, while the model has excellent

performance when soil layers are relatively shallow, the accuracy drops when soils become deep. Further, natural soils could be very heterogeneous, and thus, soil properties could be highly variable. The current model can only deal with two uniform soil layers. If the soil within the domain consists of more than two soil textures, extra calculations are needed to obtain averaged soil properties for two layers. While recent advances using stochastic theory can furnish formulas for estimating effective properties for use in the two-layer model, this does not negate the errors inherited by truncating higher-order terms and other assumptions made to derive the coupled ODEs.

The CPU times required to run the two-layer model for numerical experiments in this paper were less than that for HYDRUS. The two-layer model has fewer input parameters and uses a simple numerical method, making use of less memory and CPU than finite-element-based RE solutions. For simulations and applications from field-scale to large watershed scale where resolution of water content with depth is not needed, the two-layer model can be a reliable numerical method for simulating soil moisture spatial and temporal variability. This is especially true for watershed simulations involving relatively shallow groundwater and computing biogeochemistry of complex ecosystems. Although simple numerical tests were conducted, the strength and weakness of the two-layer model are not fully comprehended. In a follow-up paper, the model will be investigated in more detail, considering differences in hydraulic properties between the two layers and various surface and bottom BCs. In addition, model predictive uncertainty will be examined by application to field site data where climate and soil moisture data are available at high temporal resolution, along with measured soil properties. This application will provide further evidence on model robustness to simulate moisture content in the field under complex hydroclimate conditions.

Table 2.1: Soil properties for van Genuchten model (Carsel and Parrish, 1988)

Soil type	α (cm^{-1})	n	θ_r ($cm^3\ cm^{-3}$)	θ_s ($cm^3\ cm^{-3}$)	K_s ($cm\ day^{-1}$)	λ
Sandy Loam	0.075	1.89	0.065	0.41	106.1	0.5
Loam	0.036	1.56	0.078	0.43	24.96	0.5
Clay loam	0.019	1.31	0.095	0.41	6.24	0.5

Table 2.2: Upper boundary conditions

Scenario #	Rainfall intensity i (cm/day)	Potential transpiration rate T_p (cm/day)
1	0	0.2
2	0.5	0

Table 2.3: *RMSE* of soil moisture content for numerical simulations

Numerical scenarios	Soil textures	i=0 cm/day, T_p =0.2 cm/day		i =0.5 cm/day, T_p =0 cm/day	
		First layer	Second layer	First layer	Second layer
Free-drainage	Sandy Loam	0.005	0.011	0.002	0.004
	Loam	0.010	0.007	0.002	0.002
	Clay Loam	0.010	0.004	0.000	0.000
Zero-pressure head	Sandy Loam	0.004	0.008	0.006	0.005
	Loam	0.001	0.001	0.001	0.002
	Clay Loam	0.005	0.004	0.002	0.007
		i=0 cm/day, T_p =0 cm/day			
		First layer	Second layer		
Groundwater decline	Sandy Loam	0.004	0.006		
	Loam	0.001	0.000		
	Clay Loam	0.000	0.000		

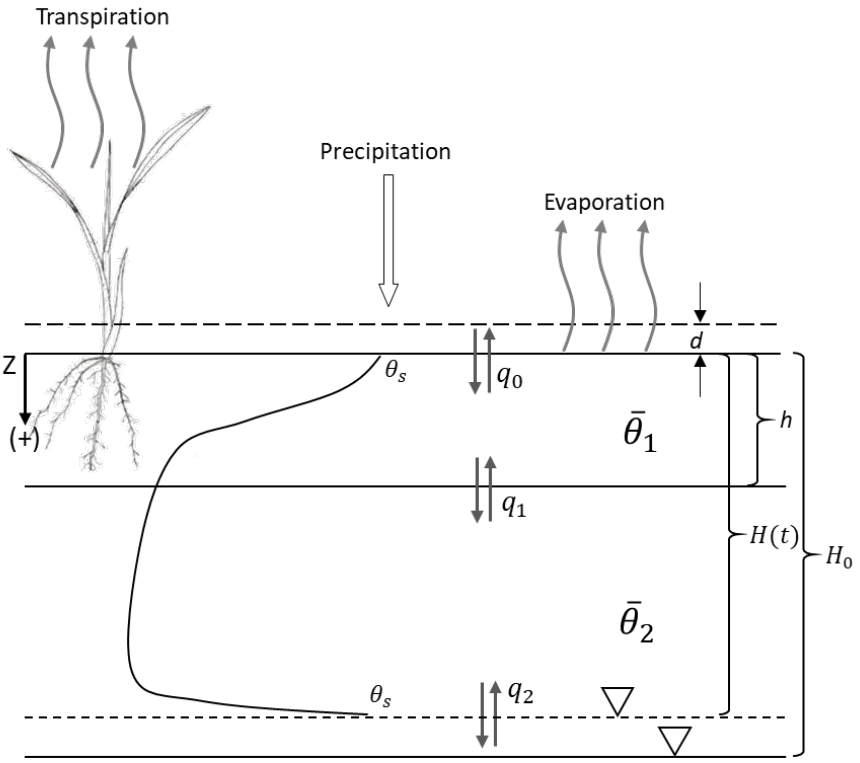

Figure 2.1: Schematic illustration of soil profile and the two-layer model depicting the root zone and vadose soil below. d is the ponding depth; h is the first layer (zoot zone) depth; $H(t)$ is depth of WT at time t; and H_0 is initial depth; q_0, q_1 and q_2 are the top, middle and bottom flux (positive downward) , respectively.

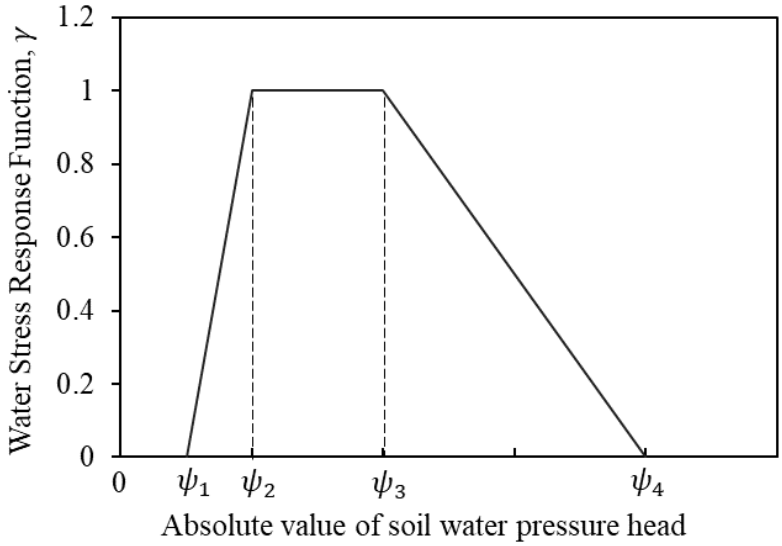

Figure 2.2: Schematic of the plant water stress response function (Eq. 41)

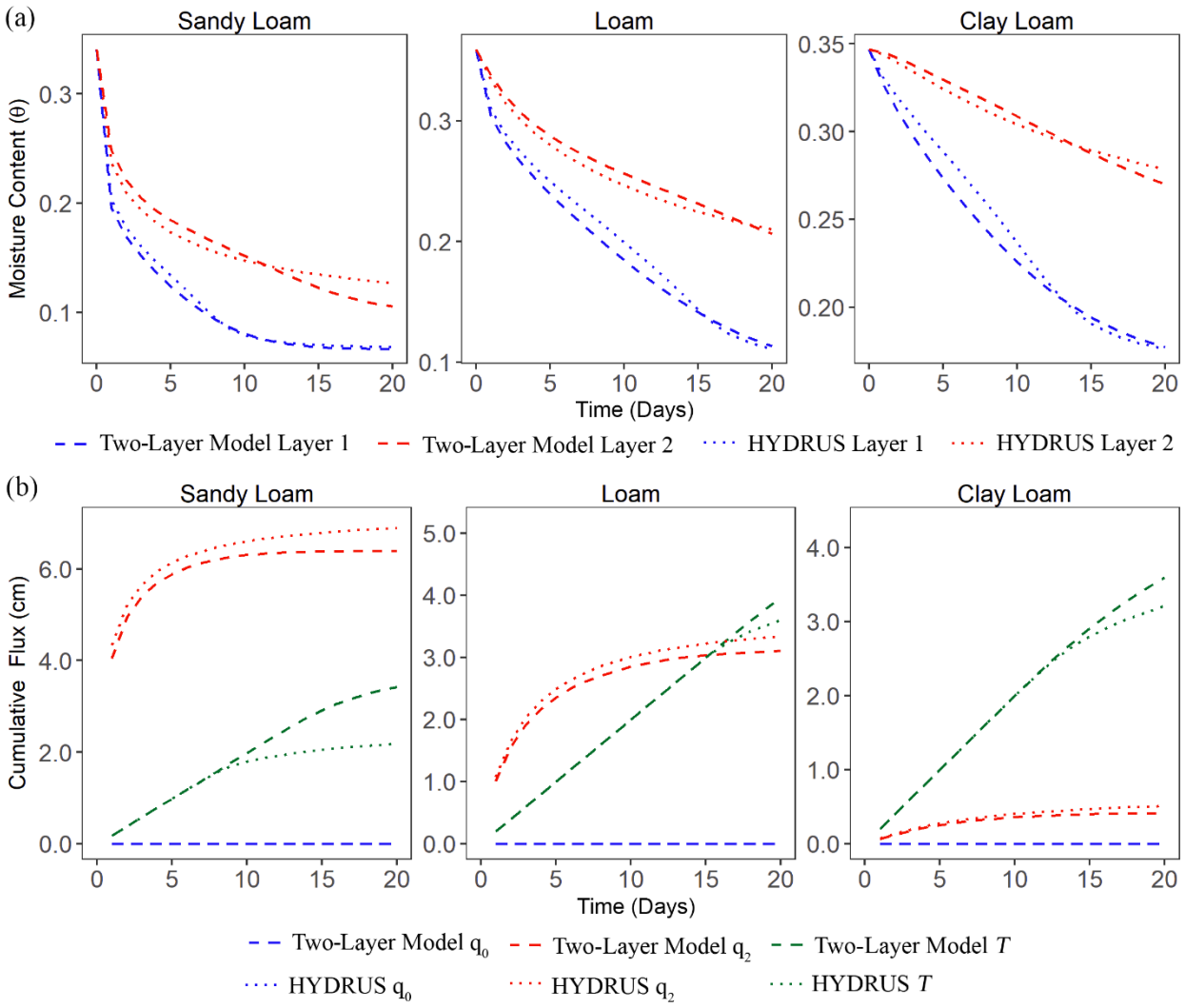

Figure 2.3: Moisture contents and cumulative fluxes with free-drainage BC, i = 0 cm/day, T_p = 0.2 cm/day. (a) represents results for soil moisture comparison between two-layer model and HYDRUS; (b) represents results for cumulative top, bottom fluxes and transpiration comparison between two-layer model and HYDRUS; where q_0 and q_2 donate top and bottom flux terms, respectively; T donates actual transpiration)

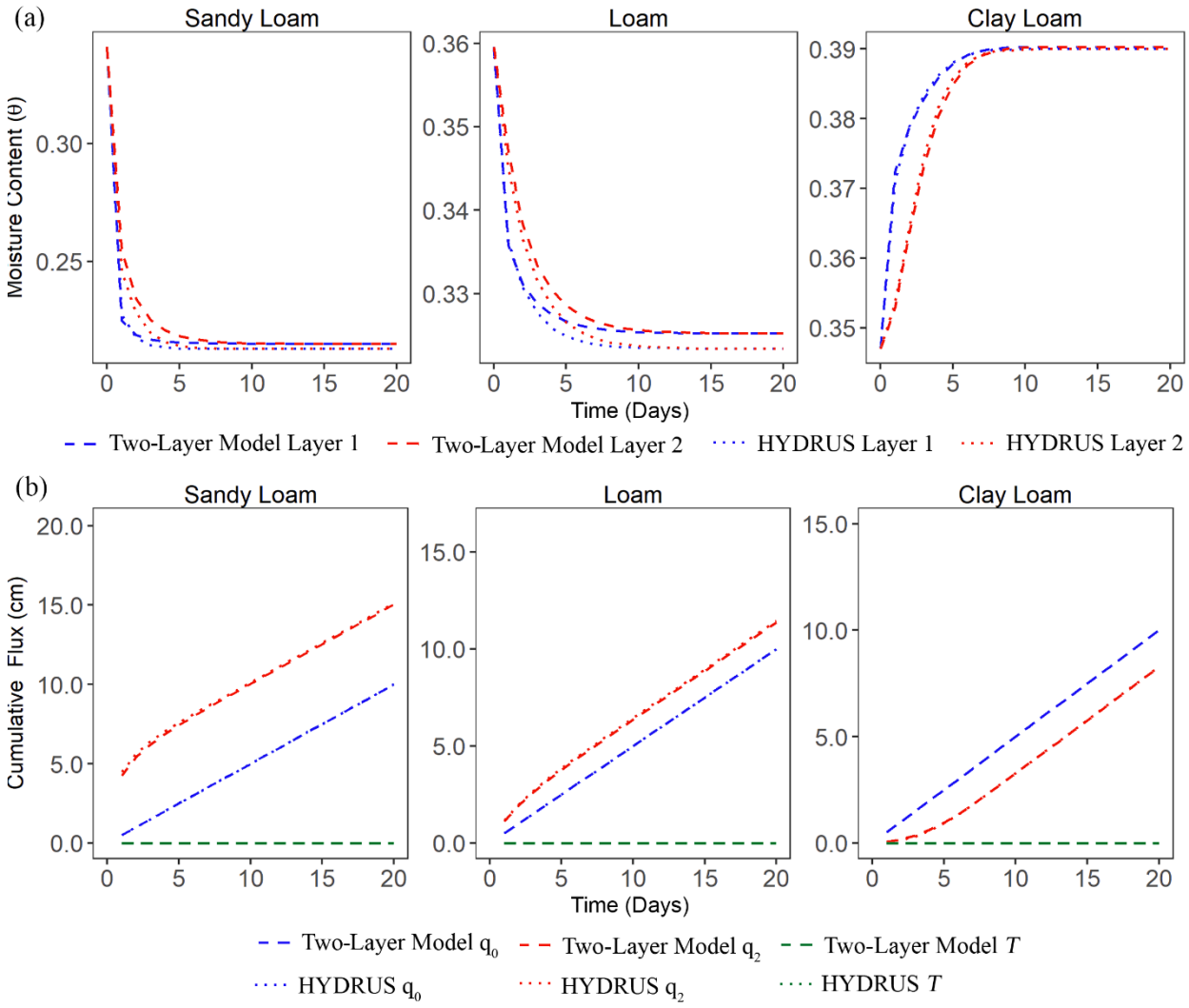

Figure 2.4: Moisture contents and cumulative fluxes with free-drainage BC, i = 0.5 cm/day, T_p = 0 cm/day (note that the top and bottom cumulative fluxes and cumulative transpiration from the two-layer model are overlapped with those from HYDRUS)

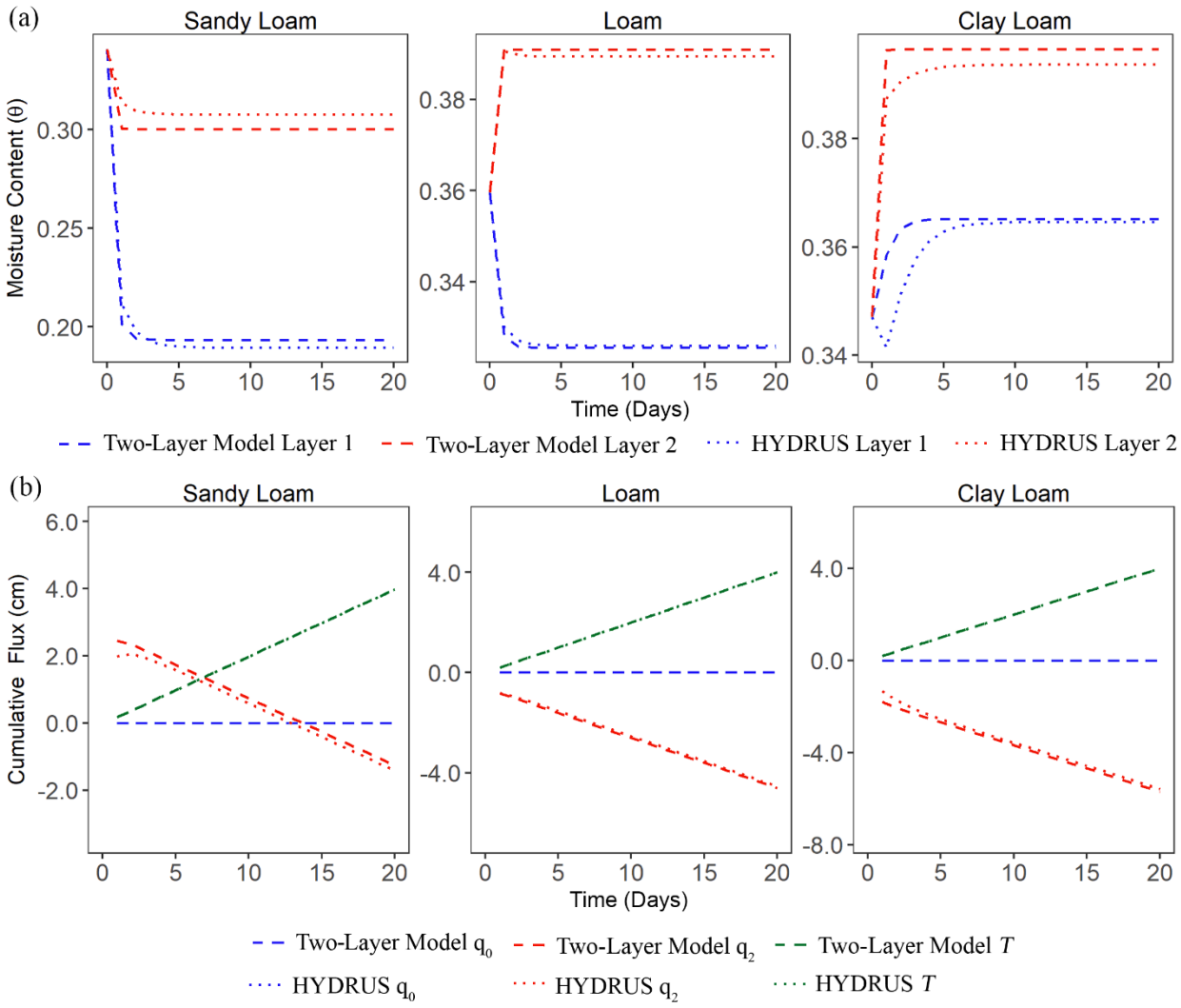

Figure 2.5: Moisture contents and cumulative fluxes with zero-pressure head BC, $i = 0$ cm/day, $T_p = 0.2$ cm/day

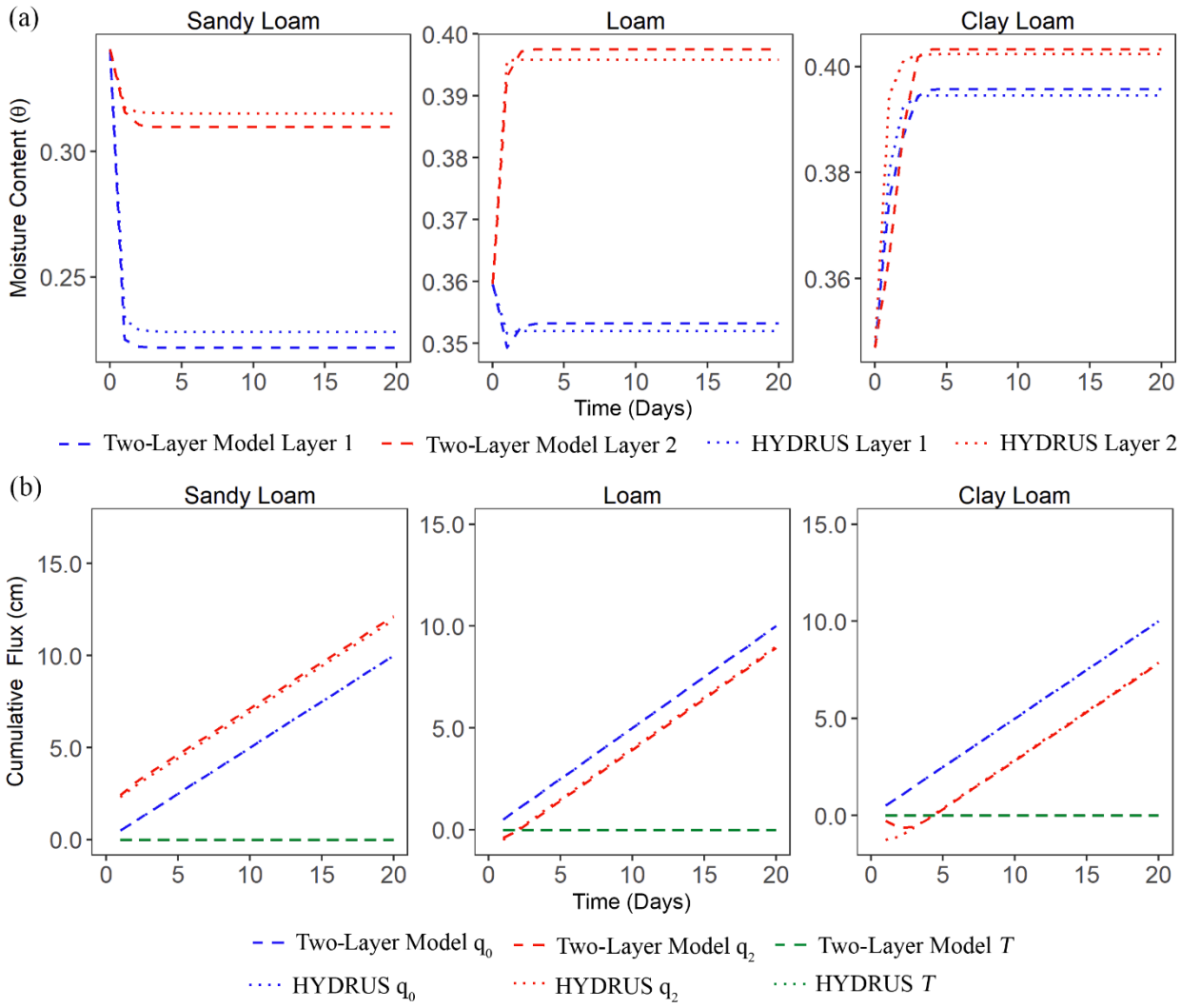

Figure 2.6: Moisture contents and fluxes with zero-pressure head BC, i = 0.5 cm/day, T_p = 0 cm/day

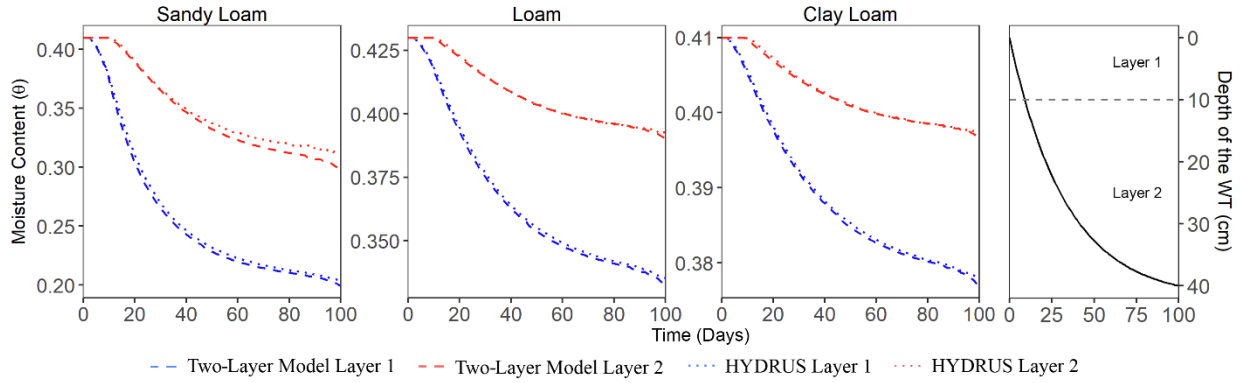

Figure 2.7: Moisture contents with declining water table, i = 0 cm/day, T_p = 0 cm/day

Chapter 3: Two-Layer Vertically Averaged Soil Moisture Dynamics: Model Assessment and Bayesian Uncertainty Estimation

Abstract

Modeling water movement in variably saturated soils with relatively shallow water table is important in land system models. A two-layer approximation of Richards' equation (RE) was recently developed by the authors for this purpose and its utility was shown for few simple cases. This study presents a comprehensive assessment of the two-layer RE model. First, the two-layer model was evaluated for 231 soil textures under varying soil layer thicknesses, with a prescribed upper boundary and two bottom boundary conditions. The vertical soil profile was assumed to be uniform. Second, the two-layer model was tested for conditions where the top and bottom soil layers have contrasting hydraulic characteristics. For this, we tested two extreme conditions with a highly permeable soil overlying a low permeability soil, and vice versa. For the first two cases, the performance of the two-layer model was evaluated by comparing the results of volumetric soil moisture contents and fluxes from the two-layer model and HYDRUS. Last, a case study of model application at a Soil Climate Analysis Network (SCAN) site was presented. The application was combined with the Bayesian Monte Carlo (BMC) method for model calibration and uncertainty analysis. Computed vertically averaged soil moisture of two delineated soil layers were compared with observed data. Results showed that when dealing with a homogeneous soil profile, the two-layer model had excellent performance. 99.8% and 87.5% of the simulations among 92,400 simulations were found to have root mean square error (*RMSE*) of moisture contents smaller than 0.015 for free-drainage and zero-pressure head bottom boundary condition, respectively. With heterogeneous soil profiles, the soil moisture contents and fluxes from the two-layer model agreed well with those from HYDRUS (Šimůnek et al., 2008). The

two-layer model combined with the BMC method showed good agreement with the observed average soil moisture of the root zone and vadose zone below. Soil moisture observation data, hydroclimate data, and model structural uncertainties contributed to the overall model uncertainty the most. The model input parameters had very small contribution to the overall model uncertainty. The posterior parameter space and their likelihood values obtained by BMC in calibration process were used for model validation. The overall *RMSE* was smaller than 0.023 and *NSE* was greater than 0.72 for both soil layers during model validation.

1. Introduction

Richards equation (RE, 1931) has widely been used to describe water movement in saturated/unsaturated flows in porous media because of its physical basis. However, due to the high nonlinearities of the partial differential expression of RE and two empirical water retention relations (unsaturated hydraulic conductivity and soil water pressure head) integrated with it, achieving a numerically stable, robust, and accurate solution of RE still remain challenging (Vereecken et al., 2016; Farthing and Ogden, 2017a). In laboratory and small-scale applications, RE has shown to provide remarkably good estimates of water flow and moisture distribution in soils (Ma et al., 2010; Selle et al., 2011; Romano, 2014; Lai and Ogden, 2015a). Nevertheless, when applying RE in large spatial and temporal scale modeling, solving RE can be computationally expensive due to its high nonlinearity. Besides, in such scale, estimation of high vertical resolution of soil moisture content is often not necessary. Simpler numerical methods have been developed as an alternative and adopted for soil water movement in watershed and large scale hydrological models, such as simplified RE scheme (e.g. Best et al., (2011)) and reservoir cascade scheme (e.g. Romano et al., (2011); Arnold et al., (2012)). Although these approaches have

provided satisfactory predictions of soil water movement and soil moisture contents for certain depth of soil, they often did not consider all soil hydrological processes due to model simplicity. Thus, there is a need for developing an efficient and stable numerical solution of RE, which considers layer-averaged moisture content and accounts for various infiltration processes and the interactions between soil and dynamic groundwater level. Recently, we have developed a two-layer approximation of RE to explicitly simulate one-dimensional vertical unsaturated flow in the root zone and the vadose soil below the root zone under dynamic atmospheric conditions (He et al., 2021a). The model computes vertically averaged soil moisture content in the roots layer and lower vadose soil as well as maintains continuity of fluxes at the soil surface and a relatively shallow groundwater. The model is described by the following coupled ordinary differential equations (refer to Figure 3.1 on flow domain schematic illustration):

$$h\frac{d\bar{\theta}_1}{dt} = q_0 - q_1 - h\bar{S} \tag{50}$$

$$(H-h)\frac{d\bar{\theta}_2}{dt} - \theta_{2s}\frac{dH}{dt} = q_1 - q_2 \tag{51}$$

in which

$$\bar{\theta}_1(t) = \frac{1}{h}\int_0^h \theta(z,t)\,dz\,, \bar{\theta}_2(t) = \frac{1}{H(t)-h}\int_h^{H(t)} \theta(z,t)\,dz \tag{2a}$$

$$q_2 = \frac{2}{H}(\beta\bar{K}_1 + (1-\beta)\bar{K}_2)(\bar{\psi}_2 - \bar{\psi}_1) + \beta\bar{K}_1 + (1-\beta)\bar{K}_2 \tag{2b}$$

where, $\bar{\theta}_1$ and $\bar{\theta}_2$ are the first (root zone) and the second layer (lower vadose soil) average moisture contents, respectively [-]; θ_{2s} is the saturated water content of the second layer [-]; h is the thickness of the first layer [L]; H is depth to water table[L]; q_0 is the moisture flux at the soil-atmosphere interface [LT^{-1}] (positive downward); q_1 is the moisture flux at the interface of the two layers [LT^{-1}] (Figure 3.1); q_2 is the moisture flux at the bottom of the second layer and accounts

for flux interactions between vadose zone and water table [LT^{-1}]; $\bar{S}$ is the transpiration rate [T^{-1}]; $\bar{K}_1$ and $\bar{K}_2$ are average unsaturated conductivities of the first and the second layer, respectively [LT^{-1}]; $\bar{\psi}_1$ and $\bar{\psi}_2$ are average soil capillary pressure heads for the first and the second layer, respectively [L]; and $\beta = (H - h)/H$. The coupled ordinary differential equations (Eqs. 1 and 2) of the two-layer model are solved by Heun's method with the iterative corrector to reduce truncation error and improve stability. Actual plant transpiration rate ($\bar{S}$) is calculated based on the moisture content of the root zone by the method proposed by Feddes (1982). The actual bare soil evaporation is evaluated according to average moisture content and moisture contents at field capacity and wilting point of the root zone layer. Details of the model description are given in He et al. (2021a).

The model was evaluated for relatively simple atmospheric and bottom soil profile boundary conditions by comparing its results to the one-dimensional finite element model HYDRUS 1-D (Šimůnek et al. 2008) as a benchmark. The assessment was performed for a homogenous soil profile with three soil textures under different prescribed pressure and flux atmospheric and bottom boundary conditions as well as for a scenario involving feedback with shallow and dynamic water table (He et al. 2021a). The two-layer model has shown good performance in terms of model accuracy and efficiency in estimating average moisture contents of the two soil layers and top and bottom fluxes as well as transpiration estimation when compared with HYDRUS under prescribed boundary conditions. However, the two-layer model was not fully tested to understand its true strengths and limitations for different soil textures and layered soil (layers with contrasting soil texture) as well as its performance under varying hydroclimate conditions. The model was also not tested with field data and its potential in predicting site-level soil moisture movement, hence, needs to be explored.

Application of RE in practice requires estimation of soil hydraulic parameters which are critical inputs to obtain accurate solutions (Baroni et al., 2010). Field-scale applications rely on field or laboratory measurements of soil hydraulic parameters. However, studies have shown that these parameters are often measured at a scale different than the scale they are applied to, which raises questions about their suitability for representing soil water movement at large scale (Jacques et al., 2002; Guber et al., 2006; Wöhling et al., 2008). Besides, direct measurement is always time-consuming and labor-intensive. Indirect methods for estimating soil parameters at the field scale can be achieved through inverse modeling, whereby differences between model simulated values and corresponding observational data are minimized using an objective function. In practice, soil information is often insufficient in modeling approaches, especially for large scales. Soil pedotransfer functions (PTFs) have been developed and applied to predict soil hydraulic parameters in many regions to large scale soil water movement studies (Sanchez et al., 2009; Jana and Mohanty, 2011; Piedallu et al., 2011; Xu et al., 2015; Bayabil et al., 2019). PTFs can provide relatively accurate predictions with limited soil information or easily measurable soil properties (such as soil separates and bulk density). However, calibration efforts still have to be carried out because uncertainties in predicted soil hydraulic parameters may have impact on soil hydrological modeling (Minasny and Mc Bratney, 2002; Loosvelt et al., 2011). Model parameters and predictive uncertainty will be estimated using Bayesian Monte Carlo, with Maximum Likelihood Estimation as the strategy for estimating statistical parameters; henceforth, referred to BMC (Hantush and Chaudhary, 2014a). The BMC technique is a noniterative formal Bayesian estimation approach that can produce results similar to the Markov Chain Monte Carlo (MCMC) and has shown good versatility in water quality applications for model calibration and uncertainty analysis (Hantush

and Chaudhary, 2014a; Chaudhary and Hantush, 2017a). Its noniterative nature and simplicity make it a suitable candidate for quantifying uncertainty associated with the highly nonlinear RE.

The main objective of this paper is to perform an in-depth evaluation of the two-layer model through the following steps:

(1) The two-layer model was evaluated on homogeneous soil profile under prescribed atmospheric condition for 231 soil textures classified by the fractions of sand, silt, and clay separate. We explored free-drainage and variable flux as the soil profile bottom boundary conditions. The latter corresponds to a relatively shallow water table. The soil thickness of the first and the second layer was varied between 10 cm to 200 cm, respectively. Estimated soil moisture contents averaged over each layer were compared with those from HYDRUS as a reference.

(2) The two-layer model was tested for two soil layers having contrasting hydraulic characteristics. In this case, we considered a highly permeable soil overlaying a soil with very low permeability and vice versa. Soil moisture estimates of two soil layers, and top and bottom fluxes along with transpiration estimations were again compared with those from HYDRUS.

(3) The two-layer model was applied at a Soil Climate Analysis Network (SCAN) site in the United States with real climate data. The BMC method was used to calibrate the two-layer model and evaluate model predictive uncertainty. The results of Bayesian soil moisture estimation along with 95% confidence band were provided by the BMC method. The model performance was evaluated by comparison with the site observations.

The structure of the paper is as follows. First, the methodology used in the evaluation of homogeneous and heterogeneous soil scenarios is presented. This is followed by the description of the SCAN site used in field-level application of the two-layer model. Next, the BMC method used in parameter and uncertainty estimation was described. The Results section provides

qualitative and quantitative comparison of the two-layer model results to HYDRUS as well as to field-measured soil moisture estimates. The strengths and weaknesses of the two-layer model are scrutinized under Discussion. The manuscript ends with Summary and Conclusions.

2. Methods

2.1. Soil Water Retention Curve

The soil hydraulic characteristic relationships $\theta(\psi)$, and $K(\theta)$ in this study were described by the Van Genuchten (1980) model.

$$K(\theta) = \begin{cases} K_{sat} S_e^{\frac{1}{2}} \left[1 - \left(1 - S_e^{\frac{1}{m}}\right)^m\right]^2 & \psi < 0 \\ K_{sat} & \psi \geq 0 \end{cases} \quad (52)$$

$$\psi(Se) = \frac{1}{\alpha}\left(Se^{-\frac{1}{m}} - 1\right)^{1-m} \quad (53)$$

$$Se = \frac{\theta - \theta_{res}}{\theta_{sat} - \theta_{res}} \quad (54)$$

where S_e is relative saturation [-]; K_{sat} is saturated hydraulic conductivity [LT^{-1}]; θ_{res} and θ_{sat} are residual and saturated water content, respectively [-]; n is pore-size distribution index [-]; m is a fitting parameter defined as $m = 1 - \frac{1}{n}$; and α is the fitting parameter [L^{-1}]. The parameters n, λ and α are considered to be empirical coefficients affecting the shape of the hydraulic functions.

2.2. Simulation Scenarios

2.2.1. Testing with homogeneous soil profile

In this test, the two-layer model was run with homogeneous soil profile with 231 soil textures and 400 soil layer thickness scenarios under one prescribed upper boundary condition and

two bottom boundary conditions. Similarly, the reference model HYDRUS was run with the same combinations of soil, layer thickness, climate, and boundaries conditions.

Each homogeneous soil profile in the numerical simulations was made up by soil texture identified by varying the percentage of soil separate of sand, silt, and clay. During simulations, the soil separates in each soil texture varied from 0% to 100%, by 5% increments. Thus, total of 231 soil textures were generated which covered all possible textures on the soil texture triangle. We used the van Genuchten (1980) soil hydraulic model to describe soil water retention characteristics. The soil hydraulic parameters including water retention parameters and saturated hydraulic conductivity (K_s) were calculated by ROSETTA3. ROSETTA3 is a Python based open-sourced PTFs model based on artificial neural network (ANN) analysis developed by Zhang and Schaap (2017). This provided us the flexibility to generate the soil hydraulic parameters and saturated hydraulic conductivity for all 231 soil textures using sand, silt, and clay percentages as input.

The thickness of the first (root zone) and the second layer (lower vadose soil) was varied from 10 to 200 cm, at 10 cm increments. Thus, the total soil depth varied from a minimum of 20 cm to a maximum of 400 cm. This resulted in 400 soil-layer-thickness combinations for each soil texture. The upper boundary condition involved an atmospheric scenario with a cycle of prescribed rainfall intensities and potential transpiration rates (Figure 3.2). The first 5 days had no rain, but there was a 0.2 cm/day potential transpiration. Days 5-10 had 2 cm/day of constant rain, but no transpiration demand. This cycle was repeated until day 50. We only considered plant transpiration, i.e. no soil evaporation to allow for consistent comparison of the two-layer model with HYDRUS. The methods applied for calculating soil evaporation in the two-layer model and HYDRUS are different. Both the two-layer model and HYDRUS adopts the root-water uptake water stress response function proposed by Feddes et al. (1978) to calculate the actual plant transpiration rate.

The parameters for the stress reduction function were set to the values in Wesseling (1991) for pasture (values of root-water uptake water stress response function parameters were: ψ_1=10 cm, ψ_2=25 cm, ψ_3=800 cm, ψ_4= 8000 cm).

Two bottom boundary conditions were applied: 1) free-drainage, which refers to zero pressure gradient boundary at the bottom. This boundary condition is suitable for situations where the water table is far below the domain of interest; 2) zero-pressure head boundary condition, which describes the situation where the water table is at the bottom of the soil column (water table depth is equal to the total depth of the soil column *H*). We set the initial moisture contents for all soil textures to the moisture content at -33 kPa (field capacity). Simulations were carried out by the two-layer model and HYDRUS for a 50-day period using a computational time step of 0.001 day. In HYDRUS, the soil domain was discretized using 101 equidistant nodes. The soil moisture estimations for the first and the second layers were obtained by averaging soil moisture contents of the nodes within each layer. We evaluated model performance using the root mean square error (*RMSE*).

Note that for fine-textured soils, which have the Genuchten water hydraulic parameter n less than 1.3 as defined by Vogel et al. (2000), van Genuchten model with -2 cm air entry value is typically recommended in HYDRUS applications to overcome the convergence issue (Vogel and Cislerova, 1988). This configuration significantly alters the hydraulic conductivity function. However, this modification in air entry pressure for fine-textured soils was not necessary for the two-layer model. In order to make the two models comparable, this option was not selected in HYDRUS. Instead, the maximum number of iterations during any time step was changed from the default value of 10 to 100. This change sacrificed efficiency for accuracy in HYDRUS using the standard van Genuchten model for fine-textured soils.

2.2.2. Testing with heterogeneous soil profile

The two-layer model was tested for a configuration where the two soil layers have contrasting permeability. We assessed the performance of the two-layer model with coarse-textured soil on top of fine-textured soil and vice versa. The coarse and fine-textured soils used in this study were loamy fine sand and silty clay loam obtained from Hills et al. (1989). The van Genuchten soil hydraulic parameter values of these two soil textures are shown in Table 3.1. The thicknesses of the two soil layers were set to 30 cm. The upper boundary condition was the same as the 5-day cycle climate pattern described earlier (Figure 3.2) for a duration of 15 days. We assigned 0.2 cm/day of potential transpiration for the first 5 days, then 2 cm/day of rain for the next 5 days, followed by 0.2 cm/day of potential transpiration. The free-drainage and zero-pressure head bottom boundary conditions were applied. The initial moisture contents of both soil textures were set to the moisture content at -33 kPa: 0.2694 for loamy fine sand and 0.4483 for silty clay loam. Results of soil moisture contents, top, and bottom flux terms, as well as estimated transpiration rates, were compared with those from HYDRUS.

2.2.3. Site level application

The two-layer model was applied to a SCAN site to assess its soil moisture prediction capability. Site Tuskegee (SCAN site ID: 2115) from Alabama, USA, was chosen as the study site, which is located at $32°26′$ N and $85°45′$ W and at an elevation of 122 meters above mean sea level (Figure 3.3). SCAN dataset provides site-level soil moisture and meteorological data at hourly and daily time step (Schaefer et al., 2007). Soil moisture was measured at five different soil depths, which are 5 cm (2 inches), 10 cm (4 inches), 20 cm (8 inches), 50 cm (20 inches), and 100

cm (40 inches). To avoid the periods that had days with air temperature below zero, data were collected at daily time interval from February 24th to October 31st in year 2018 and 2019, respectively. Data from 2018 were used for model calibration and data from 2019 were used for model validation. Based on our preliminary test, the moisture redistribution always occurred within 2 days. To eliminate the effect of the initial moisture content, the first five days from February 24th to 28th were model warm-up period. Results of the model simulated moisture contents were compared with field measurements for the period between March 1st to October 31st. To make the model outputs comparable with the observed soil moisture data, the measured soil moisture contents at different depths were grouped into two soil layers by following the logic in the two-layer model that the first layer represents the root zone where the plant water uptake occurs and the second layer acts as in the lower vadose soil. At the SCAN site, the weather station and soil moisture sampling point were installed at the same location where the area was covered by short grass or natural fallow for most of the time (Albergel et al., 2015). We consulted with the local USDA service center in Tuskegee for vegetation cover and rooting depth. The dominant species for this SCAN site is Bahiagrass (*Paspalum notatum*). The depth where the majority of root biomass located is about 18 cm. Thus, we assumed the top 20 cm thickness of soil to be the root zone layer, and the 30 cm below was the second layer. Besides, based on Web Soil Survey (Soil Survey Staff), the groundwater level at the site was below 200 cm. However, there was a small creek located about 500 meters southeast of the site. The groundwater level in the area around the creek was about 110 cm, which could potentially influence soil moisture measurement in the deeper soil (100 cm). Owing to the lack of detailed data for groundwater level, the fifth sensor was excluded for model comparison. Thus, we considered the total soil depth of interest to be 50 cm that includes the top four moisture sensors. The first two moisture sensors belonged to

the first layer and the fourth sensor belonged to the second layer. The third sensor was located at the boundary between two layers.

Soil properties for four soil horizons within 50 cm soil profile were provided by National Cooperative Soil Survey (Survey, 2017) including percentage of sand, silt, clay and organic carbon, bulk density, moisture content at field capacity, and moisture content at wilting point. Because the first and the second layer of the model domain contained several horizons, the soil physical properties of each layer were calculated by weighted average according to the depth of the horizons within the layer. Percentage of sand, silt, clay, and organic carbon, as well as moisture contents at field capacity and wilting point, were used as inputs to the ROSETTA3 model to estimate Van Genuchten soil hydraulic parameters. The prediction uncertainties of each Van Genuchten parameter were provided by ROSETTA3 in terms of their standard deviations. Meteorological data were collected at daily time step during the simulation period including precipitation, maximum and minimum air temperature, relative humidity, solar radiation, wind speed, etc. FAO-56 Penman-Monteith method (Allen et al., 1998) was applied to calculate daily potential evapotranspiration (PET) rate.

For model calibration, the two-layer model was run from February 24th, 2018 to Oct 31st, 2018. The upper boundary condition was atmospherically controlled which was described by observed precipitation and PET. Calculated PET and observed precipitation data for the model calibration period are shown in Figure 3.4. Potential evaporation for bare soil and potential transpiration rate for grass were calculated by partitioning of PET by an area index (f_s). The area index represents the fraction of bare soil (range from 0 to 1) and $1 - f_s$ stands for fraction of vegetation cover. In the study site, the area of vegetation cover was unknown. This area index can be calibrated in the model calibration process. The bottom boundary condition was set to free-

drainage. We ran the two-layer model with Δt=0.001 day (86 s) during calibration and validation periods. The initial moisture contents for the two layers were set to the values equal to the observed moisture contents at the first day.

2.2.3.1. Bayesian model calibration and uncertainty Estimation

The uncertainties introduced by input data and data used for calibration, model parameters and imperfection in model structure make the model output subject to errors. The uncertainties of the two-layer model in model applications stem mainly from the following specific sources: 1) uncertainties may be introduced due to measurement errors, limited soil moisture data and interpolation of observed data to obtain vertically averaged soil moisture contents for the two soil layers in the model domain; 2) estimation of Van Genuchten parameter from basic soil texture data using ROSETTA3; 3) averaging soil properties from different horizons to obtain averaged soil properties of two soil layers as inputs for ROSETTA3; and 4) model structural errors introduced by neglecting higher-order terms in the derivation of Equations (1) and (2) as well as not accounting for soil heterogeneity and other potentially important processes, such as lateral flow and preferential pathways. Quantifying the uncertainties of the two-layer model can provide a better idea of how the two-layer model performs at site level.

During the model calibration and uncertainty estimation, we employed the Bayesian Monte Carlo and Maximum Likelihood (referred to as BMC) estimation methodology for model calibration and uncertainty estimation. The detailed methodology and procedure of BMC can be found in Hantush and Chaudhary (2014) and Chaudhary and Hantush (2017). In this study, we considered five soil hydraulic and van Genuchten parameters and an area index $\boldsymbol{\Theta} = (\alpha, n, \theta_{res}, \theta_{sat}, K_s, f_s)$ to be random variables. Uniform distributions of the values or log values are

commonly assumed as priors for the unknown parameters (e.g., Vrugt and Bouten, 2002; Wöhling and Vrugt, 2008; Huisman et al., 2010; Mboh et al., 2012; Köpke et al., 2019). The effect of priors diminishes with the size of the observed data and the choice of the prior distribution, therefore, becomes increasingly less important. Following Scharnagl et al., (2011), here, the prior distribution of van Genuchten soil hydraulic parameters is defined as $p(x) \sim U(a_x, b_x)$, where a_x and b_x are lower and upper bounds, respectively. a_x and b_x are calculated as $\gamma \pm 4\sigma$, where γ is ROSETTA3 predicted values, and σ is the standard deviations of the predicted parameters. The predicted values and corresponding standard deviations of α, n, and K_s from ROSETTA3 were given in log form. The log values of these three parameters were assumed uniformly distributed based on their logarithmic standard deviations as prior distributions. The values of these three parameters were sampled from the uniform distributions of the $\log_{10}$ values and then inverted to their original values. The area index (f_s) is assumed uniformly distributed *a priori*, $p(f_s) \sim U(0,1)$. The upper and lower bounds of prior distributions of model input parameters are shown in Table 3.2. The relationship between site soil moisture observation at time t ($O(t)$) and the corresponding simulated output ($\theta(\mathbf{\Theta}, t)$) from the two-layer model can be expressed as: $O(t) = \theta(\mathbf{\Theta}, t) + \varepsilon$, where $\varepsilon = (\varepsilon_1, \varepsilon_2, \dots, \varepsilon_m)$, $\varepsilon_i \sim N(0, \sigma_\varepsilon^2)$ is assumed to be zero-mean, independent and normally-distributed model residual error; and m is number of observations. The error ε accounts for all sources of modeling errors described above (observational, parametric, structural, hydrometeorological inputs). We generated 1,000,000 parameter sets by randomly drawing parameter values from their prior distributions. What follows, is a summary description of the BMC methodology. Based on Bayes' theorem, the posterior joint probability density function is given by,

$$P(\mathbf{\Theta_i}|\boldsymbol{O}) = kl(\mathbf{\Theta_i})P(\mathbf{\Theta_i}) \tag{55}$$

where $\boldsymbol{O} = (O_1, O_2, \dots, O_m)$ is set of m observed moisture content values; $P(\boldsymbol{\Theta_i}|\boldsymbol{O})$ is the posterior probability mass of parameter set $\boldsymbol{\Theta} = \left[\alpha^i\ n^i\ {\theta_{res}}^i\ {\theta_{sat}}^i\ {K_s}^i\ {f_s}^i\right]$; $i = 1, 2, \dots, n$, where n is number of randomly sampled parameter sets (n = 1,000,000); $l(\boldsymbol{\Theta_i}) = P(\boldsymbol{O}|\boldsymbol{\Theta_i})$ is the likelihood of observations given $\boldsymbol{\Theta_i}$; $P(\boldsymbol{\Theta_i})$ is the prior probability mass of parameter set $\boldsymbol{\Theta_i}$; k is a normalizing factor such that $\sum_{i=1}^{n} P(\boldsymbol{\Theta_i}|\boldsymbol{O}) = 1$; that is $k = n/\sum_{i=1}^{n} l(\boldsymbol{\theta}_i)$, where we have assumed equally likely parameter sets *a prior*, $P(\boldsymbol{\Theta_i}) = \frac{1}{n}$.

The likelihood of each generated parameter set $\boldsymbol{\Theta_i}$ can be obtained by maximizing the joint log-likelihood function of ε_i, i 1,2,…m (Chaudhary and Hantush, 2017):

$$l(\boldsymbol{\Theta_i}) = \left(2\pi e\hat{\sigma}_{\varepsilon,i}^2\right)^{-\frac{m}{2}} \tag{56}$$

in which

$$\hat{\sigma}_{\varepsilon,i}^2 = \frac{1}{m}\sum_{k=1}^{m}[\varepsilon_k(\boldsymbol{\Theta_i})]^2 \tag{7a}$$

The posterior probability mass of $\boldsymbol{\Theta_i}$ is given by

$$P(\boldsymbol{\Theta_i}|\boldsymbol{O}) = \frac{\hat{l}(x_i)}{\sum_{i=1}^{n}\hat{l}(x_i)} \tag{57}$$

The Bayesian estimate of moisture content (θ) of the first and the second layer at any point in time is the conditional mean of θ given the observation,

$$E(\theta|\boldsymbol{O}) \approx \sum_{i=1}^{n} E(\theta|\boldsymbol{\Theta_i})\,P(\boldsymbol{\Theta_i}|\boldsymbol{O}) = \frac{1}{\sum_{i=1}^{n}\hat{l}(x_i)}\sum_{i=1}^{n}\theta(\boldsymbol{\Theta_i}, t)\hat{l}(x_i) \tag{58}$$

in which we made use of $E(\theta|\boldsymbol{\Theta_i}) = \theta(\boldsymbol{\Theta_i}, t)$ and Eq. (6). Posterior probability distribution functions (PDFs) of the parameters $\boldsymbol{\Theta} = \left[\alpha^i\ n^i\ \theta_{res}^i\ \theta_{sat}^i\ K_s^i\ K_c^i\right]$ can be obtained from the sampled values of each model parameter and corresponding posterior probability masses computed by Eq.

(6). The confidence band for simulated posterior (i.e., conditional on the observed data) soil moisture content at time *t* can be generated from the following cumulative distribution function (CDF) (Hantush and Chaudhary, 2014):

$$F(y|\boldsymbol{O}) \approx \frac{1}{2} + \frac{1}{2}\sum_{i=1}^{n} erf\left(\frac{y-\theta(\boldsymbol{\Theta_i},t)}{\sqrt{2}\hat{\sigma}_{\omega,i}}\right) P(\boldsymbol{\Theta_i}|\boldsymbol{O}) = \frac{1}{2} + \frac{1}{2\sum_{i=1}^{n}\hat{l}(\boldsymbol{x_i})}\sum_{i=1}^{n} erf\left(\frac{y-\theta(\boldsymbol{\Theta_i},t)}{\sqrt{2}\hat{\sigma}_{\omega,i}}\right)\hat{l}(\boldsymbol{x_i}) \quad (59)$$

This equation can be inverted using any of the root-finding techniques to obtain percentiles and construct confidence band for moisture content at any point in time given the hydroclimate data.

Model performance was evaluated by using *RMSE* and Nash Sutcliffe efficiency (E_{NS}). Because the soil moisture observations were measured at discrete distances, in order to compare model outputs with measurements for two simulated soil layers, linear interpolation method was applied to field measurements. We first interpolated the soil moisture contents along 50 cm soil column according to the observations at four depths, and then calculated averaged moisture contents for the first and the second layer by averaging interpolated values from 1 cm to 20 cm and 20 cm to 50 cm, respectively. The model performance indices were calculated for each layer separately.

3. Results

3.1. Model performance with homogeneous soil profiles

The two-layer model was tested for 231 soil textures and 400-layer thickness combinations. The results of two-layer soil moisture content were compared with those from HYDRUS (Šimůnek et al., 2008). The performance of the two-layer model was evaluated using averaged *RMSE* of soil

moisture contents. Averaged *RMSE* was calculated by averaging *RMSE* values of moisture contents from two soil layers. There are 231 plots of *RMSE* patterns each with different thicknesses of two soil layers for two bottom boundary conditions, respectively. Due to space limitations, the results of three soil textures are shown in this manuscript. All the results can be found in supplementary materials. The three selected soil textures were coarse, medium, and fine-textured soils, which are sand, loam, and clay. Specific percentages of sand, silt, and clay were selected to represent these three soil textures following the USDA soil texture classification (Soil Survey Staff, 1999). Sandy soil was 90% sand, 5% silt, and 5% clay. Loamy soil was 40% sand, 40% silt, and 20% clay, while clay soil was 10% sand, 15% silt, and 75% clay.

The *RMSE* values between the two-layer model and HYDRUS for three soil textures with free-drainage and zero-pressure head bottom boundary conditions are shown in Figure 3.5. (Figure 3.6 shows one example of the simulated moisture contents of two soil layers from the two-layer model and HYDRUS for three soil textures and two bottom boundary conditions with 50 cm thickness of the first and 50 cm thickness of the second layer) The plots show the contour lines and heat maps of *RMSE* with different thickness of the first (root zone) and the second layer (lower vadose soil). As shown in Figure 3.5, *RMSE* has an increasing trend with the increase of the thickness of either the first or the second layer. With the free-drainage bottom boundary condition, the *RMSE* for three soil textures was always lower than 0.015. With shallow root zone (less than 30 cm), *RMSE* increased rapidly with increasing thickness of the second layer. The same trend was observed with thin second layer, but this was less pronounced in the figures. When considering water table at the bottom of the soil profile (zero-pressure head), the performance of the two-layer model varied for different soil textures. The performance on coarse-textured soils dropped with increased thickness of both layers. *RMSE* was highest for sand and clay soil texture under water-

table boundary condition. The highest *RMSE* among all the soil textures was 0.048 and it was obtained with a soil with 95% sand and 5% silt (results are shown in supplementary materials). In Figure 3.5, for sand, *RMSE* was lower than 0.01 only when the first layer thickness was less than 60 cm and the second layer thickness was below 90 cm. When soil texture became finer, model performance improved. *RMSE* for loam dropped below 0.010 for all thickness scenarios whereas for clay the maximum *RMSE* was 0.020. When all 231 soil textures are pooled, the minimum and maximum *RMSE* was 0 and 0.018, respectively, for free-drainage bottom boundary condition, and 0 and 0.048 for zero-pressure head bottom boundary condition, respectively.

Figure 3.5 summarized model performances as a function of layer thicknesses for a given soil texture assuming a homogenous soil profile. Another way of assessing model performance is plotting *RMSE* as a function of soil texture on the soil texture triangle, for various soil layer thicknesses. Figure 3.7 shows one such example, where the variation of *RMSE* with soil texture is shown for 50 cm root zone depth combined with second layer thicknesses of 10, 100, and 200 cm, under the two bottom boundary conditions. *RMSE* heat maps for all other thickness combinations are available in the supplementary materials. In Figure 3.7, the two-layer model had better performance with the free-drainage bottom boundary condition compared to the water table bottom boundary condition, and this was also the case with other thickness combinations (supplementary materials). The general pattern in each soil triangle is that *RMSE* increases with sand fraction. Model performance also generally increases with increased silt fraction, which is more evident for deeper soils. The maximum *RMSE* in free-drainage bottom boundary condition was 0.008 in Figure 3.7, and it corresponds to the case with the second layer thickness being 200 cm and very high sand fraction. With the zero-pressure head (water table) boundary condition, the maximum error was 0.038 which happened with the same thickness and soil texture. The general trends for

RMSE for all other thickness combinations are similar to the ones in Figure 3.7 (see supplement). Thus, *RMSE* values from free-drainage bottom boundary condition were lower than those from zero-pressure head bottom boundary condition. With the increase of soil thickness, *RMSE* values often increased from soil textures with high percentage of sand, then from soil textures with high percentage of clay.

3.2. Model performance with heterogeneous soils

The simulations with the two-layer model and HYDRUS for 30 cm of loamy fine sand (high permeability) overlaying 30 cm of silty clay loam (low permeability) and vice versa are shown in Figures 3.8 and 3.9, respectively. Simulated soil moisture contents of the low permeability layer were always higher than the high permeability layer by both models, as shown in Figures 3.8 and 3.9. The soil moisture contents of two soil layers and flux estimations from the two-layer model matched very well with those from HYDRUS. Moisture contents for two layers varied correspondingly with atmospheric condition, i.e. moisture contents in both layers declined in response to the transpiration demand, which was followed by an increase over the next 5 days due to rain. For the soil layer configuration with high permeability soil overlaying the low permeability soil, the two-layer model showed excellent performance with free-drainage bottom boundary condition, for the *RMSE* of both layers were lower than 0.01. The cumulative top flux and cumulative bottom flux from the two-layer model were identical to those from HYDRUS, while the cumulative transpiration was little higher than from HYDRUS. With zero-pressure head bottom boundary condition, moisture content in the first layer from the two-layer model was higher than that from HYDRUS in the first 5 days with only transpiration, while in the next 5 days with precipitation, moisture content of the first layer was lower than that from HYDRUS. *RMSE* for the

first layer was 0.02, while moisture contents of the second layer matched very well with that from the reference model with *RMSE* equals to 0.002. The cumulative top flux and transpiration rate were identical to those from HYDRUS. The cumulative bottom flux for the first 5 days was higher (absolute value) than that from HYDRUS but similar for the next 10 days. When the low permeability soil overlaid the high permeability soil (Figure 3.9), soil moisture and cumulative fluxes estimated by the two-layer model were almost identical to their counterparts generated by HYDRUS for both bottom boundary conditions. *RMSE* values for the average moisture contents of the first and the second layers in both bottom boundary conditions were always lower than 0.01.

3.3. Application of two-layer model to the SCAN site

Figures 3.10 (A1) and (A2) show the two-layer model calibration results for the period from March 1st, 2018 to October 31st, 2018: the Bayesian estimates (Eq. 9), 95% confidence interval and observed soil moisture contents of the root zone and the soil layer below, respectively. The 95% confidence limits are obtained by inverting Eq. (10) using the bisection method. The Bayesian estimated, vertically averaged soil moisture contents of both layers compare well with the corresponding aggregated observations given the uncertainty and errors in preprocessing of limited and discrete observed point data set and linear interpolation of what could actually be a nonlinear soil moisture distribution. The *RMSE* and E_{NS} values are 0.016 and 0.726 for the first layer, and 0.021 and 0.622 for the second layer, respectively. All the observed soil moisture values fell within the 95% confidence bands. The 95% confidence intervals and the Bayesian estimates (*a posteriori*) of model input parameters and $\hat{\sigma}_{\varepsilon}^{2}$ calculated by BMC are shown in Table 3.3. Figures 3.10 (B1) and (B2) shows the results of BMC predicted soil moisture contents along with 95% confidence bounds and observed soil moisture contents of both soil layers for the validation period

(March 1st - October 31st, 2019). The soil variability and magnitude of moisture contents are adequately captured by the BMC estimates as shown in Figure 3.10 (B1) and (B2). Although model performance dropped somewhat for the validation period, it can still be considered good with *RMSE* values equal to 0.023 and 0.023, and E_{NS} values equal to 0.733 and 0.719 for the first layer and the second layer, respectively. The two-layer model appears robust in simulating hydrometeorological conditions outside the range used for model calibration.

4. Discussion of Results

The numerical simulations on homogeneous soil profiles revealed the performance of the two-layer model on various soil textures and layer thickness conditions. Overall, the two-layer model has better performance with the free-drainage than the zero-pressure head bottom boundary condition. With the influence of the water table, groundwater affects the soil moisture of the layer above mainly through capillary actions. In the two-layer model solution, the suction force in the second layer is averaged over the layer corresponding to the thickness. The truncation errors committed by neglecting higher than first-order terms leading to Eqs. (1) and (2) increase the error in deeper soil and can be more pronounced near the water table where capillary pressure gradient can be highly nonlinear. With the exception of coarse-textured soil with the water table at the bottom (Figure 3.5) where the two-layer model suffers with increased thickness of both layers, model performance with all other soil textures deteriorates only with relatively thicker lower vadose soil. The model still performed very well for a relatively thick roots layer (2 m), except for sandy soil and water table at the bottom. The highly nonlinear relationship between matric pressure head and moisture content in coarse soils near saturation amplifies the truncation errors in the

computed matric pressure head gradient at the water table and, consequently, the average soil moisture computed by the model.

Soil textures and thickness of the soil layers influence the accuracy of soil moisture estimates with varying degrees. Figure 3.11 shows the empirical probability densities of soil separates and the thicknesses of two layers for $RMSE \leq 0.015$ and $RMSE \geq 0.015$, assuming 0.015 as the model performance acceptability threshold. In practice, the precision of the in-situ soil moisture measurement, described by *RMSE*, with the value of 0.02 or smaller is often considered to be good (Robinson et al., 2008). $RMSE=0.015$ is a little on the conservative side in this regard. With the free-drainage bottom boundary condition, only 199 simulations among 92,400 simulations had *RMSE* greater than 0.015, which is 0.2% of total simulations. This indicates that almost all (99.8%) simulations results were nearly perfect. From Figure 3.11 (A1), the probability of inadequate model performance is higher for coarse-textured soil than for fine-textured soil. Besides, the cases with very thin thickness of the first layer showed the highest probability for poor model performance. We found that these cases generally had 10 cm thickness of the first layer and were combined with either 190 cm or 200 cm thickness of the second layer. This can be seen from the probability densities of the second layer that model performance deteriorates with increasing thickness of the second layer (also shown in Figure 3.5). With zero-pressure head bottom boundary condition (Figure 3.11 B), 87.5% of simulations had *RMSE* smaller than 0.015. 11,543 among 92,400 simulations were considered to have low model performance. Same soil texture compositions as in the case of free drainage had low model performance, which were soils with high percentage of sand and low percentage of silt and clay (Figure 3.11 B1). Very thin (10 or 20 cm) and thick (>100 cm) roots layer and thick lower vadose soil (>180 cm) had the highest probability of less than adequate model performance. Again, low model performance with thin

first layer was associated with thick lower layer. When we consider the water table at bottom of the soil, the effect of upward capillary flux on the whole soil domain is weakened by a deep soil profile. The feedback from the water table deteriorates in the two-layer model when compared to the finite element solution of RE in HYDRUS due to higher truncation errors incurred in the derivation of Eq. (2) and q_2. Furthermore, for both boundary conditions, the probability densities when $RMSE \leq 0.015$ were very low with high percentage of any one of three soil separates (Figures 3.11 (A2) and (B2)).

The two-layer model mainly focuses on simulating moisture content of the root zone, with a lower vadose zone connecting root zone and groundwater. From Figures 3.5, 3.7, 3.11 and the plots from the supplemental materials, a full-scope of model simulation capabilities and model configurations can be investigated. For a specific soil texture, if the depth of the root zone is shallow but the water table is relatively deep, using free-drainage bottom boundary condition can lead to better model performance for the lower layer. If the water table is relatively shallow, it can have a significant impact on modulating moisture exchange with the root zone. However, modeling this situation using the two-layer model is constrained by soil texture and layer depth. From the plots, to have a model performance of RMSE lower than 0.015, root zone depth can vary up to 200 cm, but the thickness of the lower layer should not exceed 100 cm. Soil textures should contain less percentage of sand (<75%) and high percentage of silt and clay (>20%).

Solving RE for layered soils has been a challenging task because of the discontinuity of moisture and hydraulic properties moving from one soil texture to another. Two phenomena are often related to this discontinuity: the capillary barrier and the hydraulic barrier (Alfnes et al., 2004; Si et al., 2011). The capillary barrier often occurs when a fine-textured soil layer overlies a coarse-textured soil. Under this condition, the saturated hydraulic conductivity of the lower layer is higher

than the upper layer. Hydraulic conductivity approaching the interface is not sufficient to transmit water downward across the interface. Besides, compared to the lower layer, the capillary pressure in the upper layer is relatively large. As a result, water tends to be retained in the upper layer. In another situation, when coarse-textured soil overlaying a fine-textured layer, the hydraulic barrier could occur. The hydraulic barrier is related to relatively low permeability of the underlying fine soil layer As a result, the rate of downward water movement is restricted by the permeability of the lower layer. To address or "smooth" the discontinuity, one attempt is to find satisfactory values of hydraulic conductivity and metric potential at the interface of two different soil textures (Miller et al., 1998; Brunone et al., 2003; Matthews et al., 2004; Szymkiewicz and Helmig, 2011). In the two-layer model, the interface flux term (q_2) is expressed as a function of the hydraulic conductivity and vertically averaged capillary pressure of the first and second layer given by Eq. (2b) (He et al., 2021a). The two-layer model handles the discontinuity of hydraulic properties properly with two extreme soil layering scenarios. The results reflected these two types of barriers. Considering free-drainage bottom boundary condition, when loamy fine sand is on top of silty clay loam and if flux from the upper layer at the interface is higher than saturated conductivity of the lower layer, the hydraulic barrier occurs and only part of water flux is transmitted downward and the excess water is initially retained in the upper layer During the first two days of the rainfall period (day 6 to day 7), when sand is on top of loam (Figure 3.8 A1), the moisture content of the upper layer started to increase at day 6, while the increase of the moisture content for the lower layer was observed at day 7 because of the hydraulic barrier. When loam is on top of sand as shown in Figure 3.9 (A1), there was a rapid increase of moisture content in the upper layer at day 6, but the moisture content in the lower layer gradually increased at day 7. This is because the unsaturated conductivity in the lower sandy layer was lower than that in the fine textured upper layer in the

dry period, which act as the hydraulic barrier, although sand has higher saturated conductivity than loamy soil. The discontinuity created by hydraulic barrier was gradually mitigated when both layers were receiving rainfall resulting in increased hydraulic conductivities for both layers. Furthermore, the capillary barrier can be observed in Figure 3.9 (A1) during rainfall period. From day 6 to day 10, moisture content of the lower layer had slower rate of increase than that in the upper layer. When compare between Figure 3.9 (A1) with Figure 3.8 (A1), the highest moisture contents of the loam textured layer were similar (0.428 in Figure 3.9 (A1) vs 0.438 in Figure 3.8 (A1)). However, the highest moisture content of the sandy soil layer in Figure 3.9 (A1) (0.143) was lower than that in Figure 3.8 (A1) (0.173), which indicates that the capillary barrier occurred during rainfall period in Figure 3.9 (A1). Our results indicate that the first order approximation of Taylor expansion of conductivity and metric potential at the interface in the two-layer model can be a solution to deal with heterogeneous soil profile.

In model application at site level, the two-layer model showed its skills in simulating layer averaged soil moisture at field scale. A noticeable increase was shown for both layers after the rainfall events. Precipitation was the only water input pathway, while evapotranspiration and gravity drainage were the two pathways for water leaving the soil domain. The actual transpiration was calculated based on soil water availability of the first soil layer which is assumed to be root zone layer in the two-layer model. When soil moisture of the root zone was decreasing during dry condition with little or no precipitation, the two-layer model calculated actual transpiration and evaporation rate according to the soil moisture of the whole root zone layer. In reality, moisture content at soil surface may be different from that at deeper soil. These differences could make the estimation of transpiration and evaporation under or overestimated for different weather conditions. Furthermore, good estimation of potential evapotranspiration could improve overall model

performance. Owing to detailed meteorology data provided by SCAN, every term in Penman-Monteith method was addressed properly. Additional uncertainty could be introduced if other simplified potential evapotranspiration calculation methods are used.

The Bayesian framework proved to be simple and robust in the two-layer model calibration and uncertainty estimation. As stated in methodology, we assumed that $\varepsilon \sim N(0, \sigma_\varepsilon^2)$. The Bayesian estimated values of residual error variance (σ_ε^2) for the first layer and the second layer showed in Table 3.3 were 2.77×10^{-4} and 4.39×10^{-4}, respectively. σ_ε^2 accounts for measurement, model structural errors and uncertainty in the forcing input hydroclimate data. We further investigated model predictive uncertainty using Eq. (10). Random samples of model predicted moisture contents at each day for each soil layer were obtained from Eq. (10). The variance of model predicted moisture contents for each day were calculated based on sampled values. The sample average of the variance (σ^2) over the simulations for the first and the second layer, respectively, are taken as measures of total model prediction uncertainty. Model prediction variances for the first and the second layer were $\sigma^2 = 2.88 \times 10^{-4}$ and 4.52×10^{-4}, respectively. As shown in Figures 3.10 (A1) and (A2), the darker grey bands are attributed to model prediction error in terms of all sources of errors (parametric, observational, hydroclimate data, and ε). The ratio $\sigma_\varepsilon^2/\sigma^2$ was 96% for the first layer and 97% for the second layer, which indicates that after conditioning on the processed observed moisture content data bulk of the modeling errors was caused by deficiencies in the model structure and errors in the observed and hydroclimate data. The contribution of parametric uncertainty to total error appears very small, up to 4% and 3% in layer 1 and 2, respectively. To obtain more specific estimate of the error variance attributed to parameters uncertainty (σ_Θ^2), we used the MC simulated moisture contents and their corresponding probability masses calculated by Eq. (8). The variance for moisture content at each day was calculated from

the MC simulated values. The variances are then averaged over the simulation to represent the parametric uncertainty variance (σ_{Θ}^2). The calculated σ_{Θ}^2 were 7.50×10^{-6} and 7.81×10^{-6} for the first layer and the second layer, respectively. Parameters uncertainty contributed very little (about 2.61% and 1.73% for the first and the second layer, respectively) to the model prediction variance. The uncertainty bands before (*a prior*) and after (*a posterior*) conditioning on the observation data are plotted as grey and blue bands in Figure 3.10, respectively. We note that the reduced posterior parametric uncertainty is obtained after conditioning on the sizable, preprocessed observed moisture content data. These findings indicate that much of the uncertainty is attributed to observational, hydroclimate data, and model structural errors, while parameters' uncertainty contributed very little to the overall model uncertainty.

The overall good match between Bayesian estimates and observed soil moisture contents of two soil layers indicates that the parameters were informed appropriately by the observations and are identifiable. Figure 3.12 shows the histograms of posterior distributions overlaying prior distributions along with BMC estimated values of model input parameters. Most of the posterior distributions of model input parameters clustered around their BMC estimated values as shown in Figure 3.12. For the root zone layer, the posterior distributions of n, θ_{res}, and θ_{sat} narrowed around a small region. The posterior distributions of α and K_s were clustered in a range narrower than the prior range, while f_s had its posterior distributions extended over a wider region of the prior ranges. For the second layer, the posterior distributions of n, θ_{res}, θ_{sat}, and K_s clustered in a small region compared to their priors, while the posterior distribution of α showed a wider range. Clustered and peaked distributions are associated with well-identifiable parameters and less parameter uncertainty, while flat and scattered distributions indicate more parameter uncertainty. From Figure 3.12, n, θ_{sat}, θ_{res}, and K_s for the first layer and the second layer were identifiable

for their posterior distributions. However, α for the two layers and f_s for the first layer seemed non-identifiable. We conducted a nonparametric statistical Kolmogorov-Smirnov (K-S) test (Massey Jr, 1951) to further evaluate the identifiability of the model parameters. The K-S test was applied to quantify the maximum distance (D_{max}) between the prior and posterior cumulative distribution functions (CDFs) of parameter sets. If D_{max} is significant at a certain confidence level, the parameter can be declared identifiable because the two distributions are statistically different. The D_{max} values from the K-S test are shown in Table 3.4. The p values that correspond to D_{max} for all model parameters were smaller than 0.001 indicating that all model parameters were identifiable. These findings indicate that all parameters in the first and the second layer can be well informed by the site-level soil moisture observations. However, the observations did not provide enough information that can be used to fully estimate the values for a water retention parameter α for the first and the second layer and area index f_s for determining the fraction of bare soil and vegetation cover. Studies have reported that in-situ measurements of soil moisture content sometimes do not contain sufficient information to constrain Van Genuchten soil hydraulic parameters due to the small variability of the observations to represent a whole range of soil water states (Wöhling and Vrugt, 2011). Nevertheless, BMC methodology constrained the parameters very well for almost all of the parameters. Besides, estimations of parameters for prior distribution using pedotransfer function take into account the correlations between soil hydraulic parameters, which is better than uninformed prior distribution. Using the informed priors can produce good results in terms of estimation of parameter values (Scharnagl et al., 2011). Application of soil moisture models requires simplifications of what otherwise a complex unsaturated flow phenomenon. The results of the two-layer model and Bayesian MC simulation show a robust

framework to model vertically averaged soil moisture and estimate soil characteristic parameters at field scale.

5. Summary and Conclusions

In this study, a numerical model for two-layer vertically-averaged solution of Richards equation was evaluated with two numerical experiments and a site-level application. In one of the numerical experiments, we ran the model for 231 soil textures under various atmospheric and bottom boundary conditions with soil profile depth varied from 10 cm to 400 cm. The thickness of the root zone layer and the second layer were varied from 10 cm to 200 cm at 10 cm intervals. Soil moisture estimates were compared with vertically averaged HYDRUS simulated nodal values as a reference. This experiment revealed the soil texture and layer thickness combinations under which the two-layer model has good or poor performance. The second numerical experiment was carried to assess the performance of the model with two layers of contrasting (high and low) permeabilities. Thirdly, the two-layer model was applied to a SCAN site to simulate site-level soil moisture content of two soil layers under real atmospheric and field conditions. BMC methodology was integrated with the two-layer model for model calibration and uncertainty estimation. The major conclusions are as follows.

1. Among 92,400 simulations, the two-layer model showed excellent performance with free-drainage boundary condition with 99.8% of the total simulations having *RMSE* ≤0.015; with the zero-pressure head boundary condition representing water table, this percentage became 87.5%.
2. The two-layer model had excellent performance (*RMSE*≤0.015) for soil textures with one of the sand, silt, and clay separates less than about 30% for free-drainage and zero-

pressure head bottom boundary conditions. In addition, the two-layer model showed good skill in estimating layer averaged moisture contents for soil domains having the root zone depth greater than 10 cm and the lower vadose soil layer thickness less than 150 cm for free-drainage bottom boundary condition. For zero-pressure head bottom boundary condition, the model performed very well with the first layer thickness between 30 cm to 70 cm and the second layer between 20 cm to 100 cm.

3. The two-layer model showed satisfactory performance in simulating soil moisture contents and top and bottom fluxes as well as actual plant water uptake in stratified soils (soil layers with contrasting permeabilities). Compared to the finite element model HYDRUS, results from the two-layer model showed *RMSE* values smaller than 0.02 for all simulations. The two-layer model solution deals with contrasting hydraulic conductivity properly.
4. The results of the model application indicate that the two-layer model can deal with layer averaged soil moisture modeling at field scale with appropriate input data. The model performance was found to be good with *RMSE* values ≤ 0.023 and *NSE* values ≥ 0.62 during both calibration and validation periods.
5. The uncertainty in soil characteristic parameters and simulated moisture content was computed using the Bayesian Monte Carlo method. Much of the uncertainty was attributed to observational, hydroclimate data, and model structural uncertainties, while parametric uncertainty was found to be very small after conditioning on the observed moisture content data. Besides, all model parameters were identifiable using the observed data as evaluated by the K-S test. BMC methodology constrained all model parameters very well using informed prior distributions.

It should be noted that the two-layer approximate solution of Richards equation was intended for simulating average moisture content in the root zone (or biologically active sediment layer) in the presence of free drainage or a relatively shallow water table. The two-layer numerical model is not designed to simulate average soil moisture and fluxes at deep soil depths. Extension of the two-layer model solution to multiple soil layers could be interesting for future work.

Appendix A. Supplementary materials

Supplementary plots of the *RMSE* of moisture contents from the simulations of homogeneous soil profile between two-layer model and HYDRUS can be found by the following links:

1. Plots of *RMSE* patterns for 231 soil textures with different thickness of two soil layers for two bottom boundary conditions: https://drive.google.com/drive/folders/1RbjpnVqAy5zFlqGppYBE1Xxyf8tmLn_w?usp=sharing
2. Plots of *RMSE* patterns on the soil texture triangle for various soil layer thicknesses and two bottom boundary conditions: https://drive.google.com/drive/folders/1f6I0VB4_koXN6m4oS11UEIP05X4J-zXa?usp=sharing

Table 3.1: Soil hydraulic properties for heterogeneous soil profiles using van Genuchten model

Soil textures	α (cm^{-1})	n	θ_{res}	θ_{sat}	θ_{-33kPa}	K_{sat} (cm/day)
Loamy fine sand	0.0280	2.2390	0.0286	0.3658	0.2694	541.0
Silty clay loam	0.0104	1.3954	0.1060	0.4686	0.4483	13.1

Table 3.2: Upper and lower bounds of Van Genuchten soil hydraulic parameters applied for BMC

Layer	Bound	α (cm^{-1})	n	θ_{res}	θ_{sat}	K_s (cm/day)
1	Lower	0.0116	1.0753	0.001	0.3068	58.8
	Upper	0.0792	1.9648	0.0737	0.4156	520.5
2	Lower	0.0121	1.1776	0.005	0.3178	30.7
	Upper	0.0477	1.6705	0.0806	0.3889	111.6

Table 3.3: Estimated values of the model parameters and their confidence intervals at the SCAN site

	Parameters	2.5th Percentile	Median	97.5th Percentile	Bayesian estimate
First Layer	α	0.0273	0.0446	0.0589	0.0404
	n	1.4934	1.6362	1.8610	1.6443
	θ_{res}	0.0018	0.0228	0.0360	0.0218
	θ_{sat}	0.3075	0.3200	0.3695	0.3208
	K_s	305.4	469.5	513.6	440.4
	f_s^*	0.032	0.427	0.693	0.438
	σ_ε^2	2.74×10^{-4}	2.77×10^{-4}	2.88×10^{-4}	2.77×10^{-4}
Second Layer	α	0.0213	0.0355	0.0458	0.0361
	n	1.4650	1.5400	1.6652	1.5675
	θ_{res}	0.0401	0.0594	0.0797	0.0598
	θ_{sat}	0.3182	0.3227	0.3415	0.3259
	K_s	67.3	94.4	110.6	94.4
	σ_ε^2	4.32×10^{-4}	4.37×10^{-4}	4.56×10^{-4}	4.39×10^{-4}

* Area index represents fraction of bare soil

Table 3.4: Summary of D_{max} values from the K-S test between prior and posterior cumulative distribution functions (CDFs) of parameter sets

	α (cm^{-1})	n	θ_{res}	θ_{sat}	K_s (cm/day)	f_s
First Layer	0.40	0.47	0.51	0.67	0.58	0.30
Second Layer	0.40	0.62	0.52	0.66	0.49	N/A

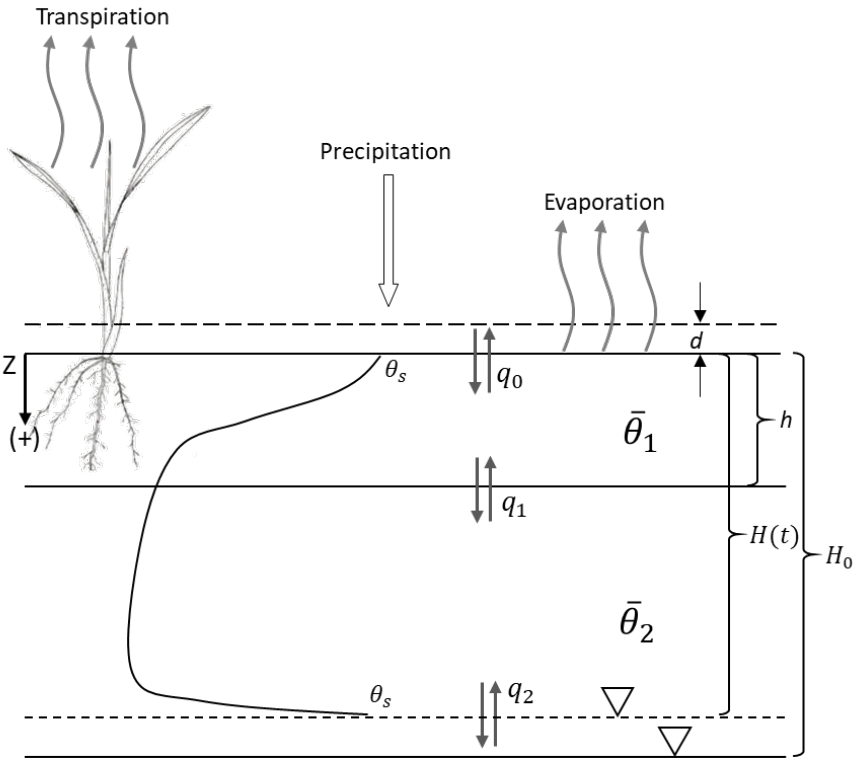

Figure 3.1: Schematic illustration of soil profile and the two-layer model depicting the root zone and vadose soil below. d is the ponding depth; h is the first layer (zoot zone) depth; $H(t)$ is depth of WT at time t; and H_0 is initial depth; q_0, q_1 and q_2 are the top, middle and bottom flux (positive downward) , respectively.

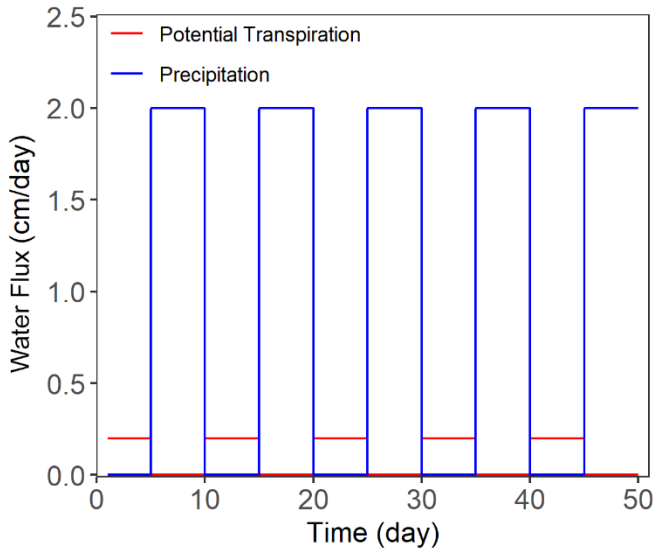

Figure 3.2: Prescribed atmospheric boundary condition applied for testing scenarios with homogeneous and heterogeneous soil profiles.

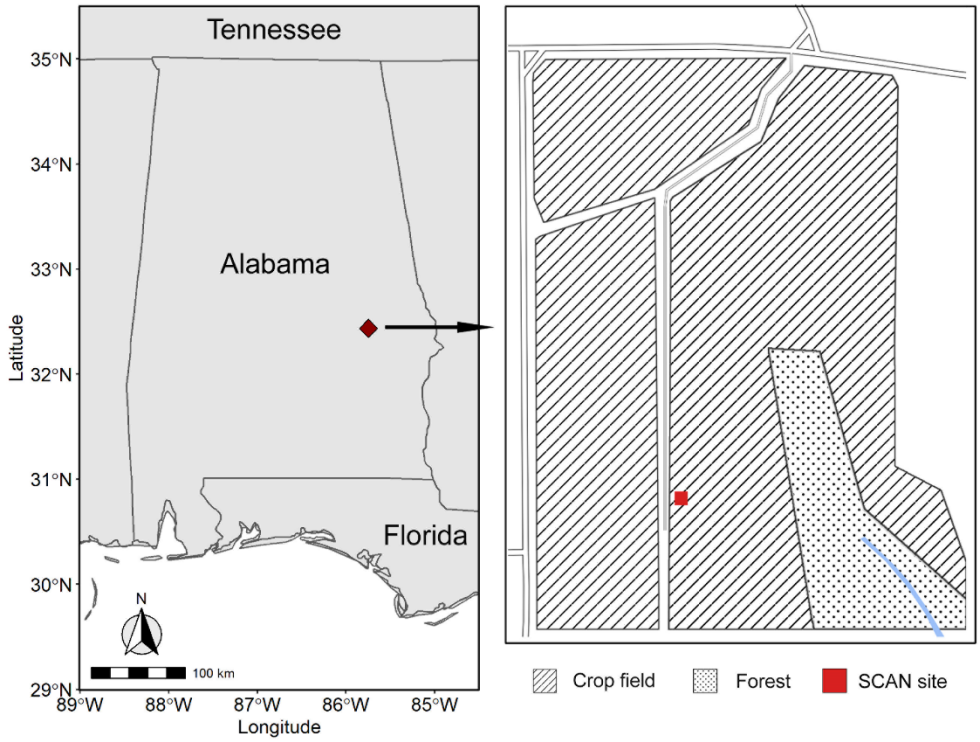

Figure 3.3: Location of study SCAN site in Alabama

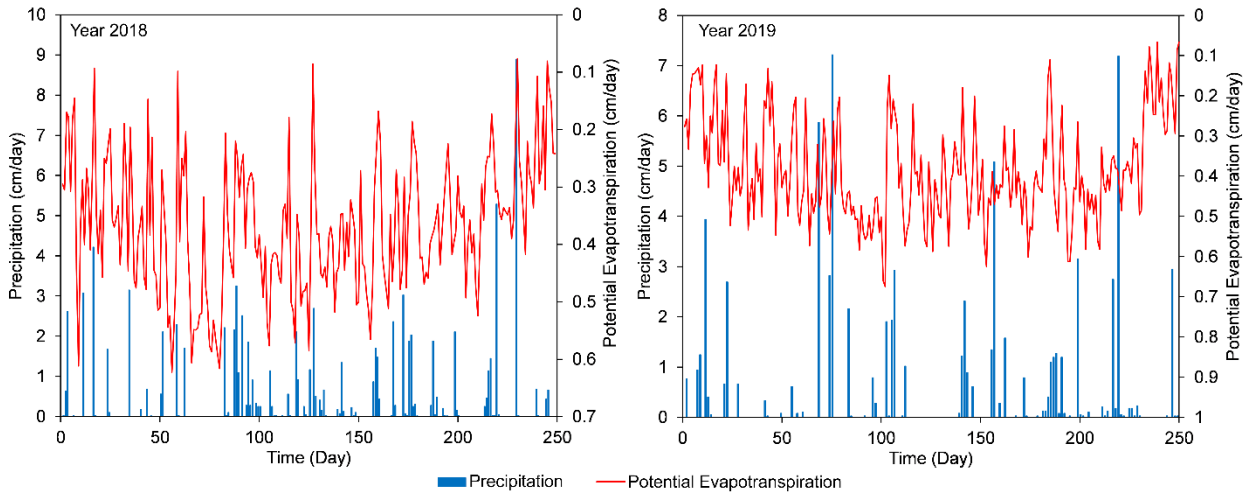

Figure 3.4: Daily potential evapotranspiration and precipitation for model calibration (year 2018) and validation (year 2019)

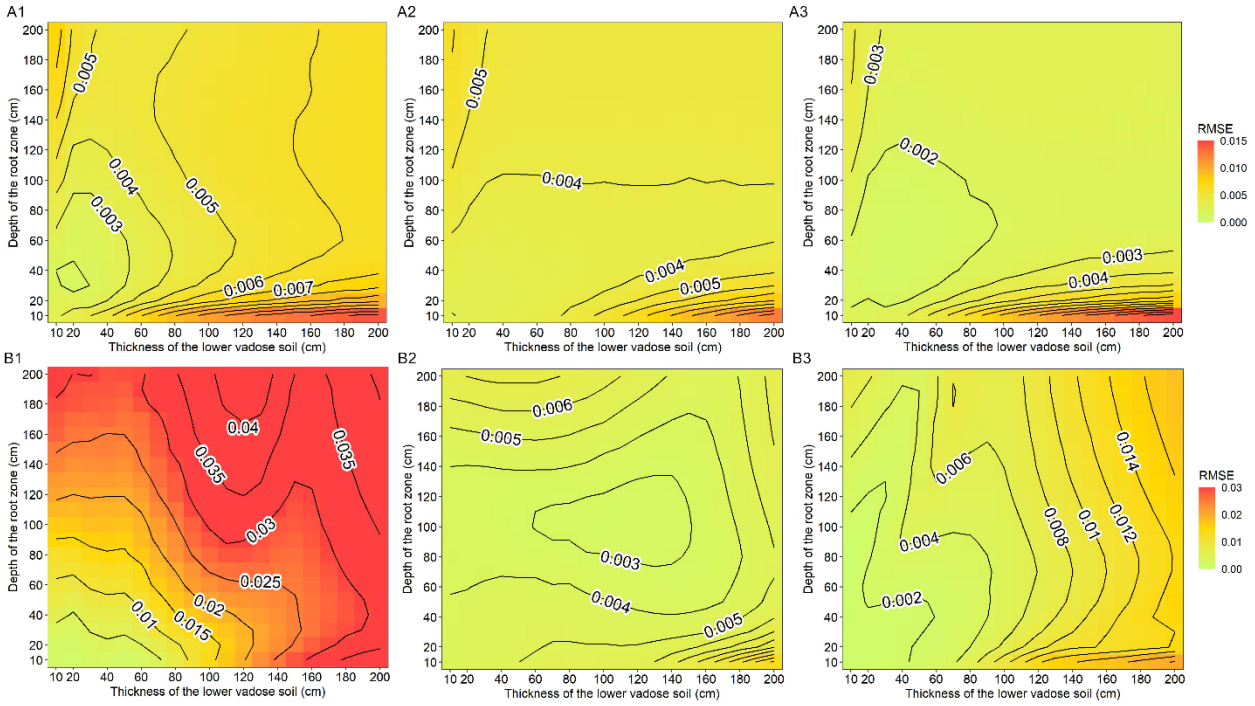

Figure 3.5: Contour plots and heat maps of average *RMSE* with different thickness of two soil layers for sand (1), loam (2) and clay (3) soil textures under free-drainage (A) and zero-pressure head (B) bottom boundary conditions (average *RMSE* was calculated by averaging *RMSE* values for moisture contents from two soil layers).

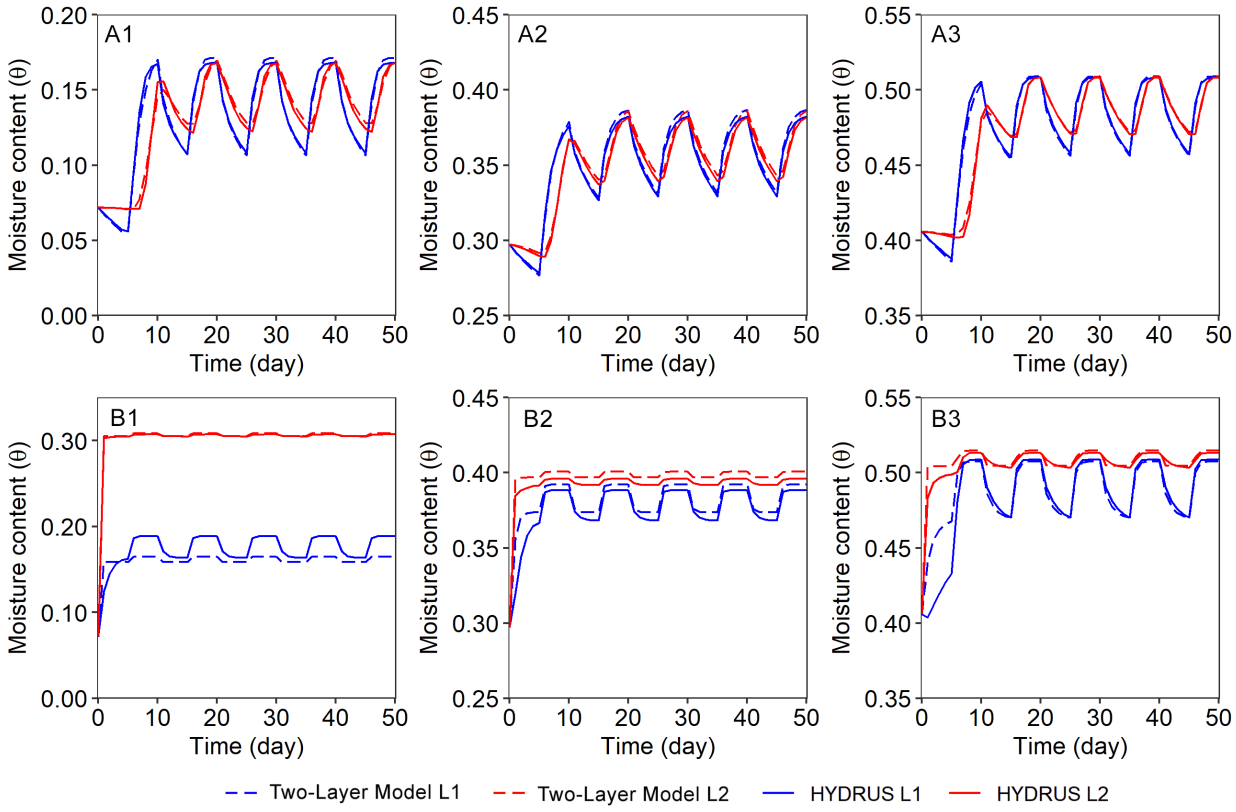

Figure 3.6: Soil moisture contents of homogeneous soil profile with 50 cm of the first layer and 50 cm of the second layer between the two-layer model and HYDRUS for sand (1), loam (2) and clay (3) soil textures under free-drainage (A) and zero-pressure head (B) bottom boundary conditions.

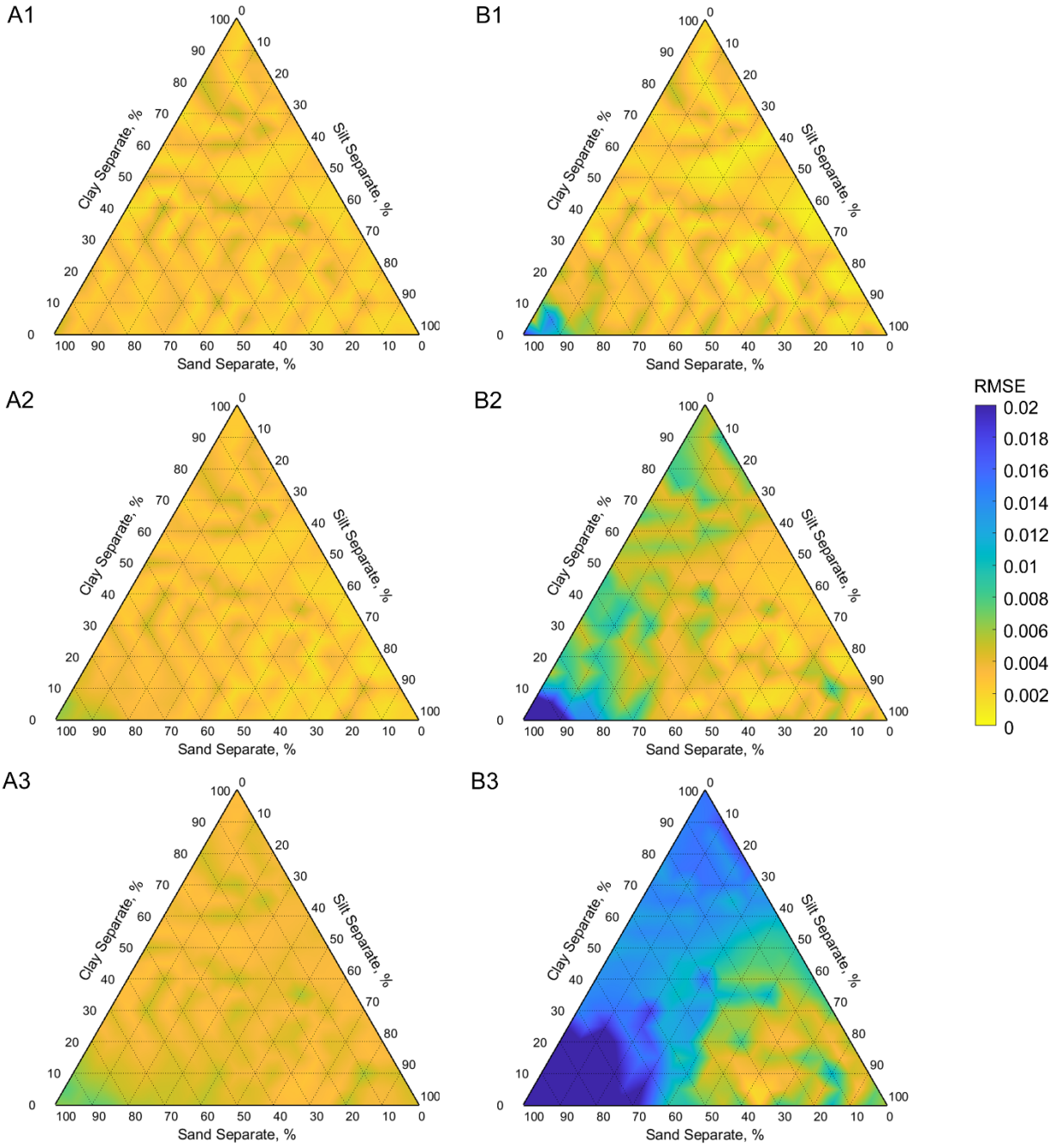

Figure 3.7: Heat maps for *RMSE* on soil triangle with 50 cm depth of the first layer and 10 cm (1), 100 cm (2), and 200 cm (3) depth of the second layer for free-drainage (A) and zero-pressure head (B) bottom boundary conditions.

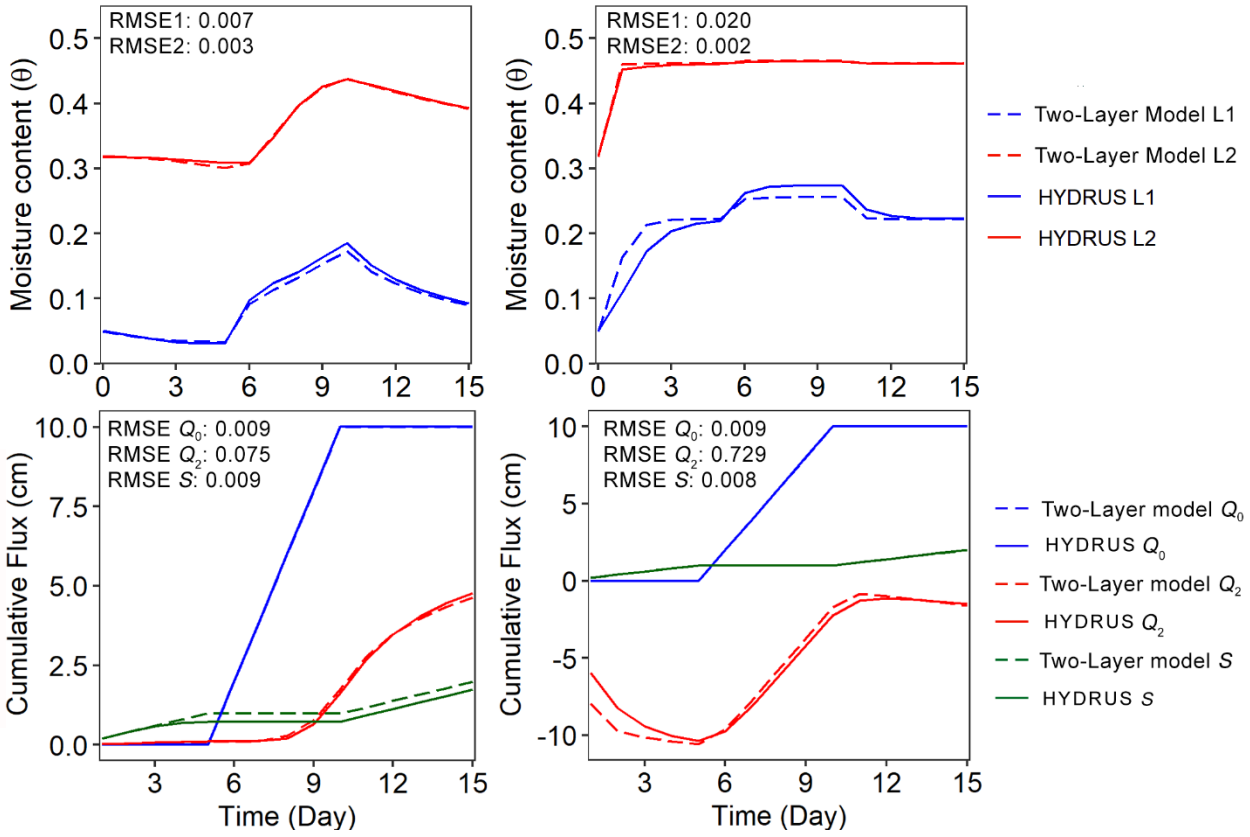

Figure 3.8: Simulated soil moisture content and fluxes by the two-layer model and HYDRUS for a soil profile where loamy fine sand (30 cm) overlays silty clay loam (30 cm). A and B represent free-drainage and zero-pressure head bottom boundary conditions, respectively. L1 and L2 represent the first and the second layer, respectively; Q_0 and Q_2 represent top and bottom cumulative flux, respectively).

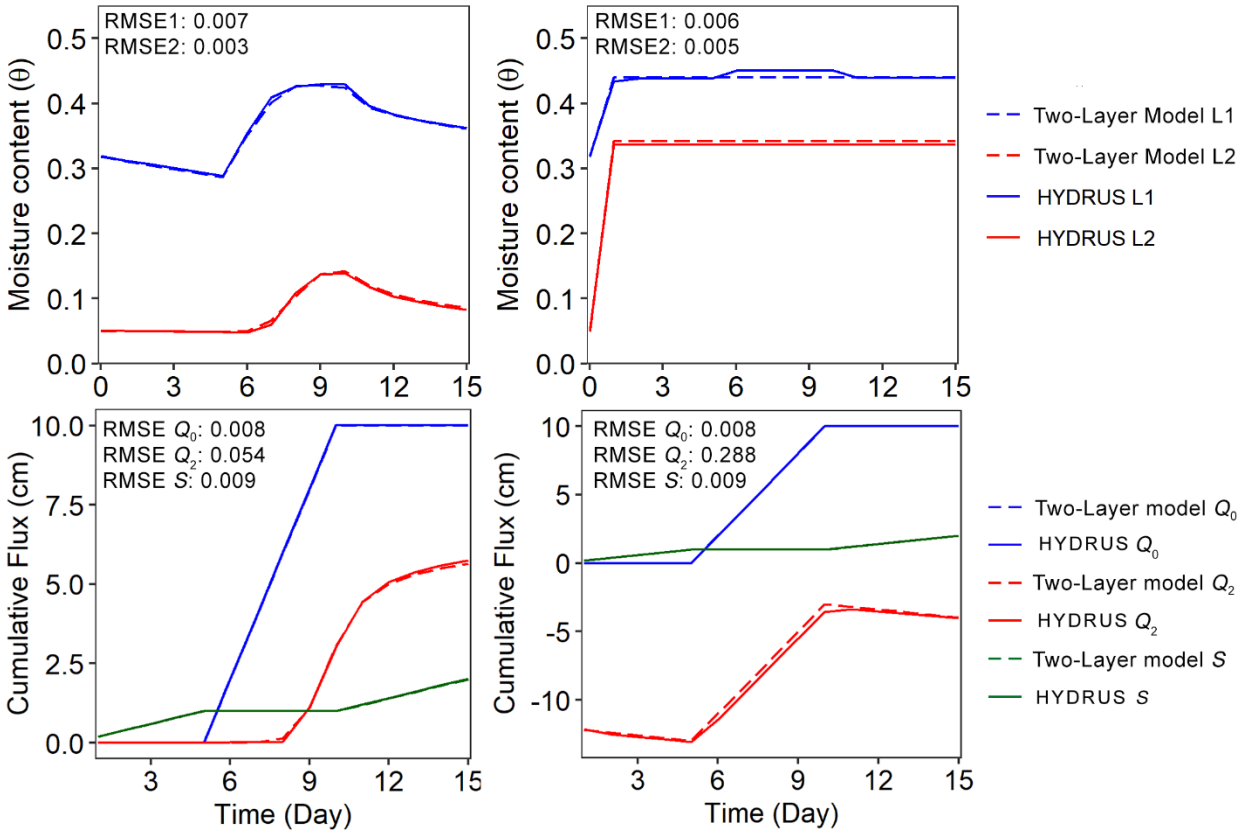

Figure 3.9: Simulated soil moisture content and fluxes by the two-layer model and HYDRUS for a soil profile where silty clay loam soil (30 cm) overlays loamy fine sand soil (30 cm). A and B represent free-drainage and zero-pressure head bottom boundary conditions, respectively. L1 and L2 represent the first and the second layer, respectively; q_0 and q_2 represent top and bottom cumulative flux, respectively).

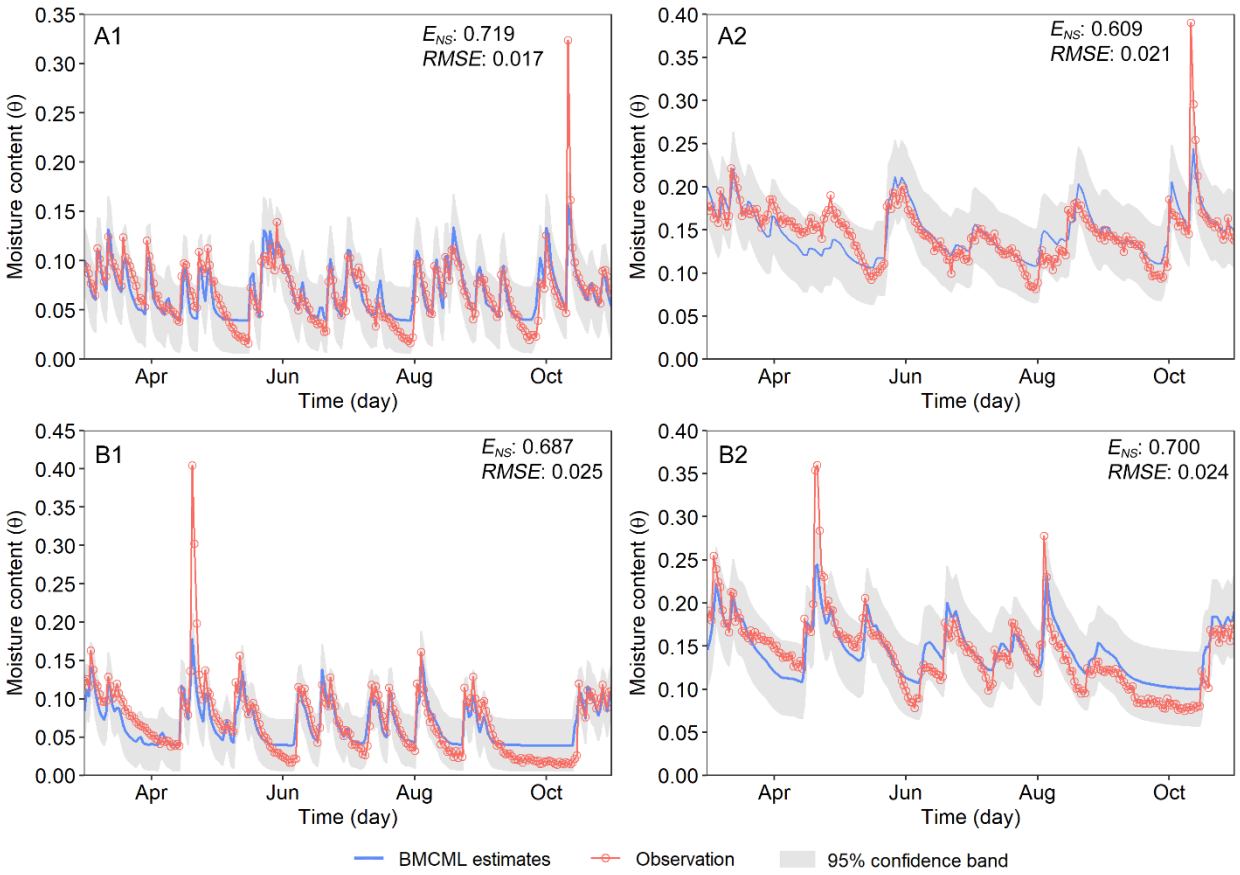

Figure 3.10: (A) Comparison with observed values of Bayesian estimates (Eq. 7) and 95% s limits of soil moisture contents of the first layer (1) and the second layer (2): (A) model calibration period, and (B) validation period.

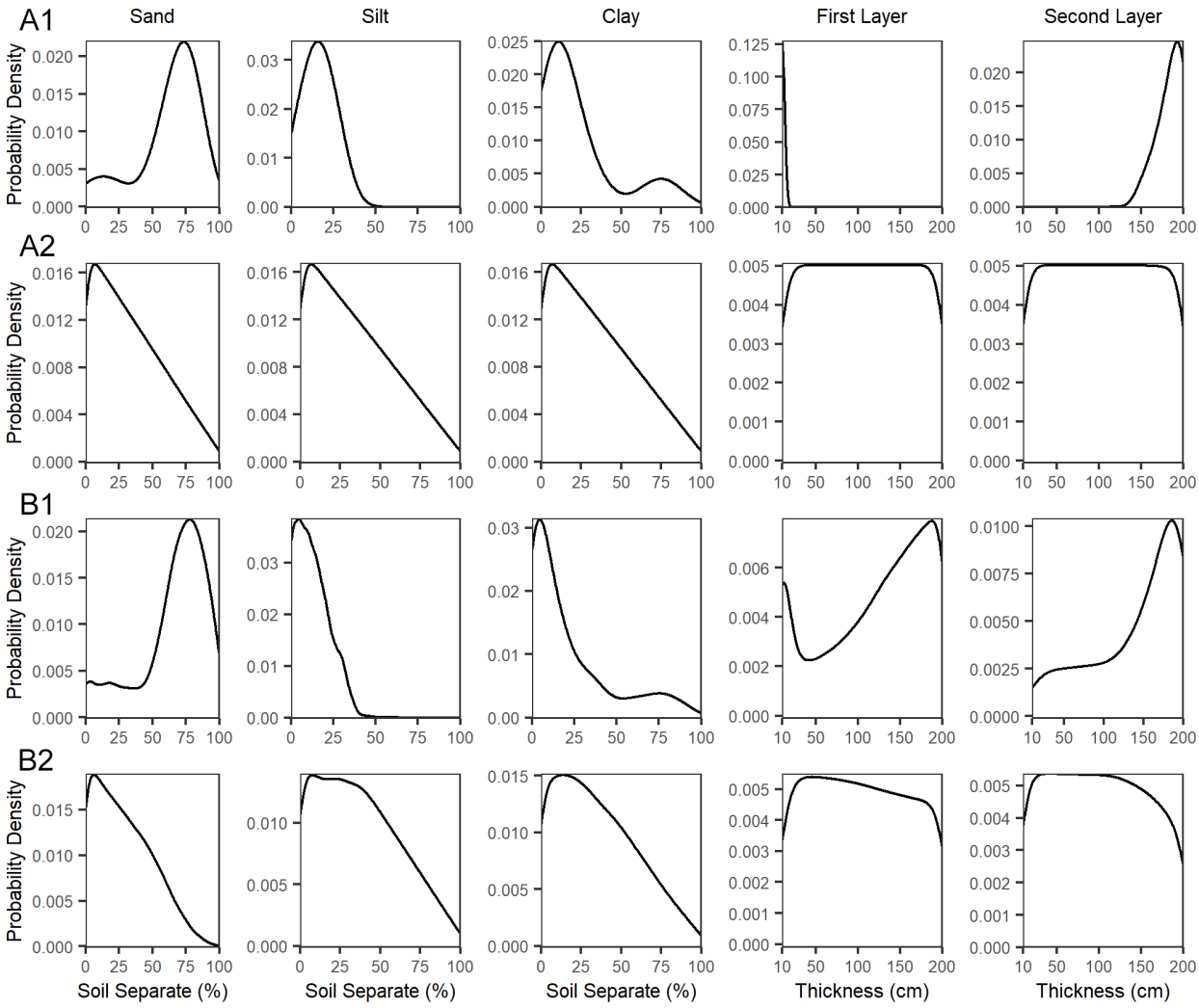

Figure 3.11: Probability densities of three soil separates and the depth of the two layers for simulations that had *RMSE* values greater than 0.015 (1) and smaller than or equal to 0.015 (2) with free-drainage (A) and zero-pressure head (B) bottom boundary conditions.

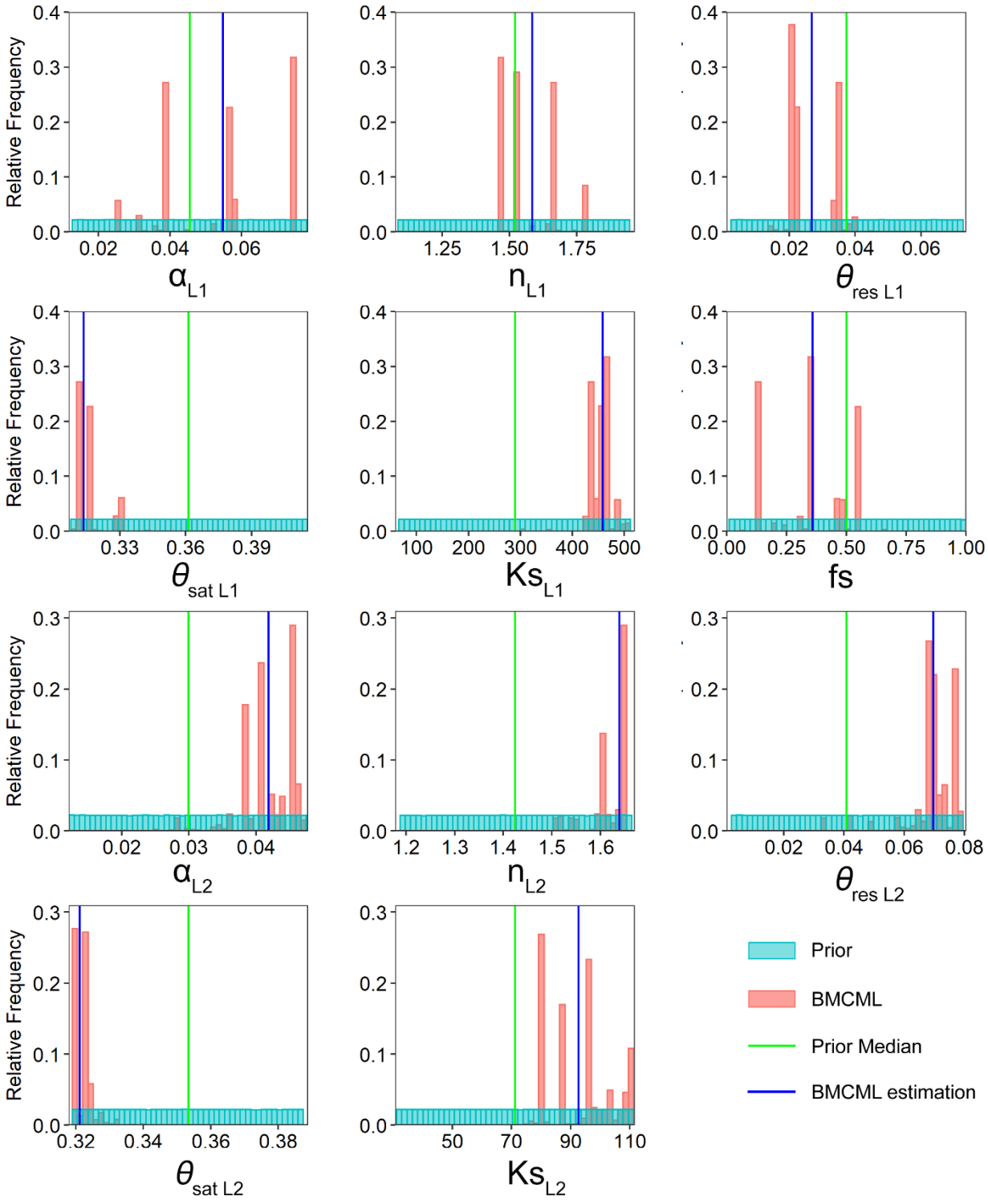

Figure 3.12: Posterior PDFs of model parameters used for BMC (green and blue vertical lines represent prior median and BMC estimated values of the parameters, respectively. L1 and L2 in subscripts stand for the first layer and the second layer, respectively. The x-axes cover the range of prior distribution of parameters listed in Table 2)

Chapter 4: A Numerical Model for Multiple Layer-Averaged Richards Equation

Abstract

Soil moisture plays an essential role in regulating hydrological and biogeochemical processes. Accurately modeling moisture content in variably saturated soil media is fundamental to land-surface coupling simulations in large-scale watershed models and land surface models (LSMs). Current large-scale watershed models and LSMs apply either reservoir cascade scheme or Richards equation (RE) to estimate vertical water movement and soil moisture content at a reasonable computational cost. RE provides relatively accurate predictions of soil moisture over other approaches due to its clear physical basis. However, solving RE numerically has always been challenging because of its high nonlinearity and computational burden, especially when RE is employed in large-scale watershed and hydro-climate applications. Recently, the authors developed a two-layer approximation of RE for the situations with shallow water table. The two-layer model has shown promising results in estimating average soil moisture contents in relatively thin soil root zone and the vadose zone below. To address situations that soil profile cannot be distinguished into two soil layers (e.g. stratified soil with varying soil textures or applications that require higher vertical resolution) and that higher vertical resolution of θ distribution is required, the two-layer model was extended to multiple layers in this study, and a numerical scheme was developed to solve coupled ordinary differential equations (ODEs) describing layer-averaged soil moisture dynamics for predefined soil layers. The multiple layer-averaged RE (LARE) solution solves the coupled ODEs using Heun's method with time adaptive algorithm and like the two-layer model it also accounts for prescribed flux and pressure head boundary conditions at the soil surface, including precipitation, ponding, soil evaporation, and plant transpiration, subject to deep

and shallow dynamic water table. LARE was evaluated by five testing scenarios against analytical solutions, HYDRUS 1-D solver, and field soil moisture observations. The model provided accurate estimations of moisture contents for multiple soil layers, and it was computationally efficient in accounting for complex, dynamic prescribed boundary conditions without any convergence issues. LARE is numerically stable and computational efficient, it is suitable for modeling water movement, and soil moisture for multiple layered soils at both field and watershed scale.

1. Introduction

Soil moisture is one of the key variables in the land-atmosphere system. It connects various hydrologic processes (such as runoff, evapotranspiration, groundwater dynamics, etc.) through unsaturated flow and further controls the terrestrial energy and biochemical cycles (McGuire et al., 2000; Seneviratne et al., 2010). Water movement in variably saturated soils has been considered an important component in watershed and land surface models (LSMs) (Pollacco and Mohanty, 2012; Vereecken et al., 2016; Lawrence et al., 2019). Appropriate and accurate estimation of water flux and moisture redistribution in root zone and vadose zone is imperative to predicting biochemical processes (Pollacco and Mohanty, 2012; Wood et al., 2013; O'Connell et al., 2018).

Many mathematical models have been developed to account for water flow and soil moisture dynamics in unsaturated media (Green and Ampt, 1911; Richards, 1931; Philip, 1957; Mahrt and Pan, 1984; Guswa et al., 2002; Ogden et al., 2015; Zhu et al., 2016; Sanchez-Mejia and Papuga, 2017). Among them, one-dimensional Richard's Equation (RE) has been widely applied in current LSMs to represent vertical water movement in variably saturated soil. RE is a physical-based model, integrating the mass conservation equation and Darcy's law, making it applicable to simulate soil moisture movement under various soil, land, and hydro-climatic conditions. RE is a

highly nonlinear, elliptic-parabolic partial differential equation, and it is coupled with two nonlinear empirical soil hydraulic relations: soil matric potential and unsaturated hydraulic conductivity. Therefore, solving the RE numerically poses several challenges (Miller et al., 2013; List and Radu, 2016). In general, numerical methods commonly applied for solving RE are finite difference (Celia et al., 1990; van Dam and Feddes, 2000; Feddes et al., 1988; Herrada et al., 2014; Rathfelder and Abriola, 1994b; Ross, 1990), finite volume (Caviedes-Voullième et al., 2013a; Kumar et al., 2009; Lai and Ogden, 2015b; Svyatskiy and Lipnikov, 2017), finite element (Forsyth et al., 1995; Lee and Abriola, 1999; Šimůnek and van Genuchten, 2008), and mixed form (Farthing et al., 2003). These numerical methods often need special design of spatial and temporal discretization schemes for certain conditions (Farthing and Ogden, 2017a). At laboratory and field-scale studies, RE has shown excellent performance in estimating soil moisture and water flux in soils under various conditions (Camporese et al., 2019; B. Chen et al., 2018; Fields et al., 2020). However, in large-scale watershed models and LSMs, traditional numerical solutions of RE are usually not considered owing to the risks that the RE solution may not convergence in complex and changing environmental conditions (such as shallow groundwater level and soil heterogeneity). These conditions can eventually create unstable situations for overall model performance (Qi et al., 2018; Sharifi et al., 2017). Besides, the overall computational cost associated with the numerical schemes listed above could be high due to their numerical complexity, which could lead to undesirably long simulation time, especially when RE is applied in a large watershed at a high vertical resolution, or RE is solved thousand or million times in a distributed regional model (Harter et al., 2004; Orgogozo et al., 2014).

To decrease the computational burden, many watershed models and LSMs often use rough parameterization schemes or consider the simplified representation of RE to simulate water

movement in the vadose zone. For example, the Soil and Water Assessment Tool (SWAT) (Neitsch et al., 2011b) model uses a simple but efficient storage routing technique to simulate water flux through soil layers. Vertical movement of soil water occurs when the water content of the upper layer exceeds field capacity and the lower layer is not saturated. The moisture contents of each layer are updated at each time step according to the mass balance of water within the soil. This method is unconditionally stable and only requires few input parameters that can be easily obtained. However, SWAT model does not directly model the unsaturated flow between soil layers. Detailed information on water movement may be lost due to the simplification of the physical process. The Gridded Surface/Subsurface Hydrologic Analysis (GSSHA) (Downer and Ogden, 2004b) model uses finite-difference solution of RE to simulate water flux and soil moisture in three soil horizons (horizon A, B, and C). The solution yields point soil moisture values (i.e., at the center of each layer) and not the thickness-averaged values. The solution in GSSHA accounts for free-drainage, water table, and moving water table as bottom boundary conditions. The computation cost is determined by user-specified discretization parameters (soil depth and vertical grid size), which require expertise in numerical analysis. The Joint UK Land Environment Simulator (JULES) (Best et al., 2011) simulates moisture contents for four soil layers with different thicknesses in a 2-meter soil domain using finite difference form of RE. This approach significantly decreases the computational time but may bring some unexpected errors because of the coarse discretization scheme being used to solve for point values of the volumetric moisture content. The early version of Organizing Carbon and Hydrology In Dynamic Ecosystems (ORCHIDEE) LSM used reservoir cascade scheme to simulate water balance of two soil layers in a 2-meter root zone (Ducoudré et al., 1993b). The updated version of ORCHIDEE adopted the Fokker-Planck equation to simulate water flow in a 2-meter soil using an implicit numerical

scheme (De Rosnay et al., 2002). 2-meter soil is discretized into 11 non-uniform vertical grid points that are finer at the top and coarser along with the depth. Nevertheless, ORCHIDEE only considers free-drainage as the bottom boundary condition, which is commonly adopted in many LSMs such as Hydrology Tiled ECMWF Scheme for Surface Exchanges over Land (HTESSEL) (Persson, 2001), Noah (Niu et al., 2011), and Variable Infiltration Capacity (VIC) Model (Gao et al., 2010). Shallow groundwater level and the effect of capillary rise cannot be appropriately treated with this bottom boundary condition. Community Land Model version 5.0 (CLM5.0) uses adaptive time-stepping algorithm to solve RE in a 50-meter depth soil column with non-uniform spatial discretization configuration (Zeng and Decker, 2009; Lawrence et al., 2019). The bedrock is specified at the bottom boundary as the default setting which assumes zero-flux boundary condition. Similar bottom boundary conditions are also applied in other LSMs such as Land Dynamics model (LM3) (Milly et al., 2014). Zero-flux boundary condition could overestimate soil water content in certain circumstances (e.g. relatively shallow simulation domain) (Chen et al., 2018).

There has been an increasing trend of development and application of high-resolution LSMs to address finer scale (1 km globally, 100 m at continental scale) hydrological and biochemical problems (Wood et al., 2011; Fatichi et al., 2016b). At such scale, parameterization of soil hydrology requires a more realistic and detailed representation of water movement in soils. When using RE to simulate soil water movement at finer scale, some challenges need to be appropriately treated. When soil switches from unsaturated condition to saturated condition, RE degenerates from parabolic type to elliptic type (Farthing and Ogden, 2017a). Saturated soil is often considered unfavorable condition for RE because the soil capillary pressure cannot be predicted correctly (for $\psi_b \geq \psi \geq 0$, $\theta = \theta_s$ and $\psi(\theta)$ is not a unique function of θ, where ψ_b is

air-entry capillary pressure). Besides, more than one type of bottom boundary condition is needed in the numerical solution that can internally switch between several bottom boundary conditions according to the position of groundwater level. In addition, soil heterogeneity has strong impact on moisture redistribution (Huang et al., 2011; Cui and Zhu, 2018). In stratified soils, soil properties can vary greatly from layer to layer. During the simulation, discontinuity of soil moisture and hydraulic conductivity between two adjacent soil textures yield sudden change of infiltration rate at the soil interface, making the numerical solution prone to convergence failure (Ma et al., 2010; Miller et al., 2013). Several approaches have been developed to resolve these discontinuities including special design of spatial discretization (Celia et al., 1990; Pan et al., 1996; Ju and Kung, 1997; Ogden et al., 2015; Dai et al., 2019) and finding the best averaging approach for equivalent hydraulic conductivity to calculate inter-nodal flux (Belfort and Lehmann, 2005; Szymkiewicz and Helmig, 2011; Belfort et al., 2013). However, the use of these approaches is mainly depending on the flow conditions and numerical scheme being applied (Szymkiewicz, 2012; Szymkiewicz et al., 2015). A universal, straightforward, and accurate formula that contributes less numerical oscillations remains challenging. Therefore, there is a need to improve the numerical solution of RE to deal with finer-scale water movement in variably saturated soils for large-scale hydrological modeling.

Recently, He et al. (2021a) developed a two-layer approximation of RE that simulates the dynamics of soil moisture contents and water flow in the root zone and vadose zone below. The two-layer model accounts for variable soil moisture flux and pressure conditions at the soil surface and effects of deep or shallow water table. The solution converts the partial differential form of RE to two coupled ordinary differential equations (ODEs). The coupled ODEs are solved explicitly using iterative Huen's method, which makes the solution computational efficient. The model was

tested for various soil profile configurations and boundary conditions and the results of soil moisture contents and fluxes were compared with the benchmark model HYDRUS-1D and field-scale observations (He, et al., 2021b). The two-layer model had excellent performance in estimating depth-averaged moisture contents with the soil profile depth less than 150 cm. However, the model performance dropped with the increasing soil depth due to greater truncation errors. Besides, the two-layer model is not designed for multiple stratified soil layers. Detailed information on soil moisture variation and fluxes are averaged out in stratified soil profiles. For example, in the two-layer model, the plant root uptake is integrated over the first layer (root layer), but it is evaluated at the average moisture content of the root zone. Plant water uptake could be over or underestimated with this simplification if the roots are dispersed in a stratified soil.

To address the need for higher vertical resolution and handle stratified soil profiles, the two-layer model was extended to multiple layers in this study, and a numerical scheme was developed to solve coupled ODEs describing layer-averaged soil moisture dynamics for predefined soil layers. The new numerical model, called LARE (**L**ayer-**A**veraged **R**ichards **E**quation), describes one-dimensional vertical unsaturated flow in layered soils. Similar to the two-layer model, LARE also considers various atmospheric conditions along with plant water uptake and water movement between soil and dynamic water table. The objectives of this study are to: 1) derive a layer-averaged approximation of RE for multiple soil layers; 2) evaluate the model performance in depth by comparing LARE solutions against analytical solutions, HYDRUS 1-D solver as well as in-situ measurement data. The overarching goal is to develop a numerically stable and efficient module for variably saturated flow in layered soils at field and watershed scale.

In the following sections, the mathematical derivation of LARE is first presented, which is followed by sections describing methods of plant root distribution, plant water uptake and soil

evaporation, soil hydraulic properties, and numerical scheme. The model is then evaluated with 5 testing scenarios. The results of soil moisture from LARE are compared with those from analytical solution, HYDRUS, and site-level observation data. Model performance and some issues are discussed after the testing scenarios. The manuscript ends with summary and conclusions.

2. Methodologies

2.1. Numerical Derivations

The equation governing the mass conservation of one-dimensional vertical water movement in porous medium is the continuity equation:

$$\frac{\partial \theta}{\partial t} = -\frac{\partial q}{\partial z} - S \tag{1}$$

where θ is the volumetric soil water content [L^3L^{-3}]; t is time [T]; z is soil depth below the surface [L], positive downward; S is a soil moisture sink term (e.g. plant transpiration) [$L^3L^{-3}T^{-1}$]; and q is the Darcy water flux [LT^{-1}], given by:

$$q = K\frac{\partial \psi}{\partial z} + K \tag{2}$$

where K is hydraulic conductivity [LT^{-1}]; ψ is the soil capillary pressure head (negative of porewater pressure) [L]. The one-dimensional Richards' equation is obtained by substituting equation (2) into (1).

The derivation of layer-averaged ODE for general layer m follows the same steps that led to the two-layer ODEs (Chapter 2). Consider the compartments within the soil domain shown in Figure 4.1. The soil column is divided into *n* layers and the layer averaged soil moisture content of the m^{th} layer ($m = 1, \dots, n$) is defined as

$$\bar{\theta}_m(t) = \frac{1}{h_m - h_{m-1}} \int_{h_{m-1}}^{h_m} \theta(z,t)\, dz \tag{3}$$

where, h_m is the depth from the ground surface to the bottom of the m^{th} layer [L].

Integrating equation (1) over the m^{th} layer, from $z = h_{m-1}$ to $z = h_m$ yields

$$\int_{h_{m-1}}^{h_m} \frac{\partial \theta}{\partial t} dz = - \int_{h_{m-1}}^{h_m} \frac{\partial q}{\partial z} dz - \int_{h_{m-1}}^{h_m} S\, dz$$

$$(h_m - h_{m-1}) \frac{d\bar{\theta}_m}{dt} = q|_{z=h_{m-1}} - q\big|_{z=h_m} - (h_m - h_{m-1})\bar{S}_m \tag{4}$$

where, $\bar{\theta}_m$ is the average moisture content of the m^{th} layer [L^3L^{-3}]; $q|_{z=h_{m-1}}$ is the flux at the top of the m^{th} layer [LT^{-1}]; $q|_{z=h_m}$ is the flux at the bottom of the m^{th} layer [LT^{-1}]; $\bar{S}$ is average transpiration rate over the m^{th} layer [$L^3L^{-3}T^{-1}$], where $\bar{S}_m = \frac{1}{h_m - h_{m-1}} \int_{h_{m-1}}^{h_m} S\, dz$. Note that when $m - 1 = 0$, $q|_{z=h_0}$ $(= q|_{z=0})$ is the top flux which is governed by atmospheric conditions. When $m = n$, $q|_{z=h_n}$ is the bottom flux described by bottom boundary conditions. $(h_m - h_{m-1})\bar{S}$ is the portion of total transpiration in the m^{th} layer. If the soil compartment is below the root zone, the last term in equation (4) drops,

$$(h_m - h_{m-1}) \frac{d\bar{\theta}_m}{dt} = q|_{z=h_{m-1}} - q\big|_{z=h_m} \tag{5}$$

Expressions for $q|_{z=h_{m-1}}$ and $q|_{z=h_m}$ are needed to solve (4). $q|_{z=0}$ and $q|_{z=h_n}$ are top and bottom boundary flux for the entire soil column, respectively, which will be explained later.

At the interface of two adjacent soil layers, at $z = h_m$, equation (2) gives

$$q|_{z=h_m} = K|_{z=h_m} \frac{\partial \psi}{\partial z}\Big|_{z=h_m} + K|_{z=h_m} \tag{6}$$

where, $K|_{z=h_m}$ is the unsaturated hydraulic conductivity at $z = h_m$ [LT^{-1}]; $\frac{\partial \psi}{\partial z}\Big|_{z=h_m}$ is the pressure gradient at the interface between layer m and $m+1$.

Following same steps as in Chapter 2, Taylor expansion of K around $z = h_m$ is

$$K(z,t) = K(h_m,t) + \frac{\partial K}{\partial z}\Big|_{z=h_m}(z-h_m) + \frac{1}{2}\frac{\partial^2 K}{\partial z^2}\Big|_{z=h_m}(z-h_m)^2 + \cdots \quad (7)$$

Integrating (7) from $z = h_{m-1}$ to $z = h_m$ and retaining zero and first-order terms, and then dividing by $h_m - h_{m-1}$ yields

$$\overline{K}_m = K(h_m,t) - \frac{1}{2}\frac{\partial K}{\partial z}\Big|_{z=h_m} h_m$$

Thus,

$$\frac{\partial K}{\partial z}\Big|_{z=h_m} = 2\frac{K(h_m,t) - \overline{K}_m}{h_m - h_{m-1}} \quad (8)$$

where $\overline{K}_m$, representing $\overline{K}_m(t)$, is the average soil hydraulic conductivity of the m^{th} layer [LT^{-1}], in which $\overline{K}_m = \frac{1}{h_m - h_{m-1}}\int_{h_{m-1}}^{h_m} K(z,t)\,dz$. We assume $\overline{K}_m \approx K(\bar{\theta}_m)$. Thus $\overline{K}_m$ can be estimated from $\bar{\theta}_m$ using any of the soil characteristics model.

Integrating (7) from $z = h_m$ to $z = h_{m+1}$ and dividing by $(h_{m+1} - h_m)$ yields

$$\overline{K}_{m+1} = K(h_m,t) + \frac{1}{2}\frac{\partial K}{\partial z}\Big|_{z=h_m}(h_{m+1} - h_m) \quad (9)$$

thus,

$$\frac{\partial K}{\partial z}\Big|_{z=h_m} = 2\frac{\overline{K}_{m+1} - K(h_m,t)}{h_{m+1} - h_m} \quad (10)$$

where $\overline{K}_{m+1}$ is average soil hydraulic conductivity of the $(m+1)^{\text{th}}$ layer [LT^{-1}], in which $\overline{K}_{m+1} = \frac{1}{h_{m+1} - h_m}\int_{h_m}^{h_{m+1}} K(z,t)\,dz \approx K(\bar{\theta}_{m+1})$.

Comparison of (8) with (10) leads to,

$$2\frac{K(h_m,\mathrm{t})-\overline{K}_m}{h_m-h_{m-1}}=2\frac{\overline{K}_{m+1}-K(h_m,\mathrm{t})}{h_{m+1}-h_m}$$

Hence,

$$K(h_m,\mathrm{t})=\gamma_m\overline{K}_m+(1-\gamma_m)\overline{K}_{m+1} \tag{11}$$

from which $\gamma_m=\frac{h_{m+1}-h_m}{h_{m+1}-h_{m-1}}$, $1-\gamma_m=\frac{h_m-h_{m-1}}{h_{m+1}-h_{m-1}}$.

Taylor series expansion of ψ around $z=h_m$ is

$$\psi(\mathrm{z},\mathrm{t})=\psi(h_m,\mathrm{t})+\left.\frac{\partial\psi}{\partial z}\right|_{z=h_m}(z-h_m)+\frac{1}{2}\left.\frac{\partial^2\psi}{\partial z^2}\right|_{z=h_m}(z-h_m)^2+\cdots \tag{12}$$

Similarly, by integrating (12) from $z=h_{m-1}$ to $z=h_m$, taking the zero and first-order terms, and dividing by (h_m-h_{m-1}), one can show

$$\left.\frac{\partial\psi}{\partial \mathrm{z}}\right|_{\mathrm{z}=h_m}=2\frac{\psi(h_m,\mathrm{t})-\bar{\psi}_m}{h_m-h_{m-1}} \tag{13}$$

where $\bar{\psi}_m$ is the average metric potential of the m^{th} layer [L] given by $\bar{\psi}_m=\frac{1}{h_m-h_{m-1}}\int_{h_{m-1}}^{h_m}\psi(\mathrm{z},\mathrm{t})\,dz$.

Integrating (12) from $z=h_m$ to $z=h_{m+1}$ and dropping the higher order terms, then dividing by $(h_{m+1}-h_m)$ yields,

$$\left.\frac{\partial\psi}{\partial \mathrm{z}}\right|_{\mathrm{z}=h_m}=2\frac{\bar{\psi}_{m+1}-\psi(h_m,\mathrm{t})}{h_{m+1}-h_m} \tag{14}$$

where $\bar{\psi}_{m+1}$ is the average metric potential of the $(m+1)^{\mathrm{th}}$ layer [L], in which $\bar{\psi}_{m+1}=\frac{1}{h_{m+1}-h_m}\int_{h_m}^{h_{m+1}}\psi(\mathrm{z},\mathrm{t})\,dz$. Thus, by (13) and (14),

$$2\frac{\psi(h_m,\mathrm{t})-\bar{\psi}_m}{h_m-h_{m-1}}=2\frac{\bar{\psi}_{m+1}-\psi(h_m,\mathrm{t})}{h_{m+1}-h_m}$$

which can be solved for $\psi(h_m,\mathrm{t})$,

$$\psi(h_m, \mathrm{t}) = \gamma_m \bar{\psi}_m + (1-\gamma_m)\bar{\psi}_{m+1} \tag{15}$$

Substituting (15) into either (13) or (14) yields,

$$\left.\frac{\partial \psi}{\partial \mathrm{z}}\right|_{\mathrm{z}=h_m} = \frac{2}{h_{m+1} - h_{m-1}}(\bar{\psi}_{m+1} - \bar{\psi}_m) \tag{16}$$

Substituting (11) and (16) into (6) yields the expression for $q|_{\mathrm{z}=h_m}$,

$$q|_{\mathrm{z}=h_m} = \frac{2}{h_{m+1} - h_{m-1}}(\gamma_m \overline{K}_m + (1-\gamma_m)\overline{K}_{m+1})(\bar{\psi}_{m+1} - \bar{\psi}_m) + \gamma_m \overline{K}_m + (1-\gamma_m)\overline{K}_{m+1} \tag{17}$$

2.2. Water Fluxes at Boundary of the Soil Profile

The top flux $q|_{\mathrm{z}=0}$ is described by atmospheric conditions (precipitation, evaporation, and ponding). At z=0, if precipitation rate $i < K_{s1}$,

$$q|_{\mathrm{z}=0} = i \tag{18}$$

where K_{s1} is saturation conductivity of the first layer [LT^{-1}]; and i is precipitation rate [LT^{-1}]. If $i > K_{s1}$, Eq.(18) holds until the top soil is saturated. If ponding occurs at depth d_P, then from Darcy's equation,

$$q|_{\mathrm{z}=0} = 2K_{s1}\frac{\bar{\psi}_1 + d}{h_1} + K_{s1} \tag{19}$$

If $i = 0$,

$$q|_{\mathrm{z}=0} = -ev_a \tag{20}$$

where ev_a is soil evaporation rate [LT^{-1}]. The calculation of evaporation rate is present in section 2.5.

At $z = h_n$, the expression of $q|_{\mathrm{z}=h_n}$ is,

$$q|_{\mathrm{z}=h_n} = K|_{\mathrm{z}=h_n}\left.\frac{\partial \psi}{\partial z}\right|_{z=h_n} + K|_{\mathrm{z}=h_n} \tag{21}$$

If the water table is at the bottom of the n[th] layer, the soil below the n[th] layer becomes saturated. Then, the hydraulic conductivity at the bottom of the n[th] layer is,

$$K|_{z=h_n} = K_{sn} \tag{22}$$

where K_{sn} is saturated hydraulic conductivity of the n^{th} layer [LT^{-1}].

Once again, we expand ψ around $z = h_n$ and integrate from $z = h_{n-1}$ to $z = h_n$ and divide by $(h_n - h_{n-1})$ to obtain,

$$\left.\frac{\partial \psi}{\partial z}\right|_{z=h_n} = 2\frac{\psi(h_n, t) - \bar{\psi}_n}{h_n - h_{n-1}} \tag{23}$$

Let $\psi(h_n, t) = \psi_b$, where ψ_b is the critical bubbling suction (i.e., negative of air-entry pressure) of the soils [L]. ψ_b is equal to 0 cm by default. Substitution of equations (22) and (23) into (21) yields,

$$q|_{z=h_n} = 2K_{sn}\frac{\psi_b - \bar{\psi}_n}{h_n - h_{n-1}} + K_{sn} \tag{24}$$

If the water table drops below h_n, free drainage condition holds at the bottom referring to zero-gradient of both soil capillary pressure ($\left.\frac{\partial \psi}{\partial z}\right|_{z=h_n} = 0$) and unsaturated conductivity ($\left.\frac{\partial K}{\partial z}\right|_{z=h_n} = 0$). Using Taylor expansion of K around $z = h_n$ to yield $K(h_n, t) = \bar{K}_n$.

Thus, bottom flux $q|_{z=h_n}$ becomes,

$$q|_{z=h_n} = \bar{K}_n \tag{25}$$

At this point, soil moisture content of each layer can be obtained by equation (4) coupled with top flux from equations (18) to (20) and bottom flux terms either from equation (24) when groundwater level is at the bottom of the soil domain or from equation (25) when groundwater level is far below the soil of interest. Moisture contents of soil layers within the soil domain are

governed by several coupled ordinary differential equations (ODEs) by the extension of equation (4). The coupled ODEs are solved explicitly by using Heun's method.

2.3. Groundwater Table Dynamics

When groundwater level is within the m^{th} $(m = 1, \dots, n)$ layer $(h_{m-1} \leq h_w < h_m)$, soil below the water table is saturated. The average moisture content of the m^{th} layer is calculated by a weighted average of moisture content in both saturated and unsaturated parts,

$$\bar{\theta}_m(t) = \frac{(h_w - h_{m-1})\bar{\theta}_{mu}(t) + (h_m - h_w)\bar{\theta}_{ms}(t)}{h_m - h_{m-1}} \tag{26}$$

where $\bar{\theta}_{mu}$ is the moisture content of unsaturated part of the m^{th} layer [L^3L^{-3}], $\bar{\theta}_{ms}$ is saturation water content of the m^{th} layer [L^3L^{-3}].

$\bar{\theta}_{mu}(t)$ is described as,

$$\bar{\theta}_{mu}(t) = \frac{1}{h_w - h_{m-1}} \int_{h_{m-1}}^{h_w} \theta(z,t)\, dz \tag{27}$$

Following similar steps, integrating (1) from $z = h_{m-1}$ to $z = h_w$ yields,

$$(h_w - h_{m-1})\frac{d\bar{\theta}_{mu}}{dt} = q|_{z=h_{m-1}} - q\big|_{z=h_w} - (h_w - h_{m-1})\bar{S}_{mu} \tag{28}$$

where $q|_{z=h_w}$ is the flux at the groundwater table [LT^{-1}], and $\bar{S}_{mu} = \frac{1}{h_w - h_{m-1}} \int_{h_{m-1}}^{h_w} S\, dz$. If the groundwater table is below the root zone, equation (28) becomes,

$$(h_w - h_{m-1})\frac{d\bar{\theta}_{mu}}{dt} = q|_{z=h_{m-1}} - q\big|_{z=h_w} \tag{29}$$

Similar approach is employed to derive $q|_{z=h_w}$ as for (24), which gives,

$$q|_{z=h_w} = 2K_{sm}\frac{\psi_b - \bar{\psi}_{mu}}{h_w - h_{m-1}} + K_{sm} \tag{30}$$

where $\bar{\psi}_{mu}$ is capillary pressure of the unsaturated part of the m^{th} layer [L].

When groundwater level is below the nth layer, a free-drainage bottom boundary condition (25) is applied at the bottom of the nth layer.

2.4. Root Distribution and Plant Transpiration Estimation

Plants extract water from root zone. The rate of water uptake mainly depends on the water availability in the root zone, the root density distribution, and the potential transpiration rate (Feddes, 1982; Perrochet, 1987b). The sink term *S* in equation (4) is defined as the volume of water removed from a unit volume of soil per unit time due to plant water uptake and it is calculated based on the following relationship

$$S_{am} = \beta(\psi) b(z) S_p \tag{31}$$

where S_{am} is actual plant water uptake rate in layer m in the root zone [$L^3L^{-3}T^{-1}$], $\beta(\psi)$ is a prescribed dimensionless root-water uptake water stress response function of the soil capillary pressure head ($0 \leq \beta \leq 1$), $b(z)$ is the normalized water uptake distribution and S_p is the potential water uptake rate [$L^3L^{-3}T^{-1}$].

In our model, we assume that the potential water uptake rate S_p is equally distributed over each soil layer within the root zone. Hence, S_p can be calculated as $S_p = T_p/(h_m - h_{m-1})$, where T_p is potential transpiration rate [LT^{-1}]. The stress response function $\beta(\psi)$ is based on Feddes, 1982. When soil is close to saturation (ψ_a) or soil moisture is above the wilting point capillary pressure head (ψ_d), water uptake is assumed to be zero ($\beta = 0$). Water uptake is considered optimal, at potential transpiration rate between certain prescribed capillary pressure heads (ψ_b and ψ_c). Water uptake decreases (or increases) linearly when $\psi_c < \psi < \psi_d$ or $\psi_a < \psi < \psi_b$. Root water uptake distribution function $b(z)$ is described by Hoffman and Van Genuchten (1983), which

assumes that the top 20% depth of the root zone contributes one-third of plant water uptake and the remaining 80% contributes two-thirds of plant water uptake.

2.5. Soil Evaporation Estimation

Actual evaporation is calculated from potential evaporation based on the soil moisture content of the first layer in the model domain. If the water content of the first layer is higher than the field capacity (θ_{fc1}), the actual evaporation rate is equal to the potential evaporation rate, whereas if the value of water content is lower than θ_{fc1} but higher than the wilting point (θ_{wp1}), the actual evaporation rate is calculated by the relationship given by Dingman (2015),

$$ev_a = ev_p \left(\frac{\bar{\theta}_1 - \theta_{wp1}}{\theta_{fc1} - \theta_{wp1}} \right)^p \tag{32}$$

where, ev_p is potential evaporation rate [LT^{-1}], θ_{wp1} is moisture content of the first layer at wilting point (-1500 kPa) [L^3L^{-3}], θ_{fc} is the water content of the first layer at field capacity (-33 kPa) [L^3L^{-3}] and p is an exponent coefficient [-]. The value of p was set to 1 in this study. Potential transpiration rate (S_p) and potential evaporation rate (ev_p) can be calculated by partitioning of potential evapotranspiration calculated either by process-based or empirical equations, such as Penman-Monteith method (Allen et al., 2005), Hargreaves equation (Jensen et al., 1997), and Priestley-Taylor equation (Priestley and Taylor, 1972).

2.6. Unsaturated Soil Hydraulic Properties

The soil hydraulic characteristic relationships between ψ and K were modeled using the Van Genuchten (1980) model.

$$K(S_e) = K_s S_e^{\frac{1}{2}} \left[1 - \left(1 - S_e^{\frac{1}{m_{VG}}} \right)^{m_{VG}} \right]^2 \tag{33}$$

$$\psi(S_e) = \frac{1}{\alpha}\left(S_e^{-\frac{1}{m_{VG}}} - 1\right)^{1-m_{VG}} \tag{34}$$

where S_e is the relative saturation and calculated by $S_e = (\theta - \theta_r)/(\theta_s - \theta_r)$; θ_r and θ_s are residual and saturated water content, respectively [L^3L^{-3}]; K_s is saturated hydraulic conductivity [LT^{-1}]; m_{VG} [-], n_{VG} [-], and α [L^{-1}] are fitting parameters where $m_{VG} = 1 - \frac{1}{n_{VG}}$.

2.7. Numerical Scheme

Soil moisture of each predefined layer in the model domain is governed by a set of coupled equations (4). The coupled ordinary differential equations can be solved explicitly by using Heun's method. First, the flux terms q_m ($m = 0, 1, \dots, n$; q_0 refers to the top flux $q|_{z=0}$, and q_m refers to the flux at the bottom of m^{th} layer $q|_{z=m}$) at the boundaries of each layer are obtained from $\bar{\psi}$ and $\bar{K}$ of that layer which are calculated at the beginning of the time step using the Van Genuchten soil characteristic relationships. Second, the slope or time derivative of the function $\bar{\theta}_i(t)$ at the beginning of the computational time interval (Euler's slope) is written as,

$$\frac{d\bar{\theta}_i{}^j}{dt} = f\left(t_j, {q_m}^j\right) \tag{35}$$

where subscript i denotes layer number; superscript j indicates time t_j; and $f\left(t_j, {q_m}^j\right)$ can be deduced from Eq. (4) after arranging terms; it is evaluated at the beginning of the computational time step (t_j). Eq. (35) is used to extrapolate $\bar{\theta}_i$ linearly to the end of the computational time step.

$$\bar{\theta}_i^0 = \bar{\theta}_i{}^j + f\left(t_j, {q_m}^j\right)\Delta t \tag{36}$$

where the superscript 0 refers to intermediate prediction of $\bar{\theta}_i$ at time t_{j+1}, which refers to the standard Euler method and Δt is the computational time step [T], $\Delta t = t_{j+1} - t_j$. Third, the fluxes

q_m^0 are obtained from $\bar{\psi}_i^0$ and $\bar{K}_i^0$ of each layer which are calculated from $\bar{\theta}_i^0$. Fourth, the slope at the end of the time interval is given by:

$$\frac{d\bar{\theta}_i^{\,j+1}}{dt} = f\left(t_{j+1}, {q_m}^0\right) \tag{37}$$

where the superscript *j+1* refers to time t_{j+1}. Last, the correction for the prediction (36) is calculated using the average slope for the interval,

$$\bar{\theta}_i^{\,j+1} = \bar{\theta}_i^{\,j} + \frac{f\left(t_j, {q_m}^j\right) + f\left(t_{j+1}, {q_m}^0\right)}{2}\Delta t \tag{38}$$

The slope in (37) is updated based on this correction ($\bar{\theta}_i^{\,j+1}$) and a revised correction is obtained using (38) once again. These steps are repeated until convergence. A termination criterion for the convergence of the corrector is provided by:

$$\varepsilon_i = \frac{\left|\bar{\theta}_i^{\,j+1,p} - \bar{\theta}_i^{\,j+1,p-1}\right|}{\bar{\theta}_i^{\,j+1}} \times 100$$

where, $\bar{\theta}_i^{\,j+1,p-1}$ and $\bar{\theta}_i^{\,j+1,p}$ are the results from the prior iteration and the present correction, respectively.

The adaptive time-step algorithm is applied to improve model efficiency to reduce computation time. When numerical solutions during iterations converge fast, larger time step could be used to decrease computation time, whereas when the absolute changes in moisture contents between consecutive time steps remain higher than prescribed error tolerance, smaller time step should be applied to ensure the accuracy of numerical estimations. We followed the procedure implemented by Šimůnek et al. (1998). The time increment is adjusted automatically during iterations but cannot be less than the predefined minimum time step, nor exceed the maximum time step. During each time step, if the numerical solution converges within certain number of iterations (predefined numbers), Δt is increased by multiplying by a constant greater than 1;

otherwise, if iterations exceed the predefined number of iterations, which indicates the convergence difficulties are encountered, Δt is decreased by multiplying it with a number smaller than 1. For the worst case when the number of iterations during a time step is greater than prescribed maximum number of iterations, Δt is reduced to $\Delta t/10$ and the iteration for this time step is repeated.

3. Results

This section presents a comprehensive evaluation of LARE, including four numerical experiments and one site-level application: (1) steady-state soil profile under constant infiltration into layered soils, (2) three homogeneous soil profiles with multiple numerical layers, (3) constant infiltration into stratified soil profile with dry initial conditions, (4) dynamic rainfall and transpiration on stratified soil profile with changing shallow groundwater level, (5) site-level model application. HYDRUS program, which solves RE numerically using finite element method with mass conservative implicit iterative scheme (Simunek et al., 2005), was used in the first four scenarios as benchmark for assessment of LARE performance. In these five numerical experiments, flat surface and no runoff were assumed at the soil surface.

3.1. Scenario 1: Steady State Soil Moisture Profile with Constant Infiltration into Layered Soil

The first scenario was steady-state soil moisture profile with constant water infiltrates into layered soils. The results were compared with those from HYDRUS and an analytical solution developed by Rockhold et al. (1997), which accounted for one-dimensional vertical steady water flow in layered soils with arbitrary hydraulic properties. As presented in the work by Rockhold et

al. (1997), a 6-meter soil profile was divided into three layers with 2 meters of each in thickness. Two soil textures were considered which were Berino loamy fine sand for the first and the third layer, and Glendale silty clay loam for the middle layer. The van Genuchten soil hydraulic properties of the two soil textures are shown in Table 4.1. The top boundary condition was set with a constant flux of 13.824 cm/day, and zero-pressure boundary condition (Eq.24) was specified at the bottom of the soil profile, which indicates existence of a water table at the soil bottom. LARE was run at two spatial discretization schemes: Δz=5 cm and Δz=40 cm, respectively. HYDRUS was run using fine spatial discretization method. It should be noted that HYDRUS uses 101 equally spaced elements as the default mesh size. We kept the default spatial discretization in HYDRUS for each simulation to ensure good prediction accuracy of the reference model. LARE and HYDRUS were run until steady state was reached. To compare the results between LARE, HYDRUS and the analytical solution, we averaged the moisture contents from the analytical solution and HYDRUS solution obtained at finer spatial resolution over 5 cm and 40 cm increments, respectively.

Results of soil moisture profiles at steady state estimated from LARE and HYDRUS along with analytical solution are shown in Figure 4.2. With fine spatial discretization scheme (Δz=5 cm), the results from LARE were almost identical to those obtained from the analytical solution and HYDRUS (Figure 4.2A). Besides, LARE captured the sudden change of moisture profile at 200 cm (moisture content increased from 0.3661 to 0.4691) and 400 cm (moisture content decreased from 0.4379 to 0.2034), respectively, where the silty clay loam was saturated in the 200 cm-thickness middle layer. However, there was a small difference between LARE and analytical solution between 100 cm and 200 cm depth. This difference was caused by the spatial discretization scheme being used. However, the purpose of developing LARE was not for such

fine spatial resolution. Thus, we tested the performance of LARE with a coarse spatial discretization too using Δz=40 cm. As shown in Figure 4.2(B), the results from LARE were almost identical to the averaged analytical solution and averaged moisture contents obtained from HYDRUS.

3.2. Scenario 2: Infiltration with Pulse Rainfall into Three Homogeneous Soil Profiles with Multiple Numerical Discretization Layers

The second scenario was to test infiltration into homogeneous soil profile with different layer configurations. In this scenario, the hypothetical homogeneous soil domains were made up of three U.S. Department of Agriculture (USDA) soil textures: sand, loam, and clay loam. The van Genuchten soil hydraulic properties of three soil textures are shown in Table 4.1. Simulations were conducted by LARE and HYDRUS on these three homogeneous soil profiles with the total soil depth varied from 20 cm to 200 cm, at 10 cm increments. The soil column was evenly divided into 2 to 10 layers for each depth setting. The upper boundary was controlled by a pulse rain condition. There was no rain for the first 5 days, followed by 2 cm/day of rain over the next 5 days, and then rain ceased for 5 days, followed by rain condition for 5 days, and so on. The pulse rain condition lasted for 50 days. Free-drainage (Eq. 25) and zero-pressure bottom boundary conditions were considered in this test. The initial conditions for three soil textures were set to the moisture content at field capacity ($-33\ kPa$). The results were compared with those from HYDRUS as reference. Because HYDRUS solves RE at multiple discretized nodes, estimation of averaged moisture content for each soil layer was obtained by averaging moisture contents over all nodes within that layer. After calculating the moisture content of each layer using each soil configuration from LARE and HYDRUS, we calculated the time series of averaged moisture contents of all layers

from the two models. The time series of moisture content averaged over the layers were used to calculate root mean square error (*RMSE*) for evaluation of model performance.

The heatmaps of *RMSE* values obtained between LARE and HYDRUS for different soil depth and soil layer configurations are shown in Figure 4.3. With free-drainage bottom boundary condition, *RMSE* values were below 0.01 for most of the simulations. There was a decreasing trend of *RMSE* with the increase of soil depth for three soil textures. Thin soil profiles (about 20 to 30 cm) tended to have relatively higher *RMSE* regardless of the number of layers. For loam and clay loam, the number of layers had little influence on model performance, since contour lines of *RMSE* showed vertical patterns. For sand, when the total soil depth was smaller than 80 cm, *RMSE* showed similar vertical patterns. However, for depths greater than 80 cm, model performance increased with increased number of layers. When the water table was at the bottom of the soil domain, sand showed the highest overall *RMSE* among other soil textures. For sand, deep soil with fewer layers tended to have high *RMSE*, while *RMSE* values dropped when more layers were added. The highest *RMSE* was found to be 0.043 for 200 cm soil profile with only two layers, while the lowest value was 0.002 for 20 cm soil with 10 layers. Same patterns were found for loam and clay loam such that deep soils with few layers had higher *RMSE* values than those with more soil layers. However, *RMSE* values from loam and clay loam were much lower than those from sand.

3.3. Scenario 3: Constant Infiltration into Stratified Soil Profiles with Two Dry Initial Conditions

The third case was water infiltrating into stratified soil. Following Hills et al. (1989), the model domain was a 1-meter heterogeneous soil column with 5 layers. Each layer was 20 cm in thickness. The first, third, and fifth layers were filled with loamy fine sand, and the second and the

fourth layer were filled with silty clay loam as listed in Table 4.1. A constant infiltration rate of 2 cm/day was specified at the soil top. Free-drainage bottom boundary condition was applied at soil bottom. Two initial conditions were applied, one with dry initial capillary pressure of 1000 cm and another with very dry initial capillary pressure of 10,000 cm. Δz of 4 cm and 10 cm were used to discretize soil profile in both LARE and HYDRUS. Besides, for consistency in comparing different models, the same temporal discretization, time adaptive algorithm, and convergence criterion were applied in two models.

Soil moisture profiles obtained from LARE and HYDRUS with infiltration into stratified soil discretized by Δz=4 cm and Δz=10 cm at t=5 days with two initial conditions were compared with those from Hills et al. (1989), who applied finite difference numerical scheme of RE, as shown in Figure 4.4. For fine discretization scheme, with $h_0 = -1000$ cm, results from LARE and HYDRUS were almost identical (Figure 4.4A). They all agreed very well with the results from Hills et al. (1989). Notice that moisture contents of the first, third, and last layers were much lower than the second and the fourth layers. LARE captured these sharp turning points on the moisture profile at the interface of different soil textures. Excellent agreement between LARE results and reference was observed with very dry initial soil profile ($h_0 = -10000$ cm). Small difference was noticed between HYDRUS and reference at the fourth layer, where the wetting front was located at t= 5 day. LARE correctly captured the movement of the wetting front. For the coarse spatial discretization scheme (Δz=10 cm), moisture profiles from LARE and HYDRUS were almost identical. However, compared with the 10 cm-averaged moisture profile of the results from Hills et al. (1989), outputs from two models showed some discrepancies for both initial conditions (Figure 4.4C and D). These differences were shown around the interface between two distinct soil textures (e.g. 40 cm and 60 cm).

3.4. Scenario 4: Dynamic Rainfall and Transpiration on Stratified Soils with Changing Shallow Ground Water Level

The fourth scenario was dynamic rainfall and transpiration on a stratified soil column with changing groundwater level in a wetland area. The purpose was to evaluate the performance of LARE with dynamic shallow groundwater level and the estimation of plant water uptake in layered soils. In this case, a numerical experiment was performed in a restored wetland located on Kent Island, Maryland. The wetland hydrological components such as inflow, outflow, precipitation, potential evapotranspiration, and average surface water level were collected by Jordan et al. (2003) from June 29, 1995 to September 30, 1995 for 94 days. Detailed information on data collection and analysis can be found in Jordan et al. (2003) and Kalin et al. (2013). The simulation was conducted in the variably saturated soil (the bank of the wetland) upgradient from the ponded part of the wetland. The total depth of the soil domain was set to 60 cm. We assumed that the groundwater was at the same level as the surface water in the wetland. During the data sampling period, the groundwater level varied between 45 cm and 55 cm of the depth from the soil surface according to the measurements of average water table level. Input data of groundwater level, precipitation, and potential evapotranspiration are shown in Figure 4.5. Soil texture data including soil separates of sand, silt, and clay, bulk density of each soil horizon were obtained from Web Soil Survey (Soil Survey Staff). There were three soil horizons within the 60 cm soil profile, each having about 20 cm thickness. The Van Genuchten soil hydraulic parameters were calculated by the ROSETTA3 model developed by Zhang and Schaap (2017). The soil physical and hydraulic properties are shown in Table 4.2. We divided the three horizons into five layers for model simulation, which were 5 cm, 5 cm, 10 cm, 20 cm, and 20 cm, respectively. Because soil moisture

was not measured, HYDRUS was applied as reference for results comparison. We only tested plant water uptake here and soil evaporation was not considered because the way LARE estimates soil evaporation is different than in HYDRUS. Whigham et al. (2002) reported that the most dominant macrophyte species in the wetland were blunt spikerush (*Eleocharis obtuse* (Willd.) Schult.), water-purslane (*Ludwigia palustris* (L.) Elliott), and American bulrush (*Schoenoplectus americanus* (Pers.) Volkart ex Schinz & R. Keller). The maximum rooting depth of these plant species was about 20 cm. The parameters for the root-water uptake water stress response functions for these wetland macrophyte species have not been reported in any literature. We borrowed the water stress function from Xu et al. (2016), who used the S-shaped model developed by Van Genuchten (1987) to evaluate the plant water uptake in a floodplain wetland. We modified the S-shaped model to fit $\beta(\psi)$ in Eq. (31). The parameters in $\beta(\psi)$ were set to: ψ_a=0 cm, ψ_b=10 cm, ψ_c=350 cm, ψ_d= 4000 cm. The bottom boundary condition was zero-pressure with variable water table depth (Eq. 30). Default spatial discretization of 101 nodes was applied in HYDRUS to get accurate estimations, while in LARE, five soil layers were used. Two models were run for two days as a warm-up with the initial moisture contents of each soil texture equaled to the values at field capacity. Simulations were then carried out for the period from July 1 to September 30 by setting the initial moisture contents equaled to the outputs from the warm-up period. The model was evaluated by *RMSE* and Nash Sutcliffe efficiency (*NSE*) calculated between outputs of moisture contents and actual transpiration rate from LARE and HYDRUS.

Simulation results of moisture contents for five soil layers and estimated actual transpiration rate from LARE and HYDRUS are shown in Figure 4.6. The performance indices of *RMSE* and *NSE* are shown in Table 4.3. As shown in Figure 4.6 (A), results from LARE matched well with those from HYDRUS. The *RMSE* values for all layers were below 0.0004. *NSE* values

were greater than 0.92 for the first three layers, while they were 0.854 and 0.882 for the fourth and the fifth layer, respectively. During the simulation period, due to the influence of the groundwater level, moisture contents of all five layers were close to saturation but showed some variations corresponding to variations of precipitation and positions of the water table. Soil moisture contents were decreasing with the decrease of water level and vice versa. The spikes in soil moisture values were in response to precipitation. Estimated plant water uptake from LARE and HYDRUS were almost identical as shown in Figure 4.6 (B).

3.5. Scenario 5: Field Scale Application

The last testing case was the application of LARE at field scale. We applied LARE to a Soil Climate Analysis Network (SCAN) site in Mason, Illinois (SCAN site ID: 2004). The site is located at $40°19'$ N and $89°54'$ W at an elevation of 174 meters above mean sea level. Soil moisture, soil physical properties data for each soil horizon along with meteorology data were provided by SCAN dataset at hourly and daily time interval (Schaefer et al., 2007). Soil moisture sensors were installed at five soil depths, which were 5 cm, 10 cm, 20 cm, 50 cm, and 100 cm. Data were collected from April 21st to October 31st, 2018 and April 21st to September 21st, 2019 to avoid the winter period with air temperature below zero and missing data. Data from 2018 were used for model calibration and data from 2019 were used for model validation. The weather station located at the study site provides meteorological data including daily precipitation, maximum and minimum air temperature, relative humidity, solar radiation, wind speed, and air pressure.FAO-56 Penman-Monteith method (Allen et al., 1998) was applied to calculate daily potential evapotranspiration (ET) rate. Figure 4.7 shows the precipitation and potential evapotranspiration applied for 2018 and 2019. The numerical soil domain was set to 120 cm in depth with five layers

that covered 5 soil moisture sensors. The first four layers had 20 cm thickness, and the thickness of the last layer was 40 cm. At the study site, there were five soil horizons from 0 cm to 126 cm. We calculated the physical properties of each soil layer by weighted average according to the portion of the soil horizon within each layer. Soil hydraulic parameters for the van Genuchten model were calculated by ROSETTA3. The soil texture for the first layer was loamy sand and it was sandy loam for the next four layers. The top three layers had high permeability (K_s varied from 80 cm/day to 130 cm/day), while the bottom two layers had relatively low conductivity (K_s≈20 cm/day). According to the Web Soil Survey, the groundwater level at the sites was below 80 feet (24.38 meters), which is deep enough for free-drainage bottom boundary condition at depth 120 cm. The upper boundary was controlled by atmospheric conditions using observed precipitation and calculated potential evapotranspiration (PET) rate. Potential evaporation and potential transpiration rate were calculated by partitioning of PET by an area index (f_s). The area index represents the fraction of bare ground at the site and $1 - f_s$ is the fraction of area covered by vegetation. PET $\times f_s$ is the potential bare soil evaporation rate and PET $\times (1 - f_s)$ is potential plant transpiration rate. At the sites, weather station and soil moisture sampling point were located at the area covered by grass or natural fallow for most of the time (Albergel et al., 2015). However, the area covered by grass was unknown. The area index (f_s) was calibrated in model calibration step to determine the fraction of bare soil and vegetation cover. In addition, the root depth of the grass was unknown. We assumed that the grass roots were dispersed anywhere between the first and the fourth layer (20 cm to 80 cm) in the soil profile. We introduced a root position index (f_r) that can take values of 1, 2, 3, and 4 to determine the position of the root in the top four layers. For example, if $f_r = 3$, the root is located in the top three layers. The model was run with Δt of 0.001 day for the simulation period. The soil moisture observations were measured at discrete points

along soil profile. To make observations comparable with model outputs, we interpolated observation data along 100 cm soil depth using measured data and then calculated layer averaged moisture content for each layer from interpolated observation data. The initial conditions for five soil layers were set to the moisture contents equaled to those from observation data on the first day of simulation. Data from 2018 were used for model calibration and those from 2019 were used for model validation. The first 10 days from April 21st to April 30th were model warm-up period. Results of the model estimated moisture contents for five soil layers were compared with observations starting from May 1st.

We consider van Genuchten parameters for five soil layers (α_i, n_i, θ_{res_i}, θ_{sat_i}, K_{s_i}, where *i* denotes layer number), area index (f_s) and root position index (f_r) as calibration parameters for which $\boldsymbol{\Theta} = (\alpha_i, n_i, \theta_{res_i}, \theta_{sat_i}, K_{s_i}, f_s, f_r)$. The prior distributions of van Genuchten parameters for each soil layer were defined as $p(x) \sim U(a_x, b_x)$, where a_x and b_x are lower and upper bounds, respectively. The values of a_x and $b_x$were calculated by $\pm 4\sigma$, where γ is ROSETTA predicted values, and σ is the standard deviations of the predicted parameters. The prior distributions of van Genuchten hydraulic parameters for five layers are shown in Table 4.4. The prior distribution of area index (f_s) and root position index (f_r) were defined as $p(f_s) \sim U(0,1)$ and $f_r = \{1, 2, 3, 4\}$, respectively. During the Monte Carlo simulations, 100,000 parameter sets were generated by randomly drawing values from their prior distributions. Model performance was evaluated by *RMSE* and *NSE* calculated between observed and model predicted moisture content of each layer.

Figure 4.8 shows the model calibration results for Bayesian estimates, 95% confidence interval, and observed soil moisture contents of five soil layers in 2018. LARE captured the variations of soil moisture by the influence of precipitation and evapotranspiration. Almost all observation data fell within the 95% confidence bounds. *RMSE* and *NSE* calculated between

Bayesian estimations and observations are also shown in Figure 4.8. LARE showed excellent performance in the model calibration. *RMSE* values were lower than 0.019 cm^3/cm^3 and *NSE* values were higher than 0.61 for 5 layers. The lowest *RMSE* was found to be 0.014 cm^3/cm^3 for layer 2, while the highest *RMSE* was 0.019 cm^3/cm^3 for layer 3. The *NSE* showed the highest value as 0.847 for layer 2 and the lowest value was 0.610 for layer 4. From the middle of July to the middle of August 2018, there was a dry period. Soil moisture stayed low in all layers during this period. Moisture observations of layer 1 showed variations in response to precipitation but lower layers did not show any response to precipitation. Precipitation in this period was consumed by the first layer by plant water uptake and surface evaporation. The lower layers contributed to plant roots uptake during the dry season indicated by the decreasing trend of observed moisture contents for layers 3 to 5 shown in Figure 4.8. The results from LARE showed this moisture variations in dry period. Bosch (2004) reported that the accuracy of the soil moisture probe (Hydro Probe) used by SCAN dataset was within 0.04 $cm^3\ cm^{-3}$. LARE predicted moisture contents showed smaller error than the accuracy of the moisture sensors for five layers. LARE did a decent job in predicting moisture contents for layered soils during model calibration.

The results of BMC predicted moisture contents along with the 95% confidence bounds and observed soil moisture contents for five soil layers for the validation period are shown in Figure 4.9. The soil variability and magnitude of moisture contents for all layers are adequately captured by the BMC estimates compared with observed soil moisture contents. During the dry period from July to August, not only the first layer showed drying trend with observation, but the deeper four layers also matched with observations, exhibiting a gradually decreasing trend. Model performance increased from layer 1 to layer 4 but dropped at layer 5. *RMSE* from the first four layers were all below 0.012 cm^3/cm^3 with the lowest value of 0.008 cm^3/cm^3 found for layer 4,

while *RMSE* was highest in layer 5 with the value of 0.020 cm^3/cm^3. *NSE* values were higher than 0.89 for all five layers with the highest value of 0.979 found in layer 4, whereas layer 5 had the lowest *NSE* value at 0.898.

We also investigated the model uncertainties. The detailed procedures of investigating model uncertainties can be found in Chaudhary and Hantush (2017), Hantush and Chaudhary (2014), and He et al. (2021). The BMC methodology assumes $\varepsilon \sim N(0, \sigma_\varepsilon^2)$, where ε is model residual error and σ_ε^2 is the residual error variance, which accounts for measurement, model structural errors and uncertainty in the forcing input hydroclimate data. The Bayesian estimated σ_ε^2 for the five layers are showed in Table 4.5. The second layer had the highest σ_ε^2 of 1.97×10^{-4}, while the fourth layer had the lowest value of σ_ε^2 of 1.60×10^{-5}. We further investigated model predictive uncertainty (σ^2). σ^2 accounts all sources of errors (parametric, observational, hydroclimate data, and ε). As shown in Table 4.5, the highest model predictive uncertainty was found in the fifth layer (3.27×10^{-3}), while the lowest value was found in the first layer (6.96×10^{-4}). The ratio $\sigma_\varepsilon^2 / \sigma^2$ for five layers were 96%, 81%, 98%, 98%, and 98%, respectively. These indicate that much of the modeling uncertainty was caused by errors in model structure, observed soil moisture and forcing data. Moreover, we investigated the parameters uncertainty (σ_Θ^2) for five soil layers (Table 4.5). We found that the parameters uncertainty contributed very little to the whole model prediction uncertainty, which were about 3%, 18%, 1%, 1%, and 1% for the five layers, respectively. The findings in uncertainty analysis indicate that much of the uncertainty is attributed to observational, forcing data, and model structural errors, while parameters' uncertainty contributed very little to the overall model uncertainty.

4. Discussion

Based on the illustrative examples, the multiple layer-averaged solution to RE has shown its robustness for the following reasons:

First, LARE produces relatively accurate layer-averaged moisture contents for multiple soil layers with various thicknesses for different environmental conditions. The solution accounts for changing upper boundary conditions including precipitation, soil evaporation, and plant transpiration. The proposed solution also deals with dynamic groundwater table within and below the soil domain by switching the bottom boundary conditions internally during iterations based on the location of groundwater level. The first-order approximations of matric gradient and hydraulic conductivity at the soil interface deal with water flux between soil layers properly.

Second, the numerical scheme of LARE uses the similar integrated form of RE applied in finite volume scheme (Eq. 4). However, the solution of LARE is different than other numerical methods. LARE considers the finite-differences approximation of layer-integrated values as opposed to nodal values (or centered values) in finite differences and finite element method. Besides, LARE transforms PDEs to ODEs and solves these using the relatively simple Huen's method. Moreover, the algorithms we proposed for the derivations of interfacial matric gradient and conductivity are different from those in finite volume and finite difference schemes. Unlike other numerical schemes, which adopt differential form of matric gradient and different methods for calculation of interface hydraulic conductivity, LARE calculates the interfacial matric gradient and conductivity directly from adjacent soil layers (or control volumes) using their capillary pressure, unsaturated conductivity, and thickness using first-order Taylor series expansion of the moisture content integrated over the layer, rather than the point value. In addition, there are many methods to calculate interface hydraulic conductivity such as arithmetic mean (Douglas Jr et al., 1959), geometric mean (Bouwer, 1969), upstream mean (Brutsaert, 1971), harmonic mean

(Chaudhari, 1971), etc. The selection of averaging method can significantly affect the performance of the numerical solution, especially with varying grid size (Belfort and Lehmann, 2005; Caviedes-Voullième et al., 2013b). The averaging approach for calculating interface hydraulic conductivity applied in LARE is based on fundamental calculus and provides accurate results with consideration of different layer thickness without the need for finding the optimal method for interface hydraulic conductivity. Note that if soil layers are evenly spaced in the model domain, Eq. (11) becomes $K(h_m, \mathrm{t}) = 0.5(\overline{K}_m + \overline{K}_{m+1})$, which is exactly the arithmetic mean. Besides, the averaging method in LARE deals with discontinuity of hydraulic conductivity appropriately. One of the cases related to discontinuity is the sharp wetting front. Generally, the sharp wetting problem is often solved by changing spatial configuration such as fine mesh to the entire soil column or adaptive mesh at the depth where wetting front is located, and temporal settings such as decreasing Δt or increasing iterations in every time step. LARE captured the movement of sharp wetting front skillfully and seamlessly when water infiltrates into dry soil with both thin and thick layer thickness without additional numerical adjustments (Figure 4.4B and D). Furthermore, no convergence issue was observed in five simulation scenarios, hence, indicating a numerically stable solution. Additionally, this approach simplifies the numerical complexity and permits elegant coding.

Third, with the proposed method for estimation of interfacial matric gradient and hydraulic conductivity, soil layer configurations with different thicknesses and textures can be considered in the modeling approach rather than fine grid size applied in finite volume or finite difference schemes. Besides, with no issues with convergence so far, the thickness of each layer can be set up arbitrarily without the implementation of additional model algorithms such as grid refinement. With this feature, soil stratification can be correctly addressed. The numerical soil domain can be

discretized by soil textures or horizons. Thus, each soil layer is treated as homogeneous. Extra calculations (such as averaging soil texture to calculate soil hydraulic parameters) become unnecessary. Moreover, relatively accurate estimations of moisture contents in certain layers of interests can be obtained. In LSMs, the exponential grid is often applied as default, which uses fine grid size near the surface to track soil moisture variation for partitioning of rainfall and energy, and coarse grid at lower soil to decrease computational burden (Downer and Ogden, 2004a). LARE further simplified this procedure. With appropriate layer setup for specific depth of soil domain and soil texture, LARE can yield accurate soil moisture estimations with low computational cost.

Last, the layer-averaged RE converted the partial differential equation of RE into coupled ordinary differential equations (Eq. 4). The coupled governing equations are solved by simple explicit Heun's method. This reduces the computational complexity. The solution further couples with time adaptive algorithm. This algorithm adjusts delta t for the next time step based on the convergence performance (number of iterations) in the current time step during the iterations, which optimizes the computational time. Compared to the complete implicit numerical scheme applied in HYDRUS, computational time (CPU time) in LARE was 5 to 10 times faster than that from HYDRUS based on the numerical simulations in testing scenarios 2 to 4. Numerical solution converged in less than 3 iterations for each time step for most of the time (not shown in this work). With homogeneous soil profile, under steady rainfall or no rain condition, Δt often switched to the maximum value predefined as model input, because the solution during each time step tended to converge fast. On the other hand, in heterogeneous soil and initially dry soil, smaller Δt was used at the beginning of the simulation to track the sharp changes in moisture content. In addition, although LARE scheme is numerically stable; no convergence problem was found in any of the testing scenarios.

5. Summary and Conclusions

In this study, we proposed a numerical scheme of layer-averaged Richards equation, named LARE. LARE was an extension of the solution of the two-layer approximation of RE developed for wetlands and larger-scale hydrologic simulations to multiple soil layers. The solution of LARE converted the partial differential equation of RE into multiple coupled ordinary differential equations derived from the integrated form of RE. Several coupled governing equations are solved by explicit Heun's method to describe layer averaged soil moisture contents for multiple soil layers. The proposed model is designed for simulating soil moisture dynamics in layered or stratified soils under various atmospheric conditions and with bottom boundary condition that is suited for deep or shallow fluctuating water table.

Four numerical experiments and one site level application were conducted to evaluate LARE. LARE performance was compared against analytical solutions, finite element RE solution by HYDRUS 1-D, and field-scale soil moisture observations from SCAN dataset. The results showed that LARE has the capability to simulate soil moisture in both homogeneous and heterogeneous soil profiles with either fine or coarse grids, for different upper and lower boundary conditions. LARE showed excellent performance with free drainage bottom boundary condition for various soil depth and layer thicknesses, while the model performance dropped for deep soil profiles with fewer layers (i.e., coarser spatial discretization) for zero-pressure head bottom boundary condition. Besides, LARE perfectly estimated layer-averaged soil moisture contents with dynamic shallow groundwater level within the soil column without any convergence issues. With the correct soil moisture prediction, the actual plant water uptake was properly estimated. At site level application, LARE showed good performance under real soil and atmospheric conditions.

The uncertainty analysis showed that the observational, hydroclimate data, and model structural uncertainties contributed to much of the uncertainty, while parametric uncertainty was found to be very small. From the numerical tests, the proposed solution is numerically stable and found to be computationally efficient for different infiltration scenarios, soil initial conditions, soil textures, and layer configurations. LARE is suitable for modeling soil moisture movement at both field and watershed scale, and it can potentially be used in large scale LSMs for land-atmosphere coupling simulations.

Table 4.1: Van Genuchten soil hydraulic properties for soil textures applied in numerical experiments 1, 2 and 3

Soil textures	α (cm^{-1})	n_{VG}	θ_{res}	θ_{sat}	K_{sat} (cm/d)
Berino loamy fine sand	0.0280	2.2390	0.0286	0.3658	541.0
Glendale silty clay loam	0.0104	1.3954	0.1060	0.4686	13.1
Sand	0.145	2.68	0.045	0.43	712.8
Loam	0.036	1.56	0.078	0.43	24.96
Clay loam	0.019	1.31	0.095	0.41	6.24

Table 4.2: Soil layer physical and van Genuchten hydraulic properties applied in numerical experiment 4

Depth	Sand (%)	Silt (%)	Clay (%)	BD (g cm^{-1})	α (cm^{-1})	n_{VG}	θ_{res}	θ_{sat}	k_s (cm day^{-1})
0-20	17	71	12	1.4925	0.0043	1.5219	0.0713	0.3879	18.40
20-40	16	70	14	1.47	0.0042	1.5171	0.0745	0.3947	17.87
40-60	15	63	22	1.6375	0.0049	1.3951	0.0884	0.3649	4.62

Table 4.3: Performance of LARE against HYDRUS in testing numerical experiment 4

	Layer 1	Layer 2	Layer 3	Layer 4	Layer 5	Transpiration
RMSE	0.0004	0.0003	0.0003	0.0003	0.0001	0.0001
NSE	0.928	0.940	0.926	0.854	0.882	1.000

Table 4.4: Upper and lower bounds of prior distributions of Van Genuchten soil hydraulic parameters applied for BMC in site-level model application

Layer	Bound	α (cm^{-1})	n	θ_{res}	θ_{sat}	K_s (cm/day)
1	Lower	0.0237	1.6239	0.0010	0.2868	117.6
	Upper	0.0274	1.8544	0.1043	0.3484	134.3
2	Lower	0.0212	1.4944	0.0117	0.2989	79. 1
	Upper	0.0254	1.7125	0.0898	0.3764	90.3
3	Lower	0.0089	1.000	0.0010	0.2000	33.7
	Upper	0.0569	3.7063	0.1500	0.7138	177.9
4	Lower	0.0113	1.2108	0.0010	0.2682	17.2
	Upper	0.0177	1.5641	0.2054	0.4749	22
5	Lower	0.0070	1.000	0.0010	0.2000	8.4
	Upper	0.0353	3.6109	0.1500	0.7119	52.1

Table 4.5: Bayesian estimates of modeling uncertainty for five soil layers

Layer	σ^2	σ_ε^2	σ_Θ^2
1	7.21×10^{-4}	1.93×10^{-5} (3%)	6.96×10^{-4} (96%)
2	1.09×10^{-3}	1.97×10^{-4} (18%)	8.88×10^{-4} (81%)
3	2.58×10^{-3}	1.93×10^{-5} (1%)	2.54×10^{-3} (98%)
4	2.66×10^{-3}	1.60×10^{-5} (1%)	2.62×10^{-3} (98%)
5	3.34×10^{-3}	3.70×10^{-5} (1%)	3.27×10^{-3} (98%)

Note: σ^2 accounts for total model prediction uncertainty, σ_ε^2 accounts for measurement, model structural errors and uncertainty in the forcing data, and σ_Θ^2 accounts for parameters uncertainty. Numbers in the parentheses are values normalized with total model prediction uncertainty.

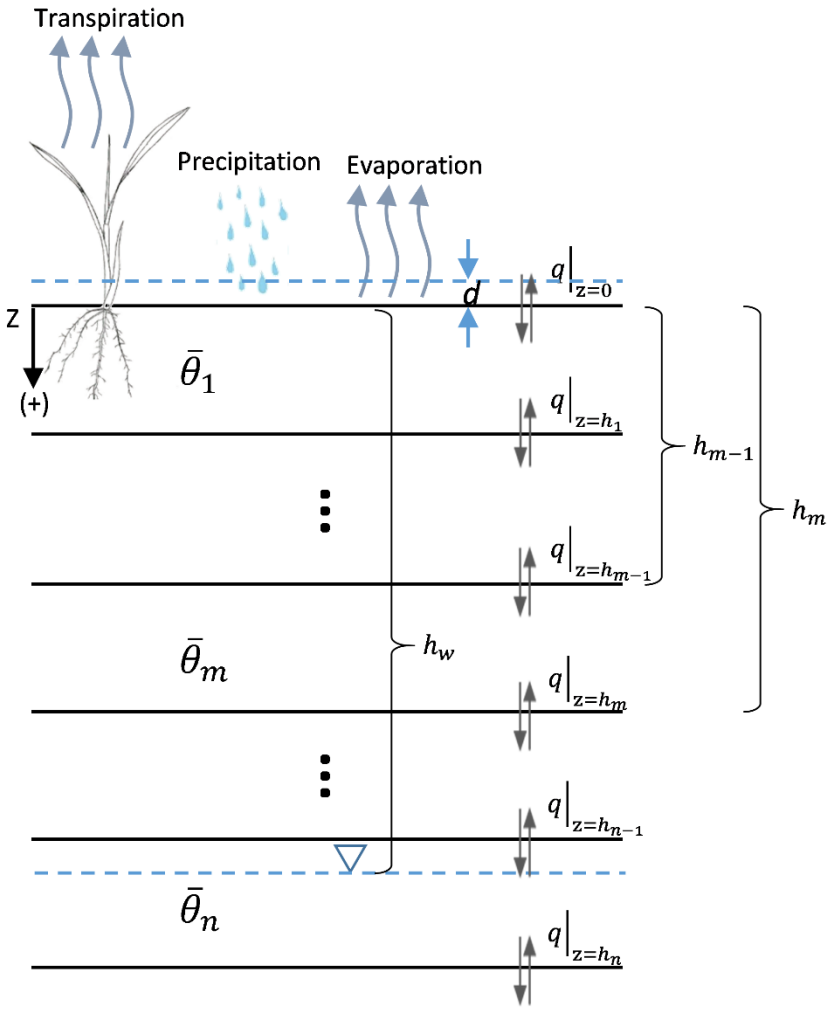

Figure 4.1: Schematic of soil profile for layer-averaged solution to Richards equation (where d is the ponding depth [L]; $\bar{\theta}_m$ is average soil moisture content of the m^{th} layer [-]; h_m is the depth of the m^{th} layer [L]; h_w is groundwater depth [L]; q_0 is the top flux (positive downward) [LT^{-1}]; q_m is the flux at the bottom of the m^{th} layer [LT^{-1}])

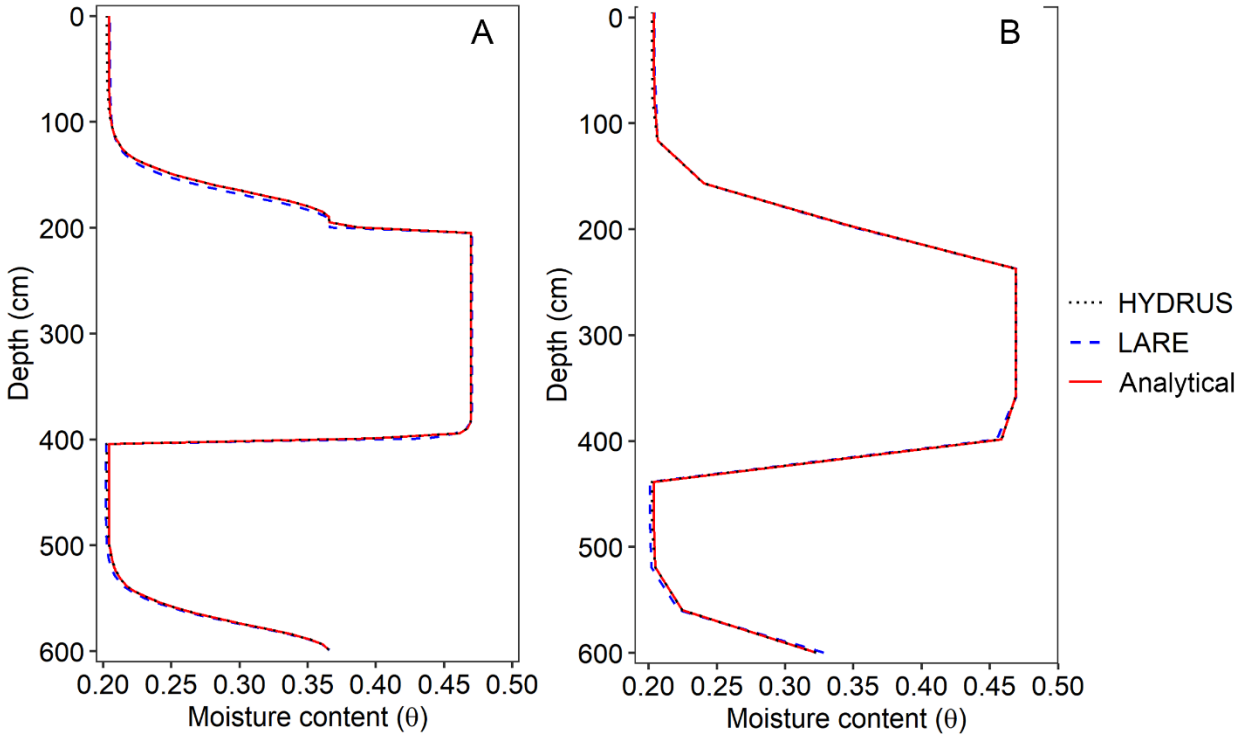

Figure 4.2: Soil moisture profile at steady state with steady infiltration into layered soil in numerical experiment 1 (Analytical solution was proposed by Rockhold et al. (1997)). A and B represent soil moisture contents calculated by LARE using $\Delta z = 5$ cm and $\Delta z = 40$ cm, respectively.

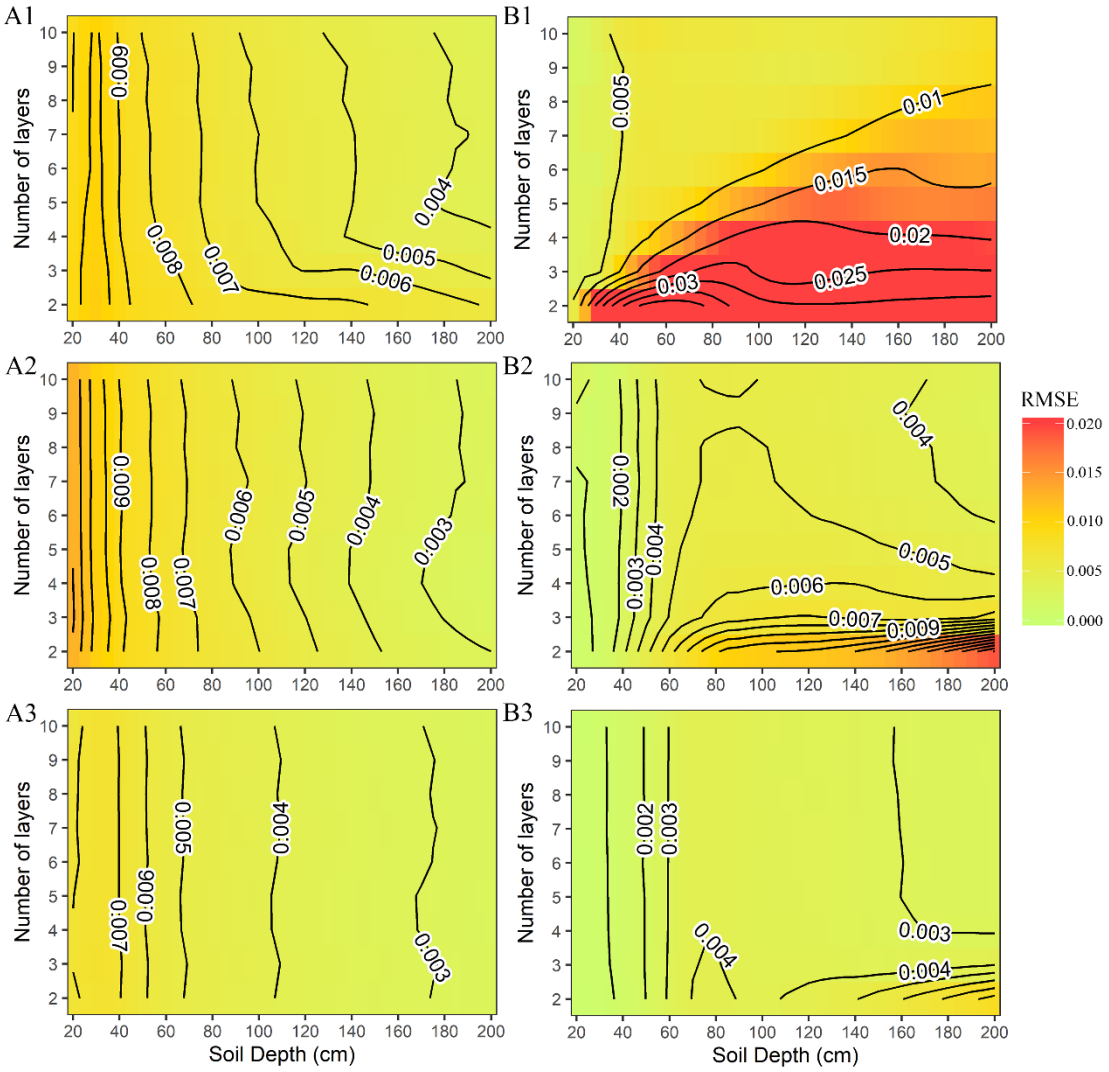

Figure 4.3: Contour plots and heat maps of *RMSE* values with different layer depth and number of layers for 1) sand, 2) loam and 3) clay loam with A) free-drainage and B) zero-pressure head bottom boundary conditions under pulse rain top boundary condition in numerical experiment 2

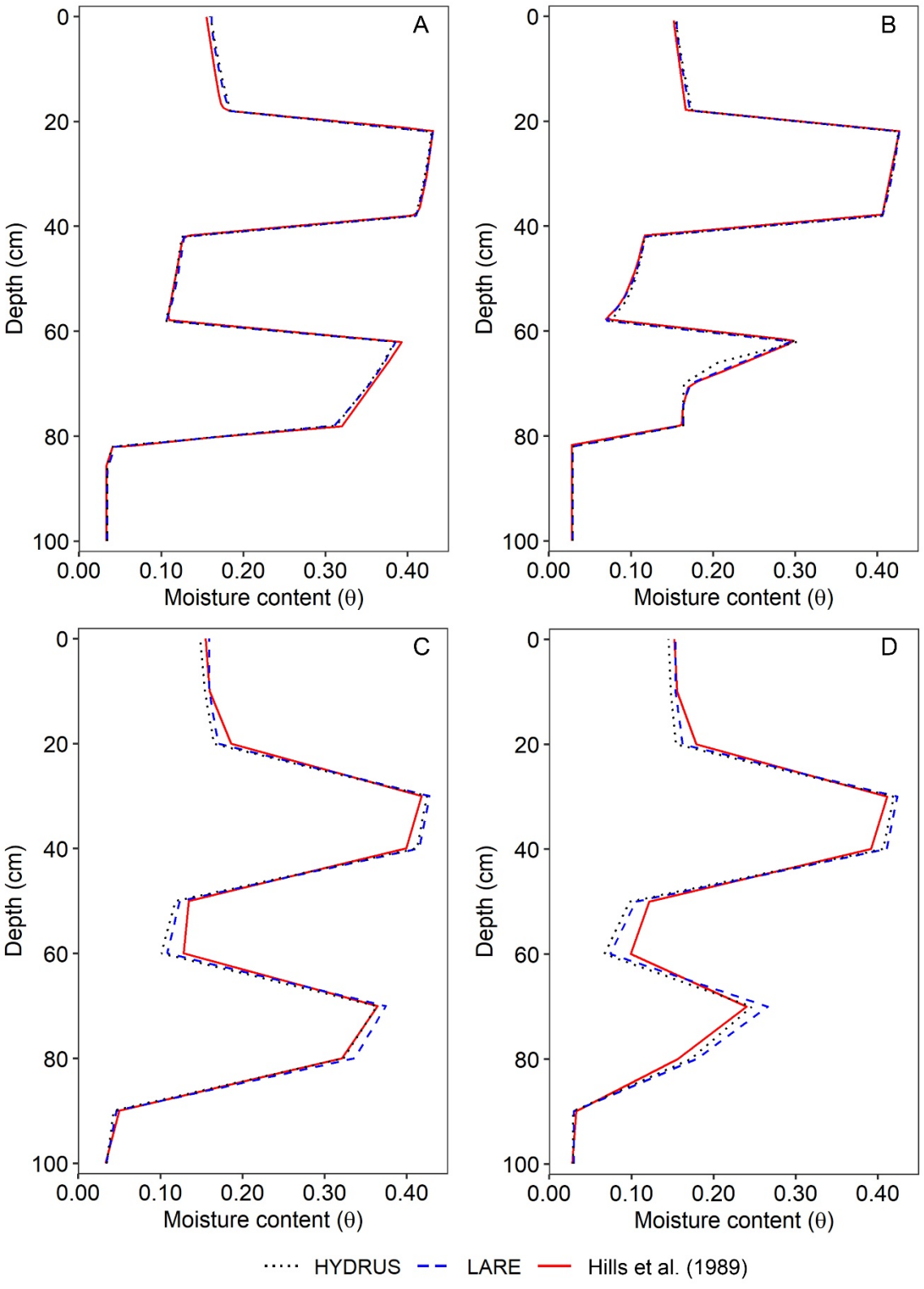

Figure 4.4: Soil moisture profiles for infiltration into heterogeneous soil column in numerical experiment 3 using Δz=4 cm (A and B) and Δz=10 cm (C and D) when t=5 days with initially dry soils (A and C) and very dry soils (B and D)

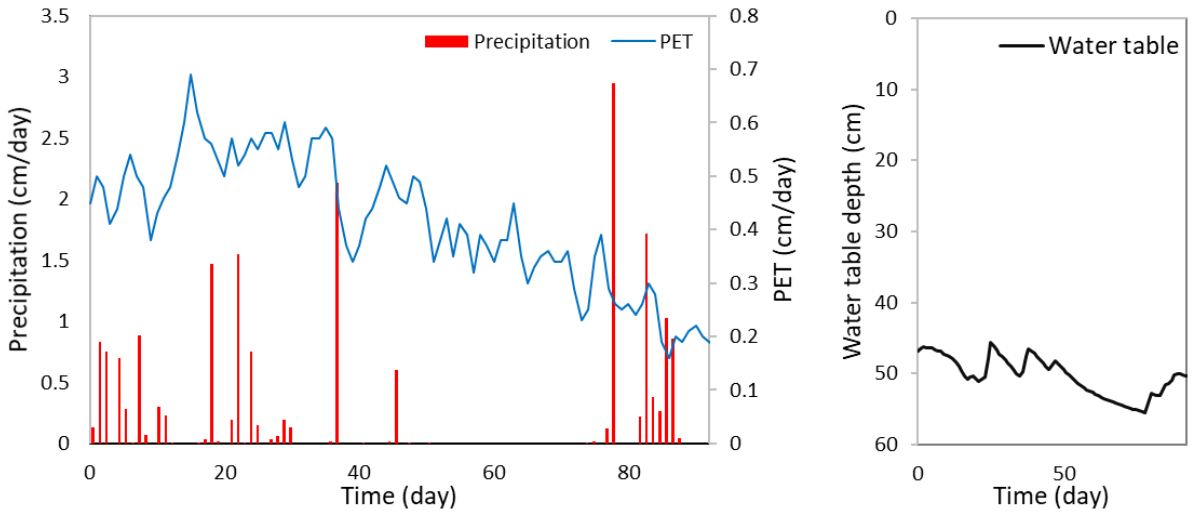

Figure 4.5: Precipitation rate, potential evapotranspiration rate and groundwater level for numerical experiment 4 (day 0 represents June 29, 1995)

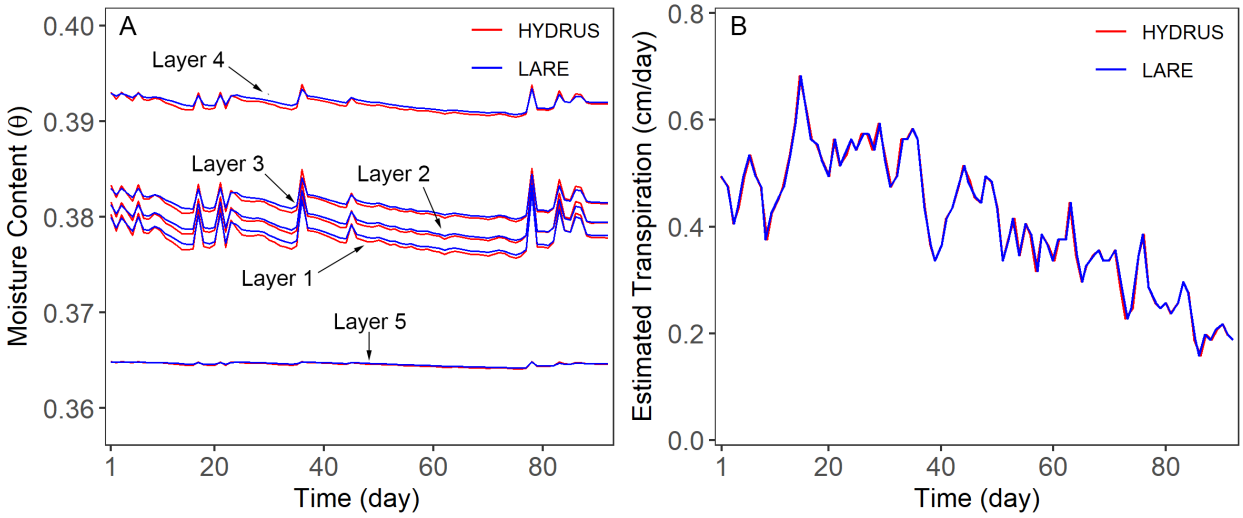

Figure 4.6: A) Moisture contents for 5 soil layers with shallow water table, and B) estimated transpiration rate between LARE and HYDRUS (day 1 represents May 1, 1995) from numerical experiment 4

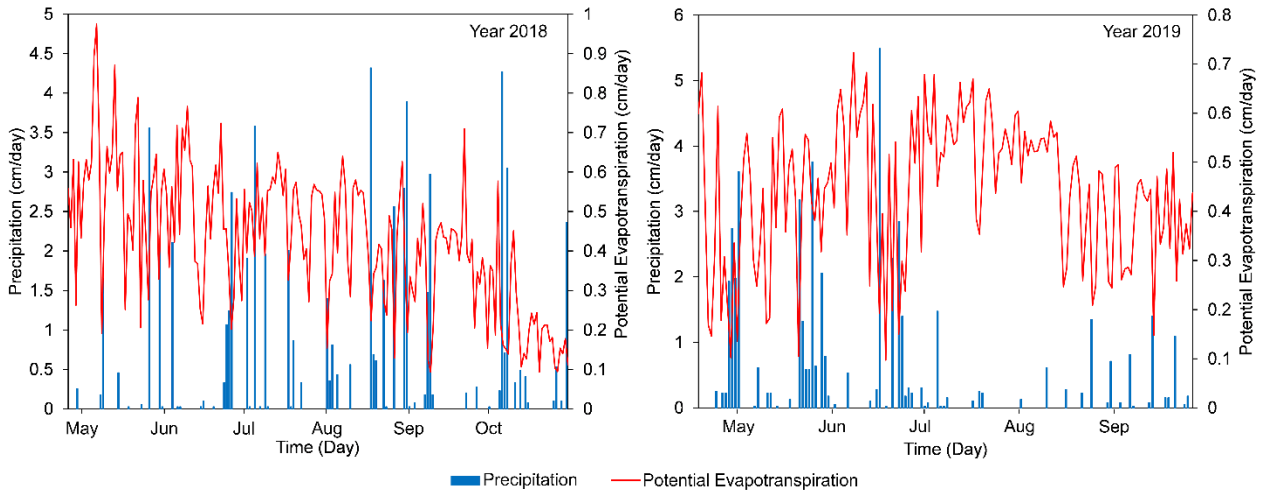

Figure 4.7: Precipitation and potential evapotranspiration rate at SCAN site Mason, Illinois applied in the model application scenario for model calibration in 2018 and model validation in 2019

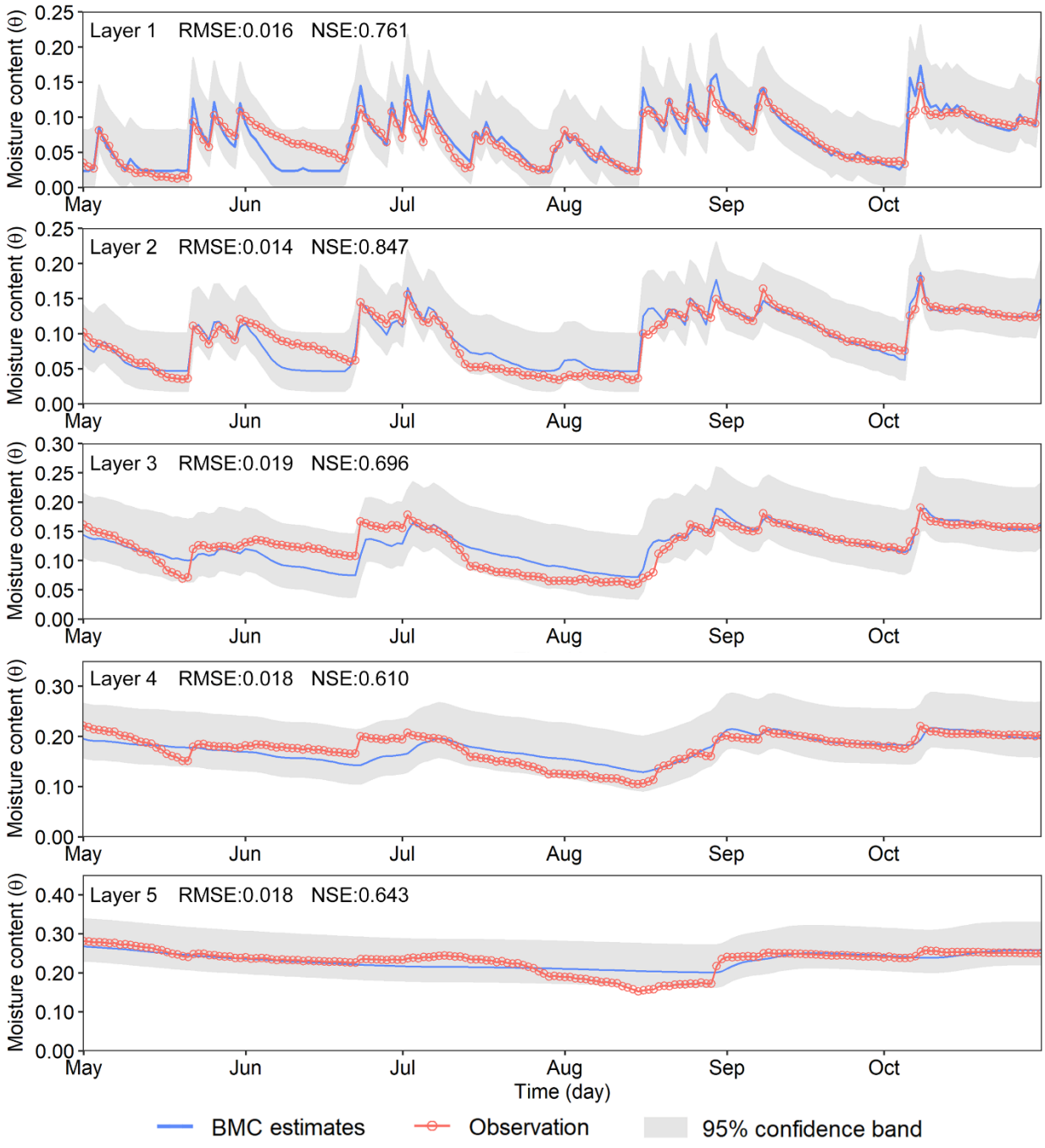

Figure 4.8: Model calibration results of BMC estimated and observations of moisture contents for five soil layers along with 95% confident intervals from May 1st to October 31st, 2018 in field-scale application scenario.

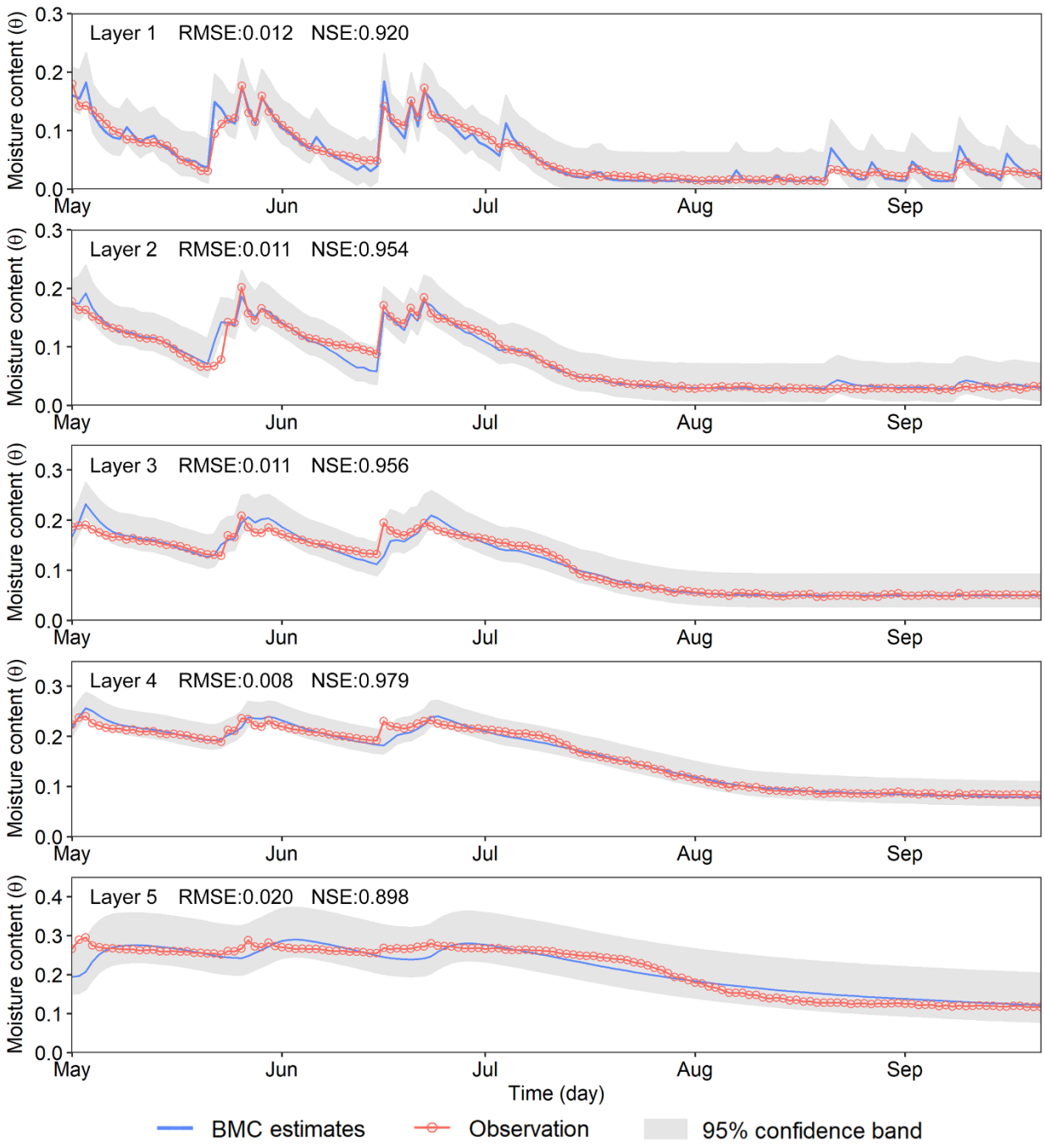

Figure 4.9: Model validation results of BMC estimated moisture contents for five soil layers along with 95% confident intervals from May 1st to Sep 21st, 2019 in field-scale application scenario.

Chapter 5: Modeling Nutrient Dynamics in Wetland Water and Variably Saturated Soils Using Wetland Model

Abstract

In this paper, the authors updated the soil moisture movement and plant growth modules in a process-based biogeochemical model *WetQual* for wetland nutrient cycling in the ponded and variably saturated compartments. The Updated model adopted a two-layer model developed by He et al. (2021a) to simulate soil moisture dynamics subjected to various atmospheric conditions at the soil surface and changing shallow groundwater level in the variably saturated compartment of the wetland. Plant water uptake was specified for plants in the wetland environment. The primary productivity module was modified to consider environmental factors including temperature stress, water stress, and plant dormancy. The updated model was evaluated by applying it to a restored wetland located on Kent Island, Maryland, USA, utilizing two numerical experiments using different bottom boundary conditions for moisture movement in the variably saturated compartment. The results showed that the model had excellent performance in estimating NO_3 and TOC loads and moderate performance in capturing ON, NH_4, and TN loads, but not as good in estimating TSS and P loads. The moisture contents in the variably saturated compartment had significant differences between the two bottom conditions. Besides, the use of the zero-pressure head and free-drainage bottom boundary conditions applied in the variably saturated compartment had significant influences on NH_4, TSS, and TOC exports but did not show influences on other nutrient constituents in the ponded compartment. Sensitivity analysis revealed that the parameters showed sensitivities in the ponded and variably saturated compartments more or less confirmed the sensitive parameters of the Original and the Expanded models, but the order of sensitivities

differed. Nevertheless, N, C, and P cycles did not show sensitivity to soil hydraulic parameters. The mass balance analysis showed that using different bottom boundary conditions for moisture flow in the variably saturated compartment had influences on N, C, and P budget. The model estimated biomass in the study wetland reflected the temperature and water stress in addition to the period of dormancy. The estimated plant biomass and nutrient uptake had good matches with field measurements. The modified equations for plant growth are capable of estimating plant biomass in wetland environments.

1. Introduction

Wetlands are defined as transitional areas between terrestrial and aquatic systems where the water table is usually at or near the surface or the land is covered by shallow water, and vegetation (also known as hydrophytes) are adapted to saturated soil conditions (Cowardin, 1979). Among different aquatic ecosystems, wetlands are important environments providing many ecosystem services such as water supply, flood storage, water quality protection and improvement, groundwater replenishment, biomass production, and habitats for aquatic animals and wildlife (Mitsch and Gosselink, 2000). Wetlands not only regulate global and regional climate through the exchange of water, heat, and energy with the atmosphere through evapotranspiration, but also they have impacts on the global biogeochemical cycle through greenhouse gas emission (Fan and Miguez-Macho, 2011; Russi et al., 2013).

Wetland hydrology is one of the most important factors driving the wetland ecosystem and describing the characteristics of the wetland. Wetlands with shallow topographical depressions situated between terrestrial and aquatic ecosystems results in complex hydrology in both spatial and temporal aspects. Wetlands can receive water from surface inflow, lateral flow, groundwater

discharge, and precipitation and lose water by outflow, groundwater recharge, and evapotranspiration. The water balance between inflow and outflow, known as a water budget, characterizes the hydrological signature of a wetland (Mitsch and Gosselink, 2000). The presence and duration of open water, known as a hydroperiod, have dynamic variations across different time scales. For example, the hydroperiod of tidal wetlands tends to change daily due to tidal movements (Montalto et al., 2006). Floodplain riparian wetlands have seasonal or annual hydroperiods with at least one dry and one wet phase (Ameli and Creed, 2017). Hydroperiod of prairie pothole wetlands can have daily, seasonal, or even interannual variations due to their geographic and climate conditions (Ewel and Myers, 1990). Isolated wetlands such as ephemeral wetlands can hold water for a few days or weeks, while water in semipermanent and permanent wetlands can stay for years (Baber et al., 2004). The water level in constructed wetlands is often managed at a certain level to maintain their function and has less variation over time (Kadlec and Wallace, 2008).

Wetland hydrology has strong influences on wetland structure, ecosystem functions, and biogeochemical cycles. Surface inflow transports sediments, nutrients, and contaminants to wetland, and further influences the biochemical condition. Water outflow flushes away biotic and abiotic materials. Inflow and outflow can modify the physicochemical environment of wetlands (Mitsch and Gosselink, 2000). Hydrology affects wetland biota by changing the physicochemical environment. Hydroperiod affects wetland size and species richness (Snodgrass et al., 2000). Water regime determines the plant community development and patterns of plant zonation in wetlands (Casanova and Brock, 2000). Also, wetland hydrology changes soil moisture content by partitioning soil into saturated and unsaturated parts as a result of water level fluctuation during different states of hydroperiods. Soil moisture regulates oxygen level in

wetland soils, which in turn has a significant impact on the microbial community structure and microbial activity, thereby changing nutrient availability during wet-dry phases (Reddy and DeLaune, 2008; Manzoni et al., 2012; Moyano et al., 2013; Chen et al., 2015; Limpert et al., 2020). In unsaturated conditions, soil moisture has a positive correlation with total microbial biomass and activity across biomes and climatic conditions (Brockett et al., 2012; Manzoni et al., 2012). Soil moisture is highly correlated with the decomposition rate of soil organic matters. The decomposition rate of soil organic material increases when soil moisture increases (Dan et al., 2016). However, when soil moisture is higher than a threshold or close to saturation, decomposition rate decreases (Murwira et al., 1990). In saturated soil condition, oxygen concentration is lower than that in unsaturated soils. Redox potential in wetland soils drops as oxygen level decreases. Consequently, wetland soil tends to become more reduced and biogeochemical processes change in response to such conditions.

Process-based models are useful tools to understand and investigate complex wetland biogeochemical processes. The *WetQual* model is a process-based numerical model that simulates hydrology and nitrogen, phosphorus, and carbon dynamics in wetlands (Hantush et al., 2013; Kalin et al., 2013; and Sharifi et al., 2013). The model accounts for nutrient dynamics in two basic wetland elements: free water and saturated soil below. The soil column is divided into aerobic and anaerobic layers to address different biogeochemical reaction rates based on oxygen availability in these two layers. In these two wetland elements, *WetQual* simulates nitrogen dynamics (including ammonification, nitrification, denitrification, and volatilization), phosphorus retention and release, and carbon cycle (including carbon storage, oxidation of carbon-related chemical species, and organic carbon export and retention). The model has been extended to account for dynamic soil moisture content in wetland soils around the ponding area with variably saturated

conditions (Sharifi et al., 2017). Nitrogen and carbon cycling was simulated in saturated and unsaturated soils separately. The biogeochemical transformation/exchanges between the ponded part and the surrounding variably saturated soils are also captured in the model (Sharifi et al., 2017). They reported that nitrogen loss due to denitrification in the variably saturated area was seven times higher than that in ponded part. Cycling of carbon-related constituents showed high sensitivity to soil moisture in the variably saturated compartment.

Sharifi et al., (2017) applied the finite difference numerical solution to Richards equation (RE) to simulate soil moisture dynamics in variably saturated soils around ponded areas of wetlands. The numerical solution considered various flux or head-controlled top boundary conditions including precipitation, soil evaporation, plant water uptake, surface ponding. The bottom boundary condition depends on the groundwater table, which can be free-drainage if the groundwater level is nonsexist or very deep, and zero-pressure head assuming water table at bottom of the soil profile. The RE solution embedded in *WetQual* was capable of tracking soil moisture in unsaturated wetland soil. However, Sharifi et al., (2017) reported that the numerical scheme crashed frequently during a Monte Carlo (MC) simulation, especially when the soil was close to saturation, which precluded a wide range of MC simulated moisture content values. Since WetQual is a compartmental model whereby constituents' concentrations are averaged over the active sediment layer, solving RE at multiple nodal points was unnecessary, given that sediment layer-averaged volumetric moisture content is what was needed in calculating various mass balances. In addition, the plant growth module in *WetQual* were based on simple mass balance equations (Hantush et al., 2013) and did not consider detailed seasonal plant phenology, such as plant dormancy and maturity, and the effects of environmental stress on plant growth, such as temperature and water stress.

In this study, we replaced the previous finite difference RE solution in the *WetQual* model with the two-layer RE solution developed by He et al. (2021a) to simulate moisture dynamics in unsaturated soils. The first layer accounts for the biologically active sediment layer (roots layer) and the second layer is intended to account for potential feedback from shallow water table in the vadose soil bellow the root zone. In the case of a relatively deep phreatic surface, free drainage can be assumed at the bottom of the active sediment layer. The plant growth component of *WetQual* was also improved to better capture the seasonal variations of primary production in wetland environments. The modified *WetQual* model was applied to a restored wetland located on Kent Island, Maryland, USA to evaluate its performance. The goals of this study are to (1) replace the soil moisture simulation algorithm in *WetQual* with a more efficient and compatible module, (2) update the plant growth equations by considering water stress and temperature stress, which will allow for interannual variation of primary productivity, (3) evaluate the overall performance of *WetQual* on simulating nutrient cycling in variably saturated wetlands, (4) explore the effect of variably saturated conditions on nitrogen, phosphorus, and carbon cycling and their budgets in the wetland.

In the following sections of this chapter, we described the improvements to *WetQual* for the variably saturated compartment. Then we describe the model application to a restored wetland and model assessment. This is followed by the presentation of results and discussion. The chapter ends with a summary and conclusions.

2. Methodology

2.1. *WetQual* Model for Variably Saturated Compartment

The *WetQual* versions developed by Hantush et al. (2013), Kalin et al. (2013), and Sharifi et al. (2013) only considered nitrogen, phosphorus, and carbon dynamics in the flooded section of a wetland. Sharifi et al. (2017) modified the model to account for both ponded and variably saturated compartments around the ponded area (Figure 5.1A). In the ponded compartment, oxygen and nutrient dynamics, primary productivities of free-floating plants, and rooted aquatic plants are explicitly simulated as presented in works by Hantush et al. (2013), Kalin et al. (2013), and Sharifi et al. (2013). When considering the variably saturated compartment in a wetland, the soil is divided into an unsaturated part and saturated part determined by the location of the water level in the wetland. The saturated soil consists of an aerobic layer and an anaerobic layer. As shown in Figure 5.1 (A), the variably saturated compartment is divided into three layers. Unsaturated soil layer ($S_{0,u}$) is at the top. A thin aerobic soil layer ($S_{1,u}$) is in the middle just below the water table, underneath which is a relatively thick layer of anaerobic soil layer ($S_{2,u}$). Nutrient constituents are calculated in each layer. Constituent concentrations are assumed as averaged values for each layer. Biochemical reactions in unsaturated soil are adjusted based on soil moisture in the unsaturated soil layer. The reaction rates are adjusted using a generic correction factor according to available soil water content in the unsaturated soil layer, which is given by

$$k(\theta) = k_{\theta_s}(\frac{\theta}{\theta_s})^{\varepsilon} \tag{60}$$

where $k(\theta)$ is the soil moisture adjusted reaction rate, k_{θ_s} is any of the first-order reaction rates for saturated soil (e.g. mineralization rate, k_{mr}), θ is the soil moisture content in unsaturated soil, θ_s is saturation moisture content or porosity, ε is an exponent ($0.01 < \varepsilon < 1$) and was treated as a calibration parameter. The soil moisture adjusted governing equations for nitrogen and carbon

related constituents are described in Sharifi et al. (2017). The relationships for phosphorus related constituents in the variably saturated compartment of the wetland are given by

$$\frac{dV_0P_0}{dt} = \beta_{px}A(F_{ds}P_1 - F_{xds}P_0) + F_{Pg}^0 - a_{pa}k_{gb}(\theta)f_0b + V_0a_{pn}k_{mr}(\theta)N_{or} + V_0a_{pn}k_{ms}(\theta)N_{os} \quad (2)$$

$$\frac{dV_1P_1}{dt} = \beta_{px}A(F_{xds}P_0 - F_{ds}P_1) + F_{Pg}^1 - a_{pa}k_{gb}(\theta)f_1b + V_1a_{pn}k_{mr}(\theta)N_{or} + V_1a_{pn}k_{ms}(\theta)N_{os} + \beta_{p2}A(f_{ds}P_2 - F_{ds}P_1) \quad (3)$$

$$\frac{dV_2P_2}{dt} = V_2a_{pn}k_{mr}(\theta)N_{or} + V_2a_{pn}k_{ms}(\theta)N_{os} - \beta_{p2}A(f_{ds}P_2 - F_{ds}P_1) + F_{Pg}^2 - a_{pa}k_{gb}(\theta)f_2b \quad (4)$$

where t is time [T]; P_0, P_1, and P_2 are total inorganic phosphorus concentration in unsaturated soil, aerobic saturated soil, and anaerobic saturated soil layer, respectively [ML^{-3}]; V_0, V_1, and V_2 are volume of the unsaturated soil column, aerobic saturated soil layer, and anaerobic saturated soil layer, respectively [L^3]; A is the area of the unsaturated part of the wetland [L^2]; f_0, f_1, and f_2 are volumetric fractions of the unsaturated soil, aerobic, and anaerobic saturated soil layer, respectively; β_{px} is the diffusive mass-transfer rates of inorganic phosphorus between unsaturated soil and saturated aerobic soil layer [LT^{-1}]; β_{p2} is the diffusive mass-transfer rates of inorganic phosphorus between saturated aerobic soil layer and anaerobic soil layer [LT^{-1}]; F_{Pg}^0, F_{Pg}^1, and F_{Pg}^2 are net advective groundwater contribution of total phosphorus to the unsaturated layer, aerobic layer, and anaerobic layer, respectively [MT^{-1}]; F_{ds}, F_{xds}, and f_{ds} are the dissolved fraction of total inorganic phosphorus in unsaturated soil, aerobic layer, and anaerobic layer, respectively; a_{pa} is gram of phosphorus per gram of Chlorophyll-a; a_{pn} is phosphorus to nitrogen mass ratio produced by mineralization of POM; b is mass of rooted plants [M *chl a*]; k_{gb} is the growth rate of the

benthic and rooted plant [T^{-1}]; k_{mr} and k_{ms} are first-order rapid and slow mineralization rate, respectively [T^{-1}]; N_{or} is the concentration of labile organic nitrogen [ML^{-3}]; N_{os} is the concentration of refractory organic nitrogen in wetland soil [ML^{-3}]; and θ is soil moisture content [L^3L^{-3}]. Those terms have been marked with a (θ) indicate soil moisture adjusted reaction rates.

Similar to Sharifi et al. (2017), the hydrology in *WetQual* was first solved over the entire simulation period by ignoring the exchange of water between the ponded and variably saturated compartments. After the wetland depth, area, volume, and outflow were determined over the simulation period, the exchange of water and nutrients between the two compartments was then simulated, To track the mass exchanges of constituents between ponded and variably saturated compartments when the inundated area expands and shrinks during simulation, a transitional compartment was introduced (blue area shown in Figure 5.1). Depending on the rising and falling of the water level at each time step, the constituent concentrations in the transitional compartment will either be those from ponded or variably saturated compartments. At the end of each time step, the transitional compartment will merge into either ponded or variably saturated compartments using the volumetric averaging algorithm to update the concentration in these two compartments. The procedure for determining the transitional compartment and the algorithm for updating concentration in ponded and variably saturated compartments can be found in Sharifi et al. (2017).

2.2. Two-layer depth-averaged solution to RE

In Sharifi et al. (2017), soil moisture dynamics in variably saturated soil was described by finite difference solution to RE developed by van Dam and Feddes (2000). However, this numerical solution was not stable in wetland soil conditions and frequent crashes were observed during Monte Carlo (MC) simulations. In this study, we replaced the finite difference solution with

the two-layer approximation of RE (hereafter two-layer model) developed by He et al. (2021a). The two-layer model focuses on vertically-averaged soil moisture contents and flow dynamics in two soil layers. The first layer is the root zone, and the second layer extends from the bottom of the root zone to the water table (Figure 5.2). It converts the partial differential equation of RE into two coupled ordinary differential equations, which are given by,

$$L_{root}\frac{d\bar{\theta}_1}{dt} = q_0 - q_1 - L_{root}\bar{S} \tag{5}$$

$$(L_{total} - L_{root})\frac{d\bar{\theta}_2}{dt} - \theta_{2s}\frac{dL_{total}}{dt} = q_1 - q_2 \tag{6}$$

where, $\bar{\theta}_1$ and $\bar{\theta}_2$ are the first (root zone) and the second layer average moisture contents, respectively [L^3L^{-3}]. $\bar{\theta}_1(t) = \frac{1}{h}\int_0^{L_{root}} \theta(z,t)\, dz$, and $\bar{\theta}_2(t) = \frac{1}{L_{total}(t) - L_{root}}\int_{L_{root}}^{L_{total}} \theta(z,t)\, dz$; θ_{2s} is the saturated water content of the second layer [L^3L^{-3}]; L_{root} is the depth of the first layer [L]; L_{total} is the depth from soil top to the water table [L]; $\bar{S}$ is the transpiration rate [T^{-1}]; q_0 is the moisture flux at the soil-atmosphere interface [LT^{-1}] (positive downward); q_1 is the moisture flux at the interface of the first and the second soil layers [LT^{-1}]; and q_2 is the moisture flux at the bottom of the second layer and accounts for flux interactions between the vadose zone and the water table [LT^{-1}]. Two coupled ordinary differential equations were solved explicitly by Heun's method. The two-layer model considers various atmospheric boundary conditions including precipitation, soil evaporation, and ponding. It also deals with varying bottom boundary conditions determined by the dynamic water table within or below the soil profile. Soil hydraulic characteristic relations of capillary pressure and unsaturated conductivity were described by van Genuchten model (1980). Details about the derivations, numerical solutions, and different boundary conditions of the two-layer model can be found in He et al. (2021a).

2.3. Plant Growth in Wetlands

The previous version of *WetQual* simulated plant productivity of two types of wetland plants, free-floating plants (e.g. algae) and rooted aquatic plants (e.g. macrophytes), using simple governing equations as a function of annual growth rates and death rates. Growth rates were adjusted by daily solar radiation. In this study, we improved the growth/death pathways for wetland plants.

A water stress factor was added to adjust the growth rate for rooted plants. The growth rate was adjusted according to the actual and potential transpiration rate, which is given by,

$$k_{gb,ws} = \frac{E_a}{E_p} k_{gb} \tag{7}$$

where $k_{gb,ws}$ is the adjusted growth rate for rooted plants [T^{-1}]; k_{gb} is the maximum growth rate for rooted plants [T^{-1}]; E_a is daily actual root water uptake rate [LT^{-1}], which is estimated by the two-layer model; and E_p is daily potential root water uptake rate [LT^{-1}].

Plant root water uptake in the variably saturated compartment was estimated by the two-layer model. The actual root water uptake rate was evaluated using the plant water stress function. The two-layer model used a plant water stress function proposed by Feddes (1982) to estimate actual plant water uptake from the root zone (Chapter 2, Eq. 41). In this study, the water stress response function was replaced with a function proposed by Van Genuchten (1987). We further modified this function to better represent root water uptake for wetland plants. In the flooded wetland, although macrophytes have adaptations to the inundated condition, they may not transpire water at the potential rate in the flooded condition because of the inhibition of plant transpiration due to hypoxia (Pezeshki, 2001). The updated equation for describing water stress response function is given by,

$$\alpha(h) = \frac{1}{1 + \left|\frac{h - h_0}{h_{50}}\right|^p} \tag{8}$$

where α is water stress response function [-]; h is negative of soil capillary pressure head [L]; h_{50} is the capillary pressure head at which the water extraction rate is reduced by 50% [L]; h_0 is the capillary pressure head at which the actual water uptake rate is equal to the potential rate [L]; and p is a constant [-]. The values of h_{50} and p depends on vegetation type, and the reported ranges in the literature are 1000 to 5000 cm for h_{50} and 1.5 to 3 for p (Van Genuchten, 1987b; Cardon and Letey, 1992; Homaee et al., 2002; Skaggs et al., 2006; Zhu et al., 2009). An example of the modified water stress response function is shown in Figure 5.3. In the ponded compartment, the actual root water uptake rate is calculated by $\alpha(0)S_p$, where S_p is potential water uptake rate [LT^{-1}].

Temperature is one of the major constraints for plant growth. Plant growth could be suppressed due to very high or low temperatures during the year but plants can experience no stress at optimum temperature. We added the following equations (Arnold et al., 2012) to describe temperature stress on the growth of free-floating plants and rooted plants,

$$T_{str} = \begin{cases} 0, & T \le T_{base} \\ \exp\left(\frac{-0.1054\left(T_{opt} - T\right)^2}{(T - T_{base})^2}\right), & T_{base} < T \le T_{opt} \\ \exp\left(\frac{-0.1054\left(T_{opt} - T\right)^2}{\left(2T_{opt} - T - T_{base}\right)^2}\right), & T_{opt} < T \le 2T_{opt} - T_{base} \\ 0, & 2T_{opt} - T_{base} < T \end{cases} \tag{9}$$

where T is daily mean air temperature [℃]; T_{base} is the minimum temperature for the plant to grow [℃]; and T_{opt} is the optimum temperature for plant to grow [℃]. Figure 5.4 shows the temperature stress variation as a function of daily air temperature.

Plant dormancy was considered in *WetQual* to simulate the plant's growth cycle during seasons (Arnold et al., 2012). Plants go dormant when daylength is close to the shortest daylength of the year. Plants do not grow, and aboveground biomass starts to decrease during dormancy. The starting and ending time of dormancy are defined by a threshold daylength, which is given as,

$$D_{dorm} = D_{min} + d_{dorm} \tag{10}$$

where D_{dorm} is the threshold daylength to initiate dormancy given in hours [T]; D_{min} is the minimum daylength for the watershed during the year [T]; and d_{dorm} is the dormancy adjustment factor [T], which is calculated based on the latitude of the wetland, where,

$$d_{dorm} = \begin{cases} 1.0, & 40^{\circ}\text{N or S} < \emptyset \\ \dfrac{\emptyset - 20}{20}, & 20^{\circ}\text{N or S} \leq \emptyset \leq 40^{\circ}\text{N or S} \\ 0, & \emptyset < 20^{\circ}\text{N or S} \end{cases} \tag{11}$$

where $\emptyset$ is the latitude given in degree. During the dormancy period, the biomass of the free-floating plants (a [M *chl a*]) and the rooted plants gradually decrease but cannot drop below their predefined minimum biomass (a_{min} and b_{min}). When the dormancy period ends, free-floating plants start to grow, and rooted plants start to sprout in the growing season. The death rate is assumed to be zero during the growing season.

In the late of the growing season, plant maturity is considered. The biomass of the wetland plants increases during the growing season. However, the biomass keeps constant or increases very little when plants reach maturity (Stefanik and Mitsch, 2017). Thus, plant growth rate keeps constant before plants reach maturity. When plants reach maturity, the growth rate is assumed to decrease linearly and reaches 0 on the day plants go dormant. The growth rate during plant maturity is adjusted by multiplying with a factor given by,

$$f_{mature} = 1 + \frac{n - n_{D_{max}}}{n_{D_{max}} - n_{D_{dorm}}} \tag{12}$$

where f_{mature} is the adjustment factor for plant growth rate during plant maturity ranging from 1 to 0 [-]; n is the day of the year [T]; $n_{D_{max}}$ is the day that has maximum daylength at the wetland site during the year [T]; $n_{D_{dorm}}$ is the day of the year that plants go dormancy [T].

With the consideration of the temperature stress, water stress, plant maturity, and plant dormancy, the governing equations for free-floating plants are given by,

$$\frac{da}{dt} = \begin{cases} T_{str}k_{ga}a - (\frac{Q_o}{\emptyset_w V_w})a, & D_n > D_{dorm}, n < n_{D_{max}} \\ T_{str}f_{mature}k_{ga}a - (\frac{Q_o}{\emptyset_w V_w})a, & D_n > D_{dorm}, n \geq n_{D_{max}} \\ -k_{da}a - \left(\frac{Q_o}{\emptyset_w V_w}\right)a, & D_n \leq D_{dorm}, a > a_{min} \\ a_{min} - \left(\frac{Q_o}{\emptyset_w V_w}\right)a, & D_n \leq D_{dorm}, a \leq a_{min} \end{cases} \quad (13)$$

where a is mass of free-floating plants [M *chl a*]; k_{ga} is the growth rate of free-floating plants [T^{-1}]; k_{da} is the death rate of free-floating plants [T^{-1}]; Q_o is wetland discharge (outflow) rate [L^3T^{-1}]; $\emptyset_w$ is the effective porosity of wetland surface water [-]; V_w is water volume of wetland surface water [L^3]; and D_n is the daylength of n^{th} day for a year [T].

Growth/death of rooted plants b are described by,

$$\frac{db}{dt} = \begin{cases} T_{str}k_{gb,ws}b, & D_n > D_{dorm}, n < n_{D_{max}} \\ T_{str}f_{mature}k_{gb,ws}b, & D_n > D_{dorm}, n \geq n_{D_{max}} \\ -k_{db}b, & D_n \leq D_{dorm}, b > b_{min} \\ b_{min}, & D_n \leq D_{dorm}, b \leq b_{min} \end{cases} \quad (14)$$

where b is the mass of rooted plants [M *chl a*]; k_{db} is the death rate of the rooted plant [T^{-1}].

2.4. Study Area

The study site is a restored wetland, named "Barnstable" as described by Jordan et al. (2003), located on Kent Island, Maryland, which is part of the Delmarva Peninsula on the eastern

shore of Chesapeake Bay (Figure 5.5). The 1.3-ha wetland was located with a 14-ha watershed with average slope less than 1% and it receives water drainage from surrounding farmlands (primarily cultivated for corn and soybean production) and forest, which cover about 82% and 18% of the watershed area, respectively. The soils in most of the study area were Typic Endoaquults of the Othello soil series, which had silt loam texture with moderate or moderately slow permeability. Most croplands in the study area were drained by ditches or channels due to the low permeability of the soils and low topographic relief of the watershed. There were two sources of water entering the wetland: surface runoff from the surrounding watershed and precipitation. Wetland output was water via a standpipe drain installed in the dike and evapotranspiration. Because the wetland lacked well-defined flow channels, when the water was deep enough to flow out of the drain, the entire 1.3-ha area of the wetland was submerged. About 0.5 m below the soil surface, there was an impermeable clay layer blocking groundwater exchanges and seepage losses.

The study site was restored and turned into to wetland from cropland in 1986 by the Chesapeake Wildlife Heritage to provide habitat for wildlife and improve the quality of runoff from surrounding agricultural fields. The wetland vegetation was established by natural succession after restoration. There were three most dominant macrophyte species: blunt spikerush (*Eleocharis obtuse* (Willd.) Schult.), water-purslane (*Ludwigia palustris* (L.) Elliott), and American bulrush (*Schoenoplectus americanus* (Pers.) Volkart ex Schinz & R. Keller) (Jordan et al., 1999; Whigham et al., 2002). During the growing season, 70% to 90% of the wetland surface was covered by emergent vegetation, while during the nongrowing season, the covered area dropped to about 10% to 20% of the wetland surface.

The water flow and water quality of the wetland were monitored for about two years from May 8, 1995 to May 12, 1997. Inflow and outflow concentrations of nitrate N, total ammonia N,

organic N, P, TSS, and total organic carbon (TOC) were collected as weekly flow averaged values (about 5 to 8 days). Precipitation was measured using a rain gauge. ET data were collected from the Wye Research Center (WRC), located 13 km away from the study wetland. The bathymetry of the wetland was extracted from the 10-cm elevation contours within the wetland basin. Detailed information about data collection and analysis can be found in Jordan et al. (2003). Figure 5.6 shows the inflow, outflow, and the mean water depth in the ponded compartment of the wetland as well as outflow concentrations of TOC, ON, NO_3, NH_4, P, and TSS from May 1995 to May 1997.

2.5. Numerical Experiments

To evaluate the performance of the additions to the model, the updated *WetQual* model was applied to Barnstable wetland to simulate carbon, nitrogen, and phosphorus constituent concentrations and wetland plant biomass in both ponded and variably saturated compartments. Two numerical experiments with different bottom boundary condition treatments in variably saturated compartments were performed. The first numerical experiment assumed that the groundwater level in the variably saturated compartment was always at the same level with the water surface in the ponded compartment (Figure 5.1A). This is also the assumption followed in Sharifi et al. (2017). Zero pressure head bottom boundary condition was applied in the two-layer model. For the second numerical experiment, we assumed that there was a deep phreatic surface in the study wetland and the soil under the ponded compartment was always saturated as a result of ponded water, but soil moisture in variably saturated compartment varied dynamically (Figure 5.1B). The effect of the deep phreatic surface on the soil in the variably saturated compartment

was assumed negligible. Free-drainage was applied at the bottom boundary condition in the two-layer model.

Wetland soil in the variably saturated compartment was divided into two layers for the two-layer model to simulate moisture contents. The maximum depth of the soil (0 at the soil top, positive downward) of the banks of the wetland in a variably saturated compartment was assumed to be 73 cm based on the bathymetry of the wetland. The soil was divided into root zone and vadose zone. The thickness of the root zone and the layer below were varied during the MC simulation in the model evaluation step as explained in section 2.5. The groundwater level varied within the soil column with the minimum and maximum depth of 26 cm and 59 cm, respectively. The moisture content for the unsaturated part (soil above groundwater level) of the soil was needed for *WetQual* to adjust biochemical reactions. The two-layer model estimated layer averaged moisture content for the root zone and the unsaturated part of the below vadose zone. The biogeochemical reaction rates were adjusted based on the moisture content of the root zone (θ_{root}).

Soil information (soil type and physical properties) was obtained from the USDA Web Soil Survey (Soil Survey Staff) at the study site. Within the 73 cm of soil, there were three horizons. Soil particles of sand, silt, and clay for the root zone and vadose zone were calculated from three horizons using the depth-weighted function. Soil hydraulic properties for van Genuchten model (Van Genuchten, 1980) were calculated by ROSETTA3 model developed by Zhang and Schaap, (2017). The physical and hydraulic properties of the root zone and vadose zone are shown in Table 5.1. The potential evapotranspiration rate of the entire wetland was divided into ponded and variably saturated compartments based on the fraction of each compartment.

To evaluate the effectiveness of the updated model, we followed the approaches described in Kalin et al. (2013), Sharifi et al., (2013), and Sharifi et al. (2017) for the two numerical

experiments described above. MC simulation were followed by the Generalized Likelihood Uncertainty Estimation technique (GLUE) and Global Sensitivity Analysis (GSA) methods (Beven and Binley, 1992; Spear and Hornberger, 1980) to investigate the model prediction uncertainty and quantitative sensitivity to model parameters. The methodology of GLUE and GSA are described in the model evaluation section. In addition, we also compared the results of the first numerical experiments with the results from the previous versions of *WetQual* reported in Sharifi et al. (2017). To avoid confusion in the text, the lumped version of *WetQual* (Hantush et al., 2013) will be referred to as the **Original** model. The model modified by Sharifi et al. (2017) will be referred to as the **Expanded** model, and the model updated in this study will be specified as the **Updated** model.

We further evaluated the updated plant growth/death module in *WetQual* by comparing the model estimated biomass of rooted plants with field measurements. Whigham et al. (2002) measured annual aboveground biomass in the study wetland from 1994 to 1996. Aboveground plant material was harvested in mid-late October each year and biomass was measured as dry weight. The mean annual aboveground biomass reported in 1994, 1995, and 1996 were 157.4 g/m^2, 171.3 g/m^2, and 415.3 g/m^2 respectively. Further information on the experiment of biomass measurement can be found in Whigham et al. (2002). To make the simulation scenario close to the reality of the study wetland, in this simulation, the assumption that groundwater level in the variably saturated compartment was equal to the depth of water table in the ponded compartment was applied in *WetQual*. The results of MC simulation in the first numerical experiment were used to calculate the best estimates of the model input parameters for carbon, based on the equation (Sharifi et al., 2013)

$$x' = \sum_{i=1}^{n} L_{k_i} x_i \tag{16}$$

where x' is the best estimate of the parameter x; x_i is the generated value of parameter x in i^{th} parameter set; L_{k_i} is likelihood estimate from the i^{th} model run of the MC simulation, which is defined in section 2.6; and n stands for the total number of MC simulation. The growth and death rates of rooted plants were calibrated during the simulation. The growth rate of rooted plants can be roughly estimated by the following relationship proposed by Hall et al. (2014),

$$k_{gb} = \frac{\ln b_1 - \ln b_0}{t_{dorm} - t_{grow}} \tag{17}$$

where b_0 is the initial biomass of the rooted plants [M *chl a*]; b_1 is the biomass before plants go dormant (harvested biomass) [M *chl a*]; t_{dorm} is the Julian day that plants go dormant [T]; and t_{grow} is the Julian day that plants start to grow [T]. The initial biomass b_0 was assumed equal to the biomass in the nongrowing season. Based on the vegetation cover in growing season and nongrowing season reported by (Jordan et al., 2003), the initial biomass in 1995 was roughly estimated around 1/8 to 1/4 of the biomass in mid-October 1995. In this study, we compared the model estimated biomass for rooted plants with field measurements in 1995 and 1996. b_1 was assumed to be equal to the biomass measured in mid-October 1995 times the total wetland area. b_0 can also be calibrated during the simulation according to its estimated value. *WetQual* simulates total plant biomass. Thus, to compare the results of above-ground biomass, the above-ground biomass was estimated using the average belowground:aboveground biomass ratio (0.40) of wetland macrophytes suggested by Whigham and Simpson (1978).

2.6. Model Evaluation

Model performance, uncertainties, and parameter sensitivities were assessed by the combination of GLUE and GSA. Here, we describe both methods briefly. The complete description of the methodology of GLUE/GSA can be found in Sharifi et al. (2013). First, 100,000 independent model parameter sets were generated for ponded and variably saturated compartments, respectively. The selected model parameters and their respective upper and lower bounds and distributions were set to those applied in the previous *WetQual* studies (Kalin et al., 2013; Sharifi et al., 2013). The ranges of soil hydraulic parameters for each soil layer were set to $\pm 5\sigma$ around their ROSETTA predicted values using uniform distribution, where σ is the standard deviations of the predicted parameters. The ranges of values for soil thickness, soil hydraulic model, plant water stress response function, and temperature stress function are shown in Table 5.2. The same 100,000 parameter sets were applied in two numerical experiments. Second, MC simulation were performed to run *WetQual* 100,000 times using generated parameters sets. 100,000 time series for each constituent concentration were generated. The initial concentrations were set to the values of the first day of simulation (May 9, 1995). Third, model performance for each constituent was evaluated by comparing against observations for the calculated weekly averaged nutrient exports using two performance criteria, mass balance error (MBE) and Nash-Sutcliffe efficiency (E_{ns}). A likelihood estimate (L_k) calculated as a function of *MBE* and E_{ns} was used to evaluate the efficiency of model predicted nutrient exports against observed data for each MC simulation (Sharifi et al., 2013).

$$L_k = \exp\left(E_{ns} - \frac{|MBE|}{100} - 1\right) \tag{18}$$

where L_k is the likelihood estimate, ranging from 0 to 1. The closer of L_k to 1, the more accurate the model is. Fourth, the parameter sets for each compartment were sorted based on their likelihood values. The top 1% (1000) parameter sets with the highest likelihood were selected as behavior

datasets ($\boldsymbol{B}$) and the rest were non-behavior datasets ($\boldsymbol{B}'$). Last, the Kolmogorov-Smirnov test (Massey Jr, 1951) was applied to evaluate the sensitivities of model parameters based on the cumulative distribution functions (CDFs) of $\boldsymbol{B}$ and $\boldsymbol{B}'$ obtained from previous step.

3. Results and Discussion

3.1. Model Performance

Model performance using the two bottom boundary conditions were evaluated by comparing simulated nutrient exports of TN, ON, NH_4, NO_3, TSS, TOC, and P with their measured data in outflow using MBE, E_{ns}, and L_k. The average model performance criteria of MBE, E_{ns}, and L_k for behavior simulations (top 1000 simulations) are shown in Table 5.3.

As shown in Table 5.3, with zero-pressure head bottom boundary condition (presence of shallow groundwater) applied in the variably saturated compartment, the model showed excellent performance in simulating NO_3 and TOC exports with E_{ns} greater than 0.90, although the model produced a high mass balance error for NO_3. The model had good performance in capturing ON, NH_4, and TN exports from the study wetland with E_{ns} ranging from 0.71 to 0.79. However, exports for TSS and P were not well captured by the model. They showed high mass balance error (-25.1% and -51.5% for TSS and P, respectively) and low E_{ns} (0.42 and 0.50 for TSS and P, respectively) compared to other nutrient constituents. Compared with the results of model performance from the Expanded model developed by Sharifi et al. (2017), the performance of the Updated model in TN, ON, and TOC export in this study showed improvement, while the performance of NH_4, NO_3, and TSS was slightly decreased. Note that the measured outflow concentration data used in this study were revised versions which had 71 data points for each constituent over 2 years, while the

observed data applied in Sharifi et al. (2017) had 47 observation points, which were included in those 71 data points. The model performance might be better quantified using these revised observation data.

For the second numerical experiment, when free-drainage was applied in the variably saturated compartment, the model performance in estimating exports of these constituents were similar to those in the first numerical experiment. The moisture contents of the soil in the banks of the wetland with free-drainage were significantly lower (p-value<0.01) than those obtained from the first numerical experiment assuming a shallow water table (Figure 5.7).

E_{ns} values from 100,000 MC simulations of the two numerical experiments were plotted against each other to see how constituent exports are impacted by the choice of the bottom boundary condition, and thus by the variation of the soil moisture content. To do this, the E_{ns} values of the same parameter sets from the two simulations were parried. Note that the same 100,000 parameter sets were utilized in both MC simulations. The results of relation between E_{ns} of TN, ON, NH_4, NO_3, TSS, TOC, and P from behavior simulations of the two numerical experiments are shown in Figure 5.8. For a given constituent, if all the points fall on the identity (1:1) line, then selection of the bottom boundary condition, and thus moisture content variability has no impact on the constituent export. The deviations between the trends of scatters and the identity lines indicate the influences of different bottom boundary conditions on export of the constituent in the ponded compartment. From Figure 5.8, the trends of scatters of TN, ON, NO_3, and P were close to the identity lines, while the trend of scatters of NH_4, TSS, and TOC deviated from the identity line. Besides, the trend lines of NH_4, TSS, and TOC were above the identity lines, indicating that the model performance on of NH_4, TSS, and TOC from two numerical experiments were different from each other and the overall performance of the second numerical experiment

was higher than the first numerical experiment. The t-test was performed to investigate whether the trend lines were different from the identity line. The results showed that the trend lines of TN, ON, NO_3, and P were statistically similar with the identity line ($p > 0.05$), indicating that the model produced similar results of exports of these constituents in the ponded compartment when using two types of lower boundary conditions in the variably saturated compartment. The application of different lower boundary conditions in the variably saturated compartment did not affect the exports of these constituents in the ponded compartment. However, the t-test showed significant differences between the trend lines of NH_4, TSS, and TOC and the identity line ($p < 0.001$). The model performance of NH_4, TSS, and TOC from the first and the second numerical experiment was different from each other. The zero-pressure head and free-drainage bottom boundary conditions applied in the variably saturated compartment had significant influences on NH_4, TSS, and TOC exports in the ponded compartment.

3.2. Soil moisture variations

Average moisture contents in the variably saturated compartment for the two numerical experiments are shown in Figure 5.7. When considering groundwater within the variably saturated compartment, water can be exchanged between groundwater and the soil above the groundwater table, causing groundwater recharge or discharge. In the first numerical experiment, the groundwater level was relatively shallow, and fine-textured soil tended to absorb water from groundwater. For most of the time during the study period, the two-layer model estimated the soil moisture content near saturation in the variably saturated compartment (Figure 5.7A). Note that there was no soil moisture data at the study site, meaning the behavior and non-behavior simulations of soil moisture cannot be determined. Thus, we calculated the standard deviations of

predicted soil moisture at each day based on the results of moisture content from 100,000 simulations to evaluate model predicted uncertainty. The standard deviation of the two-layer model predicted soil moisture contents during the study period was small (0.02 m^3m^{-3} on average). Although moisture contents were close to saturation, the two-layer model captured the dynamic variations of soil moisture in response to precipitation. Besides, during the dry period (between August 16, 1995 to October 15, 1995), the moisture content in the wetland bank (upgradient unsaturated part of the wetland at the outer perimeter with small slope) dropped accordingly in response to declining groundwater levels. Compared with the results of moisture content in the variably saturated compartment from Sharifi et al. (2017), who applied the finite difference numerical scheme to RE, the two-layer model showed promising results of the moisture contents. Sharifi et al. (2017) reported that at the first of the 80 days, moisture content increased gradually towards saturation from the initial value, while in this study, moisture content increased suddenly after one day, although fine-textured soils were applied in both studies (although the van Genuchten parameters were not the same between the two studies). Shallow water table and precipitation should cause a rapid saturation of the wetland banks. In addition, Sharifi et al. (2017) reported that the finite difference scheme to RE crashed frequently during the MC simulation. We did not observe any numerical difficulties using the two-layer model during the 100,000 simulations. The two-layer model showed its robustness over the finite difference scheme in wetland soil conditions where groundwater level was relatively shallow.

Average moisture contents in the soil of variably saturated compartment using free-drainage bottom boundary condition are shown in Figure 5.7(B). As mentioned earlier, moisture contents in the second numerical experiment were significantly lower than those in the first experiment. When the free-drainage bottom boundary condition was applied, water was lost

through plant water uptake in the upper layer and through the lower soil boundary by the force of gravity and there is no replenishing, upward flow as the case for a shallow water table. There were only two sources of soil water: precipitation and exchange between the soil and ponded water when wetland shrinks and expands. As shown in Figure 5.7(B), moisture content varied according to the average water depth in the ponded compartment and precipitation. During the dry period between August 16, 1995 to October 15, 1995, when the water table in the ponded compartment dropped to the lowest point, moisture content also reached the lowest point. After day October 15, 1995, when the water level in ponded compartment raised again, the moisture content increased to a relatively high level but never reached saturation. Moisture content varied according to precipitation. The average standard deviation of soil moisture was 0.03 m^3m^{-3}, higher than that from the first numerical experiment. This is because, with the free-drainage bottom boundary condition, soil moisture tended to vary in a wider range, while with zero-pressure head bottom boundary condition, soil moisture stayed close to saturation for most of the time due to capillary replenishment from the water table.

3.3. Plant water uptake

Seasonal variation of plant water uptake was captured well by the updated model. In the first numerical experiment, the average actual plant water uptake rate from 100,000 simulations followed the daily and seasonal variations of potential transpiration and was slightly lower than the potential rate (Figure 5.9A). Because the soil was close to saturation for most of the time, the plants experienced little water stress and the water stress response function $\alpha(h)$ was close to 1. During the dry period (August 16, 1995 to October 15, 1995), soil moisture slightly decreased. The soil capillary pressure head (absolute value of pressure head) was higher than the optimum

value h_0 at which plants transpire at the potential rate, resulting in the estimation of actual water uptake rate lower than the potential rate. When the soil was completely saturated (i.e. July 16, 1996 and August 15, 1996), actual plant water uptake was also weakened because the soil capillary pressure head was lower than h_0.

In the second numerical experiment, the daily and seasonal variations of actual plant water uptake were also captured by the two-layer model (Figure 5.9B). Compared to the first numerical experiment, the differences between the actual plant uptake rate in the second numerical experiment and potential transpiration rate were larger than those in the first numerical experiment. This is because with free-drainage bottom boundary condition, the soil was not saturated during the study period. The soil capillary pressure head was always higher than the optimum value h_0, resulting in $\alpha(h)$ always being lower than 1. In addition, the variations of actual plant water uptake reflected the soil moisture changes during the simulation. As shown in Figure 5.9B, during the dry period from August 16, 1995 to October 15, 1995, because of the decrease in the soil moisture, the actual plant uptake rate decreased to the lowest point almost to zero, although the potential uptake rate remained relatively high. Moisture contents play an important role in estimating actual plant water uptake and can eventually affect plant growth, which will be discussed in section 3.6 and section 3.8.

3.4. Sensitivity Analysis

The sensitivities of the model input parameters were evaluated by applying the Kolmogorov-Smirnov (K-S) test to the behavioral ($\boldsymbol{B}$) and non-behavioral ($\boldsymbol{B}'$) datasets of each compartment for each numerical experiment, respectively. The most sensitive parameters for ponded and variably saturated compartment for two numerical experiments in order of sensitivity

based on NH_4, NO_3, TOC, and P exports are shown from Figures 5.10 to 5.13. On the plots, the horizontal axes are the most sensitive parameters in order of their sensitivity. The vertical axes represent the D_{max} value calculated by the K-S test. Similar to Kalin et al. (2013) and Sharifi et al. (2017), the criterion for selecting the most sensitive parameters was determined by the significance level associated with D_{max} value. The parameters with the significance level smaller than 5% in the ponded and variably saturated compartments were considered as sensitive parameters.

For the parameters related to NH_4 export, the top panels of Figure 5.10 shows the D_{max} values for the most sensitive parameters in the first numerical experiment. In the ponded compartment, ammonium ion distribution coefficient, K_d, was the most sensitive parameter, followed by f_N, fraction of total ammonia nitrogen as NH_4^+, and k_{mr} (mineralization rate in soil). High sensitivity of K_d indicates the importance of adsorption of ammonium ions onto negatively charged particles. f_N captures the effects of pH and temperature on the fraction of total ammonia in ionized form and k_{mr} determines the rate of transformation of organic N to ammonia N. In the variably saturated compartment, K_d was clearly the most sensitive parameter followed by l_2 and f_N, which were also among the sensitive parameters in the ponded compartment. The sensitive parameters found in this study were similar to those found in Sharifi et al. (2017). However, the order of the sensitivity was not the same. In the second numerical experiment, the most sensitive parameters for the ponded compartment were similar to those from the first numerical experiment, while sensitive parameters differed for the variably saturated compartment. The most sensitive parameter in the variably saturated compartment was pK, followed by the growth rate of rooted plants k_{gb}. pK is a coefficient in f_N and it is a function of temperature. Without groundwater in soil, ammonia seems to be affected more by temperature that determine the amount of ionized ammonia, and the growth of plants that take up ammonia from the soil.

The parameters of the ponded compartment that ended being sensitive for NO_3 export from the wetland are shown in Figure 5.11 for both numerical experiments. Denitrification (k_{dn}), l_2, and nitrification rate in free water (k_{nw}) were the top three sensitive parameters for the ponded compartment in both numerical experiments. Other parameters with relatively lower sensitivities appeared in both numerical experiments but with different $D_{\max}$ values. However, no parameter was found to be sensitive in the variably saturated compartment because data was insufficient to evaluate the unsaturated compartment.

From Figure 5.12, k_D^1 and θ_{T^0} in the ponded compartment were two top sensitive parameters for TOC export for the first numerical experiment. k_D^1 is the maximum dissolved organic C utilization rate for aerobic respiration. θ_{T^0} is an Arrhenius coefficient for temperature adjustment. The appearance of these two parameters indicates that TOC has a high sensitivity to microbial respiration and temperature. The sensitive parameters found in the ponded compartment were similar to those results from Sharifi et al. (2013) and Sharifi et al. (2017). For the variably saturated compartment, k_O^{in} (michaelis–Menten oxygen inhabitation coefficient) and k_{gb} (growth rate of rooted plant) were two sensitive parameters associated with important processes related to TOC export (oxygen concentration and plant biomass, respectively). For the second numerical experiment shown on the bottom panel of Figure 5.12, the most sensitive parameters in ponded compartment were found similar to those from the first numerical experiment. The sensitive parameters in the variably saturated compartment were a_{ca} (ratio of carbon to chlorophyll-a in algae) and K_M^2 (maximum methane utilization rate for denitrification), which were related to plant biomass and methanogenesis, respectively..

Sensitive parameters for phosphorus export were similar between two numerical experiments. As shown in Figure 5.13, K_w (phosphorus distribution coefficient in the water

column) was the most sensitive parameter with the highest $D_{\max}$ among others, and v_s and ϕ_w (effective settling velocity and effective porosity of wetland surface water) were the second and third sensitive parameters in the ponded compartment for both numerical experiments. This result confirms the findings in Kalin et al. (2013) that settling and sorption onto soil particles were major phosphorous removal processes in water. In the variably saturated compartment, l_2 was the most sensitive parameter when groundwater level was shallow. Phosphorous in saturated soil layer is a function of sediment-bound phosphorus depositional fluxes in proportion to the respective thicknesses of the soil layer. However, none of the parameters in the variably saturated compartment was found sensitive in the second numerical experiment because the observed data was not sufficient to evaluate the unsaturated compartment.

The sensitivities of newly added parameters (e.g. soil parameters for the two-layer model, parameters in temperature stress function and water stress function, etc.) in this study were also evaluated. Figure 5.14 summarizes those added model parameters having high sensitivities for NO_3, NH_4, P, and TOC export based on the behavior simulation outputs from two numerical experiments. Van Genuchten soil parameters did not have direct impact on the nutrient exports from the wetland. Soil moisture estimations in the variably saturated compartment, which showed influences on nutrient budgets, are highly associated with these soil parameters. Besides, all nutrient exports did not show sensitive to the exponent ε in Eq. (1), indicating that the changing of reaction rate based on moisture content in the unsaturated soil did not affect the nutrient exports from the wetland. The area index K_c, which determines the fraction of bare soil and vegetation cover in the variably saturated compartment, was a sensitive parameter for NO_3, NH_4, and TOC exports in the variably saturated compartment. The potential soil evaporation rate and potential plant transpiration rate were determined by K_c times potential evapotranspiration rate of the

variably saturated compartment. Change in K_c can affect actual plant water uptake and eventually affect plant growth rate $k_{gb,ws}$. Most of the nutrient constituents were sensitive to the plant growth rate (e.g. Figures 5.10 and 5.12). Temperature related coefficients (T_{base} and T_{opt}), which adjust growth rate by affecting temperature stress and water stress, were among the most sensitive parameters in NH_4, P, and TOC exports.

3.5. Nitrogen budget

The N, C, and P budgets and their major retention and removal pathways for ponded and variably saturated compartments during the study period for two numerical experiments are summarized in Tables 4, 5, and 6, respectively. The results of N and C were compared with those borrowed from the Expanded model (Sharifi et al., 2017) (Table 5.7). The results of the P budget were compared with those results simulated from the Original model (Kalin et al., 2013) (Table 5.7). All the quantities of source and sink terms were normalized with the incoming load (shown in parentheses) to represent their absolute values. The values shown in the tables are means ± one standard deviation calculated from the behavioral set simulations.

When assuming the groundwater was within the soil in the variably saturated compartment, the nitrogen budget from the Updated model was similar to that from the Expanded model, but there were small differences in some of the components in the nitrogen budget between the two models. The N export in the Updated model was less than that obtained by Sharifi et al. (2017) (244.0 ± 38.3 kg N versus 260.5 ± 30.4 kg N) Net organic N deposition (settling minus resuspension) in the ponded compartment was slightly higher than that from the Expanded model. Denitrification in the ponded compartment was slightly higher than that from the Expanded model.

However, denitrification in the variably saturated compartment was found about 70% of that estimated in the Expanded model. Ammonia volatilization in the ponded compartment was higher than that from the Expanded model, while the amount volatilized ammonia in the variably saturated compartment was higher than that from the Expanded model. The Updated model showed lower uncertainties in net settling, ammonia diffusion in ponded compartment and in volatilization and denitrification in the variably compartment compared to the Expanded model.

For the second numerical experiment, which assumes free-drainage bottom boundary condition in the variably saturated compartment, some of the components in the nitrogen budget had different values compared with those from the first numerical experiment (Table 5.4). The major difference came from denitrification. The denitrification in the ponded compartment was higher than that in the first experiment (22.3 ± 10.6 kg N versus 14.2 ± 7.3 kg N). However, there was no denitrification in the variably saturated compartment in the second experiment. When using free-drainage bottom boundary condition in the variably saturated compartment, the entire soil in the banks of the wetland became unsaturated for most of the time. Thus, the denitrification hardly took place in the variably saturated compartment due to the aerated soil conditions. Volatilization in the variably saturated compartment was only a fraction of that obtained in the first experiment (0.06 ± 1.1 kg N versus 3.4 ± 4.4 kg N). The outflow and volatilization in the ponded compartment were slightly lower than those from the first experiment, while the net settling, ammonia diffusion, and nitrate diffusion were slightly higher than those from the first experiment.

3.6. Carbon budget

The carbon budgets in the study wetland obtained from the behavior simulation outputs for two numerical experiments are shown in Table 5.5. For the first numerical experiment, during the

simulation period, a total of 3849.2 kg of organic carbon was transported into the wetland and 283.1 kg of atmospheric carbon was fixed by wetland plants (net primary production). 2164.0 ± 115.2 kg of carbon contributing to 56.2 ± 3.0% of incoming loading was washed out through outflow and 1379.9 ± 377.6 kg (35.8 ± 9.8% of loading) of carbon was removed by microbial respiration and emitted to the atmosphere. There was a small portion of DOC diffused to the soil layer (250.7 ± 171.2 kg as 6.5 ± 4.4% of loading) and was retained in the soil as a result of settling (124.6 ± 81.9 kg as 3.2 ± 2.1% of loading). The outflow, gaseous losses, and diffusion in the Updated model were similar to those from the Expanded model. However, in the ponded compartment, the deposition was lower than those from the Expanded model. The biomass accumulation was about 20% of that from the Expanded model (32.9 ± 0.2 kg versus 180.6 ± 88.3 kg). In the variably saturated compartment, biomass accumulation showed higher value (250.2 ± 8.2 kg versus 179.7 ± 87.9 kg) compared to those values from the Expanded model. All the components, except diffusion, had lower uncertainties compared with those from the Expanded model. For the Updated model, the modified plant equations had lower biomass estimation in the ponded compartment, which results in smaller amount of carbon returned to the ponded water. The Expanded model simulates plant growth in both ponded and variably saturated components without considering the water and temperature stress in a saturated condition. The estimated biomass accumulations were similar in both compartments. For the Updated model, biomass in the ponded compartment was much lower than that in the variably saturated compartment due to the water stress.

One of the major differences between the two numerical experiments were the gaseous losses and diffusion. Although the gaseous loss in the ponded compartment was similar to that in the first experiment, the amount of gas emitted in the variably saturated compartment was much

lower than that estimated in the first experiment (1.0 ± 3.6 kg versus 105.7 ± 129.5 kg). Under the free-drainage assumption in the variably saturated compartment, the soil in the bank of the wetland hardly formed anaerobic conditions for CO_2 and CH_4 production. The diffusion in the second numerical experiment was higher than that in the first numerical experiment (384.2 ± 242.5 kg versus 250.7 ± 171.2 kg). Under the free-drainage assumption in the variably saturated compartment, when the ponded area shrank, the chemicals in the soil that belonged to the ponded compartment leached out of the soil with moisture flow. When the wetland expanded, the water took over the unsaturated part. Organic carbon diffused to the submerged soil due to the low concentration of organic carbon in the submerged soil. In addition, the biomass accumulation in the ponded compartment was similar to that from the first numerical experiment. However, the biomass in the variably saturated compartment was lower than that from the first numerical experiment (235.8 ± 10.6 kg versus 250.2 ± 8.2 kg). In the ponded compartment, soil is always saturated, plants suffered the same water stress in both numerical experiments. Moisture contents in the variably saturated compartment from the second numerical experiment were lower than those from the first numerical experiment during the simulation. Thus, plant growth was inhibited with lower soil moisture contents.

3.7. Phosphorus budget

The summary of the total phosphorus budget in the study wetland obtained from the behavior simulations is shown in Table 5.6. Compared with other nutrient constituents, the phosphorus budget is relatively simple because only a few processes can affect the phosphorus cycle. For the first numerical experiment, during the two-year study period, 42.5± 2.4 kg P (equivalent to 72.9 ± 4.1% of P load) was flushed out by outflow. 7.4 ± 2.5 kg P (12.6 ± 4.3% of

P load) was retained in the wetland through the process of settling. 5.5 ± 2.0 kg P was diffused to the bottom sediment contributing to 9.4 ± 3.4% of P load. The phosphorus budget did not show much change between the two numerical experiments. With the free-drainage bottom boundary condition applied in the second numerical experiment, the total phosphorous budget of each component was similar to those from the first numerical experiment. Sharifi et al. (2017) did not evaluate the phosphorous budget in the Expanded model. In this study, we compared our results with those from the Original model. The results of the total phosphorous budget from the Original model are shown in Table 5.7. Comparing between the results from the first numerical experiment using the Updated model and the results from the Original model, the outflow from the two versions of the model had similar estimations (42.5 ± 2.4 kg P versus 39.3 ± 5.1 kg P). The Updated model reports 19.7% less in deposition compared to the Original model. However, the diffusion was higher than those from the Original model (5.5 ± 2.0 kg P versus 4.0 ± 1.5 kg P).

3.8. Plant growth and biomass prediction

The result of the time series for simulated plant aboveground biomass in the study wetland from May 1995 to May 1997 is shown in Figure 5.15. Note that *WetQual* simulates total plant biomass (above + below ground). Above-ground biomass was calculated using the average belowground:aboveground biomass ratio (0.40) of wetland macrophytes from Whigham and Simpson (1978). The results are compared with the aboveground biomass from the once-a-year field measurements in mid-to-late October 1995 and 1996, respectively, carried out by Whigham et al. (2002). In Figure 5.15, field measurements are plotted at the time before plants go dormant in the model simulation. Model simulated biomass started from the initial value on May 9, 1995 and then gradually increased for 66 days, then then rate of increase decreased when plants

approached maturity. The biomass reached the maximum value until plants went dormant on November 7, 1995. Biomass decreased during dormancy. On February 7, 1996, plants started growing again. The growing season in 1996 was 274 days. On November 6, 1996, plants went dormant until February 5, 1997. The biomass in 1995 was lower than that in 1996 because of the water stress associated with the lower soil moisture content in the variably saturated compartment in the growing season. In 1996, there was no or little water stress to influence plant growth. The highest biomass in 1996 was 447.8 g/m^2, which was much higher than that in 1995 (214.3g/m^2). In Figure 5.15, the model estimated biomass at the end of the growing season in 1995 and 1996 were higher than those from the field measurements. Whigham et al. (2002) reported that due to the harvest time and method used, the biomass might be underestimated. It is reasonable that the model provided higher biomass estimations for two years, and the maximum biomass was simulated before the date of sampling. In addition, based on the information provided by Jordan et al. (2003), during the growing season, 70% to 90% of the wetland surface was covered by emergent vegetation, while during the nongrowing season, the covered area dropped to about 10% to 20% of the wetland surface. Based on this information, the ratio of biomass in terms of vegetation cover in the growing season and the nongrowing season varied from 3.5:1 (70%:20%) to 9:1 (90%:10%). The model simulated ratios of the maximum and the minimum biomass were 4.3:1 and 6.3:1 for 1995 and 1996, respectively. The lowest ratio in 1995 was related to the dry period. The ratios in both 1995 and 1996 within the range reported in Jordan et al. (2003). Furthermore, we communicated the results with the authors from Whigham et al. (2002), specifically the temporal biomass dynamics. They found the general shape of the biomass curve reasonable (personal communication). This simulation proved that the equations for plant growth

applied in the Updated *WetQual* model are capable to simulate seasonal biomass variations in the wetland area.

We further investigated the plant nutrient uptake in growing season in 1995 and 1996. The results of plant net primary productivity (NPP), nitrogen, and phosphorus uptake in growing season are shown in Table 5.8. The NPP represents the maximum plant biomass during the growing season. Plant uptake nitrogen in forms of ammonium-nitrogen and nitrate-nitrogen, and phosphorus in the form of inorganic phosphorus (orthophosphate). In 1995, the NPP was 214.32 g/m^2, and nitrogen and phosphorus uptake were 1.49 g/m^2 and 0.47 g/m^2, respectively. In 1996, NPP increased to 447.79 g/m^2, and nitrogen and phosphorus uptake increased to 5.41 g/m^2 and 1.50 g/m^2, respectively. The values of NPP, nitrogen, and phosphorus uptake in 1996 were 2.1, 3.6, and 3.2 times of those in 1995, respectively. The water stress in 1995 inhibited plant growth and photosynthesis resulting in lower values of NPP, nitrogen, and phosphorus uptake. Whigham et al. (2002) measured total nitrogen, phosphorus in aboveground biomass for the study wetland in 1995 and 1996. As shown in Table 5.8, the total nitrogen and phosphorus reported from Whigham et al. (2002) were 1.70 g/m^2 and 0.26 g/m^2, respectively in 1995, and 3.53 g/m^2 and 0.88 g/m^2, respectively in 1996. *WetQual* estimated plant nitrogen and phosphorus uptake higher than those reported from Whigham et al. (2002). The higher biomass estimation was likely related to higher estimated nutrient uptake.

3.9. Implications of variably saturated compartment in *WetQaul*

The results of this study showed that dividing the wetland into ponded and variably saturated compartment has impacts on biogeochemical cycles in wetland modeling. Although the Updated model showed good performance on estimating nutrient exports in the ponded

compartment, comparing the nutrient budgets from the Updated model (the first numerical experiment) to those from the Original model (results of nutrient budgets reported from the Original model are shown in Table 5.7) reveals some differences. For the nitrogen cycle, the net deposition, denitrification, and NO_3 diffusion in the ponded compartment decreased in the Updated model. The deposition and diffusion in the ponded compartment were offset by separating wetland into ponded and variably saturated compartments. For the carbon cycle, the Updated model reported less carbon gas production than the Original model. The separation of the wetland compartments reduced the total area for microbial decomposition processes, which produce gaseous carbon (CO_2+CH_4) into the atmosphere. Implementing the variably saturated compartment to the wetland model did not have much impact on the phosphorus cycle, and this is likely due to the simplicity of the phosphorus cycle.

The use of the two-layer model in the variably saturated compartment eliminates the numerical instability in the Updated model and produces reasonable moisture estimations for unsaturated soils. Besides, the two-layer model estimates actual plant water uptake that can be used to improve the wetland water budget and estimate plant water stress. The Updated model benefits from the adding of these detailed information for accurately estimating water budget and plant biomass.

4. Summary and conclusion

In this study, we modified the soil moisture movement and plant growth modules in a process-based biogeochemical model *WetQual* for wetland nutrient cycling. The two-layer model developed by He et al. (2021a) was coded into *WetQual* to simulate soil moisture dynamics in the variably saturated compartment of the wetland. The embedded two-layer model deals with various

atmospheric boundary conditions including precipitation, evapotranspiration, and ponding subjected to changing shallow groundwater levels within the soil. Plant water uptake was constrained by a water stress response function to better represent the plant water uptake in wetland environment. The primary productivity module was modified to consider environmental factors including temperature stress, water stress, and plant dormancy.

The updated *WetQual* model (Updated model) was evaluated by applying it to a restored wetland located on Kent Island, Maryland by two numerical experiments using different bottom boundary conditions of moisture movement in the variably saturated compartment. The first numerical experiment assumed a zero-pressure head bottom boundary condition indicating presence of very shallow groundwater. Free-drainage bottom boundary condition was applied in the second numerical experiment. MC simulations were conducted using 100,000 parameter sets for the two numerical experiments. The simulated TN, NO_3, NH_4, ON, TOC, TSS, and P loads were compared against observed loads. Mass balances of N, C, and P were examined to understand the differences of source/sink of nutrients between two numerical experiments. The Kolmogorov-Smirnov test was performed between the behavior and non-behavior parameter sets to evaluate the parameter sensitivity. Besides, the model was run using the best-estimated input parameters based on the results from the first numerical experiment to estimate the plant biomass under environmental stress in the study wetland.

The results showed that the Updated model estimated weekly average of nutrient loads generally matched well with observations for both numerical experiments. The model had excellent performance in estimating NO_3 and TOC loads and moderate performance in capturing ON, NH_4, and TN loads, but not as good in estimating TSS and P loads. The model performances on TN, ON, and TOC loads improved, while the performance on NH_4, NO_3, and TSS loads slightly

decreased compared to those from Sharifi et al. (2017). Soil moisture contents in the variably saturated compartment estimated by the two-layer model were higher in the first numerical experiment but significantly lower in the second numerical experiment. Besides, the use of the zero-pressure head and free-drainage bottom boundary conditions applied in the variably saturated compartment had significant influences on NH_4, TSS, and TOC exports in the ponded compartment.

Sensitivity analysis revealed that the most sensitive parameters in the ponded and variably saturated compartments more or less confirmed the sensitive parameters of the Original and the Expanded models, but the order of sensitivities were not the same. The nitrogen cycle had high sensitivity to denitrification, ammonium ion distribution, and temperature. Microbial respiration, temperature, and plant growth were the most important processes affecting the carbon cycle. The Phosphorous cycle had high sensitivity to the settling and sorption processes in the ponded compartment. However, N, C, and P cycles did not show sensitivity to soil hydraulic parameters.

Mass balance analysis showed that using different bottom boundary conditions for moisture flow in the variably saturated compartment influence N, C, and P budget. For N budget, the most notable differences appeared in the mass of volatilization and denitrification in the variably saturated compartment from the second numerical experiment, which were only a fraction of those from the first numerical experiment. The net deposition, denitrification, NH_4 diffusion, and NO_3 diffusion in the ponded compartment in the first numerical experiment were lower than those from the second numerical experiment. For C budget, the diffusion in the ponded compartment in the first numerical experiment was lower than that in the second numerical experiment. In the variably saturated compartment, the plant biomass in the first numerical experiment were higher than those in the second numerical experiment. Biomass in both numerical

experiments was lower in the ponded compartment and higher in the variably saturated compartment compared to the results from the Expanded model due to the water stress applied in the Updated model. For P, the outflow reported in the Updated model was higher than that from the Original model. Besides, the model uncertainties for sources/sinks components were generally smaller in all nutrient constituents compared to the results from Sharifi et al. (2017) and the Original model.

The time series of the model estimated biomass in the study wetland using calibrated model parameters showed seasonal variations according to temperature and water stress in addition to the period of maturity and dormancy. The model estimated annual biomass predictions for 1995 and 1996 showed reasonable seasonal variations and had a good match with field measurements. The modified equations for plant growth are capable of estimating plant biomass in wetland environment.

Table 5.1: The physical properties and van Genuchten hydraulic parameters of the root zone and vadose zone in the soil from variably saturated compartment of the study wetland

Layer	Depth (cm)	Sand (%)	Silt (%)	Clay (%)	θ_r (cm^3cm^{-3})	θ_s (cm^3cm^{-3})	α (cm^{-1})	n	K_s (cm/day)
Root zone	0-15	20	67	13	0.082	0.405	0.0034	1.566	26.7
Vadose zone	15-73	15	64	21	0.074	0.380	0.0037	1.497	15.0

Table 5.2: Model parameters considered random, their distributions and minimum and maximum values

Parameters	Distribution	Min	Max
θ_{r1} (cm^3cm^{-3})	*U*	0.039	0.126
θ_{r2} (cm^3cm^{-3})	*U*	0.037	0.110
θ_{s1} (cm^3cm^{-3})	*U*	0.363	0.447
θ_{s2} (cm^3cm^{-3})	*U*	0.333	0.428
α_1 (cm^{-1})	*U*	0.0015	0.0076
α_2 (cm^{-1})	*U*	0.0015	0.0089
n_1	*U*	1.327	1.848
n_2	*U*	1.284	1.745
K_{s1} (cm/day)	*U*	8.1	87.7
K_{s2} (cm/day)	*U*	5.1	44.4
ε	*U*	0.01	1
L_{root} (cm)	*U*	5	25
T_{opt} (℃)	*U*	0	10
T_{base} (℃)	*U*	10	20
h_0 (cm)	*U*	1	500
h_{50} (cm)	*U*	500	2000
p	*U*	1	4

Table 5.3: Maximum and minimum of MBE, NAS, and L_k of the behavioral simulation results based on mass of export from observed and simulated exports of each constituent for two numerical experiments

Numerical experiment	Measure		TN	ON	NH_4	NO_3	TSS	TOC	P
1	$MBE(\%)$	Max	3.5	-4.5	16.1	50.2	25.2	-10.7	-16.8
		Min	-23.9	-34.4	-25.8	11.2	-55.4	-14.6	-61.1
	NAS	Max	0.83	0.75	0.78	0.92	0.48	0.93	0.76
		Min	0.78	0.70	0.72	0.89	0.37	0.92	0.42
	L_k	Max	0.82	0.71	0.78	0.80	0.56	0.93	0.67
		Min	0.63	0.52	0.59	0.54	0.31	0.80	0.31
2	$MBE(\%)$	Max	8.6	-3.3	14.3	54.4	51.0	7.8	-15.4
		Min	-25.8	-34.2	-20.8	28.7	-73.3	-14.5	-57.2
	NAS	Max	0.83	0.75	0.78	0.91	0.47	0.94	0.76
		Min	0.78	0.71	0.73	0.87	0.23	0.92	0.45
	L_k	Max	0.84	0.72	0.80	0.67	0.57	0.93	0.68
		Min	0.62	0.53	0.62	0.51	0.22	0.80	0.33

Table 5.4: Nitrogen budget in the study wetland

Component	1st Numerical experiment			2nd Numerical experiment		
	Ponded Compartment	Variably saturated compartment	Total	Ponded Compartment	Variably saturated compartment	Total
Watershed runoff	3849.2	N/A	3849.2 (100%)	3849.2	N/A	3849.2 (100%)
Atmospheric deposition[a]	2164.0 ± 115.2	N/A	2164.0 ± 115.2 (56.2 ± 3.0%)	2137.8 ± 123.3	N/A	2137.8 ± 123.3 (55.5 ± 3.2%)
Outflow	1274.2 ± 248.1	105.7 ± 129.5	1379.9 ± 377.6 (35.8 ± 9.8%)	1211.3 ± 250.9	1.0 ± 3.6	1212.3 ± 254.5 (31.5 ± 6.6%)
Net deposition[b]	124.6 ± 81.9	N/A	124.6 ± 81.9 (3.2 ± 2.1%)	126.6 ± 68.1	N/A	126.6 ± 68.1 (3.3 ± 1.8%)
Volatilization	32.9 ± 0.2	250.2 ± 8.2	283.1 ± 8.3 (7.4 ± 0.2%)	32.9 ± 0.1	235.8 ± 10.6	268.7 ± 10.7 (7.0 ± 0.3%)
Denitrification	250.7 ± 171.2	N/A	250.7 ± 171.2 (6.5±4.4%)	384.2 ± 242.5	N/A	384.2 ± 242.5 (10.0 ± 6.3%)
NH_4 diffusion[c]	3849.2	N/A	3849.2 (100%)	3849.2	N/A	3849.2 (100%)
NO_3 diffusion	2164.0 ± 115.2	N/A	2164.0 ± 115.2 (56.2 ± 3.0%)	2137.8 ± 123.3	N/A	2137.8 ± 123.3 (55.5 ± 3.2%)

Note: Results of each component in the nitrogen budget are summation over the simulation period; all units are in kg; numbers in parentheses are values normalized with runoff loading + atmospheric deposition.

[a]Atmospheric deposition of nitrogen in the variably saturated compartment is assumed as water solute that is transported to the ponded part of the wetland by runoff.

[b]Net deposition is equal to net organic settling minus resuspension.

[c](+) represents from water column to sediment layer and vice versa.

Table 5.5: Carbon budget in the study wetland

Component	1st Numerical experiment			2nd Numerical experiment		
	Ponded Compartment	Variably saturated compartment	Total	Ponded Compartment	Variably saturated compartment	Total
Watershed runoff	3849.2	N/A	3849.2 (100%)	3849.2	N/A	3849.2 (100%)
Outflow	2164.0 ± 115.2	N/A	2164.0 ± 115.2 (56.2 ± 3.0%)	2137.8 ± 123.3	N/A	2137.8 ± 123.3 (55.5 ± 3.2%)
Gaseous losses[a]	1274.2 ± 248.1	105.7 ± 129.5	1379.9 ± 377.6 (35.8 ± 9.8%)	1211.3 ± 250.9	1.0 ± 3.6	1212.3 ± 254.5 (31.5 ± 6.6%)
Deposition	124.6 ± 81.9	N/A	124.6 ± 81.9 (3.2 ± 2.1%)	126.6 ± 68.1	N/A	126.6 ± 68.1 (3.3 ± 1.8%)
Biomass accumulation[b]	32.9 ± 0.2	250.2 ± 8.2	283.1 ± 8.3 (7.4 ± 0.2%)	32.8 ± 0.1	235.8 ± 10.6	268.7 ± 10.7 (7.0 ± 0.3%)
Diffusion	250.7 ± 171.2	N/A	250.7 ± 171.2 (6.5±4.4%)	384.2 ± 242.5	N/A	384.2 ± 242.5 (10.0 ± 6.3%)

Note: Results of each component in the carbon budget are summation over the simulation period; all units are in kg; numbers in parentheses are values normalized with runoff loading.

[a]Gaseous carbon is in form of CO_2 and CH_4.

[b]Biomass is measure of plant primary productivity.

Table 5.6: Phosphorous budget in the study wetland

Component	1st Numerical experiment			2nd Numerical experiment		
	Ponded Compartment	Variably saturated compartment	Total	Ponded Compartment	Variably saturated compartment	Total
Watershed runoff	58.3		58.3 (100%)	58.3		58.3 (100%)
Outflow	42.5 ± 2.4		42.5 ± 2.4 (72.9 ± 4.1%)	37.9 ± 2.5		37.9 ± 2.5 (65.0 ± 4.3%)
Deposition	7.4 ± 2.5		7.4 ± 2.5 (12.6 ± 4.3%)	7.0 ± 2.4		7.0 ± 2.4 (12.0 ± 4.1%)
Diffusion	5.5 ± 2.0		5.5 ± 2.0 (9.4 ± 3.4%)	5.7 ± 2.0		5.7 ± 2.0 (9.8 ± 3.4%)

Note: Results of each component in the phosphorous budget are summation over the simulation period; all units are in kg; numbers in parentheses are values normalized with runoff loading.

Table 5.7: Nitrogen and carbon budgets from the Expanded model and the phosphorous budget form the Original model in the study wetland

	Component	Ponded Compartment[a]	Variably saturated Compartment[a]	Total[a]	Original Model[b]
Nitrogen budget	Watershed runoff	336.3	N/A	336.3 (95.8%)	336.3 (95.8%)
	Atmospheric deposition	14.6	N/A	14.5 (4.2%)	14.5 (4.2%)
	Outflow	260.5 ± 30.4	N/A	262.3 ± 55.9 (74.3 ± 8.7%)	269.2 ± 36.7 (76.7 ± 10.5%)
	Net deposition	81.5 ± 18.4	N/A	81.5 ± 18.4 (23.2 ± 5.2%)	64.6 ± 31.3 (18.4 ± 8.9%)
	Volatilization	11.9 ± 8.5	2.4 ± 4.6	14.3 ± 13.1 (4.1 ± 3.7%)	8.1 ± 6.8 (2.3 ± 1.9%)
	Denitrification	10.3 ± 5.5	69.1 ± 67.2	79.4 ± 72.2 (22.6 ± 20.6%)	27.9 ± 5.8 (7.9 ± 1.6%)
	NH_4 diffusion	0.6 ± 3.7	N/A	0.6 ± 3.7 (0.2 ± 1.1%)	-1.1 ± 2.8 (-0.3 ± 0.8%)
	NO_3 diffusion	12.2 ± 3.5	N/A	12.2 ± 3.5 (3.5 ± 1.0%)	31.6 ± 5.0 (9.0 ± 1.4%)
Carbon budget	Watershed runoff	3849	N/A	3849 (100%)	3849 (100%)
	Outflow	2494 ± 148.5	N/A	2338.1 ± 173.4 (63.1 ± 3.9%)	2430 ± 152 (63.1 ± 4.0%)
	Gaseous losses	1308.2 ± 257.6	111.0 ± 145.8	1419 ± 403.4 (36.9 ± 10.5%)	1350 ± 269 (35.1 ± 7.0%)
	Deposition	162.5 ± 94	179.7 ± 87.9	162.5 ± 94.0 (4.2 ± 2.4%)	172 ± 79 (4.5 ± 2.1%)
	Biomass accumulation	180.6 ± 88.3	179.7 ± 87.9	360.1 ± 176.2 (9.4 ± 4.6%)	176 ± 88 (4.6 ± 4.3%)
	Diffusion	260.7 ± 117.2	N/A	260.7 ± 117.2 (6.8 ± 3.0%)	269 ± 122 (7.0 ± 3.2%)
Phosphorus budget	Watershed runoff				58.3 (100%)
	Outflow				39.3 ± 5.1 (67.4 ± 8.8%)
	Deposition				18.8 ± 5.0 (32.3 ± 8.6%)
	Diffusion				4.0 ± 1.6 (6.6 ± 2.7%)

Note: Results of each component in the nitrogen, carbon, and phosphorus budgets are summation over the simulation period; all units are in kg; numbers in parentheses from nitrogen budget are values normalized with runoff loading + atmospheric deposition; numbers in parentheses from carbon and phosphorus budgets are values normalized with runoff loading.

[a] Results of ponded compartment, variably saturated compartment, and total in nitrogen and carbon budgets are from Sharifi et al. (2017).

[b] Results of nitrogen budget and phosphorus budget are from Kalin et al. (2013); results of carbon budget are from Sharifi et al. (2013).

Table 5.8: Plant nutrient uptake during growing season in the study wetland in 1995 and 1996

	Net Primary Productivity (g/m^2)	Nitrogen Uptake[a] (g/m^2)	Phosphorus Uptake[b] (g/m^2)	Total Nitrogen reported in Whigham et al. (2002)[c] (g/m^2)	Total Phosphorus reported in Whigham et al. (2002)[d] (g/m^2)
1995	214.32	1.49	0.47	1.70	0.26
1996	447.79	5.41	1.50	3.53	0.88
Average	346.05	3.45	0.99	2.62	0.57

Note: [a] Nitrogen is in form of total ammonia-nitrogen (NH_4^+ and NH_3)

[b] Phosphorus is in form of orthophosphate (PO_4^{3-}, HPO_4^{2-}, $H_2PO_4^-$, and H_3PO_4)

[c] Total nitrogen reported in Whigham et al. (2002) was measured from aboveground biomass

[d] Total phosphorus reported in Whigham et al. (2002) was measured from aboveground biomass

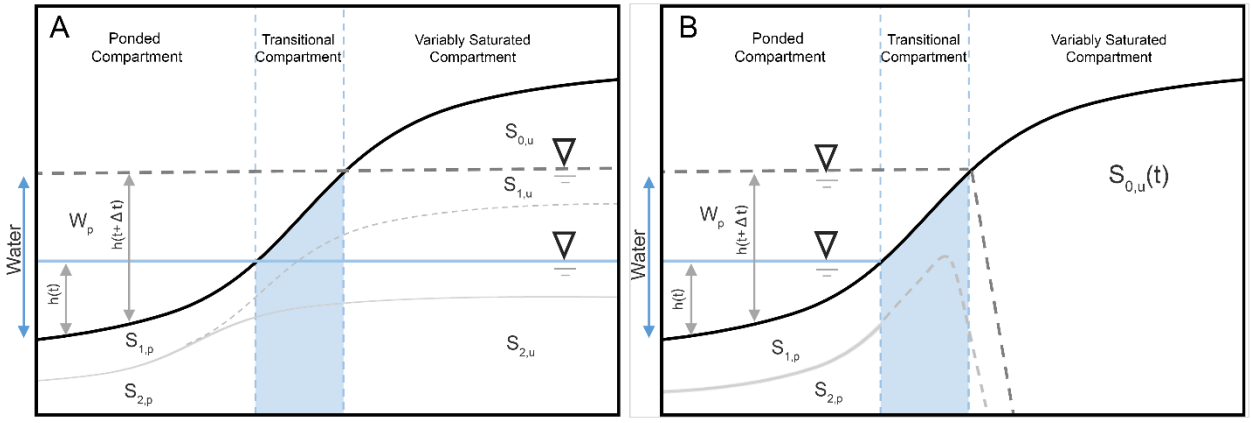

Figure 5.1: Schematic representations of the wetland compartmentalization into ponded and variably saturated compartments with A) shallow groundwater (water table same as water surface in wetland), and B) deep groundwater ; W stands for water column; S stands for soil column; 0, 1, and 2 represent unsaturated soil layer, aerobic sediment layer, and anaerobic sediment layer; subscripts p and u refer to ponded and variably saturated compartments, respectively; $h(t)$ and $h(t+\Delta t)$, represent water level in the ponded compartment at times t and $t+\Delta t$, respectively.

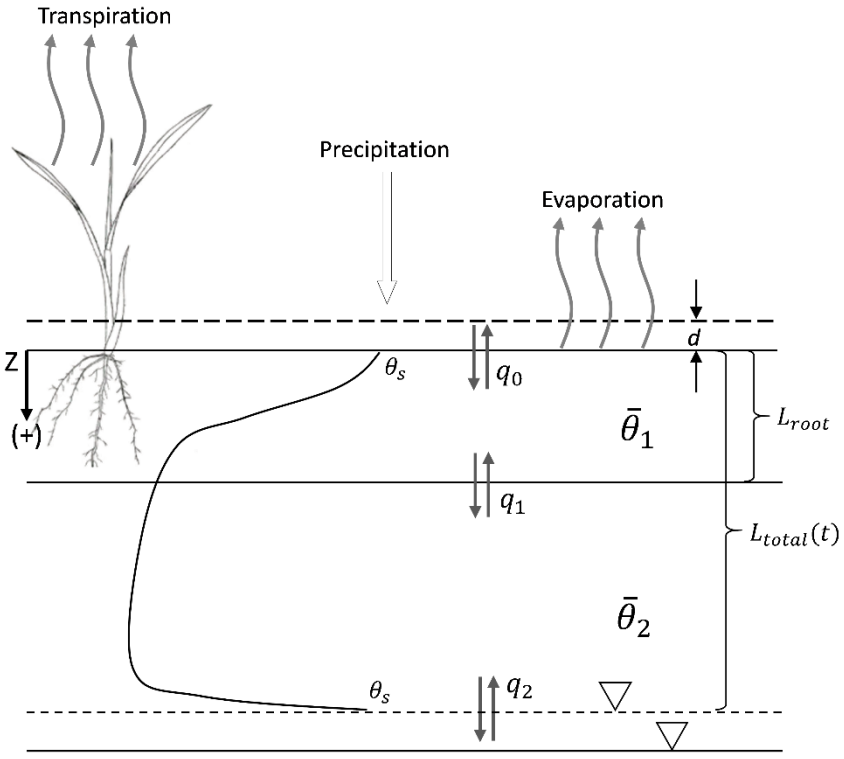

Figure 5.2: Schematic illustration of soil profile and the two-layer model depicting the root zone and vadose soil below (He et al., 2020a). d is the ponding depth; L_{root} is the first layer (zoot zone) depth; $L_{root}(t)$ is depth of water table at time t; q_0, q_1 and q_2 are the top, middle and bottom flux (positive downward), respectively.

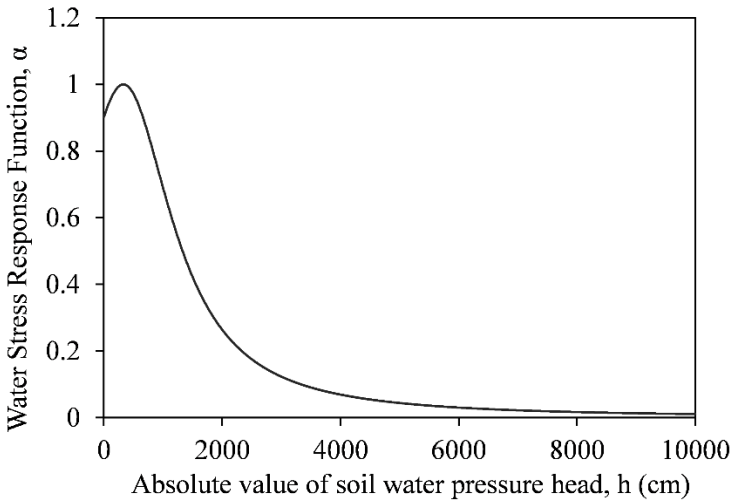

Figure 5.3: Modified water stress response function $\alpha(h)$ (Eq. 8) for wetland plants (using h_0=330 cm, h_{50}=1000 cm, and p=2)

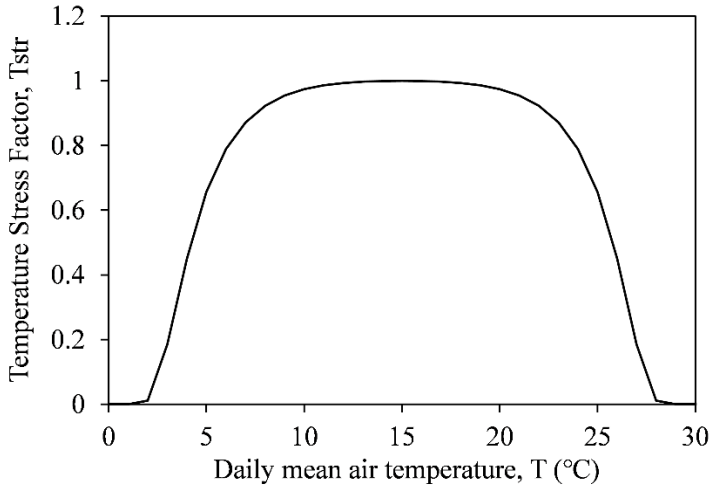

Figure 5.4: Impact of mean air temperature on plant growth for a plant with T_{base}=0℃ and T_{opt}=15℃.

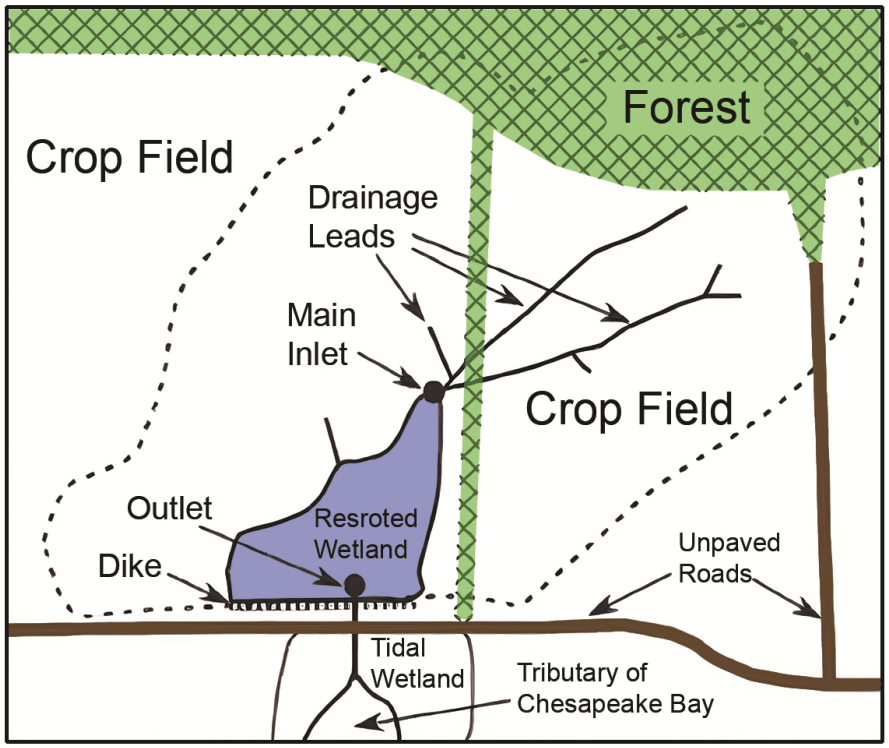

Figure 5.5: Study wetland and its watershed (dashed lines) draining into the wetland (modified from Kalin et al. (2013)).

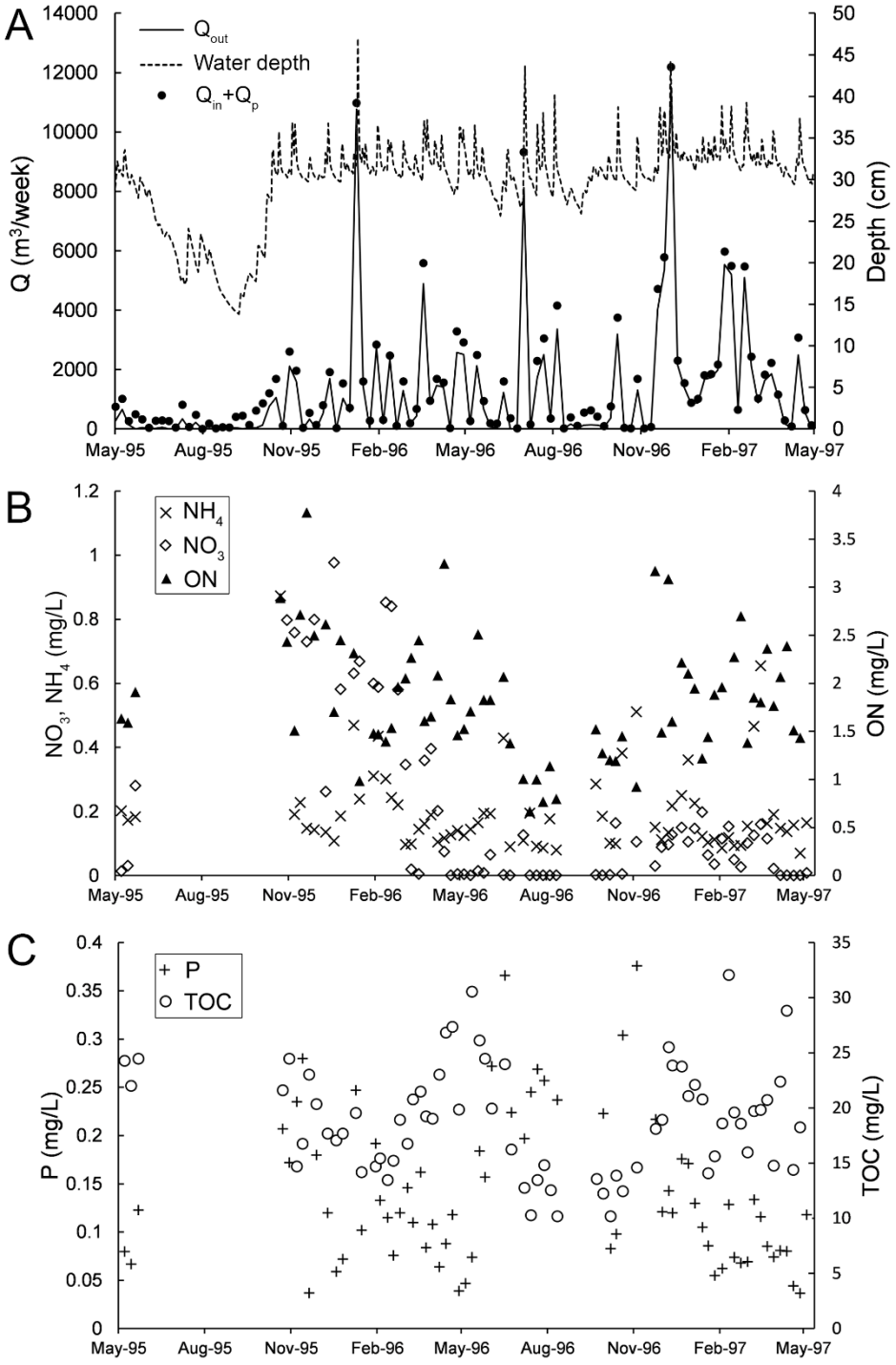

Figure 5.6: (A) Hydrology of the study wetland over the study period including average water depth, inflow, and outflow in ponded compartment; (B) Weekly-average outflow concentration of NO_3, NH_4 and ON; (C) Outflow concentration of P and TOC from May 1995 to May 1997. Q_{in} is inflow volume; Q_{out} is outflow volume; Q_p is precipitation volume falling on the wetland.

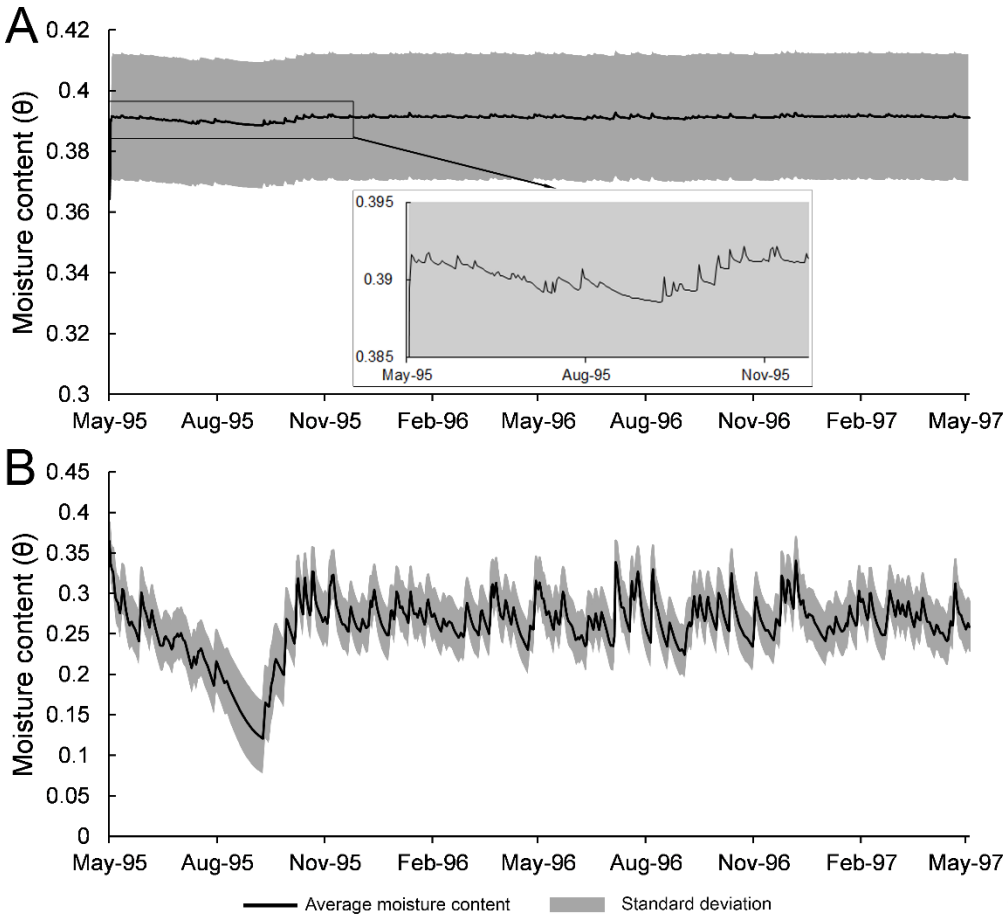

Figure 5.7: Average soil moisture content in variably saturated compartment from (A) the first numerical experiment and (B) the second numerical experiment. Grey bands represent standard deviations of moisture contents form 100,000 Monte Carlo simulation around mean values of moisture content.

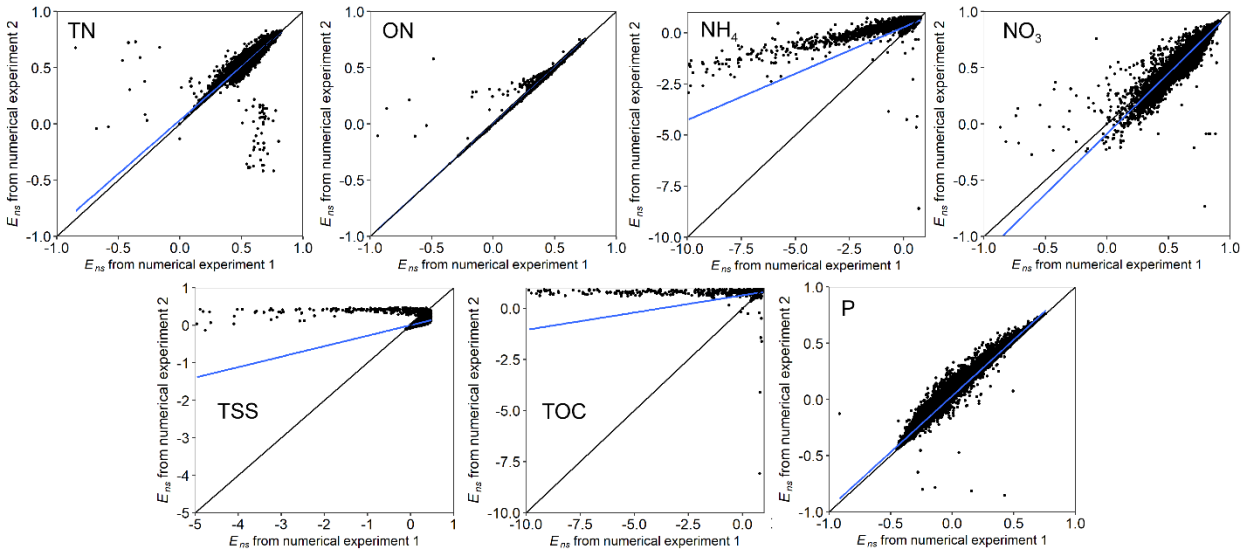

Figure 5.8: Relation between E_{ns} from 100,000 Monte Carlo simulations of two numerical experiments. Blues solid lines represent the trend lines of scatters. Black solid lines represent identity lines (1:1 line).

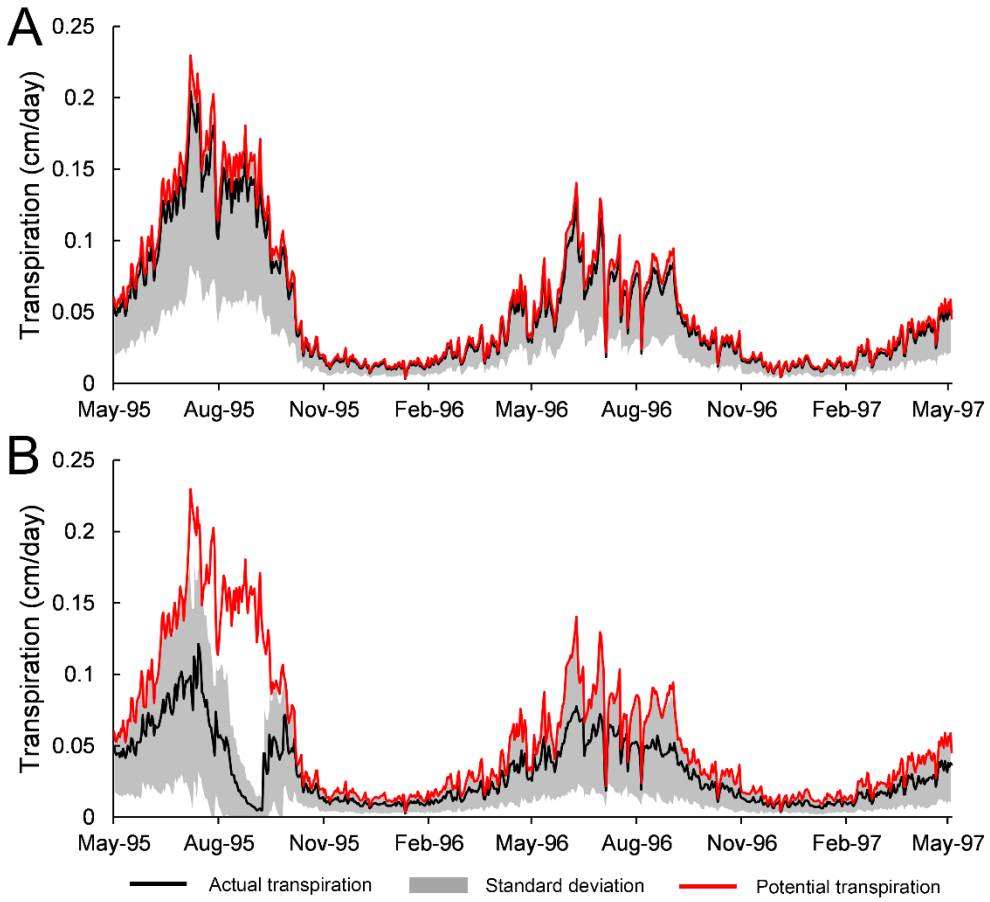

Figure 5.9: Model estimated daily actual transpiration rate compared with daily potential transpiration of plants in variably saturated compartment from (A) the first numerical experiment, and (B) the second numerical experiment.

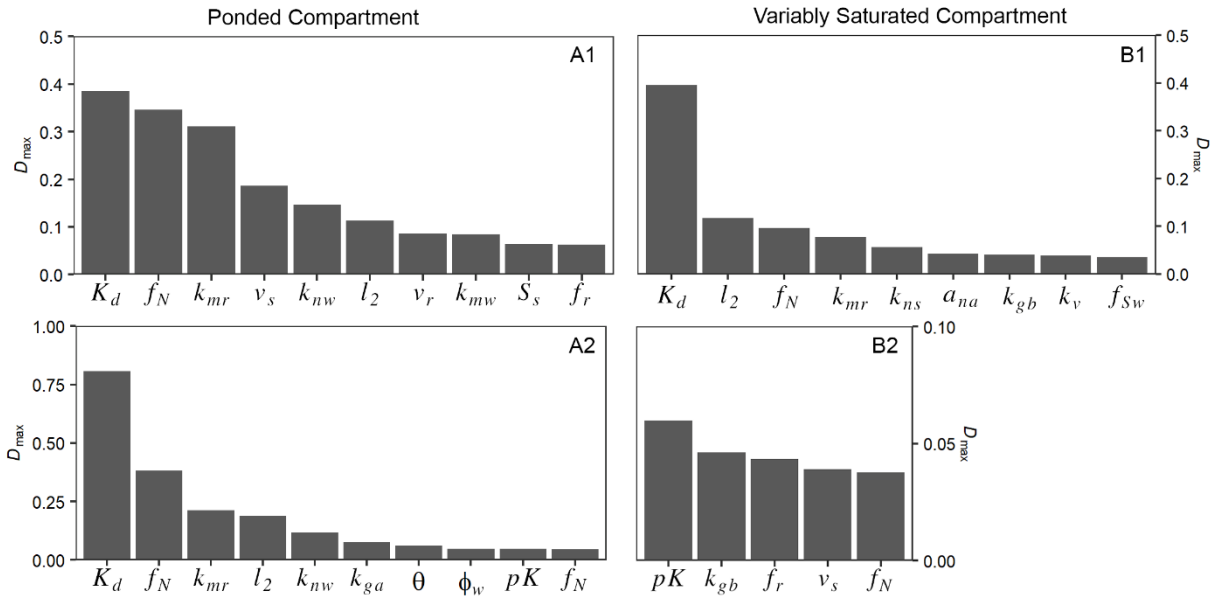

Figure 5.10: Summary of the K-S test and order of sensitivities based on NH_4 export for (A) ponded and (B) variably saturated compartments from (1) the first and (2) the second numerical experiments, respectively.

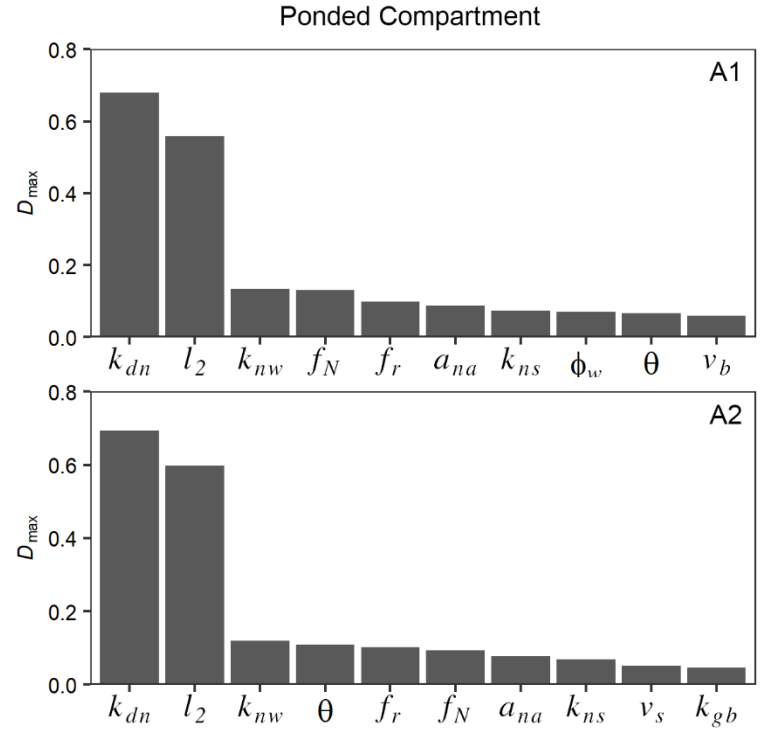

Figure 5.11: Summary of the K-S test and order of sensitivities based on NO_3 export for (A) ponded from (1) the first and (2) the second numerical experiments, respectively. No parameters were found sensitive for the variably saturated compartment.

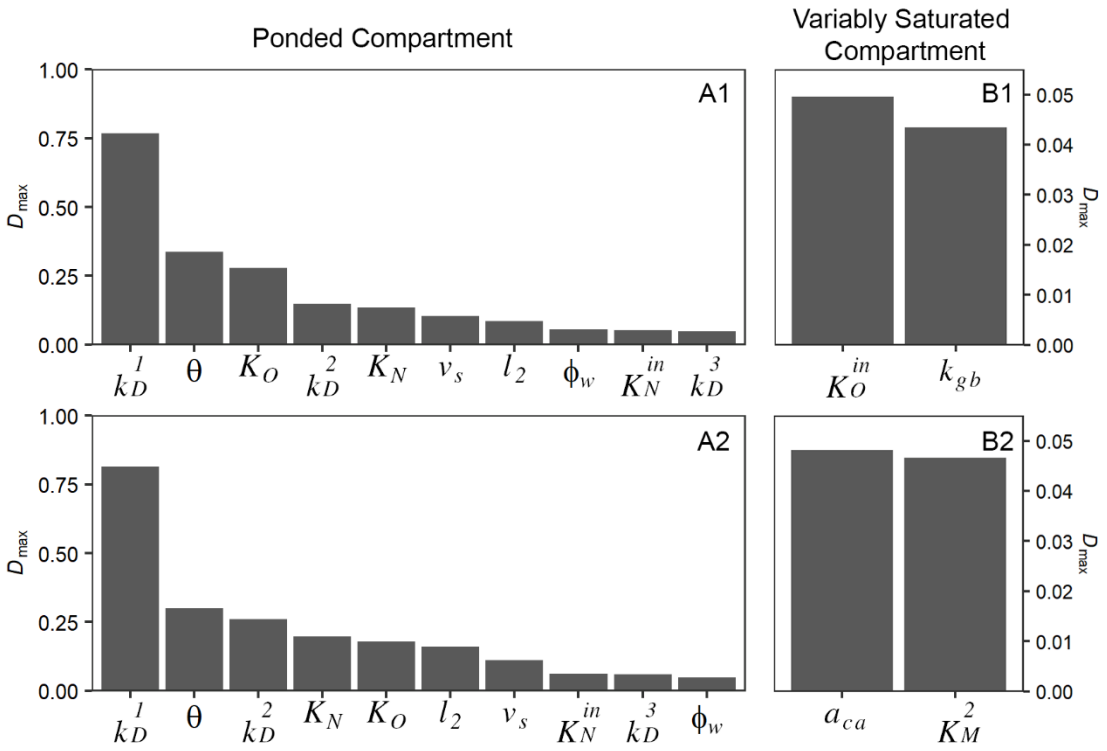

Figure 5.12: Summary of the K-S test and order of sensitivities based on TOC export for (A) ponded and (B) variably saturated compartments from (1) the first and (2) the second numerical experiments, respectively.

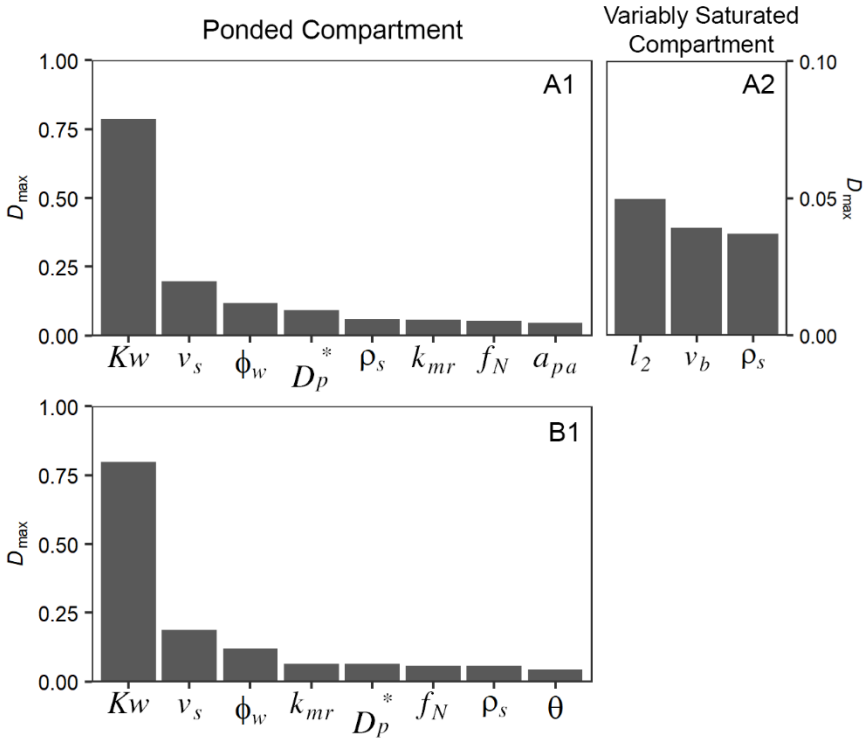

Figure 5.13: Summary of the K-S test and order of sensitivities based on P export for (1) ponded and (2) variably saturated compartments from (A) the first and (B) the second numerical experiments, respectively.

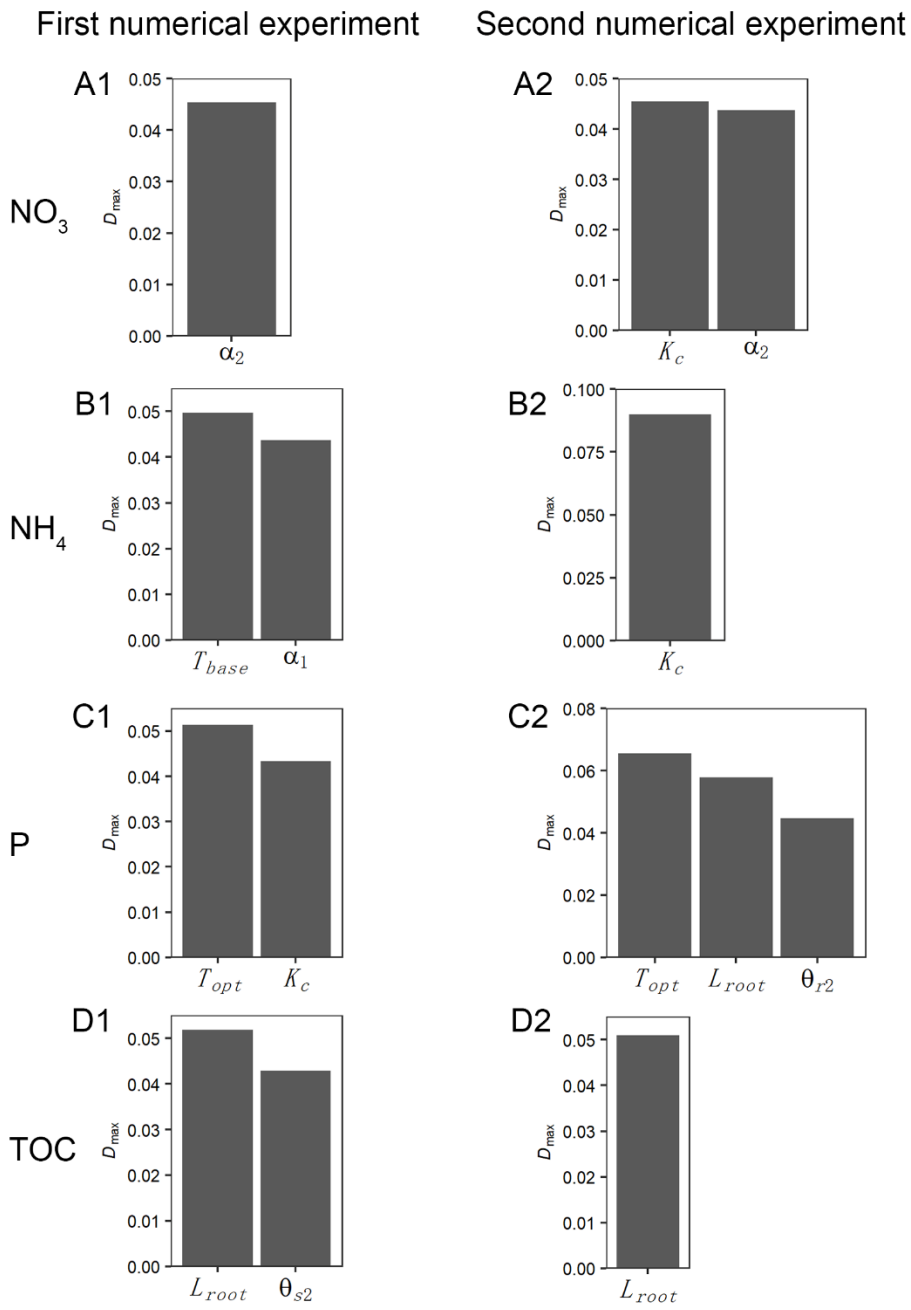

Figure 5.14: Summary of the K-S test and order of sensitivities of newly added parameters based on (A) NO_3, (B) NH_4, (C) P and (D) TOC exports, for variably saturated compartment from (1) the first and (2) the second numerical experiments, respectively.

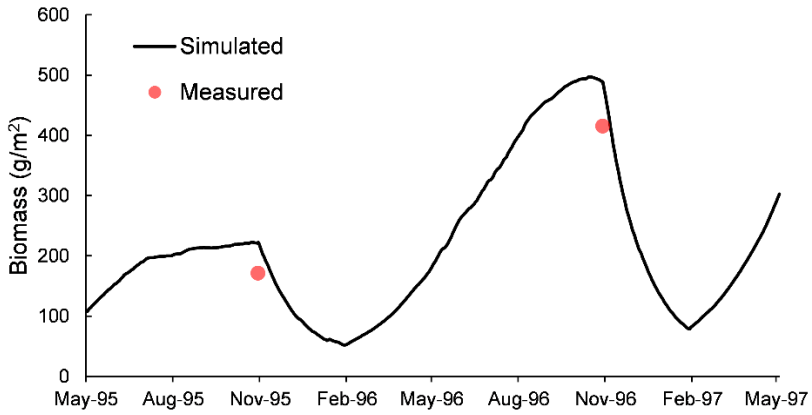

Figure 5.15: Model estimated and field measured plant biomass of the study wetland. Field measured plant biomass were obtained from Whigham et al. (2002).

Chapter 6: Conclusions

1. Summary and Conclusions

Soil moisture is one of the key variables in hydrological and biogeochemical processes. Simulating water movement in variably saturated soils in the root zone and vadose zone is important in land system models. Richard's Equation (RE) (Richards, 1931) is a commonly used, physical-based relationship that describes unsaturated flow in porous media. However, simulating water moisture flow in variably saturated soils with relatively shallow water table and dynamic atmospheric conditions is challenging due to high non-linear behavior of RE. In this study, we developed a new numerical solution to the one-dimensional (1-D) RE, which simulates depth-averaged soil moisture contents in a multiple layer soil profile under dynamic atmospheric condition including precipitation, evapotranspiration, and ponding subject to changing groundwater level. The solution converts the partial differential equation of RE to several coupled ordinary differential equations, which are solved explicitly using Heun's method. The proposed vertically-averaged RE solution was tested against analytical solutions, finite element RE solver (HYDRUS 1-D), and field observations. The results indicate that the numerical solution was robust, stable, and efficient in predicting depth-averaged soil moisture and water flux, which makes the solution trustworthy in hydrological modeling. In addition, the two-layer version of the solution was integrated into a wetland model, *WetQual*, to improve the soil moisture estimation in unsaturated soil of the wetland and further improve the biochemical processes in wetland soil. Multiple analyses were performed and the major finding emphasized the significance of the role that soil moisture dynamics play in wetland nutrient cycles and plant biomass.

In Chapter 1, four major objectives were presented. Each of these objectives is summarized below, and following that, the most important findings are listed.

1.1. Objective 1 ***Develop a two-layer vertically-averaged RE solution to simulate soil moisture dynamics under dynamic atmospheric conditions subject to relatively shallow groundwater table***

A vertically-averaged form of one-dimensional RE was derived to simulate vertical unsaturated water movement in a two-layered soil. The two-layer model simulates averaged soil moisture content by connecting hydroclimate conditions to the vadose zone with shallow and deep water tables (WTs). The numerical model was obtained by replacing RE with two-coupled ODEs and solutions are obtained numerically using the simple Huen's method. The numerical method is mass-conservative. The performance of the two-layer model was investigated in terms of computational accuracy and efficiency by comparison with HYDRUS as a reference model for three simulation scenarios, free-drainage at the bottom of the soil profile, WT at the bottom of the soil domain, and falling WT. Three soil textures with high, medium, and low permeability and different combinations of plant transpiration and rainfall rates were considered. The following conclusions are drawn:

1. The two-layer model was robust and accurate in simulating variably saturated flows. It can capture the dynamics of depth-averaged soil moisture under different surface flux boundary conditions (BCs) in the presence of deep and shallow water table. Overall, simulated cumulative fluxes agreed very well with those from HYDRUS for all scenarios. Although some relatively small discrepancies of moisture estimates between the two models were observed, the *RMSE* values, overall, indicate excellent model performance.

2. The two-layer model captured actual evaporation dynamics well in root zone, mimicking the behavior of the root zone or the biologically active sediment layer in wetlands.

3. The two-layer model can capture the dynamics of average soil moisture above the water table within the root zone and the lower vadose soil as the WT retreats.

4. The CPU time required to run the two-layer model for numerical experiments were less than that for HYDRUS.

1.2. Objective 2 Perform an in-depth assessment of the two-layer model to evaluate its strength and weakness in simulating soil moisture content under complex and changing environments

The two-layer model was evaluated with two numerical experiments and a site-level application. In the first numerical experiment, the model was ran for 231 soil textures under various atmospheric and bottom boundary conditions with soil profile depth varied from 10 cm to 400 cm. The thickness of the root zone layer and the second layer were varied from 10 cm to 200 cm at 10 cm intervals. Soil moisture estimates were compared with vertically averaged HYDRUS simulated nodal values as a reference. The second numerical experiment was carried to assess the performance of the model with two layers of contrasting (high and low) permeabilities. Thirdly, the two-layer model was applied to a SCAN site to simulate site-level soil moisture content of two soil layers under real atmospheric and field conditions. BMC methodology was integrated with the two-layer model for model calibration and uncertainty estimation. The following conclusions were drawn:

1. Among 92,400 simulations, the two-layer model showed excellent performance with free-drainage boundary condition with 99.8% of the total simulations having *RMSE* ≤0.015; with the zero-pressure head boundary condition representing water table, this percentage became 87.5%.

2. The two-layer model had excellent performance (*RMSE*≤0.015) for soil textures with one of the sand, silt, and clay separates less than about 30% for free-drainage and zero-pressure head bottom boundary conditions. In addition, the two-layer model showed good skill in estimating layer averaged moisture contents for soil domains having the root zone depth greater than 10 cm and the lower vadose soil layer thickness less than 150 cm for free-drainage bottom boundary condition. For zero-pressure head bottom boundary condition, the model performed very well with the first layer thickness between 30 cm to 70 cm and the second layer between 20 cm to 100 cm.

3. The two-layer model showed satisfactory performance in simulating soil moisture contents and top and bottom fluxes as well as actual plant water uptake in stratified soils (soil layers with contrasting permeabilities). Compared to the finite element model HYDRUS, results from the two-layer model showed *RMSE* values smaller than 0.02 for all simulations. The two-layer model solution deals with contrasting hydraulic conductivity properly.

4. The results of the model application indicate that the two-layer model can deal with layer averaged soil moisture modeling at field scale with appropriate input data. The model performance was found to be good with *RMSE* values ≤0.023 and *NSE* values ≥ 0.62 during both calibration and validation periods.

5. The uncertainty in soil characteristic parameters and simulated moisture content was computed using the Bayesian Monte Carlo method. Much of the uncertainty was attributed to observational, hydroclimate data, and model structural uncertainties, while parametric uncertainty

was found to be very small after conditioning on the observed moisture content data. Besides, all model parameters were identifiable using the observed data as evaluated by the K-S test. BMC methodology constrained all model parameters very well using informed prior distributions.

1.3. Objective 3 Extend the two-layer solution of depth-averaged RE to a multiple Layer-Averaged RE solution to predict high vertical resolution soil moisture contents and the stratified soil profile with multiple soil textures

The solution of the two-layer approximation of RE was extended to a multi-layer-averaged numerical scheme of Richards equation, named LARE. The solution of LARE converted the partial differential equation of RE into multiple coupled ordinary differential equations derived from the integrated form of RE. Several coupled governing equations are solved by explicit Heun's method to describe layer averaged soil moisture contents for multiple soil layers. The proposed model is designed for simulating soil moisture dynamics in layered or stratified soils under various atmospheric conditions and with a switching bottom boundary condition controlled by dynamic groundwater level. LARE performance was compared against analytical solutions, finite element RE solution by HYDRUS 1-D, and field-scale soil moisture observations from SCAN dataset. The following conclusions were drawn:

1. LARE has the capability to simulate soil moisture in both homogeneous and heterogeneous soil profiles with either fine or coarse grids for different upper and lower boundary conditions.

2. LARE showed excellent performance with free drainage bottom boundary condition for various soil depth and layer thicknesses, while the model performance dropped for deep soil profiles with fewer layers for zero-pressure head bottom boundary condition.

3. LARE perfectly estimated soil moisture contents with dynamic shallow groundwater level within the soil column without any convergence issues. With the correct soil moisture prediction, the actual plant water uptake was properly estimated.

4. LARE showed good performance under real soil and atmospheric conditions at site level application. The uncertainty analysis showed that parametric uncertainty contributed to the overall uncertainty the most, while the model structural uncertainty was very small.

1.4. Objective 4 Improve the soil moisture module and plant growth/death module in *WetQual* and evaluate the performance of the updated *WetQual*

We modified the soil moisture movement and plant growth modules in a process-based biogeochemical model WetQual for wetland nutrient cycling. The two-layer model developed in Chapter 2 was integrated into WetQual to simulate soil moisture dynamics in the variably saturated compartment of the wetland. The embedded two-layer model deals with various atmospheric boundary conditions including precipitation, evapotranspiration, and ponding, subjected to changing shallow groundwater levels within the soil. Plant water uptake was constrained by a modified S-shape water stress response function to better represent the plant water uptake in wetland environment. The primary productivity module was modified to consider environmental factors including temperature stress, water stress, and plant dormancy. The updated WetQual model (Updated model) was evaluated by applying it to a restored wetland located on Kent Island,

Maryland by two numerical experiments using different bottom boundary conditions of moisture movement in the variably saturated compartment. The first numerical experiment assumed a zero-pressure head bottom boundary condition indicating the presence of very shallow groundwater. Free-drainage bottom boundary condition was applied in the second numerical experiment. MC simulations were conducted using 100,000 parameter sets for the two numerical experiments. The nutrient exports of total nitrogen (TN), nitrate-nitrogen (NO_3), ammonium-nitrogen (NH_4), organic nitrogen (ON), total organic carbon (TOC), inorganic phosphorus (P), and total suspended sediment (TSS) were compared with observed data. In addition, model simulated plant biomass and plant nutrient uptake were compared with field measurements. The following conclusions were drawn:

1. The Updated model estimated weekly average of nutrient loads generally matched well with observations for both numerical experiments. The model had excellent performance in estimating NO_3 and TOC loads and moderate performance in capturing ON, NH_4, and TN loads, but not as good in estimating TSS and P loads.

2. Soil moisture contents in the variably saturated compartment estimated by the two-layer model were higher when applying zero-pressured head bottom boundary condition than those obtained by applying free-drainage bottom boundary condition.

3. The use of the zero-pressure head and free-drainage bottom boundary conditions applied in the variably saturated compartment had significant influences on NH_4, TSS, and TOC exports in the ponded compartment.

4. Sensitivity analysis revealed that the nitrogen cycle had high sensitivity to denitrification, ammonium ion distribution, temperature, and thickness of the anaerobic soil layer. Mineralization

of organic carbon under aerobic condition, oxidation of DOC, respiration, temperature, and plant growth were the most important processes affecting the carbon cycle. The phosphorous cycle had high sensitivity to the settling and sorption processes in the ponded compartment. However, soil parameters did not show sensitivity to N, C, and P exports in the ponded compartment.

5. Mass balance analysis showed that using different bottom boundary conditions for moisture flow in the variably saturated compartment influence N, C, and P budget. Comparison of nutrient budgets between the Updated model and the Original model without separating the wetland into two compartments, the differences were observed, indicating that dividing wetland into ponded and variably saturated compartment can affect wetland nutrient biogeochemical cycles.

6. The time series of the model estimated biomass in the study wetland using calibrated model parameters showed seasonal variations according to temperature and water stress in addition to the period of dormancy. The model estimated annual biomass predictions for 1995 and 1996 had a good match with field measurements.

2. Future Research

In this dissertation, we have presented a novel vertically-averaged numerical solution to RE. It brings many possibilities for future work, which can be undertaken in the following areas:

The numerical solutions of the vertically-averaged RE are based on the mixed form of RE. In a fully saturated soil condition, the mixed form of RE may underestimate the water flux between soil layers. The numerical solutions could be derived based on the head form of RE using the vertically-averaged technique. By doing this, fluxes between soil layers can be accurately estimated when the soil profile is saturated.

The solutions of the two-layer model and LARE could be used in inverse modeling studies for estimating hydraulic properties for layered soils by coupling them with the Bayesian framework or Markov chain Monte Carlo (MCMC) method. In practice, soil physical properties, such as percentage of sand, silt, and clay, bulk density, and organic content are measured for certain depth of the soil. It is very convenient to estimate soil hydraulic properties for each soil layer using vertically-averaged solution of RE. The advantage of this approach is that it can be used to estimate soil hydraulic properties at larger spatial scales.

The bottom boundary condition applied in the current solution of vertically-averaged RE is groundwater controlled, which can switch between zero-pressure head and free-drainage based on the groundwater level as model input. However, in large-scale hydrological modeling, groundwater level data is often difficult to obtain and sometimes the database has insufficient monitoring data. I suggest adding a subroutine that can track groundwater table within the soil profile. This subroutine can update groundwater depth during the iterations according to the moisture content or pressure head changes between two soil layers. By adding this feature, the two-layer model and LARE can fully connect the groundwater and atmosphere processes.

The current Earth system models hardly consider full three-dimensional (3-D) numerical solutions for surface-subsurface flow modeling because the 3-D solutions are computationally too expensive in large-scale applications. Alternatively, the quasi 3-D models, which couple 1-D variably saturated flow models with lateral flow equations, can be an alternative to model surface-subsurface flow (e.g. Yakirevich et al., 1998; Shen and Phanikumar, 2010; Hazenberg et al., 2015). The lateral flow equations can be added between grids in the model domain where 1-D vertically-averaged RE is applied to link lateral flow between grids.

LARE can be coupled with some watershed models or Earth system models to improve their performance in predicting moisture contents. For example, the Community Land Model version 5 (CLM 5) (Lawrence et al., 2019) simulates soil moisture contents in a 50-meter soil profile with 25 layers using finite-difference approximations of RE. The solution employs a zero-flux bottom boundary condition and is solved using implicit time discretization scheme. However, this lower boundary condition is relatively simple that can be improved. With several features added, LARE can be capable to simulate soil moisture in complex environmental conditions. First, more than one plant root distribution function can be added, such as those developed by Feddes (1982), Gale and Grigal (1987), and Jackson et al. (1996). These can be applied to different plant types. Second, the root growth models (such as Šimůnek and Suarez, 1993; Pagès et al., 2004; Leitner et al., 2010) can be added to represent phenology to better estimate plant water uptake across different seasons. Third, the groundwater tracking algorithm mentioned above can be added to better couple the interactions between groundwater and atmosphere.

The vertically-averaged solution to RE has shown its robustness in simulating averaged soil moisture contents. It will have great significance if this vertically-averaged numerical method is applied to another PDE, advection-dispersion differential equation, to simulate depth-averaged contaminant transport in porous media. It could be faster than current advection-dispersion equation solvers and produce relatively accurate results in simulating contaminant movement.

.

References

Albergel, C., Dutra, E., Muñoz-Sabater, J., Haiden, T., Balsamo, G., Beljaars, A., Isaksen, L., de Rosnay, P., Sandu, I., Wedi, N., 2015. Soil temperature at ECMWF: an assessment using ground-based observations. Journal of Geophysical Research: Atmospheres 120, 1361–1373. https://doi.org/10.1002/2014jd022505

Alfnes, E., Kinzelbach, W., Aagaard, P., 2004. Investigation of hydrogeologic processes in a dipping layer structure: 1. The flow barrier effect. Journal of contaminant hydrology 69, 157–172. https://doi.org/10.1016/j.jconhyd.2003.08.003

Allen, R.G., Pereira, L.S., Raes, D., Smith, M., 1998. Crop evapotranspiration-Guidelines for computing crop water requirements-FAO Irrigation and drainage paper 56. Fao, Rome 300, D05109.

Allen, R.G., Pereira, L.S., Smith, M., Raes, D., White, J.L., 2005. FAO-56 Dual Crop Coefficient Method for Estimating Evaporation from Soil and Application Extensions. Journal of Irrigation and Drainage Engineering 131, 2–13. https://doi.org/10.1061/(ASCE)0733-9437(2005)131:1(2)

Ameli, A.A., Creed, I.F., 2017. Quantifying hydrologic connectivity of wetlands to surface water systems. Hydrology and Earth System Sciences 21, 1791–1808.

Arnold, J.G., Moriasi, D.N., Gassman, P.W., Abbaspour, K.C., White, M.J., Srinivasan, R., Santhi, C., Harmel, R.D., Van Griensven, A., Van Liew, M.W., 2012. SWAT: Model use, calibration, and validation. Transactions of the ASABE 55, 1491–1508.

Baroni, G., Facchi, A., Gandolfi, C., Ortuani, B., Horeschi, D., Van Dam, J.C., 2010. Uncertainty in the determination of soil hydraulic parameters and its influence on the performance of

two hydrological models of different complexity. Hydrology and Earth System Sciences 14, 251. https://doi.org/10.5194/hess-14-251-2010

Bayabil, H.K., Dile, Y.T., Tebebu, T.Y., Engda, T.A., Steenhuis, T.S., 2019. Evaluating infiltration models and pedotransfer functions: implications for hydrologic modeling. Geoderma 338, 159–169. https://doi.org/10.1016/j.geoderma.2018.11.028

Belfort, B., Lehmann, F., 2005. Comparison of equivalent conductivities for numerical simulation of one-dimensional unsaturated flow. Vadose Zone Journal 4, 1191–1200.

Belfort, B., Younes, A., Fahs, M., Lehmann, F., 2013. On equivalent hydraulic conductivity for oscillation–free solutions of Richard's equation. Journal of Hydrology 505, 202–217. https://doi.org/10.1016/j.jhydrol.2013.09.047

Best, M.J., Pryor, M., Clark, D.B., Rooney, G.G., Essery, R.L.H., Ménard, C.B., Edwards, J.M., Hendry, M.A., Porson, A., Gedney, N., 2011. The Joint UK Land Environment Simulator (JULES), model description–Part 1: energy and water fluxes. Geoscientific Model Development 4, 677–699.

Beven, K., Binley, A., 1992. The future of distributed models: model calibration and uncertainty prediction. Hydrological processes 6, 279–298.

Bosch, D.D., 2004. Comparison of Capacitance-Based Soil Water Probes in Coastal Plain Soils. Vadose Zone Journal 3, 1380–1389. https://doi.org/10.2136/vzj2004.1380

Bouwer, H., 1969. Planning and interpreting soil permeability measurements. Journal of the Irrigation and Drainage Division 95, 391–402.

Brockett, B.F., Prescott, C.E., Grayston, S.J., 2012. Soil moisture is the major factor influencing microbial community structure and enzyme activities across seven biogeoclimatic zones in western Canada. Soil biology and biochemistry 44, 9–20.

Brunone, B., Ferrante, M., Romano, N., Santini, A., 2003. Numerical simulations of one-dimensional infiltration into layered soils with the Richards equation using different estimates of the interlayer conductivity. Vadose Zone Journal 2, 193–200. https://doi.org/10.2136/vzj2003.1930

Brutsaert, W.F., 1971. A functional iteration technique for solving the Richards equation applied to two-dimensional infiltration problems. Water Resources Research 7, 1583–1596.

Camporese, M., Paniconi, C., Putti, M., McDonnell, J.J., 2019. Fill and spill hillslope runoff representation with a Richards equation-based model. Water Resources Research 55, 8445–8462.

Cardon, G.E., Letey, J., 1992. Plant water uptake terms evaluated for soil water and solute movement models. Soil Science Society of America Journal 56, 1876–1880.

Casanova, M.T., Brock, M.A., 2000. How do depth, duration and frequency of flooding influence the establishment of wetland plant communities? Plant Ecology 147, 237–250.

Caviedes-Voullième, D., Garcı´a-Navarro, P., Murillo, J., 2013. Verification, conservation, stability and efficiency of a finite volume method for the 1D Richards equation. Journal of Hydrology 480, 69–84. https://doi.org/10.1016/j.jhydrol.2012.12.008

Celia, M.A., Bouloutas, E.T., Zarba, R.L., 1990. A general mass-conservative numerical solution for the unsaturated flow equation. Water resources research 26, 1483–1496. https://doi.org/10.1029/wr026i007p01483

Chaudhari, N.M., 1971. An improved numerical technique for solving multidimensional miscible displacement equations. Society of Petroleum Engineers Journal 11, 277–284.

Chaudhary, A., Hantush, M.M., 2017. Bayesian Monte Carlo and maximum likelihood approach for uncertainty estimation and risk management: Application to lake oxygen recovery model. Water Research 108, 301–311. https://doi.org/10.1016/j.watres.2016.11.012

Chen, B., Liu, E., Mei, X., Yan, C., Garré, S., 2018. Modelling soil water dynamic in rain-fed spring maize field with plastic mulching. Agricultural Water Management 198, 19–27.

Chen, X., Liang, X., Xia, J., She, D., 2018. Impact of Lower Boundary Condition of Richards' Equation on Water, Energy, and Soil Carbon Based on Coupling Land Surface and Biogeochemical Models. Pedosphere 28, 497–510. https://doi.org/10.1016/S1002-0160(17)60371-0

Chen, Z., Ding, W., Xu, Y., Müller, C., Rütting, T., Yu, H., Fan, J., Zhang, J., Zhu, T., 2015. Importance of heterotrophic nitrification and dissimilatory nitrate reduction to ammonium in a cropland soil: evidences from a 15N tracing study to literature synthesis. Soil Biology and Biochemistry 91, 65–75.

Cowardin, L.M., 1979. Classification of wetlands and deepwater habitats of the United States. Fish and Wildlife Service, US Department of the Interior.

Crave, A., Gascuel-Odoux, C., 1997. The Influence of Topography on Time and Space Distribution of Soil Surface Water Content. Hydrological Processes 11, 203–210. https://doi.org/10.1002/(SICI)1099-1085(199702)11:2<203::AID-HYP432>3.0.CO;2-K

Cui, G., Zhu, J., 2018. Prediction of unsaturated flow and water backfill during infiltration in layered soils. Journal of Hydrology 557, 509–521. https://doi.org/10.1016/j.jhydrol.2017.12.050

Dai, Y., Zhang, S., Yuan, H., Wei, N., 2019. Modeling Variably Saturated Flow in Stratified Soils With Explicit Tracking of Wetting Front and Water Table Locations. Water Resources Research 55, 7939–7963. https://doi.org/10.1029/2019WR025368

Dan, W., Nianpeng, H.E., Qing, W., Yuliang, L., Qiufeng, W., Zhiwei, X.U., Jianxing, Z.H.U., 2016. Effects of temperature and moisture on soil organic matter decomposition along elevation gradients on the Changbai Mountains, Northeast China. Pedosphere 26, 399–407.

Davis, T.W., Prentice, I.C., Stocker, B.D., Thomas, R.T., Whitley, R.J., Wang, H., Evans, B.J., Gallego-Sala, A.V., Sykes, M.T., Cramer, W., 2017. Simple process-led algorithms for simulating habitats (SPLASH v. 1.0): robust indices of radiation, evapotranspiration and plant-available moisture. Geoscientific Model Development 10, 689–708.

De Rosnay, P., Polcher, J., Bruen, M., Laval, K., 2002. Impact of a physically based soil water flow and soil-plant interaction representation for modeling large-scale land surface processes. Journal of Geophysical Research: Atmospheres 107, ACL 3-1-ACL 3-19.

Dickinson, J.E., Ferré, T.P.A., Bakker, M., Crompton, B., 2014. A screening tool for delineating subregions of steady recharge within groundwater models. Vadose Zone Journal 13.

Dingman, S.L., 2015. Physical hydrology. Waveland press.

Dogan, A., Motz, L.H., 2005. Saturated-unsaturated 3D groundwater model. I: Development. Journal of Hydrologic Engineering 10, 492–504.

Douglas Jr, J., Peaceman, D.W., Rachford Jr, H.H., 1959. A method for calculating multi-dimensional immiscible displacement. Transactions of the AIME 216, 297–308.

Downer, C.W., Ogden, F.L., 2004. Appropriate vertical discretization of Richards' equation for two-dimensional watershed-scale modelling. Hydrological Processes 18, 1–22. https://doi.org/10.1002/hyp.1306

Ducoudré, N.I., Laval, K., Perrier, A., 1993. SECHIBA, a new set of parameterizations of the hydrologic exchanges at the land-atmosphere interface within the LMD atmospheric general circulation model. Journal of Climate 6, 248–273.

Ewel, J.J., Myers, R.L., 1990. Ecosystems of Florida. University of Central Florida Press.

Fan, Y., Miguez-Macho, G., 2011. A simple hydrologic framework for simulating wetlands in climate and earth system models. Clim Dyn 37, 253–278. https://doi.org/10.1007/s00382-010-0829-8

Farthing, M.W., Kees, C.E., Miller, C.T., 2003. Mixed finite element methods and higher order temporal approximations for variably saturated groundwater flow. Advances in Water Resources 26, 373–394. https://doi.org/10.1016/S0309-1708(02)00187-2

Farthing, M.W., Ogden, F.L., 2017. Numerical Solution of Richards' Equation: A Review of Advances and Challenges. Soil Science Society of America Journal. https://doi.org/10.2136/sssaj2017.02.0058

Fatichi, S., Vivoni, E.R., Ogden, F.L., Ivanov, V.Y., Mirus, B., Gochis, D., Downer, C.W., Camporese, M., Davison, J.H., Ebel, B., Jones, N., Kim, J., Mascaro, G., Niswonger, R., Restrepo, P., Rigon, R., Shen, C., Sulis, M., Tarboton, D., 2016. An overview of current applications, challenges, and future trends in distributed process-based models in hydrology. Journal of Hydrology 537, 45–60. https://doi.org/10.1016/j.jhydrol.2016.03.026

Feddes, R.A., 1982. Simulation of Field Water Use and Crop Yield. Pudoc.

Feddes, R.A., Kabat, P., Van Bakel, P.J.T., Bronswijk, J.J.B., Halbertsma, J., 1988. Modelling soil water dynamics in the unsaturated zone — State of the art. Journal of Hydrology 100, 69–111. https://doi.org/10.1016/0022-1694(88)90182-5

Feddes, R.A., Kowalik, P., Kolinska-Malinka, K., Zaradny, H., 1976. Simulation of field water uptake by plants using a soil water dependent root extraction function. Journal of Hydrology 31, 13–26.

Fields, J.S., Owen Jr, J.S., Stewart, R.D., Heitman, J.L., Caron, J., 2020. Modeling water fluxes through containerized soilless substrates using HYDRUS. Vadose Zone Journal 19, e20031.

Fierer, N., Schimel, J.P., 2002. Effects of drying–rewetting frequency on soil carbon and nitrogen transformations. Soil Biology and Biochemistry 34, 777–787.

Forsyth, P.A., Wu, Y.S., Pruess, K., 1995. Robust numerical methods for saturated-unsaturated flow with dry initial conditions in heterogeneous media. Advances in Water Resources 18, 25–38. https://doi.org/10.1016/0309-1708(95)00020-J

Gale, M.R., Grigal, D.F., 1987. Vertical root distributions of northern tree species in relation to successional status. Canadian Journal of Forest Research 17, 829–834.

Gao, H., Tang, Q., Shi, X., Zhu, C., Bohn, T., Su, F., Pan, M., Sheffield, J., Lettenmaier, D., Wood, E., 2010. Water budget record from Variable Infiltration Capacity (VIC) model.

Green, W.H., Ampt, G.A., 1911. Studies on Soil Phyics. The Journal of Agricultural Science 4, 1–24.

Guber, A.K., Pachepsky, Y.A., Van Genuchten, M.T., Rawls, W.J., Simunek, J., Jacques, D., Nicholson, T.J., Cady, R.E., 2006. Field-scale water flow simulations using ensembles of

pedotransfer functions for soil water retention. Vadose Zone Journal 5, 234–247. https://doi.org/10.2136/vzj2005.0111

Guswa, A.J., Celia, M.A., Rodriguez-Iturbe, I., 2002. Models of soil moisture dynamics in ecohydrology: A comparative study. Water Resources Research 38, 5-1-5–15. https://doi.org/10.1029/2001WR000826

Hall, B.G., Acar, H., Nandipati, A., Barlow, M., 2014. Growth rates made easy. Molecular biology and evolution 31, 232–238.

Hantush M M., Kalin L., Isik S., Yucekaya A., 2013. Nutrient Dynamics in Flooded Wetlands. I: Model Development. Journal of Hydrologic Engineering 18, 1709–1723. https://doi.org/10.1061/(ASCE)HE.1943-5584.0000741

Hantush, M.M., Chaudhary, A., 2014. Bayesian Framework for Water Quality Model Uncertainty Estimation and Risk Management. Journal of Hydrologic Engineering 19, 04014015. https://doi.org/10.1061/(ASCE)HE.1943-5584.0000900

Harter, T., Hopmans, J.W., Feddes, R.A., 2004. Role of vadose zone flow processes in regional scale hydrology: Review, opportunities and challenges. Kluwer.

Hazenberg, P., Fang, Y., Broxton, P., Gochis, D., Niu, G.-Y., Pelletier, J.D., Troch, P.A., Zeng, X., 2015. A hybrid-3D hillslope hydrological model for use in E arth system models. Water Resources Research 51, 8218–8239.

Helmig, R., 1997. Multiphase flow and transport processes in the subsurface: a contribution to the modeling of hydrosystems. Springer-Verlag.

Herrada, M.A., Gutiérrez-Martin, A., Montanero, J.M., 2014. Modeling infiltration rates in a saturated/unsaturated soil under the free draining condition. Journal of Hydrology 515, 10–15. https://doi.org/10.1016/j.jhydrol.2014.04.026

Hillel, D., 1998. Environmental soil physics: Fundamentals, applications, and environmental considerations. Elsevier.

Hills, R.G., Porro, I., Hudson, D.B., Wierenga, P.J., 1989. Modeling one-dimensional infiltration into very dry soils: 1. Model development and evaluation. Water Resources Research 25, 1259–1269. https://doi.org/10.1029/WR025i006p01259

Hirschi, M., Mueller, B., Dorigo, W., Seneviratne, S.I., 2014. Using remotely sensed soil moisture for land–atmosphere coupling diagnostics: The role of surface vs. root-zone soil moisture variability. Remote sensing of environment 154, 246–252.

Hoffman, G.J., Van Genuchten, M.T., 1983. Soil properties and efficient water use: Water management for salinity control. Limitations to efficient water use in crop production 73–85.

Homaee, M., Feddes, R.A., Dirksen, C., 2002. Simulation of root water uptake: III. Non-uniform transient combined salinity and water stress. Agricultural water management 57, 127–144.

Huang, M., Lee Barbour, S., Elshorbagy, A., Zettl, J.D., Cheng Si, B., 2011. Infiltration and drainage processes in multi-layered coarse soils. Can. J. Soil. Sci. 91, 169–183. https://doi.org/10.4141/cjss09118

Huisman, J.A., Rings, J., Vrugt, J.A., Sorg, J., Vereecken, H., 2010. Hydraulic properties of a model dike from coupled Bayesian and multi-criteria hydrogeophysical inversion. Journal of Hydrology 380, 62–73. https://doi.org/10.1016/j.jhydrol.2009.10.023

J. Baber, M., Fleishman, E., J. Babbitt, K., L. Tarr, T., 2004. The relationship between wetland hydroperiod and nestedness patterns in assemblages of larval amphibians and predatory macroinvertebrates. Oikos 107, 16–27.

Jackson, R.B., Canadell, J., Ehleringer, J.R., Mooney, H.A., Sala, O.E., Schulze, E.D., 1996. A global analysis of root distributions for terrestrial biomes. Oecologia 108, 389–411. https://doi.org/10.1007/bf00333714

Jacques, D., Mohanty, B.P., Feyen, J., 2002. Comparison of alternative methods for deriving hydraulic properties and scaling factors from single-disc tension infiltrometer measurements. Water Resources Research 38, 25-1-25–14. https://doi.org/10.1029/2001wr000595

Jana, R.B., Mohanty, B.P., 2011. Enhancing PTFs with remotely sensed data for multi-scale soil water retention estimation. Journal of hydrology 399, 201–211. https://doi.org/10.1016/j.jhydrol.2010.12.043

Jensen, D.T., Hargreaves, G.H., Temesgen, B., Allen, R.G., 1997. Computation of ETo under nonideal conditions. Journal of Irrigation and Drainage Engineering 123, 394–400. https://doi.org/10.1061/(asce)0733-9437(1997)123:5(394)

Jordan, T.E., Whigham, D.F., Hofmockel, K., Gerber, N., 1999. Restored wetlands in crop fields control nutrient runoff. Nutrient cycling and retention in natural and constructed Wetlands.

Jordan, T.E., Whigham, D.F., Hofmockel, K.H., Pittek, M.A., 2003. Nutrient and Sediment Removal by a Restored Wetland Receiving Agricultural Runoff. Journal of Environmental Quality 32, 1534–1547. https://doi.org/10.2134/jeq2003.1534

Ju, S.-H., Kung, K.-J., 1997. Mass types, element orders and solution schemes for the Richards equation. Computers & Geosciences 23, 175–187.

Kadlec, R.H., Wallace, S., 2008. Treatment wetlands. CRC press.

Kalin L., Hantush M M., Isik S., Yucekaya A., Jordan T., 2013. Nutrient Dynamics in Flooded Wetlands. II: Model Application. Journal of Hydrologic Engineering 18, 1724–1738. https://doi.org/10.1061/(ASCE)HE.1943-5584.0000750

Köpke, C., Irving, J., Roubinet, D., 2019. Stochastic inversion for soil hydraulic parameters in the presence of model error: An example involving ground-penetrating radar monitoring of infiltration. Journal of Hydrology 569, 829–843. https://doi.org/10.1016/j.jhydrol.2018.12.016

Korzoun, V.I., 1978. World water balance and water resources of the earth.

Koster, R.D., Dirmeyer, P.A., Guo, Z., Bonan, G., Chan, E., Cox, P., Gordon, C.T., Kanae, S., Kowalczyk, E., Lawrence, D., 2004. Regions of strong coupling between soil moisture and precipitation. Science 305, 1138–1140.

Koster, R.D., Schubert, S.D., Suarez, M.J., 2009. Analyzing the concurrence of meteorological droughts and warm periods, with implications for the determination of evaporative regime. Journal of Climate 22, 3331–3341.

Kumar, M., Duffy, C.J., Salvage, K.M., 2009. A second-order accurate, finite volume–based, integrated hydrologic modeling (FIHM) framework for simulation of surface and subsurface flow. Vadose Zone Journal 8, 873–890.

Lai, W., Ogden, F.L., 2015. A mass-conservative finite volume predictor–corrector solution of the 1D Richards' equation. Journal of Hydrology 523, 119–127. https://doi.org/10.1016/j.jhydrol.2015.01.053

Laio, F., Porporato, A., Ridolfi, L., Rodriguez-Iturbe, I., 2001. Plants in water-controlled ecosystems: active role in hydrologic processes and response to water stress: II. Probabilistic soil moisture dynamics. Advances in water resources 24, 707–723.

Lawrence, D.M., Fisher, R.A., Koven, C.D., Oleson, K.W., Swenson, S.C., Bonan, G., Collier, N., Ghimire, B., Kampenhout, L. van, Kennedy, D., Kluzek, E., Lawrence, P.J., Li, F., Li, H., Lombardozzi, D., Riley, W.J., Sacks, W.J., Shi, M., Vertenstein, M., Wieder, W.R., Xu, C., Ali, A.A., Badger, A.M., Bisht, G., Broeke, M. van den, Brunke, M.A., Burns, S.P., Buzan, J., Clark, M., Craig, A., Dahlin, K., Drewniak, B., Fisher, J.B., Flanner, M., Fox, A.M., Gentine, P., Hoffman, F., Keppel-Aleks, G., Knox, R., Kumar, S., Lenaerts, J., Leung, L.R., Lipscomb, W.H., Lu, Y., Pandey, A., Pelletier, J.D., Perket, J., Randerson, J.T., Ricciuto, D.M., Sanderson, B.M., Slater, A., Subin, Z.M., Tang, J., Thomas, R.Q., Martin, M.V., Zeng, X., 2019. The Community Land Model Version 5: Description of New Features, Benchmarking, and Impact of Forcing Uncertainty. Journal of Advances in Modeling Earth Systems 11, 4245–4287. https://doi.org/10.1029/2018MS001583

Lee, D.H., Abriola, L.M., 1999. Use of the Richards equation in land surface parameterizations. Journal of Geophysical Research: Atmospheres 104, 27519–27526. https://doi.org/10.1029/1999JD900951

Leitner, D., Klepsch, S., Bodner, G., Schnepf, A., 2010. A dynamic root system growth model based on L-Systems. Plant and soil 332, 177–192.

Limpert, K.E., Carnell, P.E., Trevathan-Tackett, S.M., Macreadie, P.I., 2020. Reducing emissions from degraded floodplain wetlands. Wetland Biogeochemistry: Response to Environmental Change.

List, F., Radu, F.A., 2016. A study on iterative methods for solving Richards' equation. Computational Geosciences 20, 341–353. https://doi.org/10.1007/s10596-016-9566-3

Loosvelt, L., Pauwels, V.R.N., Cornelis, W.M., Lannoy, G.J.M.D., Verhoest, N.E.C., 2011. Impact of soil hydraulic parameter uncertainty on soil moisture modeling. Water Resources Research 47. https://doi.org/10.1029/2010WR009204

Ma, Y., Feng, S., Su, D., Gao, G., Huo, Z., 2010. Modeling water infiltration in a large layered soil column with a modified Green–Ampt model and HYDRUS-1D. Computers and Electronics in Agriculture, Special issue on computer and computing technologies in agriculture 71, S40–S47. https://doi.org/10.1016/j.compag.2009.07.006

Mahrt, L., Pan, H., 1984. A two-layer model of soil hydrology. Boundary-Layer Meteorol 29, 1–20. https://doi.org/10.1007/BF00119116

Manabe, S., 1969. Climate and the ocean circulation: I. The atmospheric circulation and the hydrology of the earth's surface. Monthly Weather Review 97, 739–774.

Manu, M.K., Li, D., Liwen, L., Jun, Z., Varjani, S., Wong, J.W.C., 2021. A review on nitrogen dynamics and mitigation strategies of food waste digestate composting. Bioresource Technology 334, 125032. https://doi.org/10.1016/j.biortech.2021.125032

Manzoni, S., Schimel, J.P., Porporato, A., 2012. Responses of soil microbial communities to water stress: results from a meta-analysis. Ecology 93, 930–938.

Massey Jr, F.J., 1951. The Kolmogorov-Smirnov test for goodness of fit. Journal of the American statistical Association 46, 68–78.

Matthews, C.J., Braddock, R.D., Sander, G.C., 2004. Modeling Flow Through a One-Dimensional Multi-Layered Soil Profile Using the Method of Lines. Environmental Modeling & Assessment 9, 103–113. https://doi.org/10.1023/B:ENMO.0000032092.10546.c6

Maxwell, R.M., Condon, L.E., 2016. Connections between groundwater flow and transpiration partitioning. Science 353, 377–380. https://doi.org/10.1126/science.aaf7891

Mboh, C.M., Huisman, J.A., Zimmermann, E., Vereecken, H., 2012. Coupled hydrogeophysical inversion of streaming potential signals for unsaturated soil hydraulic properties. Vadose Zone Journal 11, vzj2011.0115. https://doi.org/10.2136/vzj2011.0115

McGuire, A.D., Melillo, J.M., Randerson, J.T., Parton, W.J., Heimann, M., Meier, R.A., Clein, J.S., Kicklighter, D.W., Sauf, W., 2000. Modeling the effects of snowpack on heterotrophic respiration across northern temperate and high latitude regions: Comparison with measurements of atmospheric carbon dioxide in high latitudes. Biogeochemistry 48, 91–114. https://doi.org/10.1023/A:1006286804351

Miller, C.T., Abhishek, C., Farthing, M.W., 2006. A spatially and temporally adaptive solution of Richards' equation. Advances in Water Resources 29, 525–545.

Miller, C.T., Dawson, C.N., Farthing, M.W., Hou, T.Y., Huang, J., Kees, C.E., Kelley, C.T., Langtangen, H.P., 2013. Numerical simulation of water resources problems: Models, methods, and trends. Advances in Water Resources 51, 405–437. https://doi.org/10.1016/j.advwatres.2012.05.008

Miller, C.T., Williams, G.A., Kelley, C.T., Tocci, M.D., 1998. Robust solution of Richards' equation for nonuniform porous media. Water Resour. Res. 34, 2599–2610. https://doi.org/10.1029/98WR01673

Milly, P.C., Malyshev, S.L., Shevliakova, E., Dunne, K.A., Findell, K.L., Gleeson, T., Liang, Z., Phillipps, P., Stouffer, R.J., Swenson, S., 2014. An enhanced model of land water and energy for global hydrologic and earth-system studies. Journal of Hydrometeorology 15, 1739–1761.

Minasny, B., Mc Bratney, A.B., 2002. Uncertainty analysis for pedotransfer functions. European Journal of Soil Science 53, 417–429. https://doi.org/10.1046/j.1365-2389.2002.00452.x

Mitsch, W.J., Gosselink, J.G., 2000. Wetlands (3rd edn). Wetlands. New York: Wiley.

Molz, F.J., 1981. Models of water transport in the soil-plant system: A review. Water resources research 17, 1245–1260.

Molz, F.J., Remson, I., 1971. Application of an Extraction-Term Model to the Study of Moisture Flow to Plant Roots 1. Agronomy Journal 63, 72–77.

Montalto, F.A., Steenhuis, T.S., Parlange, J.-Y., 2006. The hydrology of Piermont Marsh, a reference for tidal marsh restoration in the Hudson river estuary, New York. Journal of Hydrology 316, 108–128.

Moyano, F.E., Manzoni, S., Chenu, C., 2013. Responses of soil heterotrophic respiration to moisture availability: An exploration of processes and models. Soil Biology and Biochemistry 59, 72–85.

Murwira, H.K., Kirchmann, H., Swift, M.J., 1990. The effect of moisture on the decomposition rate of cattle manure. Plant and Soil 122, 197–199.

Neitsch, S.L., Arnold, J.G., Kiniry, J.R., Williams, J.R., 2011. Soil and water assessment tool theoretical documentation version 2009. Texas Water Resources Institute.

Niu, G.-Y., Yang, Z.-L., Mitchell, K.E., Chen, F., Ek, M.B., Barlage, M., Kumar, A., Manning, K., Niyogi, D., Rosero, E., 2011. The community Noah land surface model with multiparameterization options (Noah-MP): 1. Model description and evaluation with local-scale measurements. Journal of Geophysical Research: Atmospheres 116.

O'Connell, C.S., Ruan, L., Silver, W.L., 2018. Drought drives rapid shifts in tropical rainforest soil biogeochemistry and greenhouse gas emissions. Nature communications 9, 1–9.

Ogden, F.L., Lai, W., Steinke, R.C., Zhu, J., Talbot, C.A., Wilson, J.L., 2015. A new general 1-D vadose zone flow solution method. Water Resources Research 51, 4282–4300. https://doi.org/10.1002/2015WR017126

Ojha, C.S.P., Rai, A.K., 1996. Nonlinear root-water uptake model. Journal of irrigation and drainage engineering 122, 198–202.

Oki, T., Kanae, S., 2006. Global hydrological cycles and world water resources. science 313, 1068–1072.

Or, D., Lehmann, P., Assouline, S., 2015. Natural length scales define the range of applicability of the R ichards equation for capillary flows. Water Resources Research 51, 7130–7144.

Orgogozo, L., Renon, N., Soulaine, C., Hénon, F., Tomer, S.K., Labat, D., Pokrovsky, O.S., Sekhar, M., Ababou, R., Quintard, M., 2014. An open source massively parallel solver for Richards equation: Mechanistic modelling of water fluxes at the watershed scale. Computer Physics Communications 185, 3358–3371. https://doi.org/10.1016/j.cpc.2014.08.004

Orth, R., Koster, R.D., Seneviratne, S.I., 2013. Inferring soil moisture memory from streamflow observations using a simple water balance model. Journal of Hydrometeorology 14, 1773–1790.

Pagès, L., Vercambre, G., Drouet, J.-L., Lecompte, F., Collet, C., Le Bot, J., 2004. Root Typ: a generic model to depict and analyse the root system architecture. Plant and soil 258, 103–119.

Pan, L., Warrick, A.W., Wierenga, P.J., 1996. Finite element methods for modeling water flow in variably saturated porous media: Numerical oscillation and mass-distributed schemes. Water Resources Research 32, 1883–1889.

Perrochet, P., 1987. Water uptake by plant roots—a simulation model, I. Conceptual model. Journal of hydrology 95, 55–61.

Persson, A., 2001. User guide to ECMWF forecast products.

Pezeshki, S.R., 2001. Wetland plant responses to soil flooding. Environmental and Experimental Botany, Plants and Organisms in Wetland Environments 46, 299–312. https://doi.org/10.1016/S0098-8472(01)00107-1

Philip, J.R., 1957. The theory of infiltration: 1. The infiltration equation and its solution. Soil science 83, 345–358.

Picek, T., Šimek, M., Šantrůčková, H., 2000. Microbial responses to fluctuation of soil aeration status and redox conditions. Biology and Fertility of Soils 31, 315–322.

Piedallu, C., Gégout, J.-C., Bruand, A., Seynave, I., 2011. Mapping soil water holding capacity over large areas to predict potential production of forest stands. Geoderma 160, 355–366. https://doi.org/10.1016/j.geoderma.2010.10.004

Pollacco, J.A., Mohanty, B.P., 2012. Uncertainties of water fluxes in soil–vegetation–atmosphere transfer models: Inverting surface soil moisture and evapotranspiration retrieved from remote sensing. Vadose Zone Journal 11, vzj2011.0167.

Pop, I.S., 2002. Error estimates for a time discretization method for the Richards' equation. Computational geosciences 6, 141–160.

Prasad, R., 1988. A linear root water uptake model. Journal of Hydrology 99, 297–306.

Priestley, C.H.B., Taylor, R.J., 1972. On the assessment of surface heat flux and evaporation using large-scale parameters. Monthly weather review 100, 81–92. https://doi.org/10.1175/1520-0493(1972)100<0081:OTAOSH>2.3.CO;2

Qi, J., Zhang, X., McCarty, G.W., Sadeghi, A.M., Cosh, M.H., Zeng, X., Gao, F., Daughtry, C.S.T., Huang, C., Lang, M.W., Arnold, J.G., 2018. Assessing the performance of a physically-based soil moisture module integrated within the Soil and Water Assessment Tool. Environmental Modelling & Software 109, 329–341. https://doi.org/10.1016/j.envsoft.2018.08.024

Raffelli, G., Previati, M., Canone, D., Gisolo, D., Bevilacqua, I., Capello, G., Biddoccu, M., Cavallo, E., Deiana, R., Cassiani, G., 2017. Local-and plot-scale measurements of soil moisture: Time and spatially resolved field techniques in plain, hill and mountain sites. Water 9, 706.

Rathfelder, K., Abriola, L.M., 1994. Mass conservative numerical solutions of the head-based Richards equation. Water Resources Research 30, 2579–2586. https://doi.org/10.1029/94wr01302

Reddy, K.R., DeLaune, R.D., 2008. Biogeochemistry of wetlands: science and applications. CRC press.

Richards, L.A., 1931. Capillary conduction of liquids through porous mediums. Physics 1, 318–333. https://doi.org/10.1063/1.1745010

Roberti, J.A., Ayres, E., Loescher, H.W., Tang, J., Starr, G., Durden, D.J., Smith, D.E., de la Reguera, E., Morkeski, K., McKlveen, M., 2018. A robust calibration method for continental-scale soil water content measurements. Vadose Zone Journal 17, 1–19.

Robinson, D.A., Campbell, C.S., Hopmans, J.W., Hornbuckle, B.K., Jones, S.B., Knight, R., Ogden, F., Selker, J., Wendroth, O., 2008. Soil Moisture Measurement for Ecological and Hydrological Watershed-Scale Observatories: A Review. Vadose Zone Journal 7, 358–389. https://doi.org/10.2136/vzj2007.0143

Rockhold, M.L., Simmons, C.S., Fayer, M.J., 1997. An analytical solution technique for one-dimensional, steady vertical water flow in layered soils. Water Resources Research 33, 897–902. https://doi.org/10.1029/96WR03746

Romano, N., 2014. Soil moisture at local scale: Measurements and simulations. Journal of Hydrology, Determination of soil moisture: Measurements and theoretical approaches 516, 6–20. https://doi.org/10.1016/j.jhydrol.2014.01.026

Romano, N., Palladino, M., Chirico, G.B., 2011. Parameterization of a bucket model for soil-vegetation-atmosphere modeling under seasonal climatic regimes. Hydrol. Earth Syst. Sci. 15, 3877–3893. https://doi.org/10.5194/hess-15-3877-2011

Ross, B., 1990. The diversion capacity of capillary barriers. Water Resources Research 26, 2625–2629. https://doi.org/10.1029/WR026i010p02625

Russi, D., ten Brink, P., Farmer, A., Badura, T., Coates, D., Förster, J., Kumar, R., Davidson, N., 2013. The economics of ecosystems and biodiversity for water and wetlands. IEEP, London and Brussels 78.

Sanchez, P.A., Ahamed, S., Carré, F., Hartemink, A.E., Hempel, J., Huising, J., Lagacherie, P., McBratney, A.B., McKenzie, N.J., de Lourdes Mendonça-Santos, M., 2009. Digital soil map of the world. Science 325, 680–681. https://doi.org/10.1126/science.1175084

Sanchez-Mejia, Z.M., Papuga, S.A., 2017. Empirical Modeling of Planetary Boundary Layer Dynamics Under Multiple Precipitation Scenarios Using a Two-Layer Soil Moisture Approach: An Example From a Semiarid Shrubland. Water Resources Research 53, 8807–8824. https://doi.org/10.1002/2016WR020275

Schaefer, G.L., Cosh, M.H., Jackson, T.J., 2007. The USDA natural resources conservation service soil climate analysis network (SCAN). Journal of Atmospheric and Oceanic Technology 24, 2073–2077. https://doi.org/10.1175/2007jtecha930.1

Scharnagl, B., Vrugt, J.A., Vereecken, H., Herbst, M., 2011. Inverse modelling of in situ soil water dynamics: investigating the effect of different prior distributions of the soil hydraulic parameters. Hydrology and Earth System Sciences 15, 3043–3059. https://doi.org/10.5194/hess-15-3043-2011

Schaufler, G., Kitzler, B., Schindlbacher, A., Skiba, U., Sutton, M.A., Zechmeister-Boltenstern, S., 2010. Greenhouse gas emissions from European soils under different land use: effects of soil moisture and temperature. European Journal of Soil Science 61, 683–696.

Selle, B., Minasny, B., Bethune, M., Thayalakumaran, T., Chandra, S., 2011. Applicability of Richards' equation models to predict deep percolation under surface irrigation. Geoderma 160, 569–578. https://doi.org/10.1016/j.geoderma.2010.11.005

Seneviratne, S.I., Corti, T., Davin, E.L., Hirschi, M., Jaeger, E.B., Lehner, I., Orlowsky, B., Teuling, A.J., 2010. Investigating soil moisture–climate interactions in a changing climate: A review. Earth-Science Reviews 99, 125–161. https://doi.org/10.1016/j.earscirev.2010.02.004

Sharifi A., Hantush M M., Kalin L., 2017. Modeling Nitrogen and Carbon Dynamics in Wetland Soils and Water Using Mechanistic Wetland Model. Journal of Hydrologic Engineering 22, D4016002. https://doi.org/10.1061/(ASCE)HE.1943-5584.0001441

Sharifi, A., Kalin, L., Hantush, M.M., Isik, S., Jordan, T.E., 2013. Carbon dynamics and export from flooded wetlands: A modeling approach. Ecological Modelling 263, 196–210. https://doi.org/10.1016/j.ecolmodel.2013.04.023

Shen, C., Phanikumar, M.S., 2010. A process-based, distributed hydrologic model based on a large-scale method for surface–subsurface coupling. Advances in Water Resources 33, 1524–1541. https://doi.org/10.1016/j.advwatres.2010.09.002

Si, B., Dyck, M., Parkin, G., 2011. Flow and transport in layered soils: preface. Canadian Journal of Soil Science 91, 127–132. https://doi.org/10.4141/cjss11501

Šimůnek, J., Huang, K., Van Genuchten, M.T., 1998. The HYDRUS code for simulating the one-dimensional movement of water, heat, and multiple solutes in variably-saturated media. US Salinity Laboratory Research Report 144.

Šimůnek, J., Suarez, D.L., 1993. Modeling of carbon dioxide transport and production in soil: 1. Model development. Water Resources Research 29, 487–497.

Simunek, J., Van Genuchten, M.T., Sejna, M., 2005. The HYDRUS-1D software package for simulating the one-dimensional movement of water, heat, and multiple solutes in variably-saturated media. University of California-Riverside Research Reports 3, 1–240.

Šimůnek, J., van Genuchten, M.Th., 2008. Modeling Nonequilibrium Flow and Transport Processes Using HYDRUS. Vadose Zone Journal 7, 782. https://doi.org/10.2136/vzj2007.0074

Šimůnek, J., van Genuchten, M.Th., Šejna, M., 2008. Development and Applications of the HYDRUS and STANMOD Software Packages and Related Codes. Vadose Zone Journal 7, 587. https://doi.org/10.2136/vzj2007.0077

Skaggs, T.H., Shouse, P.J., Poss, J.A., 2006. Irrigating forage crops with saline waters: 2. Modeling root uptake and drainage. Vadose Zone Journal 5, 824–837.

Sleutel, S., Moeskops, B., Huybrechts, W., Vandenbossche, A., Salomez, J., De Bolle, S., Buchan, D., De Neve, S., 2008. Modeling soil moisture effects on net nitrogen

mineralization in loamy wetland soils. Wetlands 28, 724–734. https://doi.org/10.1672/07-105.1

Snodgrass, J.W., Komoroski, M.J., Bryan Jr, A.L., Burger, J., 2000. Relationships among isolated wetland size, hydroperiod, and amphibian species richness: implications for wetland regulations. Conservation biology 14, 414–419.

Soil Survey Staff, 1999. Soil taxonomy: A basic system of soil classification for making and interpreting soil surveys. 2nd edition. Natural Resources Conservation Service. U.S. Department of Agriculture Handbook 436.

Soil Survey Staff. Natural Resources Conservation Service, United States Department of Agriculture. Soil Survey Geographic (SSURGO) Database. Available online at https://sdmdataaccess.sc.egov.usda.gov. Accessed, 2019.

Spear, R.C., Hornberger, G.M., 1980. Eutrophication in peel inlet—II. Identification of critical uncertainties via generalized sensitivity analysis. Water Research 14, 43–49.

Stefanik, K.C., Mitsch, W.J., 2017. Vegetation productivity of planted and unplanted created riverine wetlands in years 15–17. Ecological Engineering, Ecological Engineering of Sustainable Landscapes 108, 425–434. https://doi.org/10.1016/j.ecoleng.2017.07.001

Survey, N.C.S., 2017. National Cooperative Soil Survey Characterization Database.

Svyatskiy, D., Lipnikov, K., 2017. Second-order accurate finite volume schemes with the discrete maximum principle for solving Richards' equation on unstructured meshes. Advances in Water Resources 104, 114–126. https://doi.org/10.1016/j.advwatres.2017.03.015

Szymkiewicz, A., 2012. Modelling water flow in unsaturated porous media: accounting for nonlinear permeability and material heterogeneity. Springer Science & Business Media.

Szymkiewicz, A., Helmig, R., 2011. Comparison of conductivity averaging methods for one-dimensional unsaturated flow in layered soils. Advances in Water Resources 34, 1012–1025. https://doi.org/10.1016/j.advwatres.2011.05.011

Szymkiewicz, A., Tisler, W., Burzyński, K., 2015. Examples of numerical simulations of two-dimensional unsaturated flow with VS2DI code using different interblock conductivity averaging schemes. Geologos 21, 161–167.

Tocci, M.D., Kelley, C.T., Miller, C.T., 1997. Accurate and economical solution of the pressure-head form of Richards' equation by the method of lines. Advances in Water Resources 20, 1–14.

Trenberth, K.E., Fasullo, J.T., Kiehl, J., 2009. Earth's global energy budget. Bulletin of the American Meteorological Society 90, 311–324.

van Dam, J.C., Feddes, R.A., 2000. Numerical simulation of infiltration, evaporation and shallow groundwater levels with the Richards equation. Journal of Hydrology 233, 72–85. https://doi.org/10.1016/S0022-1694(00)00227-4

Van Genuchten, M.T., 1987. A Numerical Model for Water and Solute Movernent.

Van Genuchten, M.T., 1980. A closed-form equation for predicting the hydraulic conductivity of unsaturated soils. Soil science society of America journal 44, 892–898. https://doi.org/10.2136/sssaj1980.03615995004400050002x

Vereecken, H., Schnepf, A., Hopmans, J.W., Javaux, M., Or, D., Roose, T., Vanderborght, J., Young, M.H., Amelung, W., Aitkenhead, M., Allison, S.D., Assouline, S., Baveye, P., Berli, M., Brüggemann, N., Finke, P., Flury, M., Gaiser, T., Govers, G., Ghezzehei, T., Hallett, P., Franssen, H.J.H., Heppell, J., Horn, R., Huisman, J.A., Jacques, D., Jonard, F., Kollet, S., Lafolie, F., Lamorski, K., Leitner, D., McBratney, A., Minasny, B., Montzka,

C., Nowak, W., Pachepsky, Y., Padarian, J., Romano, N., Roth, K., Rothfuss, Y., Rowe, E.C., Schwen, A., Šimůnek, J., Tiktak, A., Dam, J.V., Zee, S.E.A.T.M. van der, Vogel, H.J., Vrugt, J.A., Wöhling, T., Young, I.M., 2016. Modeling Soil Processes: Review, Key Challenges, and New Perspectives. Vadose Zone Journal 15. https://doi.org/10.2136/vzj2015.09.0131

Vogel, T., Cislerova, M., 1988. On the reliability of unsaturated hydraulic conductivity calculated from the moisture retention curve. Transport in porous media 3, 1–15. https://doi.org/10.1007/bf00222683

Vogel, T., van Genuchten, M.Th., Cislerova, M., 2000. Effect of the shape of the soil hydraulic functions near saturation on variably-saturated flow predictions. Advances in Water Resources 24, 133–144. https://doi.org/10.1016/S0309-1708(00)00037-3

Vrugt, J.A., Bouten, W., 2002. Validity of first-order approximations to describe parameter uncertainty in soil hydrologic models. Soil Science Society of America Journal 66, 1740–1751. https://doi.org/10.2136/sssaj2002.1740

Wesseling, J.G., 1991. Meerjarige simulatie van grondwaterstroming voor verschillende bodemprofielen, grondwatertrappen en gewassen met het model SWATRE. DLO-Staring Centrum.

Whigham, D., Pittek, M., Hofmockel, K.H., Jordan, T., Pepin, A.L., 2002. Biomass and nutrient dynamics in restored wetlands on the outer coastal plain of Maryland, USA. Wetlands 22, 562–574. https://doi.org/10.1672/0277-5212(2002)022[0562:BANDIR]2.0.CO;2

Whigham, D.F., Simpson, R.L., 1978. The relationship between aboveground and belowground biomass of freshwater tidal wetland macrophytes. Aquatic Botany 5, 355–364.

Wickland, K.P., Neff, J.C., 2008. Decomposition of soil organic matter from boreal black spruce forest: environmental and chemical controls. Biogeochemistry 87, 29–47.

Wöhling, T., Vrugt, J.A., 2011. Multiresponse multilayer vadose zone model calibration using Markov chain Monte Carlo simulation and field water retention data. Water Resources Research 47.

Wöhling, T., Vrugt, J.A., 2008. Combining multiobjective optimization and Bayesian model averaging to calibrate forecast ensembles of soil hydraulic models. Water resources research 44. https://doi.org/10.1029/2008wr007154

Wöhling, T., Vrugt, J.A., Barkle, G.F., 2008. Comparison of three multiobjective optimization algorithms for inverse modeling of vadose zone hydraulic properties. Soil Science Society of America Journal 72, 305–319. https://doi.org/10.2136/sssaj2007.0176

Wood, E.F., Roundy, J.K., Troy, T.J., Beek, L.P.H. van, Bierkens, M.F.P., Blyth, E., Roo, A. de, Döll, P., Ek, M., Famiglietti, J., Gochis, D., Giesen, N. van de, Houser, P., Jaffé, P.R., Kollet, S., Lehner, B., Lettenmaier, D.P., Peters-Lidard, C., Sivapalan, M., Sheffield, J., Wade, A., Whitehead, P., 2011. Hyperresolution global land surface modeling: Meeting a grand challenge for monitoring Earth's terrestrial water. Water Resources Research 47. https://doi.org/10.1029/2010WR010090

Wood, T.E., Detto, M., Silver, W.L., 2013. Sensitivity of soil respiration to variability in soil moisture and temperature in a humid tropical forest. PLoS One 8, e80965.

Xu, L., He, N.P., Yu, G.R., Wen, D., Gao, Y., He, H.L., 2015. Differences in pedotransfer functions of bulk density lead to high uncertainty in soil organic carbon estimation at regional scales: Evidence from Chinese terrestrial ecosystems. Journal of Geophysical Research: Biogeosciences 120, 1567–1575. https://doi.org/10.1002/2015jg002929

Xu, X., Zhang, Q., Li, Y., Li, X., 2016. Evaluating the influence of water table depth on transpiration of two vegetation communities in a lake floodplain wetland. Hydrology Research 47, 293–312. https://doi.org/10.2166/nh.2016.011

Yakirevich, A., Borisov, V., Sorek, S., 1998. A quasi three-dimensional model for flow and transport in unsaturated and saturated zones: 1. Implementation of the quasi two-dimensional case. Advances in water resources 21, 679–689.

Zeng, X., Decker, M., 2009. Improving the Numerical Solution of Soil Moisture–Based Richards Equation for Land Models with a Deep or Shallow Water Table. Journal of Hydrometeorology 10, 308–319. https://doi.org/10.1175/2008JHM1011.1

Zha, Y., Yang, J., Yin, L., Zhang, Y., Zeng, W., Shi, L., 2017. A modified Picard iteration scheme for overcoming numerical difficulties of simulating infiltration into dry soil. Journal of Hydrology 551, 56–69.

Zhang, Y., Schaap, M.G., 2017. Weighted recalibration of the Rosetta pedotransfer model with improved estimates of hydraulic parameter distributions and summary statistics (Rosetta3). Journal of Hydrology 547, 39–53. https://doi.org/10.1016/j.jhydrol.2017.01.004

Zhu, Y., Lü, H., Horton, R., Yu, Z., Ouyang, F., 2016. A Modified Soil Moisture Model for Two-Layer Soil. Groundwater 54, 569–578. https://doi.org/10.1111/gwat.12387

Zhu, Y., Ren, L., Skaggs, T.H., Lü, H., Yu, Z., Wu, Y., Fang, X., 2009. Simulation of Populus euphratica root uptake of groundwater in an arid woodland of the Ejina Basin, China. Hydrological Processes: An International Journal 23, 2460–2469.